Effects of low-severity fire on species composition and structure in montane forests of the Sierra Nevada, California, USA

Kendall M. L. Becker

A thesis

submitted in partial fulfillment of the

requirements for the degree of

Master of Science

University of Washington

2014

Committee:

Gregory J. Ettl

James A. Lutz

Donald McKenzie

Program Authorized to Offer Degree:

School of Environmental and Forest Sciences

University of Washington

Abstract

Effects of low-severity fire on species composition and structure in montane forests of the Sierra Nevada, California, USA

Kendall M. L. Becker

Chair of the Supervisory Committee:

Gregory J. Ettl, Associate Professor

School of Environmental and Forest Sciences

Climate, topography, and fire influence the species composition and structure of montane forest communities in the Sierra Nevada. This thesis uses data from 97, 0.1 ha plots (46 unburned since 1930; 51 burned at moderate-severity or below since 1946) in Yosemite and Sequoia & Kings Canyon National Parks to describe relationships between (1) climatic water balance and species composition, (2) recent fire and species composition, (3) climatic water balance and forest diameter distributions, and (4) recent fire and forest diameter distributions. These analyses are presented in two parts. Chapter I examines the effects of moderate-severity fire and below (hereafter, lower-severity fire) on individual tree species and characterizes the relationships between species composition and (1) modeled climatic water balance and (2)

lower-severity fire. Chapter II parallels the approach of Chapter I but categorizes trees by diameter class rather than species. Chapter II examines the effects of lower-severity fire on individual diameter classes and characterizes the relationships between diameter class assemblages (i.e., structural communities) and (1) modeled climatic water balance and (2) lower-severity fire. This thesis recognizes species composition and structural composition as unique but interrelated attributes of forest systems. These analyses suggest that lower-severity fire reduces the density of smaller-diameter trees but that reintroduction of fire will not restore historical species composition given the abundance of shade-tolerant species that have attained fire-resistant size during the fire exclusion of the previous century. Land management strategies designed to conserve forest structure rather than species composition may therefore become increasingly important.

TABLE OF CONTENTS

List of Figures

List of Tables

CHAPTER I

EFFECTS OF LOWER-SEVERITY FIRE ON SPECIES COMPOSITION IN MONTANE FORESTS OF THE SIERRA NEVADA

ABSTRACT

Change in tree species composition is an important aspect of forest community development, but the relationships among compositional change, fire, physiography, and climate in the montane forests of the Sierra Nevada are not fully understood. Fire is a key process in this region, but nearly a century of fire suppression has altered the landscape. In some lower montane forests tree density has increased three-fold, primarily driven by greater abundance of shade-tolerant, fire-sensitive species. Additionally, the accumulation of ground and ladder fuels may increase fire severity and heighten the risk associated with using fire to restore more characteristic species composition and tree density. In contrast, the effects of both fire exclusion and fire reintroduction in upper montane forests are less studied. I used tree diameter and species data from 97, 0.1 ha plots (46 unburned since 1930; 51 burned between one and four times since 1946) located in montane forests of Yosemite and Sequoia & Kings Canyon National Parks to identify the effects of moderate-severity fire and below (i.e., lower-severity fire) on the density and basal area of individual tree species and to illustrate those fire effects along compositional and biophysical gradients. Distributions of small-diameter *Abies concolor* (<45 cm diameter at breast height; dbh), *Abies magnifica* (<30 cm dbh), and *Calocedrus decurrens* (<15 cm dbh) density and basal area differed significantly between burned and unburned plots (Mann Whitney *U* test; $\alpha = 0.05$), suggesting species-specific thresholds of sensitivity to lower-severity fire. However, comparisons of historical and contemporary diameter distributions suggest that many

A. concolor and *C. decurrens* individuals have attained fire-resistant size during the period of fire suppression. Therefore, it is improbable that even multiple lower-severity fires over a prolonged period could fully restore historical species composition, highlighting the importance of focusing management efforts on the maintenance of forest structure and ecosystem function.

INTRODUCTION

Changes in species composition are an important aspect of forest community development, but the relationships among compositional change, intermediate disturbance, and the physical and climatological template are not completely understood. Species composition affects the trajectory and pace of forest structural development (Kobe et al. 1995; Shugart et al. 1981), constrains the rate of biomass accumulation and nutrient cycling (Pacala and Deutschman 1995; Peet 1981; Van Cleve and Viereck 1981; Marks and Bormann 1972), and influences the magnitude of subsequent disturbances (Johnstone et al. 2011; Thode et al. 2011; Sugihara et al. 2006; Agee 1993). Species presence and abundance are simultaneously a function of biophysical variables and the disturbance regime, which is, in turn, a product of local climate and weather, physiography, vegetation, and anthropogenic influence (Miller et al. 2012a; Fites-Kaufman et al. 2007; van Wagtendonk and Fites-Kaufman 2006; McKenzie et al. 2003; Agee 1993). The inherently continuous nature of climate and topography and the episodic nature of disturbance events cause species' distributional bounds and demography to vary across the landscape and through time.

In the Sierra Nevada, the explanatory factors behind species composition have been studied at two separate temporal scales, one that relates species composition to long-term physiographic and climate variables (Lutz et al. 2010; Parker 1989, 1984, 1982; Vankat 1982; Oosting and Billings 1943; Klyver 1931) and another that quantifies the effects of short-term fire disturbance (van Mantgem et al. 2013; Collins et al. 2011; van Mantgem et al. 2011; Webster and Halpern 2010; North et al. 2007; Schwilk et al. 2006). The inferences drawn from such studies rarely encompass both fire-independent and fire-dependent community variation: samples are either controlled for burn status to highlight fire-independent community variation

(Parker 1989, 1984, 1982; Vankat 1982; Vankat and Major 1978) or are limited by geographic extent and examine fire-dependent community variation over only a fraction of the landscape (Collins et al. 2011; van Mantgem et al. 2011; Scholl and Taylor 2010; Webster and Halpern 2010; North et al. 2007; Schwilk et al. 2006).

Climate and topography are primary in determining the distribution of plant communities across the Sierra Nevada. Seasonal weather patterns in the Sierra Nevada are closely tied to incoming high (summer) and low (winter) pressure systems from the Pacific Ocean. As these systems encounter the western slope of the range orographic lift increases precipitation. Coupled with the lower temperatures associated with higher altitudes, a greater proportion of precipitation falls as snow (van Wagtendonk and Fites-Kaufman 2006). This hydrologic gradient affects both water availability and soil chemistry. The greater water surplus and higher sand content of soils at higher elevations facilitate leaching of cations (Parker 1989). Higher elevation species must therefore be adapted to a deeper snowpack, a shorter growing season, and shallower and more acidic soil. Lower elevation species, in contrast, must tolerate a prolonged summer drought: the earlier melting of a shallower snowpack overrides the compensatory effects of deeper soils with higher water-holding capacity. Previous studies have observed *Pinus ponderosa-Calocedrus decurrens* and *Abies concolor-Pinus lambertiana* forest alliances at lower elevations (1200-1900 m), *Abies magnifica* and *Pinus jeffreyi* forest alliances at mid elevations (1900-2500 m), and *Pinus contorta* and *Tsuga mertensiana* forest alliances at high elevations (2500-3300 m; Parker 1989, 1982; Vankat 1982; Klyver 1931). Within these elevational bands, aspect drives fine-scale variation in the distribution of plant communities. Evaporative demand decreases with rising elevation but increases with southwestern aspect (Fites-Kaufman et al. 2007). Therefore, a southerly shift in aspect will typically accompany an increase in the elevation of a given forest

alliance. Of the Sierra Nevada tree species, *Abies* spp. favor more mesic conditions, either higher elevations or northeasterly aspects, whereas *Pinus* spp. occupy more xeric sites characterized by higher evaporative demand (Scholl and Taylor 2010; Beaty and Taylor 2007; Parker 1989, 1982; Vankat 1982).

Potential evapotranspiration (PET), actual evapotranspiration (AET), and climatic water deficit (Deficit) are biophysical variables that describe the plant-water relations mechanistically responsible for the strong relationship between species composition and elevation and aspect. These water balance parameters reflect the quantity and timing of precipitation and temperature, which determine snowpack depth and residence time; soil water-holding capacity, which determines how long liquid water remains available to plants; and the flux of photosynthetically active radiation (PAR), which, in combination with temperature, dictates evaporative demand. Elevation is closely tied to the quantity of precipitation through the effects of orographic lift and also negatively correlates with (1) temperature, as atmospheric pressure decreases with increasing altitude, and (2) soil water-holding capacity, as lower elevation (e.g., unglaciated) soils are deeper, having undergone a longer period of development. Aspect and elevation together determine evaporative demand. Southwestern aspects at lower elevations experience the highest evaporative demand, driven by the southerly position of the sun over the northern hemisphere (e.g., southern aspects), higher afternoon temperatures (e.g., western aspects), and the lapse rate. PET, the amount of water that could be transpired by a hypothetical standard crop given unlimited water resources, is a product of temperature and PAR (Stephenson 1998, 1990). By definition, PET is the sum of AET, the actual amount of water that could be transpired by a standard crop given water limitations, and Deficit, the unmet water demand (PET = AET + Deficit; Stephenson 1990). In ecosystems with highly seasonal precipitation, such as the Sierra

Nevada, the dynamics of water storage in the snowpack and in soil determine the amount and timing of water available to plants. Stephenson (1998) demonstrated the utility of AET and Deficit as biologically based correlates of plant community distributions in the Sierra Nevada.

The distribution of vegetation also reflects characteristic disturbance regimes, which vary with elevation, topography, and plant community (Caprio and Swetnam 1995). Severity and frequency are attributes commonly used to typify disturbance regimes. Severity is defined as the magnitude of the effect of a disturbance on an ecosystem and is directly related to plant mortality in forest systems (Thode et al. 2011; National Wildfire Coordination Group 2007; Agee 1993).

Fire is a seasonal disturbance in the Sierra Nevada. Although higher elevation sites receive more lightning strikes, lower elevation sites experience more ignitions due to earlier snowmelt, higher site productivity, and the accumulation of dry surface fuels (van Wagtendonk and Fites-Kaufman 2006; van Wagtendonk 1994). In the lower montane zone, *Pinus* spp., which occupy sites characterized by more frequent fire, produce thicker bark for a given stem diameter, have higher live crowns, and develop larger, more protected buds (van Wagtendonk and Fites-Kaufman 2006). Historically, short fire return intervals prevented heavy fuel accumulation, leading to a low-severity fire regime at *Pinus*-dominated sites. In contrast, *Abies* spp. occupy sites characterized by less frequent fire and have comparatively thinner bark at small diameters. While longer fire return intervals and reduced moisture stress facilitate fuel accumulation, fire severity at these sites is mitigated by higher fuel moisture and compact litter that limits oxygen availability during combustion (Thode et al. 2011; van Wagtendonk 2006; van Wagtendonk and Fites-Kaufman 2006).

In the upper montane zone wind supersedes fire as a dominant disturbance (Parker 1986a). *Abies magnifica* forests exhibit high rates of mortality balanced by high rates of

reproduction. Regeneration is most successful in gaps opened by windthrow of mature individuals because rapid growth is required for saplings to transition to subcanopy status from a niche beneath the surface of the snowpack that is protected from high-speed winds (Parker 1986a, 1984; Oosting and Billings 1943).

In the Sierra Nevada anthropogenic influence on species composition has manifested itself in the form of fire suppression since 1890 (van Wagtendonk 2007). Vankat and Major (1978) were the first to document compositional changes in the lower montane zone and ascribed the primary cause to fire exclusion. Subsequent studies have temporally linked fire exclusion to a three-fold increase in tree density driven by burgeoning populations of fire-sensitive, shade-tolerant *Abies concolor* (Gordon) Lindley ex Hildebrand (white fir) and *Calocedrus decurrens* (Torr.) Florin (incense-cedar; Scholl and Taylor 2010; Beaty and Taylor 2007). Large-diameter trees, particularly large *Pinus* individuals, have concurrently decreased in abundance, potentially due to increased susceptibility to pathogens (e.g., *Heterobasidium annosum* and *Cronartium ribicola*), bark beetles (e.g., *Dendroctonus* spp.), and resource limitation induced by high tree density (Lutz et al. 2009a).

Maintaining forests with drought-tolerant and fire-resistant constituents is an important management objective, particularly considering the projected effects of warmer global temperatures and more variable precipitation patterns on fire size, frequency, and severity (Littell et al. 2009; Lutz et al. 2009b; IPCC 2007; Westerling et al. 2006). Since 1968 wildland fire use and prescribed burns have been employed with the purpose of restoring historical species composition, reducing tree density, and removing surface and ladder fuels that facilitate high-severity fire (van Wagtendonk 2007). In general, species survivorship reflects species' tolerances: Higher proportions of small-diameter (<10 cm) *Abies* are killed in prescribed burns

than small-diameter *Pinus* (van Mantgem et al. 2013; Collins et al. 2011; Schwilk et al. 2006; but see North et al. 2007).

However, while the outcomes of fire use have been documented in lower montane forests, where the effects of fire exclusion appear most prominently, few studies examine the influence of fire on species composition along a gradient that spans both lower and upper montane forests – areas altered by marked departures from historical disturbance regimes and areas that still reside within their historical range of variability. Here I compare recently burned and unburned sites distributed along the compositional gradient that characterizes montane forests of Yosemite National Park (Yosemite) and Sequoia & Kings Canyon National Park (Sequoia). My objectives are to: (1) illustrate the relationships between species composition and water balance parameters, and (2) identify diameter thresholds of sensitivity to moderate-severity fire and below for seven tree species to inform inferences regarding the effects of lower-severity fire on species composition.

STUDY AREA

Physical environment

Yosemite National Park and Sequoia & Kings Canyon National Park are located on the western slope of the central and southern Sierra Nevada (Figure 1.1). The geology and physiography of the Sierra Nevada are most recently the result of uplift associated with the expansion of the Great Basin and glacial activity during the last 100,000 years that exposed the granitic core of the mountain range. Soils of the Sierra Nevada comprise seven orders, with the more fertile *Alfisols* strongly associated with forest cover. Elevation ranges from 150 m along the American River near Sacramento to 4,418 m at the crest of Mt. Whitney (Yosemite: 648 m to 3,997 m; Sequoia: 520 m to 4,418 m; van Wagtendonk and Fites-Kaufman 2006).

The climate is Mediterranean, with cold, wet winters and warm, dry summers. Climate normals from 1981 to 2010 reflect mean January temperatures ranging from -7.3° to 7.0° C in Yosemite and from -10.0° to 9.1° C in Sequoia, mean July temperatures ranging from 8.1° to 24.9° C in Yosemite and from 5.7° to 27.7° C in Sequoia, and mean annual precipitation of 870 mm to 1802 mm in Yosemite and from 398 mm to 1614 mm in Sequoia (PRISM, 2012). Temperatures decrease approximately 6.5° C with each 1,000 m increase in elevation (van Wagtendonk and Fites-Kaufman 2006). Consequently, a greater proportion of precipitation falls as snow at higher elevations, and the duration of snowpack is longer. At the lower limit of contiguous forest cover (1,400 m) 20% to 25% of annual precipitation falls as snow, whereas in the upper montane zone (1,950 m to 2,100 m) 70% to 90% falls as snow (Fites-Kaufman et al. 2007). Cooler temperatures in the upper montane zone maintain snow coverage for up to 200 days per year, and maximum snow depths typically vary between 2.5 m and 4.0 m (van

Wagtendonk and Fites-Kaufman 2006). Lightning strikes also increase with elevation, with more strikes per unit area above 2,625 m than below (van Wagtendonk 1994).

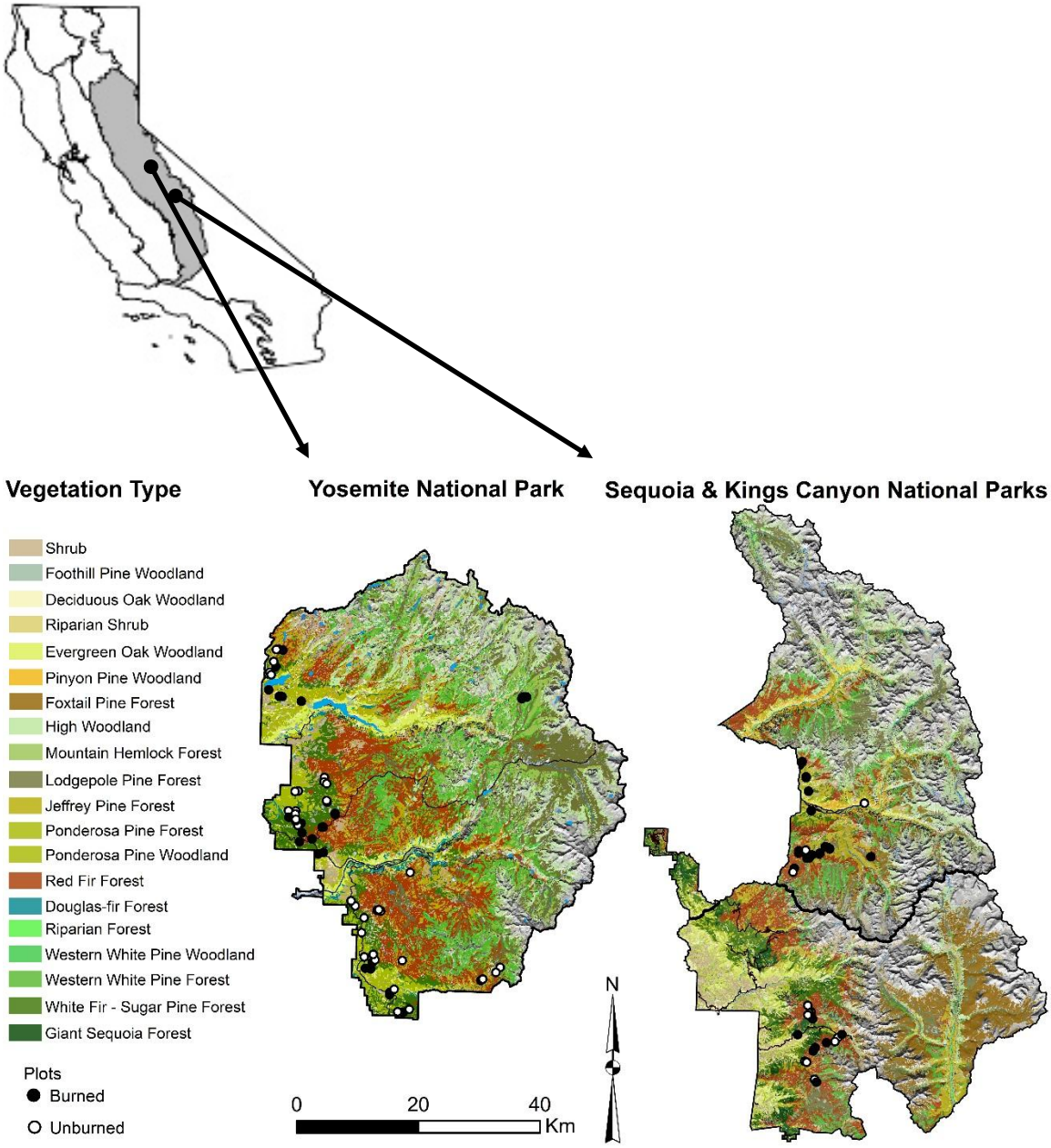

Figure 1.1. Locations of 105 study sites in Yosemite and Sequoia & Kings Canyon National Parks, California, USA, superimposed on lower and upper montane vegetation types.

Vegetation

Lower montane mixed-conifer stands predominate between 1,500 m and 1,650 m (van Wagtendonk and Fites-Kaufman 2006). Site moisture, light availability, and fire history interact

with species' tolerances and life-history traits to determine the relative dominance of the principal tree species: *Abies concolor*, *Calocedrus decurrens*, *Pinus lambertiana* Douglas (sugar pine), *Pinus ponderosa* Douglas ex C. Lawson (ponderosa pine), and *Quercus kelloggii* Newb. (California black oak; Table 1.1). *Pinus ponderosa* and *Q. kelloggii* typically occupy lower elevations, where decreased water availability restricts *A. concolor* abundance. *Abies concolor*-mixed-conifer forest generally occupies higher elevation sites with deeper soils. Patches of shrubs, including *Ceanothus cordulatus* Kellogg (mountain whitethorn), *Quercus vaccinifolia* Kellogg (huckleberry oak), and *Prunus emarginata* (Dougl. ex Hook.) Eaton (bitter cherry), are common in stands dominated by *A. concolor* (Fites-Kaufman et al. 2007). *Calocedrus decurrens* and *P. lambertiana* extend throughout the full lower montane range.

Upper montane mixed-conifer stands occur between 1,950 m and 2,100 m (van Wagtendonk and Fites-Kaufman 2006). *Abies magnifica* A. Murray (red fir) coexists with *A. concolor* at lower elevations and with *Pinus contorta* var. *murrayana* Douglas (lodgepole pine), *Pinus jeffreyi* Balf. (Jeffrey pine), *Pinus monticola* Douglas ex D. Don (western white pine), and *Tsuga mertensiana* (Bong.) Carr. (mountain hemlock) at higher elevations. *Juniperus occidentalis*-*P. jeffreyi* woodlands occupy granitic domes.

Table 1.1. Relative tolerances and responses to fire of mixed-conifer species in lower and upper montane forests (Fites-Kaufman et al. 2007; van Wagtendonk and Fites-Kaufman 2006).

Tree species	Drought tolerance	Shade tolerance	Fire resistance	Fire adaptations
Abies concolor	low	high	low (young) moderate (mature)	thick bark (mature)
Abies magnifica	high	high (seedling) moderate (sapling)	low (young) moderate (mature)	thick bark (mature)
Calocedrus decurrens	high	high	low (young) moderate (mature)	thick bark (mature)
Pinus contorta	high, also high tolerance for poor drainage	--	low/moderate	thin bark (mature)
Pinus jeffreyi	high	low	high	thick bark (young); elevated crown (mature); protected buds
Pinus lambertiana	moderate	low (dense shade) high (moderate shade)	low (young) moderate (mature)	thick bark (mature); elevated crown
Pinus monticola	--	--	very low (young) moderate (mature)	thick bark (mature); elevated crown
Pinus ponderosa	high	low	high	thick bark (young); elevated crown (mature); protected buds
Quercus kelloggii	high	moderate (young) low (mature)	high	sprouting capability

Disturbance history

Nearly a century of fire suppression has resulted in a threefold increase in tree density and a greater abundance of ladder fuels throughout lower montane forests (Scholl and Taylor 2010; Parsons and DeBenedetti 1979). The greater fuel load has increased the likelihood of high-severity fire, precipitating a shift in the fire regimes of Yosemite and Sequoia from generally low severity to mixed severity (Thode et al. 2011). Since 1972 in Yosemite and since 1968 in Sequoia, park managers have used prescribed fire and lightning ignitions in an effort to restore historical fire regimes (van Wagtendonk 2007; Kilgore and Briggs 1972). This has created a mosaic of forest patches, some that have burned up to five times in the last 40 years and others that have not burned since the adoption of fire suppression policies in 1890 (van Wagtendonk et al. 2012). Between 1972 and 2010, 182 fires >40 ha burned 106,106 ha in Yosemite, and between 1968 and 2010, 188 fires >400 ha burned 83,525 ha in Sequoia (Lutz et al. 2011; Monitoring Trends in Burn Severity database, Eidenshink et al. 2007).

Historically, a mean fire return interval (FRI) of 2 to 20 years characterized the lower montane zone (van Wagtendonk and Fites-Kaufman 2006). In Yosemite between 1984 and 2003, over a third of the area occupied by *P. ponderosa* stands burned at low to moderate severity through a combination of prescribed fire, wildland fire use, and wildfire (Thode et al. 2011). During this same period, nearly a third of the area dominated by *A. concolor* in Yosemite burned almost exclusively at low severity, likely due to the short needles of *A. concolor* that form compact litter and resist ignition (Thode et al. 2011) and the controlled severity of prescribed fires. A report of area burned by forest type and fire severity is lacking for Sequoia.

Less frequent fire characterized upper montane forests where longer periods of snowpack retention reduced the likelihood of ignition despite the higher density of lightning strikes (van

Wagtendonk and Fites-Kaufman 2006). Estimates of historical upper montane median FRI range from 12 to 69 years (van Wagtendonk and Fites-Kaufman 2006). Although high fuel moisture generally maintained a low-severity regime, where high-severity fire did occur in *A. magnifica* stands, patches of montane chaparral often colonized the area within five years; theoretically, conifers would eventually overtop the shrubs, reinstating conifer prevalence (Thode et al. 2011). Across Yosemite, between 1984 and 2003, 23.4% of the area occupied by *A. magnifica* stands and 28.0% of the area occupied by *P. jeffreyi*-shrub stands burned mostly at low to moderate severity; 3.7% of the area occupied by *P. contorta* stands burned at mostly low severity (Thode et al. 2011).

METHODS

Site selection and sampling design

I used a geographic information system to select plot locations based on forest type (Keeler-Wolf et al. 2012**;** Sequoia and Kings Canyon National Parks Photo Interpretation Report 2007); burn status; fire severity; representativeness of area; slope; and distance from streams, roads, and trails. Plots were at least 50 m within the intended forest type and burned or unburned patch; had slopes between 0° and 35°; and were at least 100 m from streams, roads, and trails. In the field we assessed the forest type and burn status and relocated plots to better meet specifications if necessary. I sought balanced representation of burned and unburned forests dominated by *P. ponderosa, A. concolor, P. jeffreyi,* and *A. magnifica.* Collection of data from burned sites in forests dominated by *P. contorta* was prioritized due to the availability of similar data collected in 2010 from unburned stands of *P. contorta* in Sequoia.

Data acquisition

Between June and September of 2011 I worked with a field crew to establish 105, 0.1 ha circular plots, 46 that had not burned since at least 1930 (hereafter, unburned; Yosemite: 35 plots; Sequoia: 11 plots; Figure 1.1) and 59 that had burned between one and five times since 1930 (hereafter, burned; Yosemite: 32 plots; Sequoia: 27 plots). A GPS set to the datum NAD83 determined the UTM coordinates at plot center. To characterize species composition and forest structure we recorded species and diameter at breast height (1.37 m; dbh) of all live trees and snags >15.0 cm dbh. Stems with dbh between 2.5 cm and 15.0 cm were recorded in at least one quadrant of every plot. To assign plots to forest alliances and associations, we ocularly estimated percent canopy cover by species and percent shrub cover by species that occupied ≥2.5 m^2.

Mean potential evapotranspiration (PET), actual evapotranspiration (AET), and climatic water deficit (Deficit) from 1980 to 2010 were calculated for each plot based on the Thornthwaite-type methods of Lutz et al. (2010), with some modifications. Inputs included latitude; number of days per month; soil water-holding capacity in the top 150 cm of soil; PRISM-generated monthly temperature and precipitation; slope; aspect; and derived values for monthly melt factor, average monthly day length, and saturation vapor pressure at mean monthly temperature. Because high resolution soil data were unavailable for Sequoia, I used the importance values of tree species (Equation 1; Scholl and Taylor 2010; Parker 1984; Curtis and McIntosh 1951) at each Sequoia plot and the mean soil water-holding capacity associated with each tree species across its range in Yosemite (Lutz et al. 2010) to calculate a weighted average of soil water-holding capacity for each Sequoia plot.

Equation 1. Species importance value represents the sum of the relative basal area (BA) and relative density (Density) of a species at a plot.

$$\text{Importance value} = (BA_{sp})/(BA_{plot})+(Density_{sp})/(Density_{plot})$$

The fire history of each plot was expressed in number of fires since 1930 and severity of the most recent fire. These data were obtained from the Yosemite fire atlas compiled by Lutz et al. (2011) and the Monitoring Trends in Burn Severity (MTBS) database (Eidenshink et al. 2007). The spatial record of fire history in Yosemite extends to 1930, thus defining the temporal threshold for unburned plots in this study. The spatial record of fire history in Sequoia extends to 1921, maintaining the validity of the 1930 threshold for unburned plots.

I used the Relative differenced Normalized Burn Ratio (RdNBR), a satellite-derived metric developed by Miller and Thode (2007), to characterize fire severity (Table 1.2). RdNBR data were available for fires that occurred in 1984 or later and were >40 ha in Yosemite and >400 ha in Sequoia. I created 1 ha circular buffers around each plot and extracted all 30 m × 30

m RdNBR pixels with centers that fell within each buffer. The pixel values associated with each plot were averaged to obtain RdNBR values that minimized the potential effects of georectification error (Kolden et al. 2012; Key and Benson 2006).

Table 1.2. Fire severity thresholds for the Relative differenced Normalized Burn Ratio (RdNBR; Miller and Thode 2007). Landsat-undifferentiated fire severity refers to areas within fire perimeters with RdNBR values that do not differ from adjacent unburned areas (Kolden et al. 2012). Plots are categorized by RdNBR of the most recent fire.

Fire severity	Number of plots	RdNBR
Undifferentiated	8	<69
Low	30	69-315
Moderate	13	316-640
High	--	>640

Data reduction

All unburned plots and the 51 burned sites with RdNBR values <641 (i.e., undifferentiated to moderate severity) for the most recent fire were retained for analysis (97 plots: 46 unburned, 28 burned once, 16 burned twice, 6 burned thrice, and 1 burned four times). I used the percent canopy and shrub cover data to assign each plot to a forest alliance and association based on park-specific vegetation community identification keys (Yosemite: Keeler-Wolf et al. 2012**;** Sequoia: Sequoia and Kings Canyon National Parks Photo Interpretation Report 2007).

I classified the stems of each species by their diameter into nine 15 cm bins (Table 1.3). I further stratified the data into four categories by mortality status (live tree vs. snag) and burn status (burned plot vs. unburned plot). Slope-corrected basal area and stem density were calculated for each diameter class at each plot.

Table 1.3. Diameter class bins.

Diameter class	Diameter range (cm)
DC1	2.5 – 15.0
DC2	15.1 – 30.0
DC3	30.1 – 45.0
DC4	45.1 – 60.0
DC5	60.1 – 75.0
DC6	75.1 – 90.0
DC7	90.1 – 105.0
DC8	105.1 – 120.0
DC9	>120.0

Ordination

I analyzed species composition with nonmetric multidimensional scaling (NMDS) ordination. A species composition matrix of plot (row) by species (column) was populated with values of basal area. I standardized by the total basal area of each plot, removing differences in total basal area among plots. Site positions in ordination space therefore reflect the proportional contribution of each species to plot basal area (hereafter, relative basal area).

NMDS ordination uses a distance measure to translate the similarities between plots into theoretical distances, which are the basis for the rank ordering of plots. The procedure seeks to preserve this order by placing similar plots closer to one another and dissimilar plots further apart in ordination space. NMDS ordination is an iterative process. After each run, the actual distances between plots in the ordination space are compared to the theoretical distances between plots as calculated by the distance measure. When the differences between the actual and theoretical distances are minimized, the "stress" of the ordination is, by definition, also minimized. I used the Bray-Curtis dissimilarity measure and 200 random reruns to ordinate data along two axes. The Bray-Curtis dissimilarity is a robust semi-metric distance measure that is appropriate for multivariate species data; when abundance data are previously standardized by row totals, the plot rankings that are indicated by Bray-Curtis dissimilarity strongly correlate

with those of Euclidean distance in ecological space (Faith et al. 1987). Ordination was executed in the R statistical language (version 3.0.2; R Development Core Team, 2013) with the function "metaMDS" from the vegan package (version 2.0-10; Oksanen et al. 2013).

I depicted correlations between compositional and biophysical gradients by coloring plots in ordination space by elevation, PET, AET, and Deficit. Because modeled values of PET, AET, and Deficit for plots in Sequoia were calculated with compositionally based estimates of soil water-holding capacity, only plots from Yosemite were included in this analysis.

Diameter distributions

Diameter distributions depicting the distribution of live tree and snag density and basal area were generated for the seven most common species. Burned and unburned plots were represented separately to expose potential effects of fire on species' demography. For each species Mann-Whitney *U* tests were performed on each diameter class to identify significant differences between burned and unburned populations. To support the assumption that differences between burned and unburned populations were attributable to recent fire occurrence I compared the distribution of elevation, slope, aspect, AET, and Deficit of the burned and unburned plots that contained the species in question (Mann-Whitney *U* test; $\alpha = 0.05$). No significant differences in these physical site attributes were detected, except for plots that included *P. jeffreyi*, where slopes differed ($p = 0.04$) between burned and unburned plots ($\mu_{burned} = 10°$; $\mu_{unburned} = 15°$). The validity of attributing differences between the burned and unburned populations to recent fire occurrence was further based on the assumption that the burned and unburned samples represented a similar range of historical (i.e., pre-1890) disturbance patterns.

RESULTS

Six forest alliances and 19 forest associations were sampled (Table 1.4). Fifteen forest associations were represented among unburned sites (46 plots), which ranged in elevation from 1,377 m to 2,645 m; burned sites (51 plots) represented 13 forest alliances and ranged in elevation from 1,338 m to 2,705 m (Table 1.5). Ranges of climatic water balance parameters were approximately equivalent between burned and unburned plots ($AET_{unburned}$ = 211-453 mm; AET_{burned} = 212-422 mm; $Deficit_{unburned}$ = 107-330 mm; $Deficit_{burned}$ = 72-361 mm; Figure 1.2).

Burned plots represented sites that had experienced fire between one and four times since 1946 (Figure 1.3). Ten locations had RdNBR records for the two most recent fires. In eight of these instances the more recent fire burned at higher severity; in all 10 instances the later fire year was ranked above the 25^{th} percentile when compared with Yosemite fire normals (Lutz et al. 2011), either maintaining or exceeding the percentile ranking of the year of the previous fire (Table 1.6).

Table 1.4. Frequency of forest alliances and forest associations among 97 plots located in lower and upper montane forests of Yosemite and Sequoia & Kings Canyon National Parks.

Codes	Forest Alliance	Forest Association	Frequency of Occurrence
1	*Abies concolor-Pinus lambertiana*		**26**
1		*Abies concolor-Pinus lambertiana*	2
2		*Abies concolor-Pinus lambertiana-Calocedrus decurrens*†	21
3		*Abies concolor-Pinus lambertiana-Pinus jeffreyi*	3
2	*Abies magnifica*		**11**
4		*Abies magnifica*	4
5		*Abies magnifica-Pinus contorta*	1
6		*Abies magnifica-Pinus monticola*	3
7		*Abies magnifica-Pinus monticola-Pinus contorta*	3
3	*Abies magnifica-Abies concolor*		**11**
8		*Abies concolor-Pinus lambertiana-Abies magnifica*	1
9		*Abies magnifica-Abies concolor*	9
10		*Abies magnifica-Abies concolor-Pinus jeffreyi*	1
4	*Pinus contorta*		**7**
11		*Pinus contorta woodland*	5
12		*Pinus contorta xeric superassociation*†	2
5	*Pinus jeffreyi woodland*		**23**
13		*Juniperus occidentalis woodland*	2
14		*Pinus jeffreyi-Abies concolor*	9
15		*Pinus jeffreyi-Abies magnifica*	1
16		*Pinus jeffreyi-Quercus chrysolepis*	1
17		*Pinus jeffreyi woodland*†	10
6	*Pinus ponderosa-Calocedrus decurrens*		**19**
18		*Pinus ponderosa-Calocedrus decurrens/Chamaebatia*	16
19		*Pinus ponderosa-Calocedrus decurrens-Quercus kelloggii*	3

†Absence of shrubs and lack of herb data precluded assigning some sites to associations.

Table 1.5. Attributes of forest alliances and associations of 97 plots located in lower and upper montane forests of Yosemite and Sequoia & Kings Canyon National Parks.

Alliance Assoc.	Number of fires					RdNBR of most recent fire mean (range)	Elevation (m) mean (range)		Slope (°) mean (range)		Aspect (°) mean (range)	
	0	1	2	3	4		Unburned	Burned	Unburned	Burned	Unburned	Burned
1	**15**	**8**	**2**	**1**	**0**	**213 (-10-481)**	**1,707 (1,460-1,895)**	**1,855 (1,610-2,115)**	**14 (4-22)**	**13 (4-34)**	**225 (10-359)**	**183 (0-330)**
1	2	0	0	0	0	--	1,850 (1,810-1,890)	--	8 (4-12)	--	203 (176-230)	--
2	13	7	0	1	0	187 (-10-412)	1,684 (1,460-1,895)	1,782 (1,610-2,000)	15 (4-22)	14 (4-34)	229 (10-359)	224 (0-330)
3	0	1	2	0	0	282 (176-481)	--	2,049 (2,012-2,115)	--	10 (4-12)	--	72 (45-122)
2	**8**	**3**	**0**	**0**	**0**	**79 (-10-142)**	**2,477 (2,045-2,645)**	**2,590 (2,525-2,705)**	**13 (5-29)**	**13 (9-20)**	**213 (27-348)**	**218 (23-332)**
4	4	0	0	0	0	--	2,399 (2,045-2,645)	--	14 (5-29)	--	230 (27-331)	--
5	1	0	0	0	0	--	2,382	--	17	--	56	--
6	1	2	0	0	0	124 (105-142)	2,600	2,532 (2,525-2,540)	14	15 (10-20)	348	178 (23-332)
7	2	1	0	0	0	-10	2,621 (2,607-2,635)	2,705	8 (6-9)	9	191 (63-319)	298
3	**4**	**4**	**3**	**0**	**0**	**191 (126-279)**	**2,176 (1,880-2,335)**	**2,358 (2,030-2,545)**	**16 (9-23)**	**17 (8-27)**	**180 (0-276)**	**190 (28-327)**
8	1	0	0	0	0	--	1,880	--	15	--	270	--
9	2	4	3	0	0	191 (126-279)	2,245 (2,200-2,290)	2,358 (2,030-2,545)	12 (9-16)	17 (8-27)	225 (174-276)	190 (28-327)
10	1	0	0	0	0	--	2,335	--	23	--	0	--
4	**1**	**4**	**2**	**0**	**0**	**179 (19-444)**	**2,550**	**2,481 (2,180-2,680)**	**11**	**9 (1-13)**	**50**	**183 (54-340)**
11	1	4	0	0	0	117 (19-174)	2,550	2,621 (2,550-2,680)	11	11 (9-13)	50	181 (90-340)
12	0	0	2	0	0	302 (160-444)	--	2,200 (2,180-2,220)	--	6 (1-11)	--	187 (54-320)
5	**9**	**5**	**5**	**4**	**0**	**288 (-174-548)**	**2,242 (1,770-2,490)**	**2,099 (1,580-2,490)**	**14 (4-24)**	**10 (0-29)**	**222 (140-277)**	**212 (12-333)**
13	2	0	0	0	0	--	2,138 (1,905-2,372)	--	12 (12-13)	--	203 (140-266)	--
14	3	3	2	1	0	315 (95-535)	2,340 (2,245-2,490)	2,282 (2,000-2,490)	24 (23-24)	15 (7-29)	244 (194-277)	252 (191-333)
15	0	0	1	0	0	164	--	2,360	--	10	--	105
16	0	1	0	0	0	480	--	1,595	--	15	--	210
17	4	1	2	3	0	249 (-174-548)	2,219 (1,770-2,389)	1,955 (1,580-2,390)	8 (4-10)	6 (0-12)	215 (160-277)	190 (12-300)
6	**9**	**4**	**4**	**1**	**1**	**207 (45-400)**	**1,606 (1,377-1,775)**	**1,628 (1,338-2,010)**	**11 (5-23)**	**14 (4-25)**	**225 (115-356)**	**185 (0-292)**
18	8	4	3	0	1	208 (45-400)	1,605 (1,377-1,775)	1,584 (1,338-1,790)	12 (5-23)	14 (4-25)	235 (115-356)	208 (110-292)
19	1	0	1	1	0	203 (178-228)	1,620	1,805 (1,600-2,010)	5	14 (11-18)	146	92 (0-184)

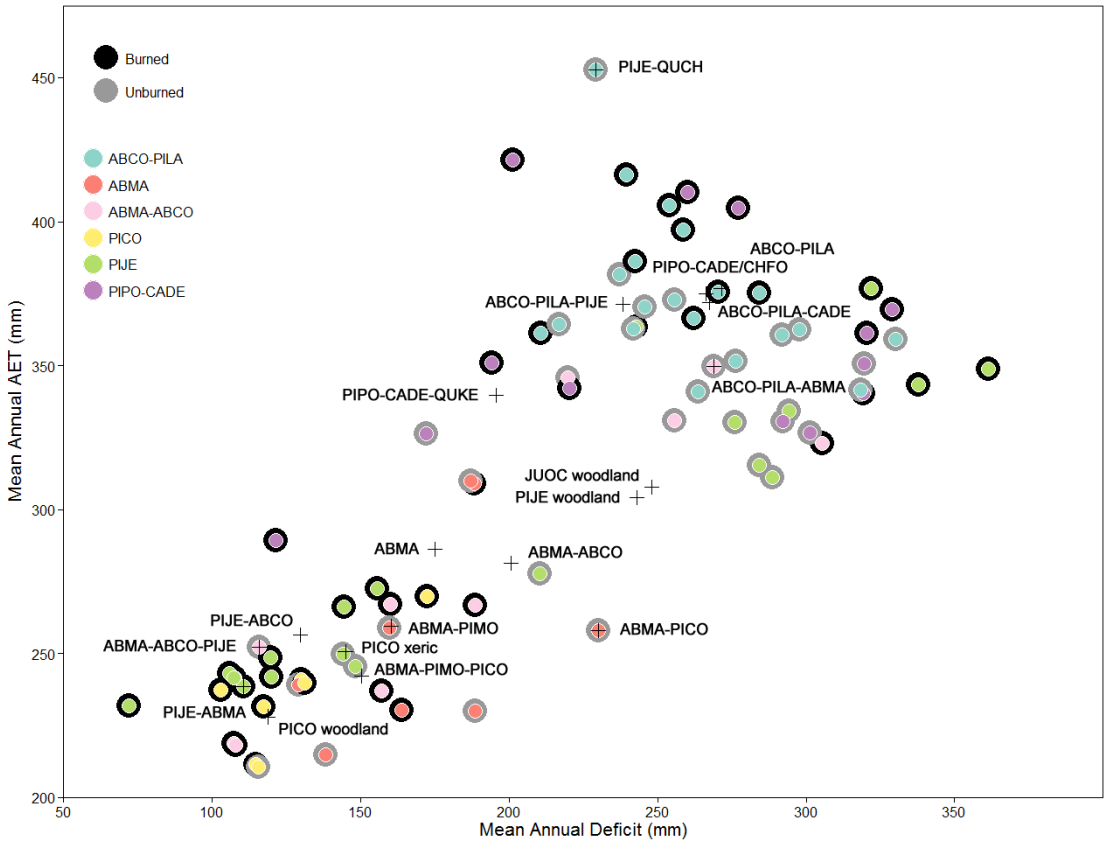

Figure 1.2. Distribution by AET and Deficit of 97 plots located in lower and upper montane forests of Yosemite and Sequoia & Kings Canyon National Parks. Unburned plots have not experienced fire since at least 1930; burned plots have experienced fire between one and four times since 1946. Six forest alliances and 19 forest associations are represented (Table 1.4). Four letter species codes are defined in Table A.1 of Appendix I.

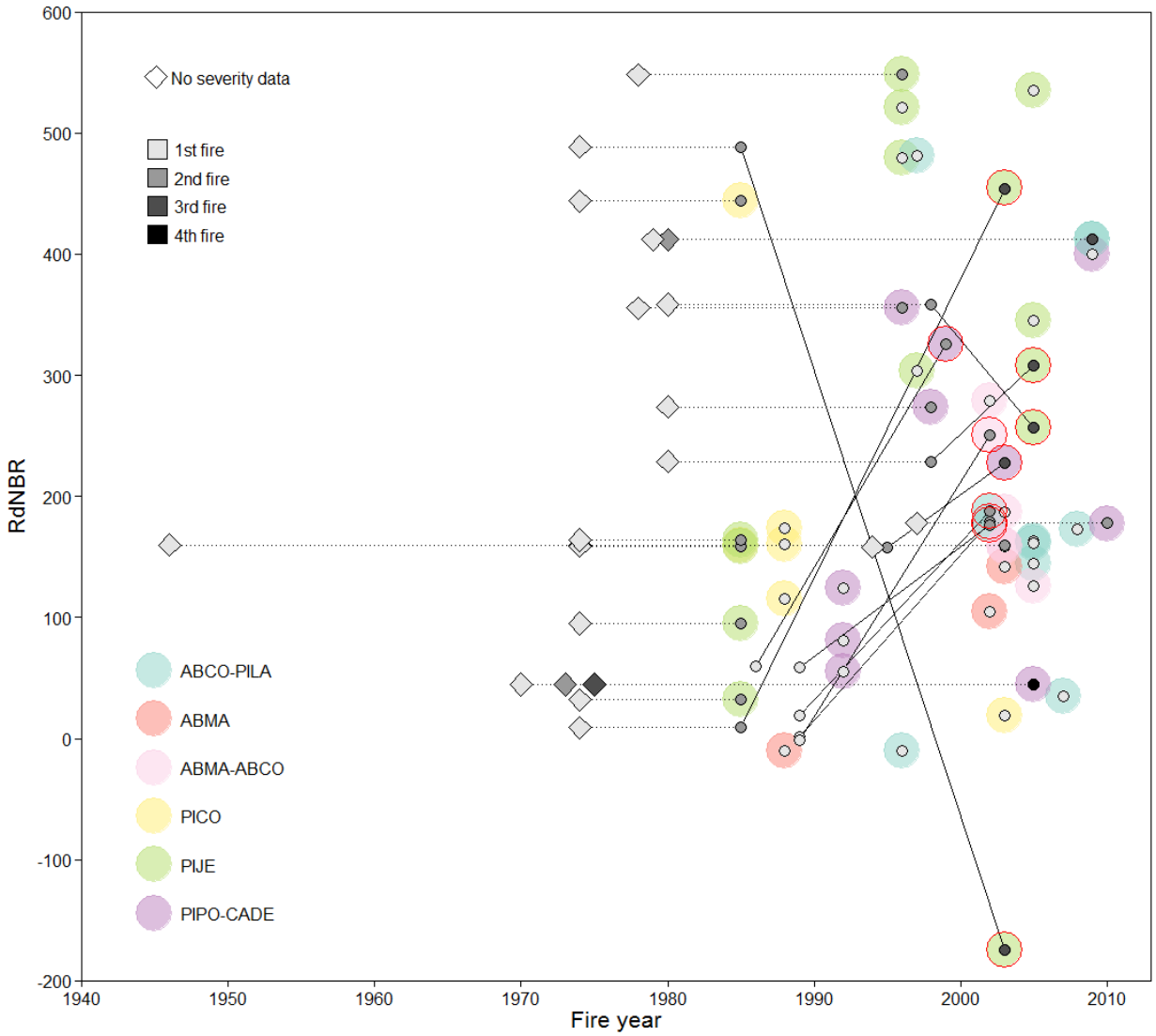

Figure 1.3. Fire history decomposed into fire year and severity as indicated by the satellite-derived Relative differenced Normalized Burn Ratio (RdNBR) for 51 plots from lower and upper montane forests in Yosemite and Sequoia & Kings Canyon National Parks. RdNBR data were available for fire events in and after 1984 that were >40 ha in Yosemite National Park and >400 ha in Sequoia & Kings Canyon National Park. Lines connect fires that occurred at the same plot. Solid lines indicate that RdNBR data were available for the fires at both endpoints of the line segment; red circles indicate the most recent fire event in these pairs. Dotted lines indicate that RdNBR data were not available for at least one of the fires at the endpoints of the line segment. Six forest alliances are represented (Table 1.4). Four letter species codes are defined in Table A.1 of Appendix I.

Table 1.6. Attributes of 10 plots located in lower and upper montane forests of Yosemite (Yosemite) and Sequoia & Kings Canyon (Sequoia) National Parks with two satellite-derived Relative differenced Normalized Burn Ratio (RdNBR) fire severity records. Four letter species codes are defined in Table A.1 of Appendix I. Letters following fire year, RdNBR, and fire size values indicate, respectively, whether the number of fires, RdNBR, or fire size associated with that year fell in the upper quartile (H), the middle two quartiles (M), or the lower quartile (L) of fire normals data developed from 26 years of Yosemite fire history (Lutz et al. 2011). Data associated with the eight plots where the more recent fire was of higher severity are bolded. Coincidentally, the Yosemite sites were burned twice, and the Sequoia sites were burned 3 times; in both cases these data represent the two most recent events.

	P061	**P062**	**P068**	**P087**	**P088**	**P148**	P168	**P170**	**P195**	P251
Park	**Yosemite**	**Yosemite**	**Yosemite**	**Yosemite**	**Yosemite**	**Sequoia**	Sequoia	**Sequoia**	**Sequoia**	Sequoia
Alliance	**ABMA-ABCO**	**ABMA-ABCO**	**PIPO-CADE**	**ABCO-PILA**	**ABCO-PILA**	**PIPO-CADE**	PIJE	**PIJE**	**PIJE**	PIJE
Association	**ABMA-ABCO**	**ABMA-ABCO**	**PIPO-CADE/ CHFO**	**ABCO-PILA-PIJE**	**ABCO-PILA-PIJE**	**PIPO-CADE-QUKE**	PIJE woodland	**PIJE woodland**	**PIJE-ABCO**	PIJE woodland
Attributes										
Elevation	**2,030**	**2,030**	**1,750**	**2,012**	**2,021**	**2,010**	1,960	**1,985**	**2,355**	2,390
Slope	**20**	**19**	**6**	**12**	**5**	**11**	12	**6**	**7**	6
Aspect	**NW**	**NE**	**SW**	**NE**	**NE**	**S**	SW	**S**	**S**	S
AET	**323**	**323**	**410**	**386**	**366**	**351**	266	**266**	**243**	242
DEF	**305**	**305**	**260**	**242**	**262**	**194**	144	**144**	**106**	107
Previous fire										
Year	**1989 L**	**1989 L**	**1986 M**	**1989 L**	**1989 L**	**1995 L**	1998 L	**1998 L**	**1985 H**	1985 H
RdNBR	**1 L**	**-1 L**	**60 M**	**19 L**	**59 L**	**158 M**	358 L	**229 L**	**9 M**	489 M
Size (ha)	**688 L**	**688 L**	**584 M**	**688 L**	**688 L**	**843 L**	645 L	**645 L**	**1,152 M**	1,152 M
Cause	**MI**	**MI**	**LTG**	**MI**	**MI**	**MI**	MI	**MI**	**LTG**	LTG
Name	**Pw3**	**Pw3**	**Eleanor**	**Pw3**	**Pw3**	**Mineral 1**	Lewis Creek	**Lewis Creek**	**Sugarloaf**	Sugarloaf
Recent fire										
Year	**2002 M**	**2002 M**	**1999 H**	**2002 M**	**2002 M**	**2003 H**	2005 H	**2005 H**	**2003 H**	2003 H
RdNBR	**179 M**	**251 M**	**326 M**	**188 M**	**176 M**	**228 H**	257 M	**308 M**	**454 H**	-174 H
Size (ha)	**1,360 M**	**1,360 M**	**1,042 H**	**1,360 M**	**1,360 M**	**1,098 H**	3,947 M	**3,947 M**	**14,05 H**	1,405 H
Cause	**MI**	**MI**	**LTG**	**MI**	**MI**	**MI**	LTG	**LTG**	**LTG**	LTG
Name	**PW-3 Gin Flat**	**PW-3 Gin Flat**	**Eleanor**	**PW-3 Gin Flat**	**PW-3 Gin Flat**	**Atwood**	Comb	**Comb**	**Williams**	Williams

Species composition

NMDS ordination of the relative basal area attributed to 14 tree species revealed a gradient relationship along NMDS axis 1 from the lower montane species of *P. ponderosa*, *Pseudotsuga menziesii* (Mirb.) Franco, *Q. kelloggii*, and *C. decurrens* to the upper montane species of *T. mertensiana*, *P. monticola*, and *P. contorta* (Figure 1.4). *Pinus lambertiana*, *A. concolor*, *Cornus nuttallii* Audubon ex Torr. & A. Gray, and *A. magnifica* were located midway along NMDS axis 1 but associated with lower values of NMDS axis 2; *P. jeffreyi*, *Juniperus occidentalis* Hook., and *Quercus chrysolepis* Liebm., which were also located midway along NMDS axis 1, were associated with higher values of NMDS axis 2. The *A. concolor* centroid was centrally located, marking the convergence of four forest alliances, *P. ponderosa-C. decurrens*, *A. concolor-P. lambertiana*, *A. magnifica-A. concolor*, and *P. jeffreyi*, and reflecting that live individuals of *A. concolor* were present in more plots (63) than any other species (Figure 1.4 A; Table 1.7). High tree density was associated with the *P. ponderosa-C. decurrens*, *A. concolor-P. lambertiana*, and *P. contorta* alliances (Figure 1.4 C). High basal area characterized *A. concolor-P. lambertiana*, *A. magnifica-A. concolor*, and *A. magnifica* forests as well as and some members of the *P. ponderosa-C. decurrens* alliance (Figure 1.4 E). Both burned and unburned plots spanned the full compositional gradient (Figure 1.4 B). The *A. magnifica* and *P. contorta* alliances were exclusively associated with single fires of low or undifferentiated severity (Figure 1.4 D and F). The remaining alliances represented the full spectrum of number of fires (1 to 4) and RdNBR (undifferentiated to moderate; Figure 1.4 D and F).

Thoroughly sampled species were represented near both the modes and extremes of their ranges (Table 1.7). Live trees of *A. magnifica*, *P. jeffreyi*, *P. contorta*, *A. concolor*, and *P.*

ponderosa were present in >15 plots and made the largest mean, median, and maximum contributions to relative basal area and the largest maximum contributions to relative density (Table 1.7); *A. magnifica*, *P. jeffreyi*, *P. contorta,* and *A. concolor* made the largest mean and median contributions to relative density. Concurrently, however, minimum density and basal area of these species could have been no lower; indeed, all species with live trees in >4 plots exhibited minimum density of 10 trees ha^{-1} (i.e., 1 tree $plot^{-1}$).

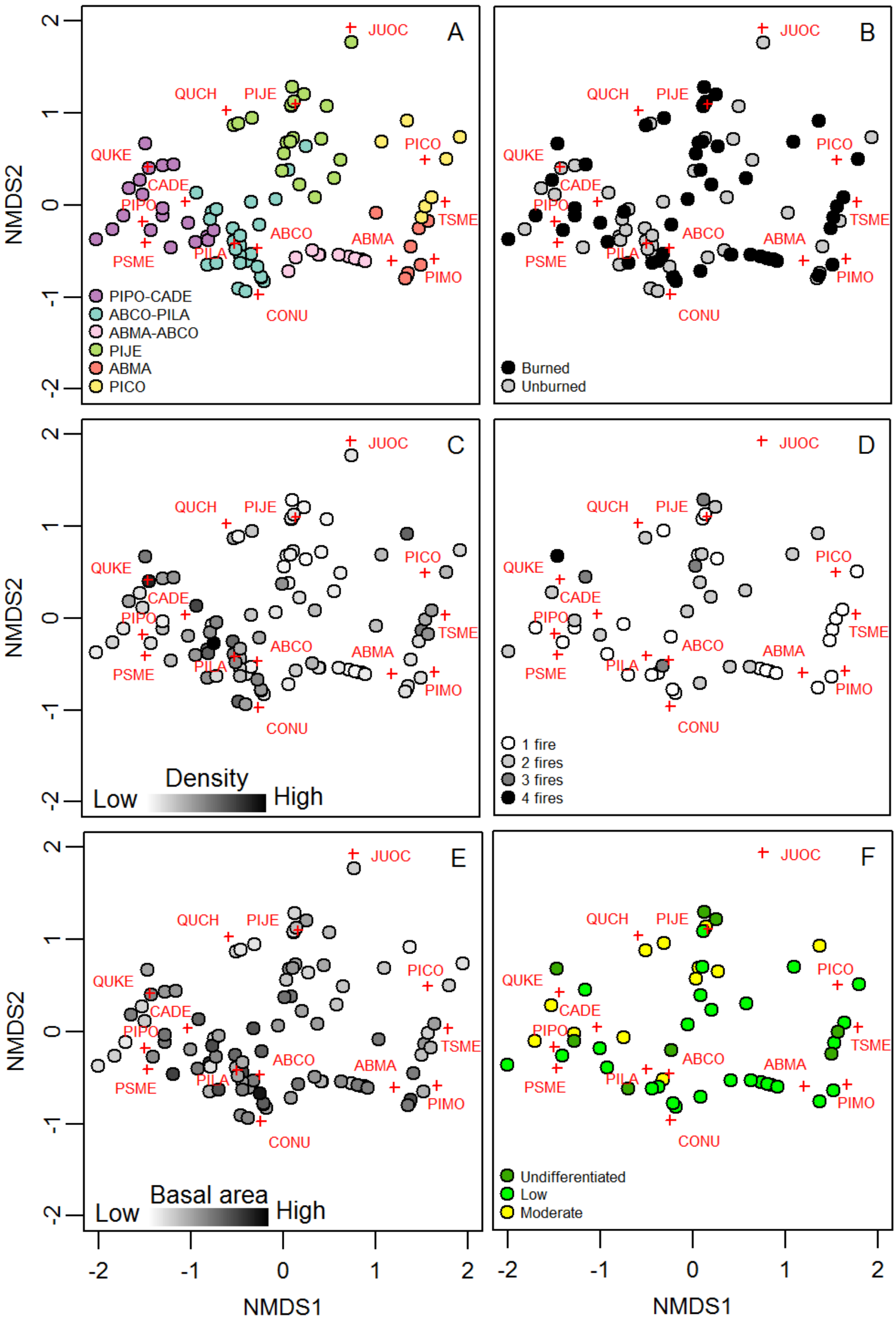

Figure 1.4. Distribution of forest alliances, burned and unburned plots, total tree density, total basal area, number of fires, and fire severity across an NMDS ordination (stress = 0.120) of the relative basal area attributed to each of 14 tree species in 97 plots located in lower and upper montane forests of Yosemite and Sequoia & Kings Canyon National Parks. Plots are colored by forest alliance (A) and burn status (B). Total density and total basal area of each plot are represented by a linear color gradient from white to black (C and E). Total density ranged from 30 to 2,082 trees ha^{-1}; total basal area ranged from 4.29 to 134.56 m^2 ha^{-1}. Plots are colored by number of fires since 1946 and RdNBR of the most recent fire (D and F). Four letter species codes are defined in Table A.1 of Appendix I.

Table 1.7. Proportional contributions of 14 tree species to the relative basal area and relative tree density of plots that include that species. Species are ordered by maxima. Abundance mean and range values were determined using only plots that contained ≥1 live tree of that species.

Species	Abundance			Median	Mean	Max.
Basal area (m^2 ha^{-1})	mean (range)		Plots			
A. magnifica	35.5	(0.6-115.7)	34	0.51	0.54	1.00
P. jeffreyi	22.1	(0.7-66.7)	33	0.60	0.56	1.00
P. contorta	14.7	(2.4-29.7)	16	0.32	0.42	0.97
A. concolor	22.7	(<0.1-95.1)	63	0.30	0.35	0.96
P. ponderosa	16.3	(0.6-42.1)	28	0.32	0.33	0.91
J. occidentalis	7.6	(2.6-21.8)	4	0.08	0.25	0.75
P. lambertiana	12.7	(<0.1-46.9)	36	0.11	0.19	0.68
C. decurrens	14.6	(0.4-54.9)	44	0.22	0.25	0.67
Q. kelloggii	7.0	(0.1-27.3)	17	0.06	0.12	0.54
P. monticola	5.8	(0.1-13.6)	7	0.08	0.12	0.31
T. mertensiana	3.9	(2.2-5.6)	2	0.07	0.07	0.10
P. menziesii	2.8	(0.5-5.2)	2	0.05	0.05	0.08
Q. chrysolepis	0.1	(0.1-0.2)	2	0.01	0.01	0.01
C. nuttallii	0.2	--	1	<0.01	<0.01	<0.01
Tree density (trees ha^{-1})	mean (range)		Plots			
A. magnifica	184	(10-722)	34	0.50	0.52	1.00
P. jeffreyi	77	(10-259)	33	0.43	0.44	1.00
P. contorta	326	(10-1210)	16	0.44	0.50	0.97
A. concolor	254	(10-952)	63	0.39	0.43	0.96
P. ponderosa	124	(10-870)	28	0.09	0.21	0.95
J. occidentalis	82	(30-225)	4	0.22	0.37	0.92
Q. kelloggii	117	(10-610)	17	0.06	0.16	0.91
C. decurrens	249	(10-1149)	44	0.30	0.31	0.81
P. lambertiana	73	(10-468)	36	0.07	0.12	0.43
Q. chrysolepis	88	(10-166)	2	0.18	0.18	0.35
P. monticola	36	(10-101)	7	0.11	0.10	0.17
T. mertensiana	106	(70-142)	2	0.12	0.12	0.17
P. menziesii	22	(11-32)	2	0.06	0.06	0.11
C. nuttallii	43	--	1	0.05	0.05	0.05

Biophysical variables

Elevation, PET, AET, and Deficit correlated with species compositional gradients as represented by ordination of relative basal area (Figure 1.5). Elevation increased along NMDS axis 1. The centroids of *P. ponderosa*, *C. decurrens*, *P. lambertiana*, and *A. concolor* were surrounded by lower elevation sites. *Pinus jeffreyi* was associated with mid-elevation sites, and *A. magnifica* and *P. contorta* were associated with high elevation sites (Figure 1.5 A). This pattern was reversed by PET (Figure 1.5 B). *A. magnifica*, *T. mertensiana*, *P. monticola*, and *P. contorta* were associated with low PET, while *P. ponderosa*, *C. decurrens*, *P. lambertiana*, and *A. concolor* were associated with high PET. *Pinus jeffreyi* was prevalent at some sites with low PET and others with high PET. Sites with low PET were generally characterized by both low AET and low Deficit (Figure 1.5 C and D). Two sites near the *P. contorta* centroid, however, exhibited moderately low PET that represented the sum of midrange AET and low Deficit. The most pronounced difference between elevation and biophysical variables manifested in the *A. magnifica-A. concolor* alliance. These sites were characterized by high elevation but also relatively high PET, AET, and Deficit.

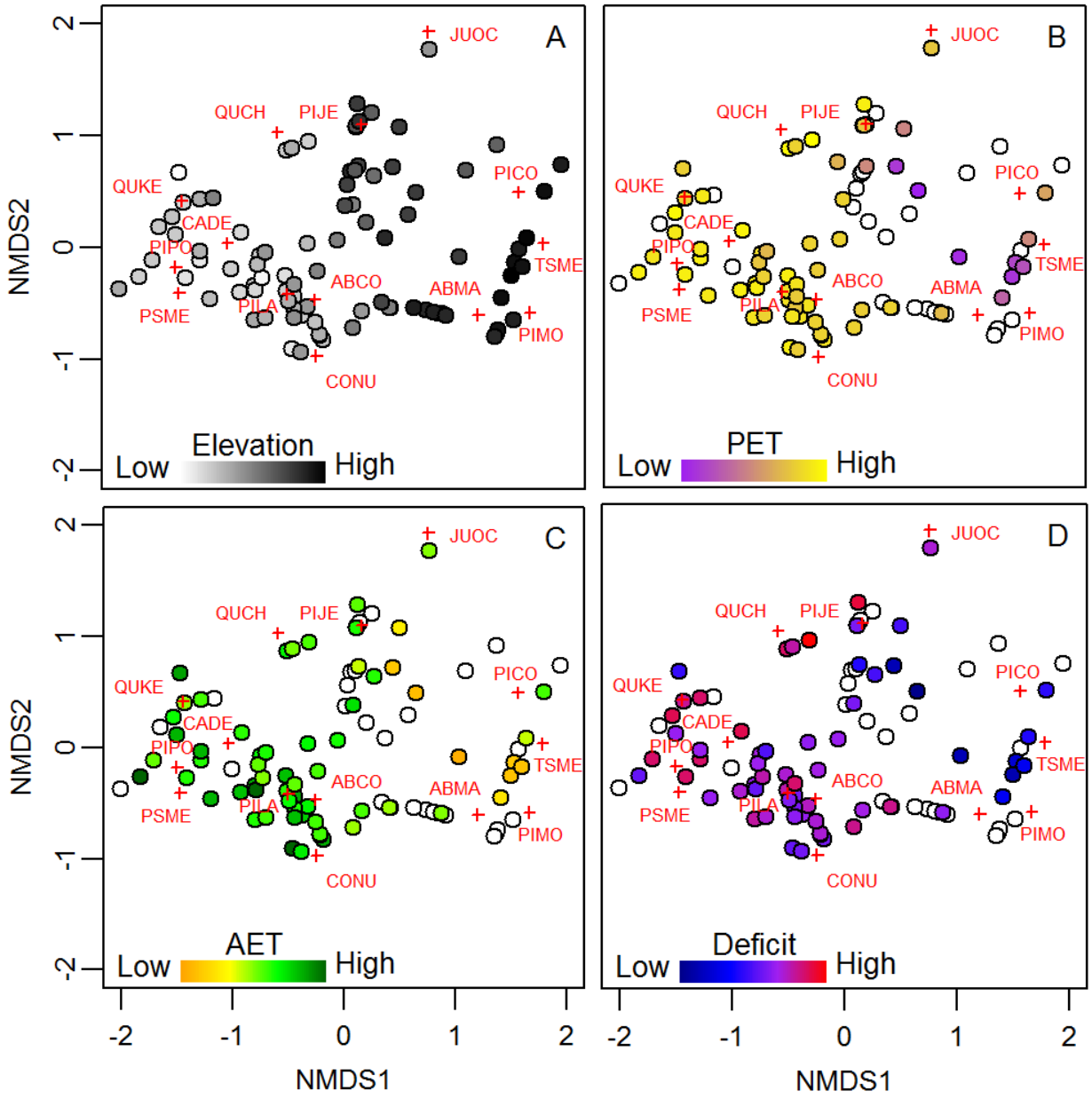

Figure 1.5. Distribution of elevation, PET, AET, and Deficit across an NMDS ordination (stress = 0.120) of relative basal area attributed to each of 14 tree species in 97 plots located in lower and upper montane forests of Yosemite and Sequoia & Kings Canyon National Parks. Linear color gradients represent the relative values of elevation, PET, AET, and Deficit associated with each plot. PET, AET, and Deficit are only shown for plots from Yosemite; plots from Sequoia are represented by white circles. Elevation ranged from 1,338 to 2,705 m; PET ranged from 304 to 710 mm; AET ranged from 211 to 453 mm; Deficit ranged from 72 to 361 mm. Four letter species codes are defined in Table A.1 of Appendix I.

Diameter distributions

Diameter distributions were developed for the seven most prevalent conifer species: *A. concolor*, *A. magnifica*, *C. decurrens*, *P. contorta*, *P. jeffreyi*, *P. lambertiana*, and *P. ponderosa* (Figures 1.6 and 1.7). Median density by diameter class for three species, *A. concolor*, *A. magnifica*, and *C. decurrens*, exhibited a reverse-J distribution among unburned plots (Figures 1.6.a, 1.6.b, and 1.6.c). These species exhibited such low density of trees <15.0 cm dbh among burned plots, however, that the reverse-J shape was severely truncated. *P. contorta* represented a counter example to this pattern, exhibiting a reverse-J distribution among burned plots and low density of trees <15.0 cm dbh among unburned plots (Figure 1.7.d). In contrast, the distribution of *P. ponderosa*, *P. lambertiana*, and *P. jeffreyi* was relatively uniform among both burned and unburned plots (Figures 1.7.a, 1.7.b, and 1.7.c).

Diameter distributions of basal area highlighted variability in the larger diameter classes among species (Figures 1.6 and 1.7). *Abies magnifica* had the most consistent representation of the larger diameter classes and was associated with the maximum basal area attributed to one species in a single diameter class (DC7 50.54 m^2 ha^{-1}). *Pinus jeffreyi*, followed by *P. ponderosa* and *A. concolor*, were also characterized by large-diameter trees at a large proportion of plots. *Calocedrus decurrens* and *P. lambertiana* included some outlier plots with high basal area in the larger diameter classes, but as subdominant species, a smaller proportion of plots included individuals that belonged to multiple large diameter classes. *Pinus contorta* expressed the lowest basal area and contained no individuals >90.0 cm dbh.

Burned and unburned populations of density and basal area differed for *A. concolor* (DC1, DC2, and DC3), *A. magnifica* (DC1 and DC2), and *C. decurrens* (DC1; p <0.03; Table 1.8). No *Pinus* spp. exhibited significant differences between burned and unburned populations.

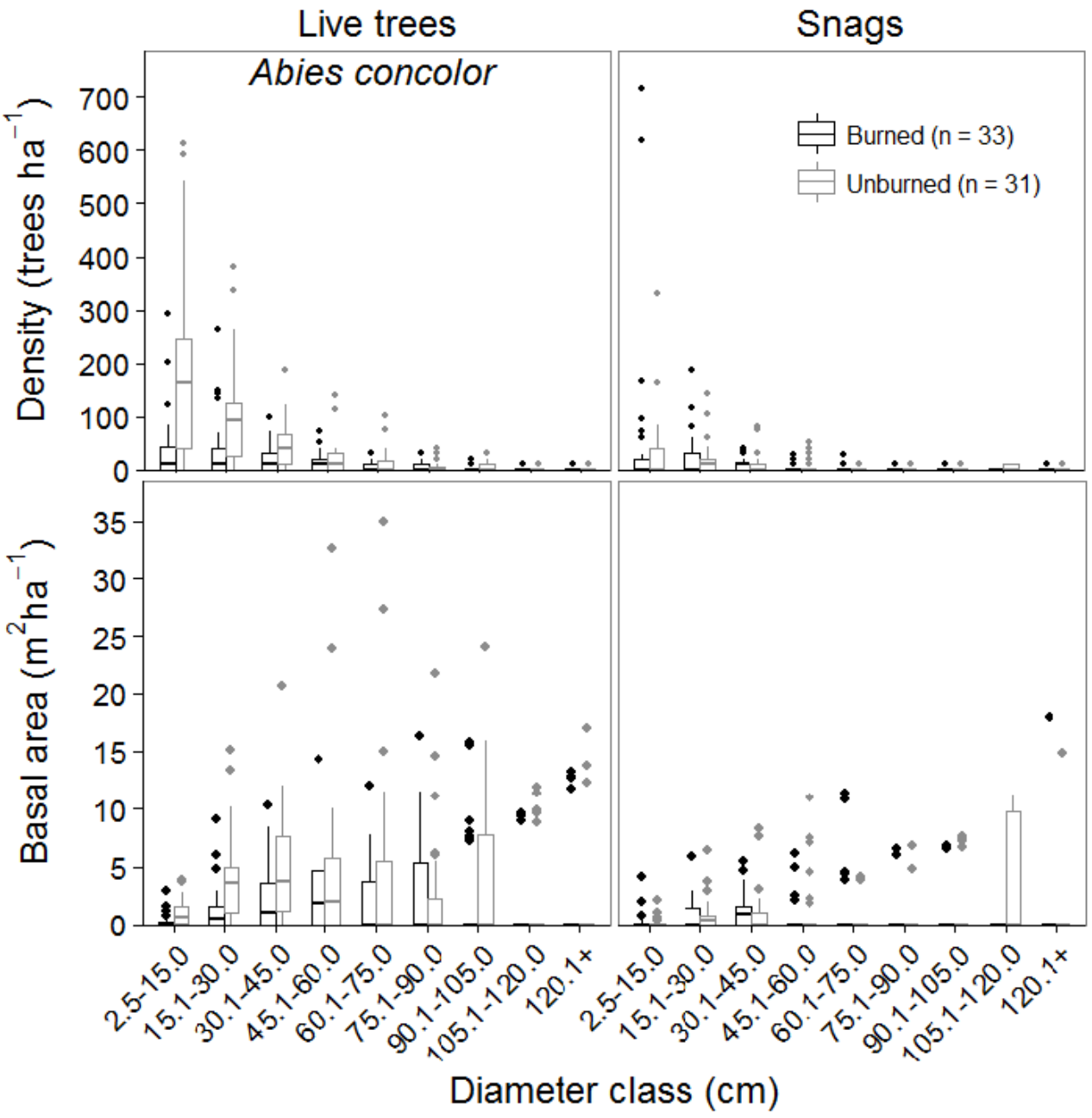

Figure 1.6.a. Diameter distributions by density and basal area of *A. concolor*, a fire-sensitive, shade-tolerant tree species characteristic of lower montane forests of Yosemite and Sequoia & Kings Canyon National Parks. The distribution of density by diameter class is depicted in the upper panels; distribution of basal area by diameter class is depicted in the lower panels. Plots were included that contained a minimum of one live tree or snag of *A. concolor*.

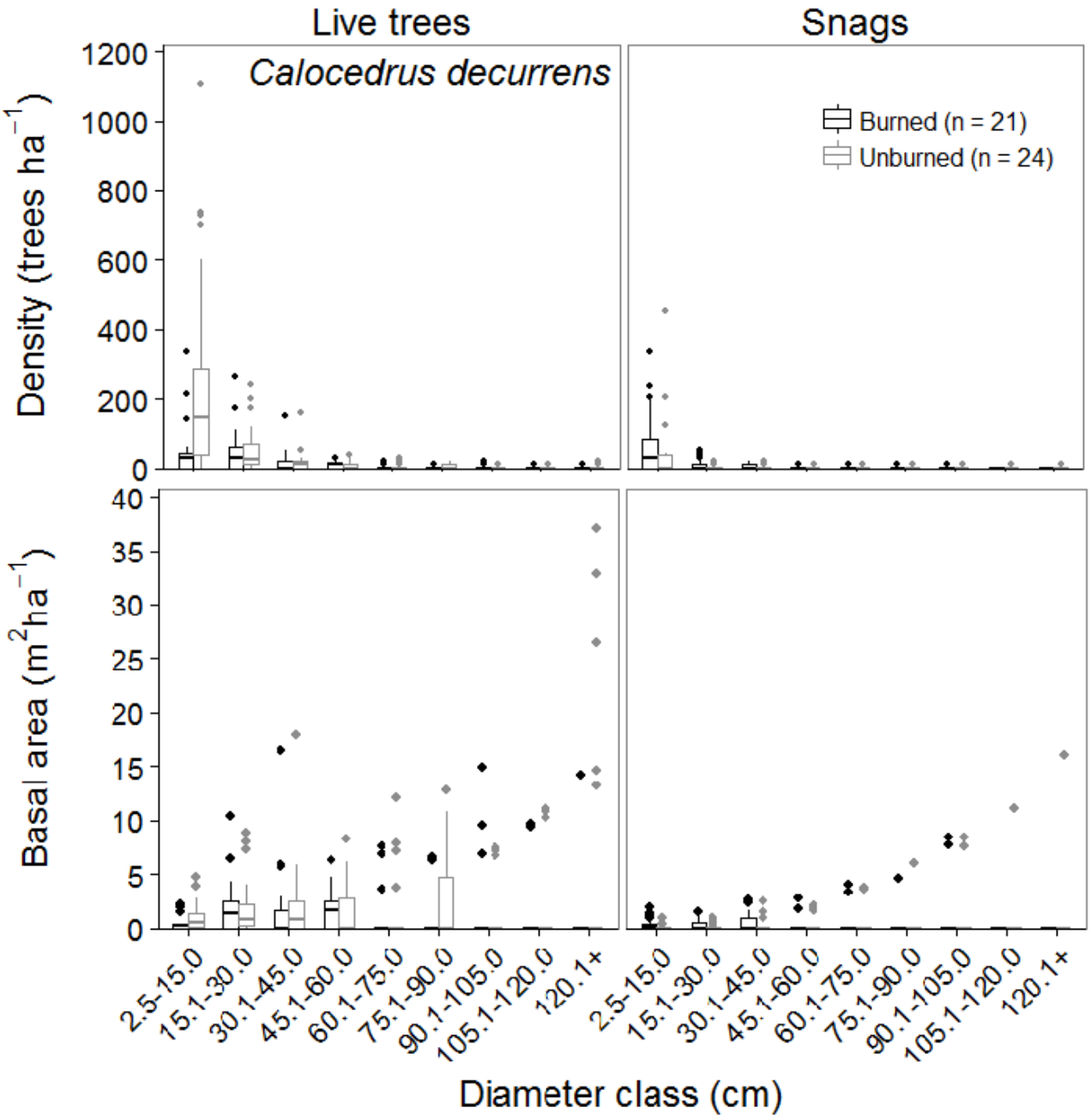

Figure 1.6.b. Diameter distributions by density and basal area of *C. decurrens*, a fire-sensitive, shade-tolerant tree species characteristic of lower montane forests of Yosemite and Sequoia & Kings Canyon National Parks. The distribution of density by diameter class is depicted in the upper panels; distribution of basal area by diameter class is depicted in the lower panels. Plots were included that contained a minimum of one live tree or snag of *C. decurrens*.

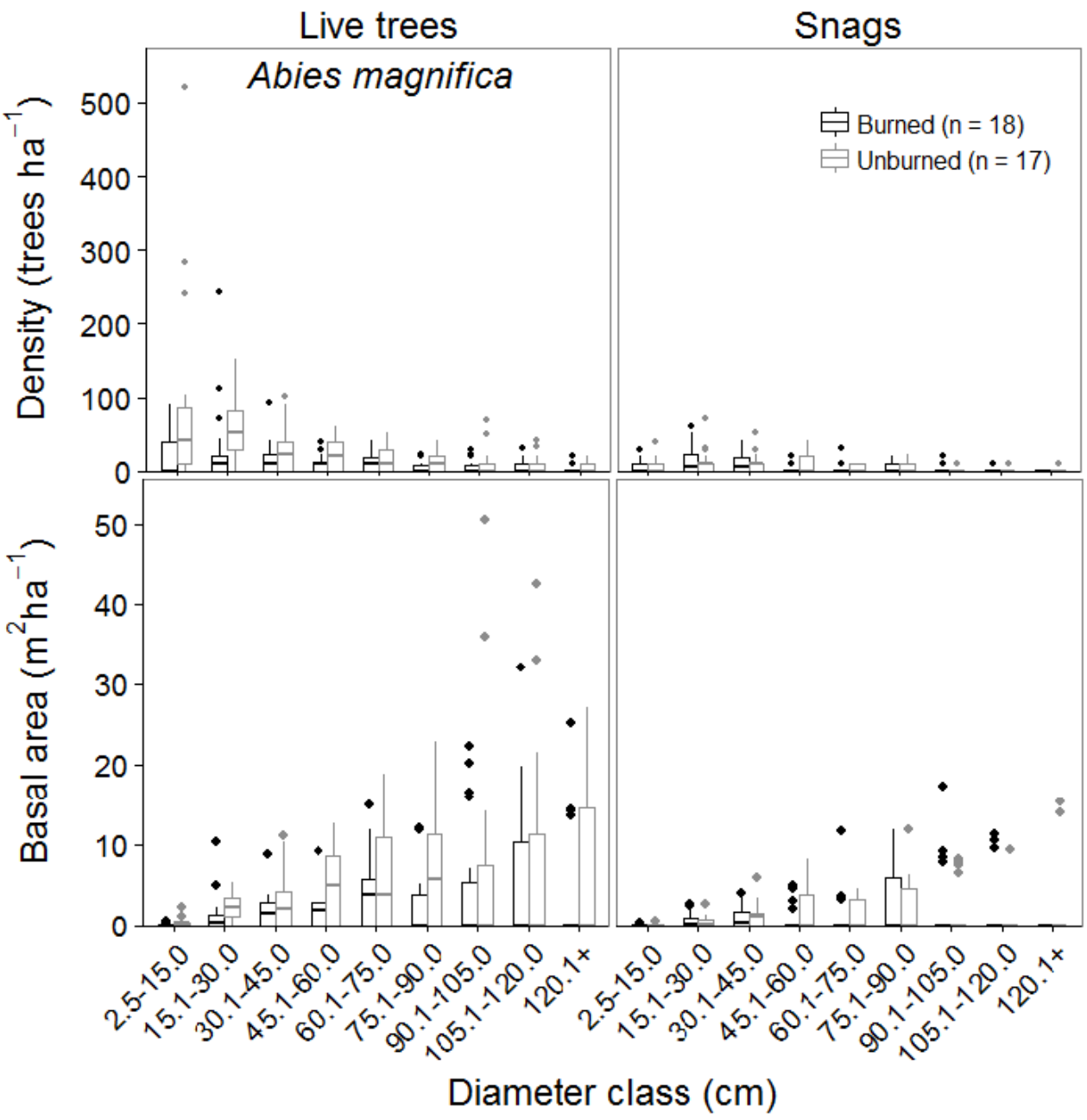

Figure 1.6.c. Diameter distributions by density and basal area of *A. magnifica*, a fire-sensitive, shade-tolerant tree species characteristic of upper montane forests of Yosemite and Sequoia & Kings Canyon National Parks. The distribution of density by diameter class is depicted in the upper panels; distribution of basal area by diameter class is depicted in the lower panels. Plots were included that contained a minimum of one live tree or snag of *A. magnifica*.

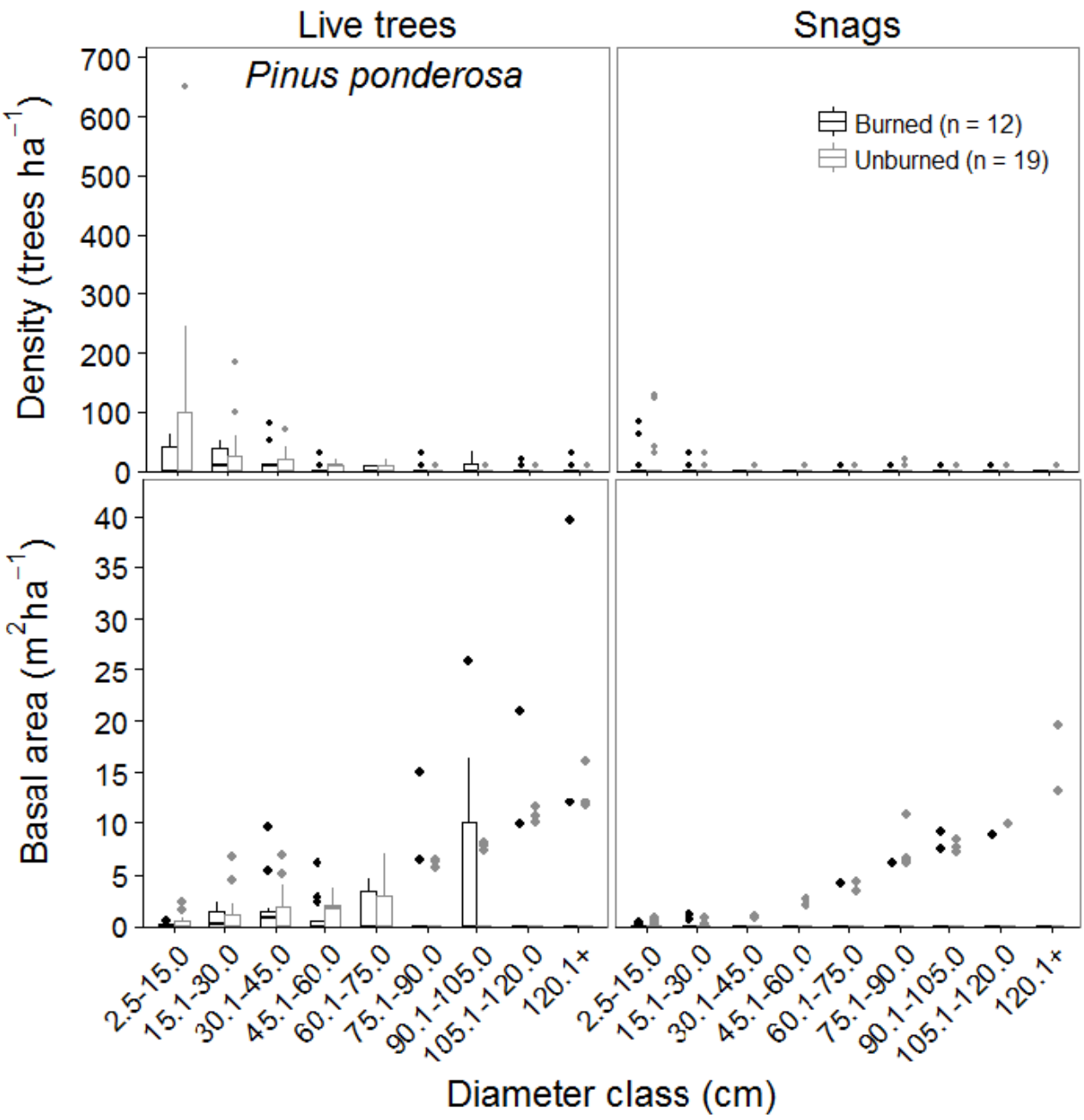

Figure 1.7.a. Diameter distributions by density and basal area of *P. ponderosa*, a fire-resistant, shade-intolerant tree species characteristic of lower montane forests of Yosemite and Sequoia & Kings Canyon National Parks. The distribution of density by diameter class is depicted in the upper panels; distribution of basal area by diameter class is depicted in the lower panels. Plots were included that contained a minimum of one live tree or snag of *P. ponderosa*.

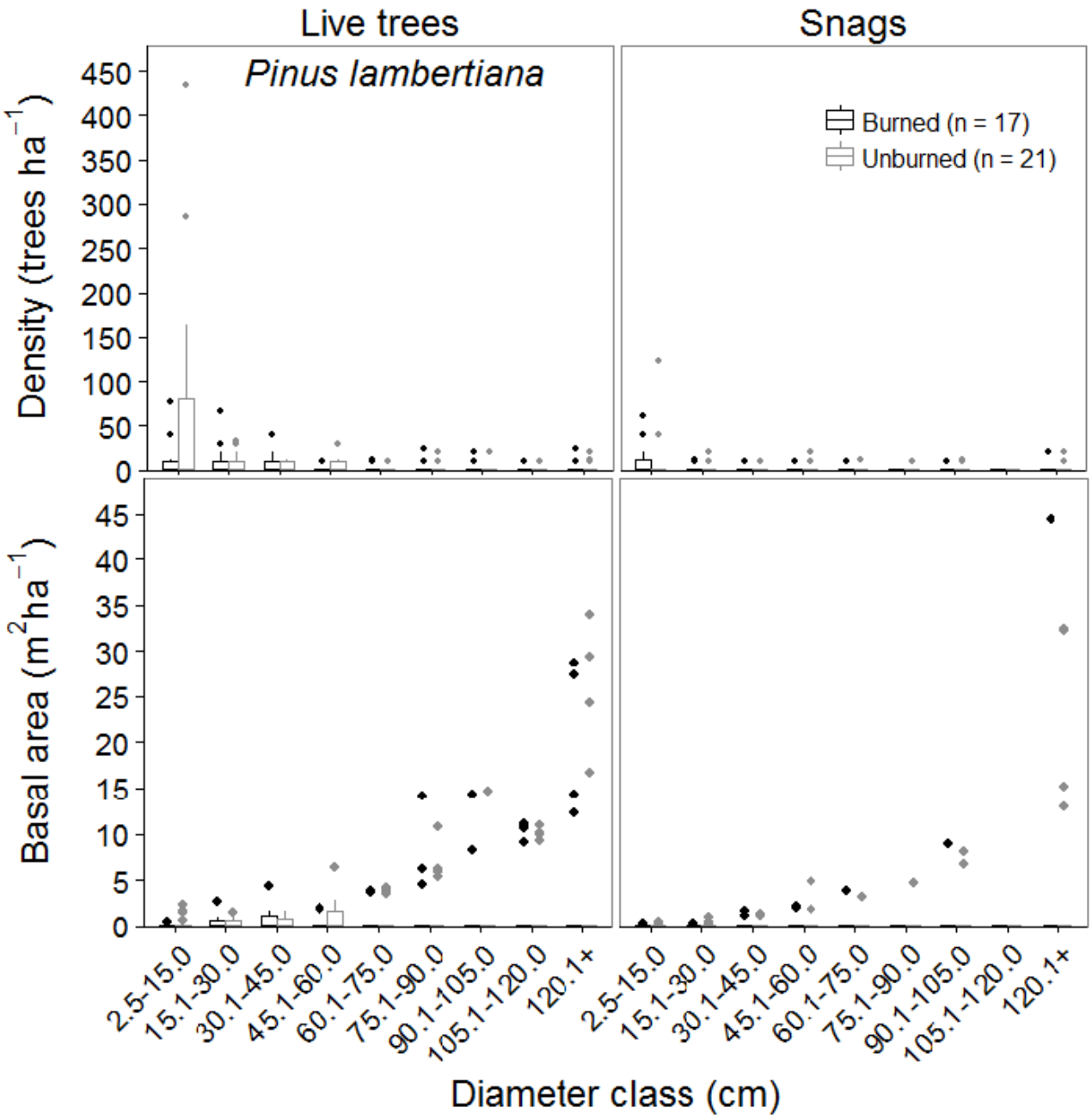

Figure 1.7.b. Diameter distributions by density and basal area of *P. lambertiana*, a fire-resistant, shade-intolerant tree species characteristic of lower montane forests of Yosemite and Sequoia & Kings Canyon National Parks. The distribution of density by diameter class is depicted in the upper panels; distribution of basal area by diameter class is depicted in the lower panels. Plots were included that contained a minimum of one live tree or snag of *P. lambertiana*.

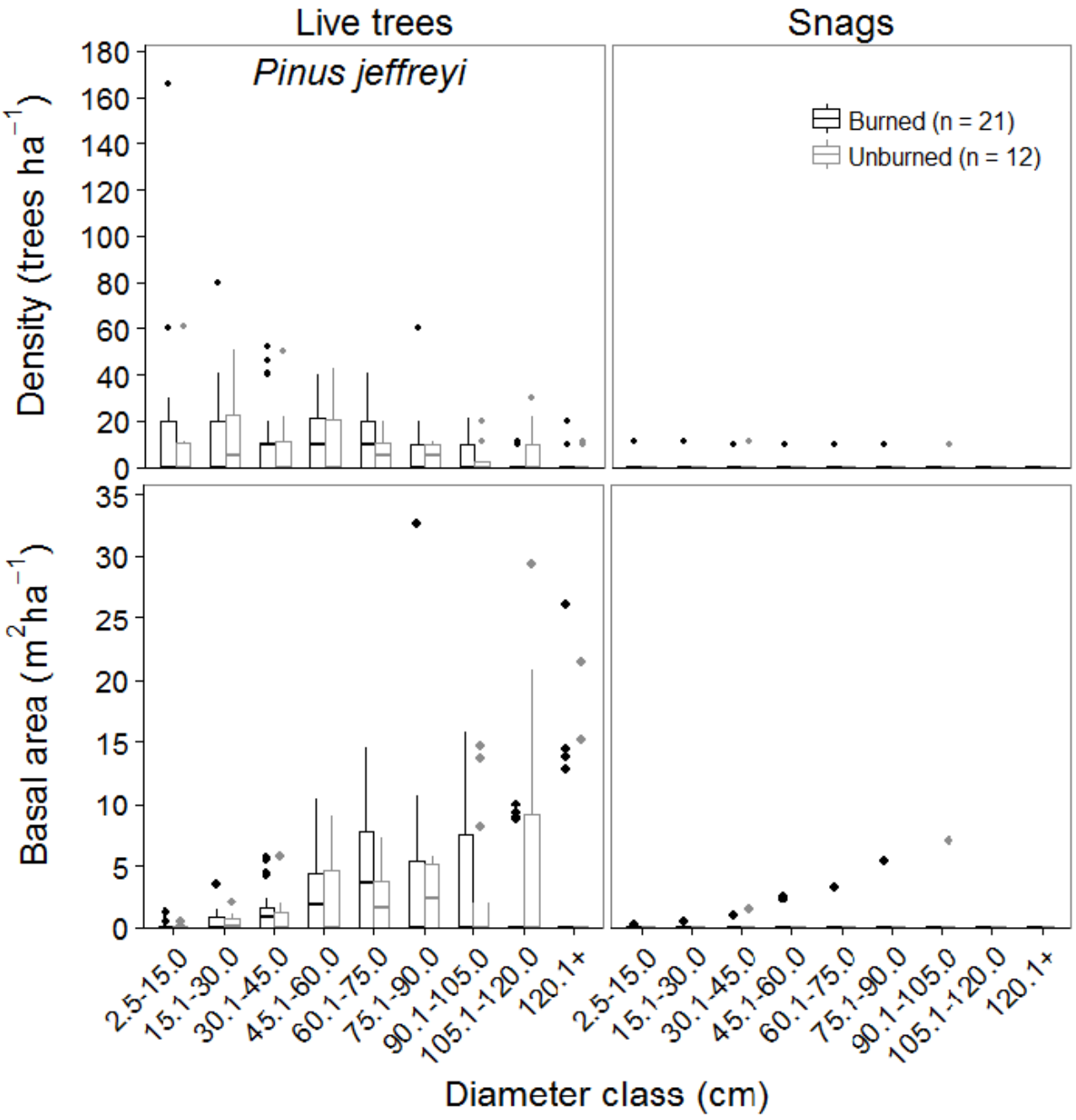

Figure 1.7.c. Diameter distributions by density and basal area of *P. jeffreyi*, a fire-resistant, shade-intolerant tree species characteristic of upper montane forests of Yosemite and Sequoia & Kings Canyon National Parks. The distribution of density by diameter class is depicted in the upper panels; distribution of basal area by diameter class is depicted in the lower panels. Plots were included that contained a minimum of one live tree or snag of *P. jeffreyi*.

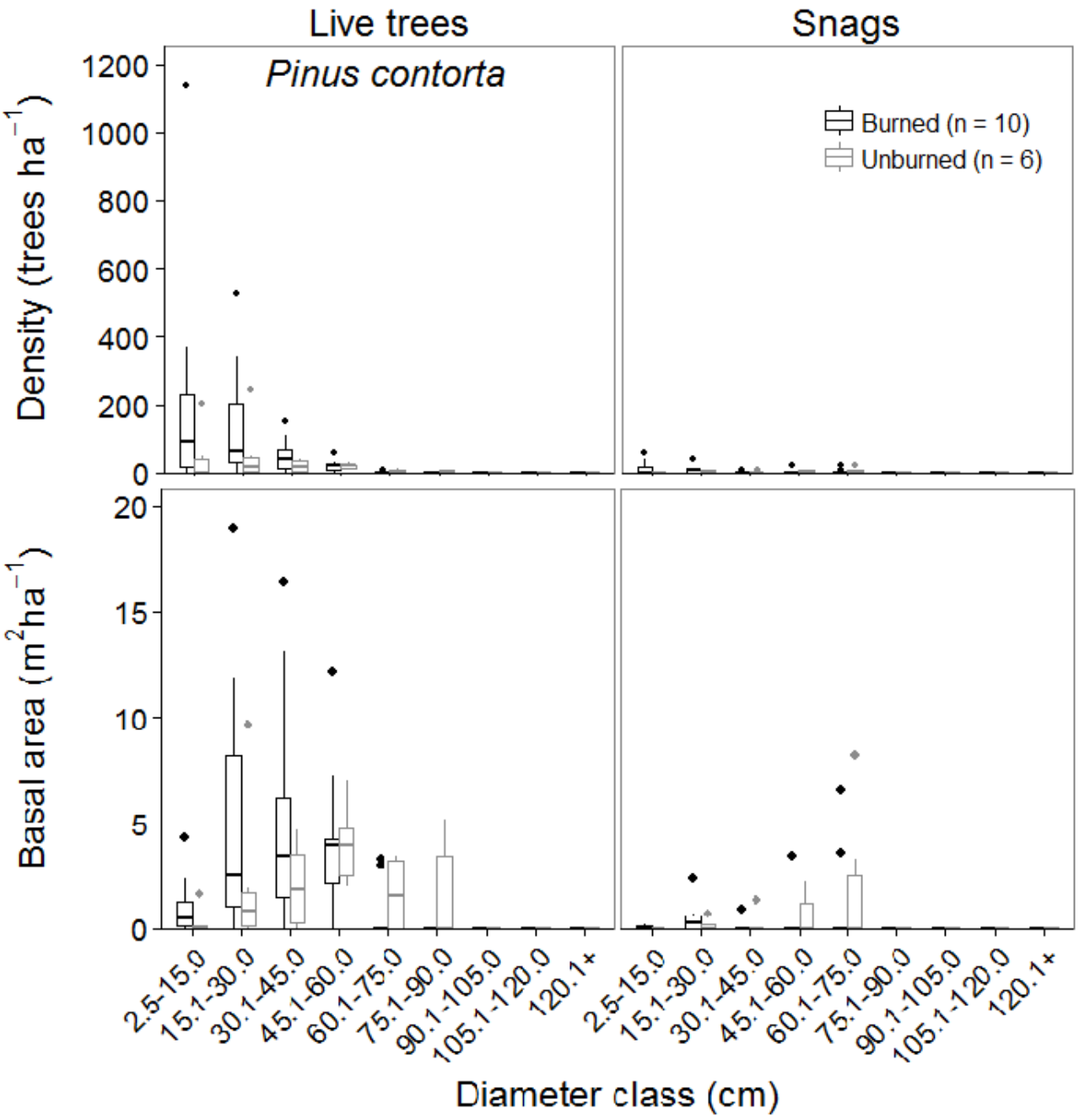

Figure 1.7.d. Diameter distributions by density and basal area of *P. contorta*, a tree species characteristic of upper montane forests of Yosemite and Sequoia & Kings Canyon National Parks. The distribution of density by diameter class is depicted in the upper panels; distribution of basal area by diameter class is depicted in the lower panels. Plots were included that contained a minimum of one live tree or snag of *P. contorta*.

Table 1.8. Mann Whitney *U* tests comparing burned and unburned populations of nine diameter classes (DC) for seven tree species sampled in 97 montane forest plots located in Yosemite and Sequoia & Kings Canyon National Parks; *p*-values <0.05 are bolded. Diameter classes are defined in Table 1.3.

	DC1	DC2	DC3	DC4	DC5	DC6	DC7	DC8	DC9
Density									
A. concolor	**<0.001**	**<0.001**	**0.008**	0.709	0.499	0.747	0.297	0.624	0.710
A. magnifica	**0.016**	**0.004**	0.428	0.194	0.745	0.052	0.545	0.696	0.682
C. decurrens	**0.004**	0.671	0.573	0.679	0.787	0.134	1.000	0.738	0.110
P. contorta	0.126	0.142	0.208	0.739	0.205	0.073	-	-	-
P. jeffreyi	0.633	0.546	0.418	0.686	0.204	0.564	0.382	0.237	0.911
P. lambertiana	0.465	0.475	0.496	0.384	0.740	0.741	0.490	0.755	0.837
P. ponderosa	0.437	0.694	0.781	0.177	0.517	0.899	0.065	0.824	0.899
Basal area									
A. concolor	**0.001**	**<0.001**	**0.011**	0.624	0.539	0.728	0.352	0.578	0.823
A. magnifica	**0.004**	**0.007**	0.354	0.219	0.733	**0.048**	0.520	0.654	0.478
C. decurrens	**0.027**	0.827	0.533	0.524	0.759	0.134	0.928	0.677	0.110
P. contorta	0.157	0.174	0.299	1.000	0.210	0.073	-	-	-
P. jeffreyi	0.587	0.632	0.293	0.794	0.148	0.718	0.373	0.241	0.978
P. lambertiana	0.696	0.587	0.557	0.325	0.592	0.726	0.490	0.665	0.885
P. ponderosa	0.464	0.600	0.750	0.240	0.477	0.825	0.077	0.975	0.924

DISCUSSION

Multiple fires and fire severity

The examination of the impacts of multiple fires on forests is an area of growing relevance to land managers given expected increases in area burned and number of fires (Lutz et al. 2009b; Westerling et al. 2006). Contrary to van Wagtendonk et al. (2012), who found that multiple intersecting fires in the Illilouette Creek basin of Yosemite reduced subsequent fire severity, my study identified eight out of 10 instances, five in Yosemite and three in Sequoia, where multiple fires were linked to higher subsequent severity, as measured by satellite-derived indices (Figure 1.3; Table 1.6). I present three viable explanations for the higher severity of later fires. First, differences in annual fire behavior could have been associated with short-term fluctuations in climate; this is supported by the higher rankings of later fire years relative to Yosemite fire normals (Table 1.6; Lutz et al. 2011). Alternatively, antecedent fires could have stimulated shrub species, which then burned in the subsequent fire; although the higher pre-fire NBR would have decreased the RdNBR value, it is possible that complete ignition of shrub cover could nevertheless result in a higher RdNBR. This second hypothesis is supported by the greater proportion of burned plots (76.5%) than unburned plots (39.1%) with $\geq$2.5 m^2 shrub cover. Third, previous fires could have accelerated the accumulation of ground fuels due to the deposition of scorched needles and other debris, thereby increasing the intensity of subsequent fires. These results and potential mechanisms suggest that (1) a history of multiple recent fires may not reduce fire severity when fire weather is extreme, and (2) RdNBR may not be the best indicator of fire effects on trees given its propensity to weight shrub and tree mortality equally.

Abundance trends and species composition

Patterns of total basal area and tree density among vegetation communities generally supported previous work of Parker (1989) in Yosemite and Vankat (1982) in Sequoia. The high tree density of lower montane and *P. contorta* alliances and low tree density of *P. jeffreyi* and *J. occidentalis* woodlands were common among previous studies, as was the high basal area of the *A. magnifica-A. concolor* alliance (Figure 1.4; Parker 1989; Vankat 1982).

Biophysical variables and species composition

Distributions of forest alliances, associations, and species were strongly associated with biophysical variables (Figure 1.5). All four biophysical parameters, however, were strongly collinear, with low elevation coinciding with high PET, AET, and Deficit and high elevation associated with low PET, AET, and Deficit (Figure 1.5). Higher AET at lower elevation is a product of the longer growing season and greater soil water-holding capacity; higher Deficit at the same sites reflects the longer summer drought, driven by higher temperatures and a shallower snowpack. Low elevation sites were dominated by *P. ponderosa, C. decurrens, Q. kelloggii, P. lambertiana*, and *A. concolor* with *P. menziesii* and *C. nuttallii* as lesser associates. At higher elevations *A. magnifica, P. contorta, T. mertensiana,* and *P. monticola* were the primary constituents, suggesting that these species are adapted to deep snow, a shorter growing season, and shallower soils.

Similar trends were identified by Parker (1989, 1982) and Vankat (1982) with regard to forest communities and by Lutz et al. (2010) with regard to individual tree species. Parker (1984) found that *A. magnifica* was more dominant on steeper slopes, at higher elevations, in more open forests, and on more acidic and nutrient poor substrates, whereas *A. concolor* was more prevalent on shallower slopes, at lower elevations, in more closed canopy settings, and on more fertile

soils. Because elevation, soil acidity and fertility, canopy closure, AET, Deficit, and PET are correlated, my findings support and reframe previous work on mixed-conifer plant communities in the context of climatic water balance.

Fire and tree species

The occurrence of lower-severity fire most strongly affected three tree species. Density of small-diameter individuals of *A. concolor*, *A. magnifica*, and *C. decurrens* was significantly higher at unburned sites relative to burned sites, corroborating previous work in this region on unburned (Scholl and Taylor 2010; Beaty and Taylor 2007; Vankat and Major 1978) and burned forests (Figures 1.6.a, 1.6.b, and 1.6.c; Table 1.8; van Mantgem et al. 2013; Collins et al. 2011; Schwilk et al. 2006).

In contrast, fire had a negligible effect on *P. ponderosa*, *P. lambertiana*, *P. jeffreyi* and *P. contorta*, evidenced by the lack of significant differences between populations of burned and unburned individuals (Figures 1.7.a, 1.7.b, 1.7.c, and 1.7.d; Table 1.8). The diameter distributions of *P. contorta* were unique in that burned sites were characterized by a reverse-J distribution and unburned sites were associated with a lower density of small-diameter trees (Figure 1.7.d). This likely reflects a combination of three factors: (1) the capacity of *P. contorta* to rapidly germinate post-fire and eventually self-thin on more productive sites, (2) the ability of *P. contorta* to persist, albeit at small diameters, on unproductive sites where establishment is inhibited and fire severity is very low due to lack of fuel, and (3) the lack of unburned *P. contorta*-dominated sites in this dataset (Table 1.5), meaning that *P. contorta*, by definition, was found at low density among most unburned stands where it was present. Among the other *Pinus* spp. lack of fire effects is likely explained by the low abundance of small-diameter, fire-susceptible individuals across all plots. These *Pinus* spp. are shade-intolerant, and widespread

regeneration is improbable unless preceded by a disturbance severe enough to alter the light environment. No median density value of small-diameter *P. ponderosa*, *P. lambertiana*, or *P. jeffreyi* exceeded zero at unburned plots, suggesting that >50% of the plots that contained these species did not support their regeneration.

This study demonstrates that lower-severity fire reduces the density of small-diameter, shade-tolerant species (Table 1.8). Lack of effects on larger diameter classes supports the utility of lower-severity fire as a management tool to reduce high tree density and potentially relieve stress on larger-diameter individuals that sequester the majority of forest carbon (Lutz et al. 2012; Lutz et al. 2009a). Subsequent studies, however, are needed to determine whether lower-severity fire is sufficient to stimulate regeneration of *Pinus* spp. and to establish diameter thresholds of fire sensitivity for *Pinus* spp. in instances where regeneration has occurred.

Fire and species composition

Despite evidence that lower-severity fire reduces density of shade-tolerant species, particularly *A. concolor* and *C. decurrens*, this study also indicates that lower-severity fire is incapable of restoring characteristic species composition in lower montane forests of the Sierra Nevada. Scholl and Taylor (2010) compared historical (1899) and contemporary (2002) diameter distributions of *A. concolor* and *C. decurrens* and found that density of *A. concolor* <60 cm dbh and *C. decurrens* <40 cm dbh had increased over the course of fire suppression. These results were corroborated by Lutz et al. (2009a) who compared Yosemite-wide historical (1932-1936) and contemporary (1988-1999) inventory data and found that modern density of *A. concolor* <60 cm dbh and *C. decurrens* <30 cm dbh exceeded that of historical levels. Given that lower-severity fire failed to impact *A. concolor* >45 cm dbh and *C. decurrens* >15 cm dbh (Table 1.8), this study suggests that fire reintroduction has come too late. On productive sites, greater

proportions of shade-tolerant individuals of fire-resistant size have developed and will persist as long-term seed sources, perpetuating high tree density and ladder fuel generation. Additionally, increased prevalence of fire-resistant *A. concolor* that established during the era of fire suppression may amplify the effects of fire exclusion on species composition not only by increased reproductive capacity, but also via increased deposition of acidic litter (Parker 1989). Parker (1989) identified a correlation between *P. ponderosa* and basic soils, suggesting that some *Pinus* spp. may be less well adapted to acidic soils. Increased abundance of *A. concolor* could therefore result in an instance of self-synergism, whereby the light environment and soil conditions created by *A. concolor* perpetuate its dominance.

Conclusions

This study explored the interactions between overstory communities, individual tree species, and the environmental and fire-related variables that drive compositional change in the Sierra Nevada. Lower-severity fire altered species composition at a small scale, primarily through effects on small-diameter individuals of shade-tolerant species, along the compositional gradient represented in this study. However, these lower-severity disturbances may amount to no more than perturbations along a steady trajectory of compositional change. Many shade-tolerant individuals have attained fire-resistant size, increasing the proportion of shade-tolerant seed inputs and shading out *Pinus* juveniles. These results counter the generally accepted model of multiple fires as a panacea for restoration of historical species composition and, instead, suggest that neither single nor multiple applications of lower-severity fire can accomplish this task. Irreversible changes in species composition that likely exceed the historic range of variability emphasize the importance of managing for other ecosystem attributes, including forest structure and function.

CHAPTER II

EFFECTS OF LOWER-SEVERITY FIRE ON DIAMETER DISTRIBUTIONS IN MONTANE FORESTS OF THE SIERRA NEVADA

ABSTRACT

Conservation of forest species composition within current land management units may be difficult in the face of changing climate. Land managers may therefore need to increasingly prioritize the maintenance of forest structure (e.g., abundance of large-diameter trees) and function (e.g., biomass accumulation). Shifting management perspectives from species-centric paradigms will require a better understanding of forest structure at a regional scale. I characterized the forest structure of Yosemite and Sequoia & Kings Canyon National Parks with techniques traditionally used to describe species composition. I grouped tree diameter data from 97, 0.1 ha plots (46 unburned since 1930; 51 burned between one and four times since 1946) that span six forest alliances in Yosemite and Sequoia & Kings Canyon National Parks into nine diameter classes and used ordination to visualize diameter class assemblages (i.e., structural communities). I described the range of structural communities associated with six forest alliances and explored relationships between structural communities, biophysical variables (elevation, potential evapotranspiration, actual evapotranspiration, and climatic water deficit), and occurrence of lower-severity fire. Structural composition of forest alliances overlapped considerably, foreshadowing the weak relationship between structural communities and biophysical variables and suggesting that different species throughout the region are adapted to filling similar structural niches. Lower-severity fire reduced the abundance of trees <30.0 cm dbh, influencing structural communities as defined by the proportion of density attributed to each

diameter class. Structural communities as defined by the proportion of basal area attributed to each diameter class, however, were unchanged. These results suggest that: (1) structural communities are similar among a wide range of lower and upper montane forests, and (2) lower-severity fire is effective at reducing density of small-diameter trees while conserving forest structural communities.

INTRODUCTION

Environmental correlates of tree species distribution have been thoroughly studied in forest systems (Lutz et al. 2010; McKenzie et al. 2003; Stephenson 1998; Parker 1989; Vankat 1982), but the distribution of forest structure at similar spatial scales has not. A comprehensive understanding of forest structure at a regional scale will be increasingly relevant to land managers given projected shifts in species distribution (Iverson and McKenzie 2013). Climate models project mean temperature increases of 2-4° C over the next century (IPCC 2007), conditions likely to increase insect- and drought-related mortality (Logan et al. 2010; Allen et al. 2010) as well as more frequent fires, larger fire size, and greater annual area burned (Miller et al. 2012b; Lutz et al. 2009b; Westerling et al. 2006; McKenzie 2004). As plant communities change in response to climate and altered disturbance regimes, the maintenance of structural attributes (e.g., large-diameter trees, Lindenmayer et al. 2012) and ecosystem functions (e.g., biomass accumulation, Stephenson et al. 2014) may supplant the retention of historical species composition as a management priority. Such a shift in management paradigms for the southern and central Sierra Nevada, however, cannot occur without a better understanding of the current forest structure.

Yosemite National Park (Yosemite) and Sequoia & Kings Canyon National Parks (Sequoia) present a complex setting for forest structural analysis. Climatic variability along elevational gradients imposes differential influences of water and energy limitation on lower and upper montane forests (Das et al. 2013) but also influences disturbance regimes. The six-month growing season characteristic of lower montane forests increases water stress during the summer drought and also reduces fuel moisture, leading to a higher proportion of lightning ignitions relative to lightning strikes (Lutz et al. 2009b; van Wagtendonk 1994). In contrast, upper

montane forests experience a shorter growing season and fewer lightning ignitions but greater mechanical damage from quarto-centennial windstorms and seasonal snow loading (Parker 1986a; Oosting and Billings 1943). Application of the same fire suppression management strategy to lower and upper montane forests, which were historically governed by different disturbance regimes, has resulted in a more acute departure from historical tree density in lower relative to upper montane forests (Vankat and Major 1978). Current forest structure reflects a combination of fire-excluded areas that have not burned since the late 19th century and areas that have burned up to five times since fire was reintroduced in 1968 (van Wagtendonk et al. 2012; van Wagtendonk 2007). Moreover, the effects of fire reintroduction vary with fire weather, topography, recent fire history, site productivity, and vegetation type (Kane et al. in press; Kane et al. 2013; Scholl and Taylor 2010; Agee 1993). Forest structure in this setting therefore represents an intersection between physiography, historical climate and disturbance, former and contemporary management practices, and the stochasticity of ignition.

In the Sierra Nevada, the consequences of lower-severity fire are crucial to land management, particularly because area burned at lower severity is projected to increase. Although area burned at all fire severities may increase due to changes in climate, area burned at undifferentiated (i.e., where fire effects are undetectable by satellite) to moderate severity is projected to exhibit proportionally larger growth due to natural ignitions and prescribed fires aimed at reducing the risk of large, high-severity conflagrations (Miller et al. 2012a; Lutz et al. 2009b; van Wagtendonk and Lutz 2007). Nevertheless, the effects of lower-severity fire on forest structure are not well understood. Lower-severity fires in the Sierra Nevada may change forest structure by removing smaller-diameter trees and surface fuels and potentially decreasing the severity of subsequent fires.

Previous examinations of forest structure have generally exhibited one or more of the following limitations: (1) a fixation on current large-diameter trees that neglects individuals poised for recruitment into large diameter classes (e.g., Lutz et al. 2009a), (2) a preference for analyzing stem density that highlights small-diameter structural elements (e.g., Bekker and Taylor 2010; Scholl and Taylor 2010; Beaty and Taylor 2007; Taylor and Halpern 1991), (3) large diameter class bin sizes (e.g., Collins et al. 2011; Lutz et al. 2009a; Fellows and Goulden 2008), (4) small geographic extent (e.g., Collins et al. 2011; Scholl and Taylor 2010; Beaty and Taylor 2007; Taylor and Halpern 1991), and (5) methods that combine plots to establish structural norms while ignoring variability (Collins et al. 2011; Scholl and Taylor 2010; Lutz et al. 2009a). Some research has focused on relationships between disturbance processes and structural variability (Lutz et al. 2013; Franklin et al. 2002); however, this approach confines the scope of inference to areas dominated by similar sets of processes, a shortcoming given that both the resource dynamics and disturbance regime that control tree demography vary along an elevational gradient within the montane forest zone (Das et al. 2013; Caprio and Swetnam 1995). Furthermore, few studies have examined the effects of recent disturbance superimposed on gradients of historical disturbance regime attributes.

Here I characterize forest structure by applying techniques traditionally used to describe patterns of species composition. I substituted species with diameter class and used ordination to: (1) establish the concept of structural composition and (2) describe structural norms and variability among lower and upper montane forests that span a gradient of historical fire return intervals (FRIs). I compared recently burned and unburned sites to evaluate the impact of lower-severity fire on structural communities. My objectives were to: (1) characterize structural composition across the montane forests of the Sierra Nevada, (2) assess whether structural

community varies with water balance parameters, and (3) identify diameter thresholds of sensitivity to lower-severity fire to inform inferences regarding the effects of lower-severity fire on structural composition.

METHODS

Data reduction

The study area, data collection procedures, and data reduction criteria are described in Chapter I. The same 97 plots were retained for structural analysis, but here I classified stems by their diameters into nine 15 cm bins regardless of species (Table 1.3). I stratified these data into four categories by mortality status (live tree vs. snag) and burn status (burned plot vs. unburned plot) and calculated slope-corrected estimates of basal area and stem density for each diameter class at each plot.

Ordinations

I analyzed forest structural communities with NMDS ordination. Whereas the ordination in Chapter I depicted species composition, these ordinations depicted diameter class composition based on live tree (1) density and (2) basal area. I standardized abundances as proportions of the total for each plot, removing differences in total density and basal area among plots. Site positions in each ordination space therefore reflected the proportional contribution of each diameter class to plot tree density (hereafter, relative density) or basal area (hereafter, relative basal area). I used the Bray-Curtis distance measure and 200 random reruns to ordinate data along two axes. A comparison of the Bray-Curtis and Euclidean distance measures is provided in Appendix V. Ordinations were executed in the R statistical language (version 3.0.2; R Development Core Team, 2013) with the function "metaMDS" from the vegan package (version 2.0-10; Oksanen et al. 2013).

I depicted correlations between structural and biophysical gradients by coloring plots in ordination space by elevation, PET, AET, and Deficit. Because modeled values of PET, AET, and Deficit for plots in Sequoia were calculated with compositionally based estimates of soil

water-holding capacity, only plots from Yosemite were included in this analysis.

Diameter distributions

Diameter distributions depicting the distribution of live tree and snag density and basal area were generated for all stems. Burned and unburned plots were grouped separately to expose potential effects of fire on each diameter class. Mann-Whitney *U* tests were performed on each diameter class to identify significant differences between burned and unburned populations. To support the assumption that differences between burned and unburned populations were attributable to recent fire occurrence I compared the distribution of elevation, slope, aspect, AET, and Deficit of the burned and unburned plots (Mann-Whitney *U* test; $\alpha = 0.05$). No significant differences in these physical site attributes were detected. The validity of attributing differences between the burned and unburned populations to recent fire occurrence was further based on the assumption that the burned and unburned samples captured a similar range of historical (i.e., pre-1890) disturbance patterns.

RESULTS

The ranges of total tree density and basal area overlapped between burned and unburned plots, but the variation among unburned plots was greater (burned: $\mu_{density} = 365$, $SD_{density} = 302$; $\mu_{ba} = 47$, $SD_{ba} = 22$; unburned: $\mu_{density} = 684$, $SD_{density} = 446$; $\mu_{ba} = 64$, $SD_{ba} = 30$; Figure 2.1). Both maximum live tree and snag density differed by a factor of two between burned and unburned plots. The higher density of live trees was associated with unburned plots (burned: 1,280 trees ha^{-1}; unburned: 2,082 trees ha^{-1}), while the higher density of snags was associated with burned plots (burned: 1,347 snags ha^{-1}; unburned: 628 snags ha^{-1}). Maximum live basal area was greater among unburned plots (134.6 m^2 ha^{-1}) than burned plots (97.1 m^2 ha^{-1}), while maximum snag basal area was greater among burned plots (71.7 m^2 ha^{-1}) than unburned plots (64.8 m^2 ha^{-1}). Minimum live tree density and basal area were both four-fold greater at unburned plots (130 trees ha^{-1}; 17.0 m^2 ha^{-1}) relative to burned plots (30 trees ha^{-1}; 4.3 m^2 ha^{-1}). Minimum snag density and basal area were zero for both burned and unburned plots.

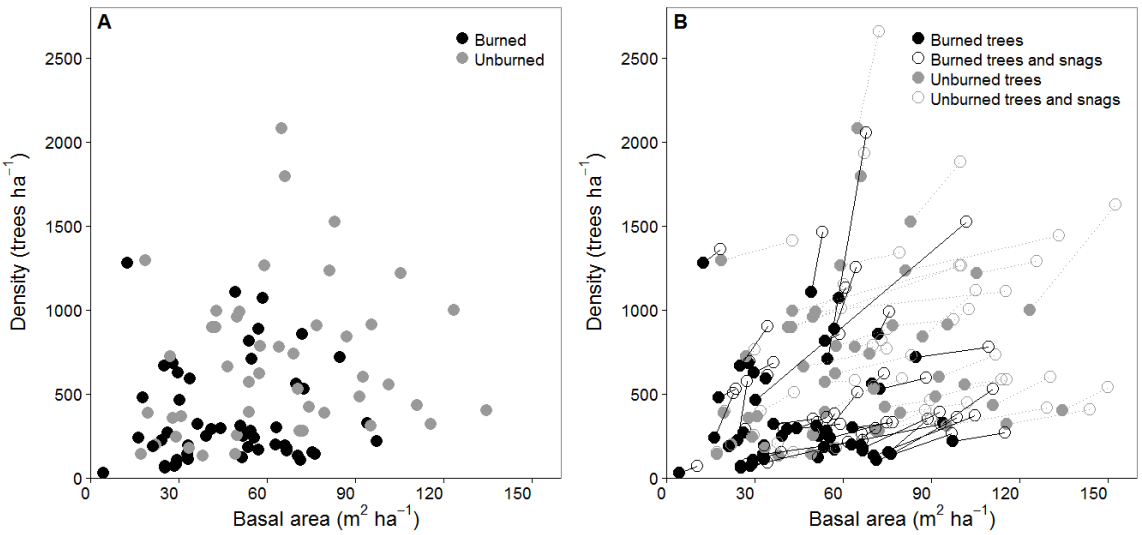

Figure 2.1. Basal area by density for 97, 0.1 ha plots from lower and upper montane forests of Yosemite and Sequoia & Kings Canyon National Parks. Live tree basal area is compared to live tree density (A). Live tree and snag basal area and density are depicted for each plot (B). Lines connect markers of live tree basal area and density (solid circles) to markers of total stem (live tree and snag) basal area and density (hollow circles) for each plot. Eight plots contained no snags and are not associated with lines in figure B. Horizontal slopes characterize plots with a small number of snags, while vertical slopes characterize plots with snags of small basal area. The slope value indicates the number of snags a plot contains per m^2 of snag basal area.

Structural composition

NMDS ordination of relative density produced one isolated diameter class (DC1) and an oblong cluster of the remaining classes that tilted away from DC1 (Figure 2.2 A). DC1 was closer to DC2, DC3, DC4, and DC9, which populated one half of the cluster, than DC5 through DC8, which occupied the other half. The isolation of the DC1 centroid indicated that a high proportion of density in DC1 corresponded with comparatively lower proportions of density in the remaining diameter classes. The capacity of DC1 to attain densities higher than any other diameter class was the primary mechanism behind the isolation of DC1 in ordination space: In nine plots the density of DC1 (611-1,642 trees ha^{-1}) exceeded the maximum density of DC2 (607 trees ha^{-1}).

NMDS ordination of relative basal area revealed a crescent-shaped, curvilinear relationship among diameter class centroids (Figure 2.2 B). The centroids of DC1 and DC2 occupied one extreme, DC7 and DC8 formed the other, and DC3 through DC6 filled in the gradient along the curve from the smaller to the larger diameter classes. The mouth of the crescent faced the DC9 centroid, which was equidistant from DC1 through DC6 and slightly closer to DC7 and DC8. The proximity of diameter class centroids reflected the inherent relationship between diameter class and basal area. When a small diameter class represents a large proportion of the basal area of a plot, the plot necessarily contains few large individuals. It follows that the majority of the residual basal area would comprise the remaining smaller diameter classes. Therefore, the separation of the smaller diameter classes in ordination space simultaneously isolated the larger diameter classes. DC9 was an extreme instance of this circumstance. Although no more than four DC9 individuals co-occurred in a given plot, the contribution to plot basal area of these trees (120.1-189.3 cm dbh) exceeded that of stems in any

other diameter class (Table 2.1). Its isolation in ordination space demonstrated that no other diameter class routinely matched the contribution of DC9 to basal area on the same sites; its position in ordination space showed that the other diameter classes contributed comparably to the basal area complement in the 40 plots that contained DC9 individuals.

Higher total density was more closely associated with plots where DC1 contributed more to relative density and basal area (Figure 2.2 C and D). Higher total basal area occurred centrally in both relative density and relative basal area ordinations, indicating that maximal basal area was achieved at sites populated with a combination of small- and large-diameter individuals (Figure 2.2 E and F).

Forest alliances

The distribution of forest alliances across ordination space of relative density indicated considerable structural overlap among plots regardless of species composition (Figure 2.2 A). *Pinus ponderosa-C. decurrens* and *A. concolor-P. lambertiana* plots were more concentrated near DC1 and in the space between DC1 and the larger diameter classes, indicating the ubiquity of small-diameter trees among these sites. *Abies magnifica-A. concolor* plots were less variable and occupied a narrow, horizontal band stretching from between the DC1 and DC2 centroids to the DC4 and DC7 centroids. *Pinus jeffreyi* plots were the most evenly dispersed throughout the ordination space, while *P. contorta* sites exhibited the least structural diversity, populating a triangular region bordered by DC1, DC2, and DC3. In contrast to the other alliances, *A. magnifica* formed two distinct groups, one concentrated near DC1 and another that spanned from DC3 to DC7.

The structural overlap of forest alliances with regard to relative density remained evident when the structural communities were characterized by relative basal area (Figure 2.2 B). *Pinus*

ponderosa-C. decurrens and *A. concolor-P. lambertiana* sites represented a wide array of diameter distributions, evidence that large-diameter trees occupied some but not all plots. In contrast, *A. magnifica-A. concolor*, *P. jeffreyi,* and *A. magnifica* sites were more closely associated with DC4 through DC9, demonstrating the consistent presence of larger diameter trees at these sites. Patterns of relative basal area mirrored those of relative density at *P. contorta* sites, indicating that the *P. contorta* constituency was primarily confined to DC1, DC2, and DC3.

Recent lower-severity fire potentially explained some structural variability within the *P. ponderosa-C. decurrens*, *A. concolor-P. lambertiana*, and *A. magnifica-A. concolor* alliances. Unburned sites of these alliances were more closely associated with DC1 than were burned sites in the relative density ordination space (Figure 2.2 A). In contrast, both burned and unburned sites of *P. jeffreyi* and *A. magnifica* were distributed throughout.

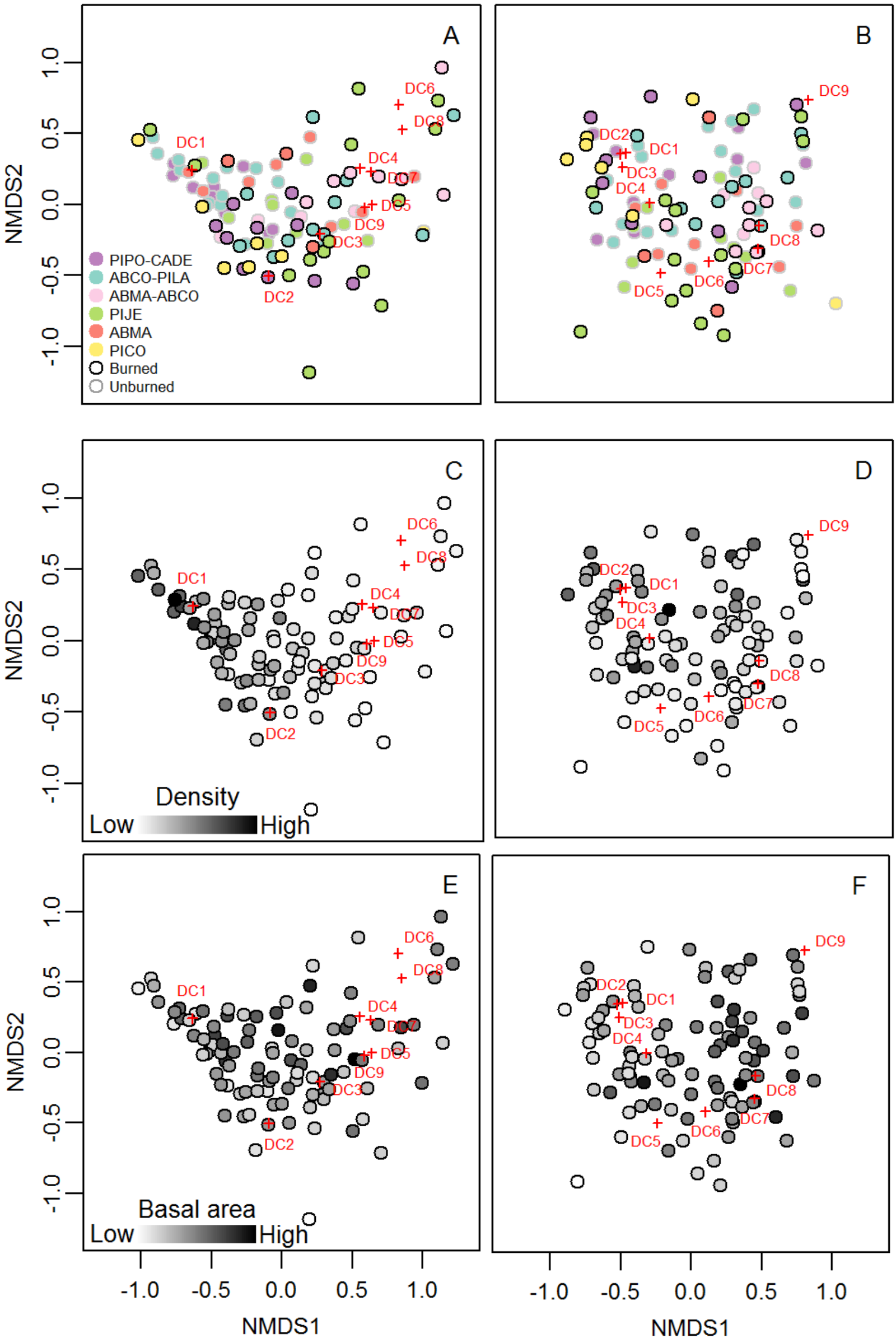

Figure 2.2. Distribution of forest alliances, total density, and total basal area across NMDS ordinations of relative density (stress = 0.130; left column) and relative basal area (stress = 0.218; right column) attributed to each of nine diameter classes in 97 plots located in lower and upper montane forests of Yosemite and Sequoia & Kings Canyon National Parks. Plots are colored by forest alliance and burn status (A and B). Total density (C and D) and total basal area (E and F) of each plot are represented by a linear color gradient from white to black. Total density ranged from 30 to 2,082 trees ha^{-1}; total basal area ranged from 4.29 to 134.56 m^2 ha^{-1}. Four letter species codes are defined in Table A.1 of Appendix I. Diameter classes are defined in Table 1.3.

Table 2.1. Proportional contributions of nine diameter classes to the relative basal area and relative tree density of plots that include that diameter class. Minimum for all diameter classes was zero for both tree density and basal area. Diameter classes are defined in Table 1.3.

Structural attribute	Diameter class	Median	Mean	Maximum
Tree density				
	1	0.33	0.38	0.93
	2	0.25	0.25	0.69
	3	0.13	0.15	0.37
	4	0.09	0.10	0.36
	5	0.05	0.07	0.34
	6	0.04	0.06	0.38
	7	0.04	0.06	0.22
	8	0.03	0.04	0.17
	9	0.03	0.04	0.18
Basal area				
	1	0.02	0.03	0.27
	2	0.07	0.10	0.53
	3	0.11	0.13	0.51
	4	0.13	0.14	0.41
	5	0.15	0.17	0.68
	6	0.16	0.18	0.56
	7	0.18	0.21	0.46
	8	0.18	0.20	0.51
	9	0.29	0.31	0.69

Biophysical variables

Relationships between structural communities and elevation, PET, AET, and Deficit were weak regardless of whether structure was represented by relative density or relative basal area (Figure 2.4). The highest values of AET and Deficit were associated with different sites dominated by high relative density in DC1 (Figure 2.3 E and G). In general, however, low, medium, and high values of biophysical variables were broadly distributed throughout the relative density ordination space (Figure 2.3 A, C, E, and G). No trends characterized the relationships between relative basal area and biophysical variables (Figure 2.3 B, D, F, and H).

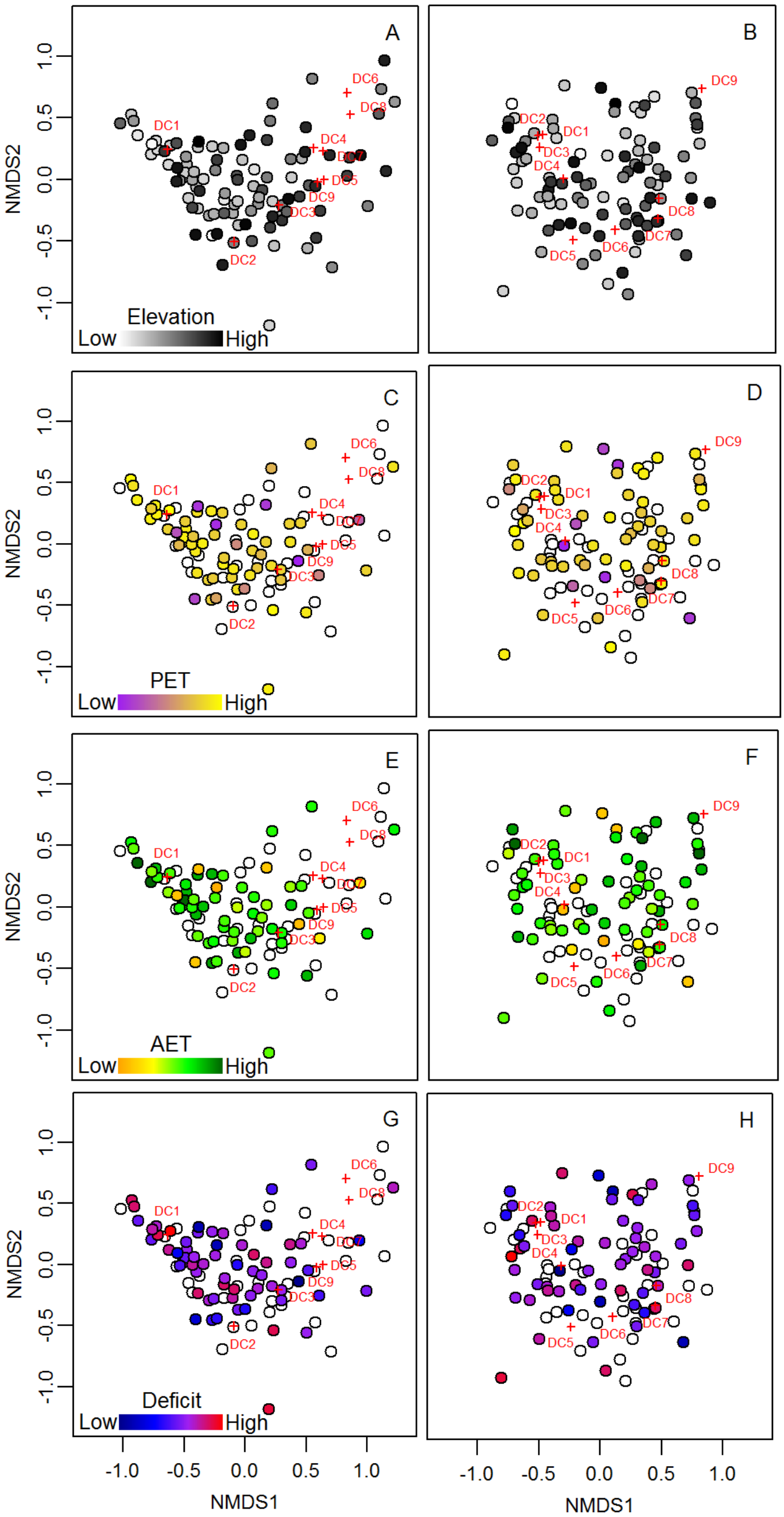

Figure 2.3. Distribution of elevation, PET, AET, and Deficit across NMDS ordinations of relative density (stress = 0.130; left column) and relative basal area (stress = 0.218; right column) attributed to each of nine diameter classes in 97 plots located in lower and upper montane forests of Yosemite and Sequoia & Kings Canyon National Parks. Linear color gradients represent the relative values of elevation, PET, AET, and Deficit associated with each plot. PET, AET, and Deficit are only shown for plots from Yosemite; plots from Sequoia are represented by white circles. Elevation ranged from 1,338 to 2,705 m; PET ranged from 304 to 710 mm; AET ranged from 211 to 453 mm; Deficit ranged from 72 to 361 mm. Diameter classes are defined in Table 1.3.

Diameter distributions

Diameter distributions of density showed distinct differences between burned and unburned populations (Figure 2.4). A reverse-J distribution characterized median density of unburned, while a uniform distribution characterized median density of burned plots (Figure 2.4, upper panels). In contrast, diameter distributions of basal area displayed similar patterns regardless of burn status. Among both burned and unburned plots, the maximum basal area associated with each diameter class was higher among the larger diameter classes, while median basal area was bimodal and peaked at DC4 and DC7 (Figure 2.4, lower panels). Burned and unburned populations of density and basal area differed for DC1 and DC2 (p <0.01; Table 2.2).

Fire and structural composition

Structural communities were more sensitive to recent fire occurrence when defined by relative density than by relative basal area (Figure 2.5 A and B). Unburned plots were more concentrated near DC1 in the ordination of relative density, while burned plots were the sole occupants of a curved, vertical band that paralleled the oblong cluster of larger diameter classes and sat opposite the DC1 centroid. Therefore, while similar patterns of relative density characterized many plots regardless of burn status, fire occurrence shifted the range of variability away from the smallest diameter class (Figure 2.5 A). In contrast, burned and unburned plots were evenly distributed throughout the ordination of relative basal area (Figure 2.5 B). Among burned plots, no relationships emerged between structural communities, number of fires, and RdNBR (Figure 2.5 C, D, E, and F).

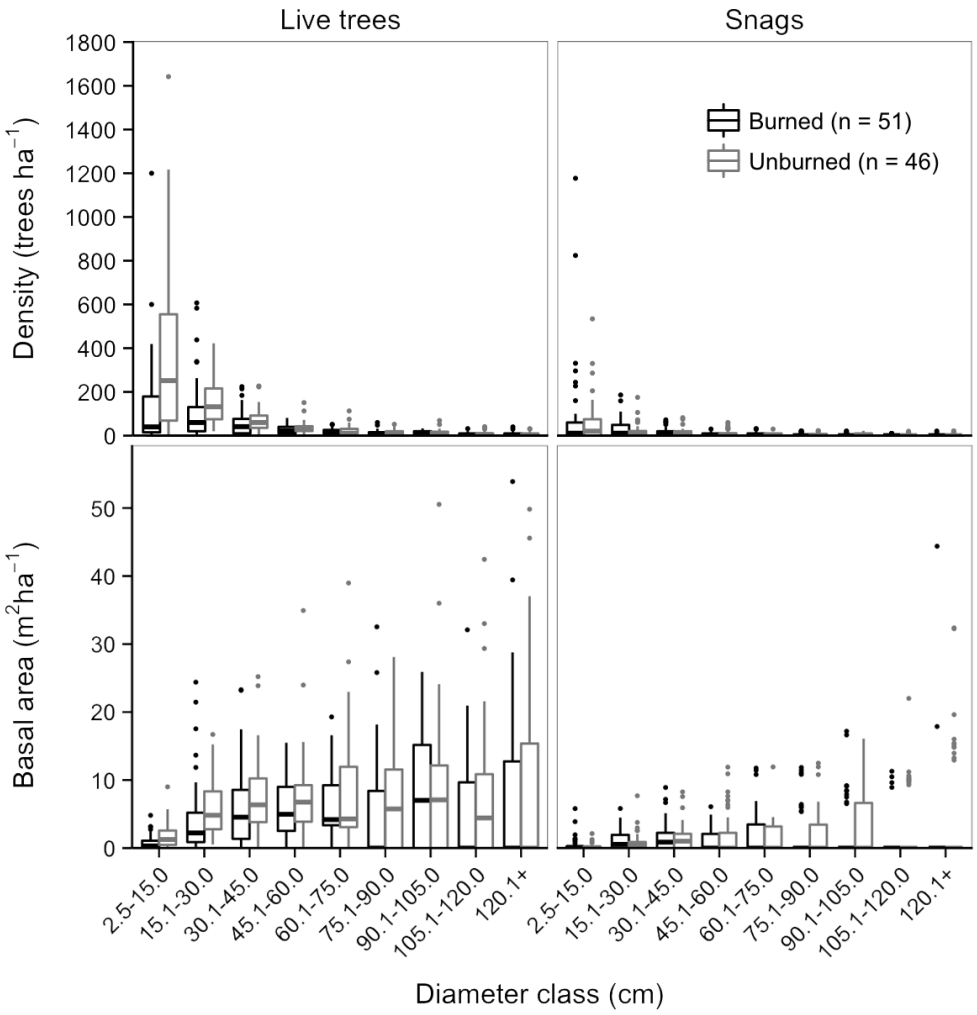

Figure 2.4. Diameter distributions by density and basal area of all stems >2.5 cm dbh from 97 plots located in lower and upper montane forests of Yosemite and Sequoia & Kings Canyon National Parks. The distribution of density by diameter class is depicted in the upper panels; distribution of basal area by diameter class is depicted in the lower panels.

Table 2.2. Mann Whitney *U* tests compared burned and unburned populations of nine diameter classes for 97 montane forest plots in Yosemite and Sequoia & Kings Canyon National Parks; *p*-values <0.05 are bolded. Diameter classes are defined in Table 1.3.

	DC1	DC2	DC3	DC4	DC5	DC6	DC7	DC8	DC9
Density	**<0.001**	**0.001**	0.071	**0.044**	0.514	0.091	0.631	0.266	0.411
Basal area	**<0.001**	**0.003**	0.074	0.077	0.511	0.106	0.719	0.206	0.284

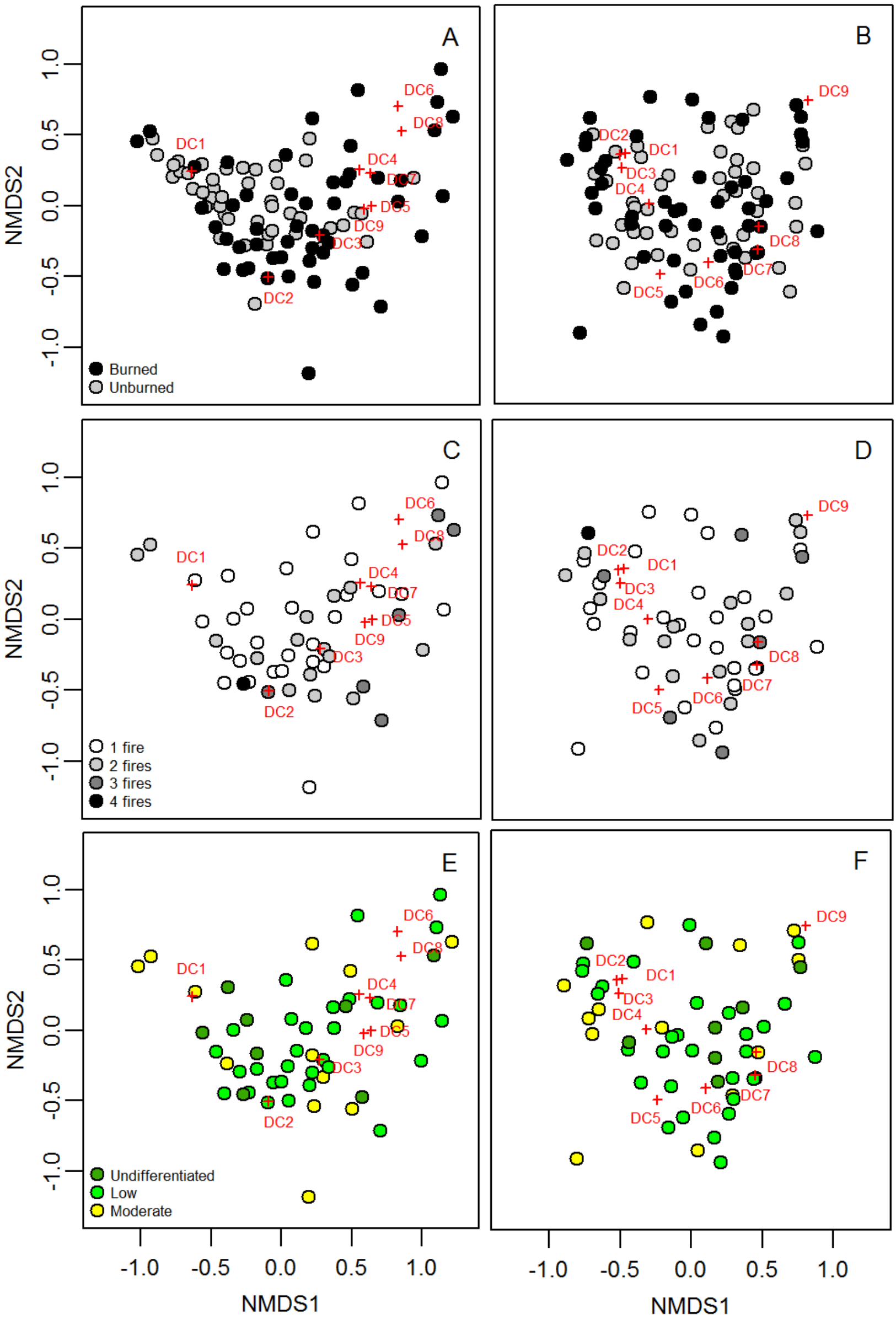

Figure 2.5. Distribution of burned and unburned plots, number of fires, and fire severity across NMDS ordinations of relative density (stress = 0.130; left column) and relative basal area (stress = 0.218; right column) attributed to each of nine diameter classes in 97 plots located in lower and upper montane forests of Yosemite and Sequoia & Kings Canyon National Parks. Plots are colored by burn status (A and B), number of fires since 1946 (C and D), and RdNBR of the most recent fire (E and F). Only burned plots are shown in C, D, E, and F. Diameter classes are defined in Table 1.3.

DISCUSSION

Structural composition

Ordination of the relative density and basal area attributed to each diameter class improved upon traditional methods of landscape-scale structural analysis. Previous approaches have used diameter distribution means to express forest structure, averaging plots together that represent the same forest type (Lutz et al. 2009a), burn status (Collins et al. 2011), or time of measurement (Collins et al. 2011; Scholl and Taylor 2010; Lutz et al. 2009a). While such methods may be useful for establishing structural norms, they ignore variability among sites. When structural variability has been of interest, studies have limited their scope by assessing one diameter class at a time (Figure 2.5; Collins et al. 2011; Lutz et al. 2009a), which ignores patterns of co-occurrence among diameter classes. Because these approaches obscure the diameter distributions of each site, they limit the type of research questions that can be addressed. Ordination, in contrast, includes the diameter distribution of each site as an individual entity while combining complex data structures into a single interpretable figure. The ordinations in this study simultaneously displayed structural norms, variability among plots, and detailed accounts of diameter class assemblage.

Abundance trends and structural composition

Overlaying total density and total basal area on ordinations of relative density and basal area revealed important points of intersection between two distinct approaches of quantifying forest structure: that which analyzes between-plot patterns (total density and basal area) and that which analyzes within-plot patterns (relative density and relative basal area; Figure 2.2 C, D, E, and F, Table 2.1). The strong correlation between total density and relative density suggested that sites with higher or lower density tended to have particular within-plot density

configurations (Figure 2.2 C). The highest total densities, for instance, were contingent upon DC1 representing a large proportion of relative density; due to physical spacing requirements between boles and limits to crown plasticity and resource availability, no other diameter class could attain the high-density extremes of DC1. However, a high proportion of density in DC1 did not necessarily equate to high total density; such a scenario could represent a sparsely populated site with a few small trees. This incongruence between total and relative density could explain the midrange total density of the sites associated with more negative NMDS axis 1 values than the DC1 centroid (Figure 2.2 C).

In contrast, the relationship between total and relative basal area was not as pronounced (Figure 2.2 F). This is likely because high total basal area is primarily driven by the presence of a few large individuals. The large-diameter contingent could, however, comprise six large-diameter trees (~90 cm dbh) or three very large-diameter trees (~120 cm dbh). Because these abundances are low, there are more ways in which a large total basal area could be distributed among the larger diameter classes.

Structural composition and fire response of forest alliances

Ordinations of relative density and relative basal area presented structural communities from separate perspectives and were therefore most descriptive in combination (Figure 2.2 A and B). Relative density ordinations emphasized the widespread prevalence of DC1 in *P. ponderosa-C. decurrens* and *A. concolor-P. lambertiana* forests, while relative basal area ordinations indicated that some of these sites also included large-diameter individuals (Figure 2.2 A and B). Conversely, some *P. jeffreyi* and *A. magnifica* sites were located near DC1 in the relative density ordination, while none were in the relative basal area ordination, reflecting the presence of large-diameter trees in all plots but the presence of small-diameter trees only in some (Figure 2.2 A

and B). In contrast, *A. magnifica-A. concolor* and *P. contorta* sites expressed similar patterns in both ordinations, suggesting that the same diameter classes dominated density as well as basal area (Figure 2.2 A and B). *A. magnifica-A. concolor* sites were spatially removed from DC1 in both ordinations, indicating that both density and basal area were dominated by the larger diameter classes; *P. contorta* sites were located near DC1, DC2, and DC3 in both ordinations, reflecting that these diameter classes figured prominently in both tree density and basal area.

The structural communities associated with each forest alliance corresponded with previous characterizations of structure and may explain differential effects of lower-severity fire among alliances. High density of small-diameter, shade-tolerant *C. decurrens* and *A. concolor* has been consistently observed in lower montane *P. ponderosa-C. decurrens* and *A. concolor-P. lambertiana* forests, potentially driving the position of these sites toward the DC1 centroid in the relative density ordination; the same studies showed that large-diameter trees were less abundant, increasing the probability that a 0.1 ha sample plot could include few or none and corroborating the result of this study that large-diameter trees occurred at some sites (Scholl and Taylor 2010; Lutz et al. 2009a). Unsurprisingly, fire-induced mortality of small-diameter trees was primarily evident in *P. ponderosa-C. decurrens* and *A. concolor-P. lambertiana* forests, where suppressed, shade-tolerant trees are typically abundant (Figure 2.2 A).

Similarly, the even distribution of *P. jeffreyi* sites across the gradient of structural composition was unsurprising, given that *P. jeffreyi* occupies productive sites where it coexists with *A. concolor*, and dry, rocky sites where other species cannot survive (Fites-Kaufman et al. 2007). At seemingly inhospitable sites, *P. jeffreyi* can root deeply into fissures and attain large size (Hubbert et al. 2001). In these locations regeneration is practically non-existent, enabling large-diameter stems to dominate both density and basal area. The wide range of environmental

conditions under which *P. jeffreyi* forests persist was captured in this dataset. Both low (72 mm) and high (361 mm) Deficit extremes occurred at *P. jeffreyi* sites, which, in turn, reflected this variability in their species complements and structural expression. Some sites contained both small-diameter, shade-tolerant constituents and larger trees, while others included just large-diameter individuals. Relative basal area and density configurations varied widely among *P. jeffreyi* stands regardless of burn status, indicating that variability in stand structure due to fire may nest within a broader framework of variability in stand structure due to physical site characteristics.

Although *A. magnifica* exhibited a similar structural trend to *P. jeffreyi* sites, the mechanisms differed. In *A. magnifica* stands, heavy snow loading and high wind speeds across the snow surface often preclude the development of a subcanopy tree layer (Parker 1986a; Oosting and Billings 1943). These data include some instances of minimal or suppressed regeneration as well as some sites where large- and small-diameter individuals coexist. Interestingly, however, lower-severity fire at these sites was not associated with reductions in small-diameter trees. This indicates that some of the fires may have skipped patches within their perimeters, an inference that is supported by the low mean RdNBR of 79 (Table 1.5).

At *P. contorta* sites, in contrast, the smaller diameter classes contained the majority of the basal area and density. Parker (1986b) sampled four *P. contorta* stands in a similar elevational range that were characterized by a reverse-J diameter distribution and strongly dominated by individuals <5 cm dbh. While Parker's sites would have overlapped with the *P. contorta* sites of this study in the relative density ordination, their position in the relative basal area ordination may have differed considerably, given that the maximum dbh ranged from 70 to 115 cm (D5 to DC8 in this study). The smaller diameters at *P. contorta* sites in this study (maximum dbh 63.1

cm) could be due to stand age or physical site attributes. Strong age-diameter relationships identified by Parker (1986b) suggest that the stands in this dataset may have primarily included individuals <150 years old. Alternatively, these plots could disproportionately represent the subset of *P. contorta* stands that occupies marginal sites where both productivity and annual growth are low, resulting in populations of small stature (Fites-Kaufman et al. 2007). This second hypothesis is supported by the widespread survival of small-diameter trees at burned sites. Low fuel abundance could have caused fire in these areas to burn at such low intensity that fire-related mortality was negligible.

Biophysical variables and structural composition

Only ordinations of relative density demonstrated any relationship to biophysical variables (Figure 2.4). Evidence of this relationship was confined to the concentration of the low elevation and high AET and Deficit extremes near the DC1 centroid. This suggests a link between high AET and Deficit and the presence of shade-tolerant *A. concolor* and *C. decurrens*. However, some sites near DC1 were characterized by low AET and Deficit and represented stands dominated by *A. magnifica* and *P. contorta* where small-diameter trees were prevalent (Figure 2.2 A). Another contributor to the weak relationship may have been that fire effects confounded biophysical effects on structural communities. Recent fire occurrence shifted the positions of burned plots away from DC1, while unburned plots remained near DC1, regardless of whether these sites were characterized by identical biophysical properties (Figure 2.5 A and B).

The weak relationships between structural composition and biophysical variables indicate that lower and upper montane forests represented a similar range of structural communities. Of

particular interest is that the prevalence of large-diameter trees was not confined to either lower or upper montane species or environments.

Fire and structural composition

Occurrence of lower-severity fire reduced tree density and basal area among stems <30.0 cm dbh (Figure 2.5; Table 2.2). These findings corroborate numerous studies that have documented fire-induced mortality of small-diameter trees. van Mantgem et al. (2011) found that prescribed fire reduced tree density by 67% but biomass by just 32% in an *A. concolor-P. lambertiana* forest. Similarly, Schwilk et al. (2006) reported higher rates of mortality in mixed-conifer forest among stems 10-40 cm dbh than among stems >40 cm dbh due to the immediate effects of prescribed fire and subsequent beetle attack. A regional analysis of *Pinus* and *Abies* further demonstrated that prescribed fire proportionately increased greater mortality of small-diameter trees (van Mantgem et al. 2013). Kane et al. (2013) used LiDAR to compare structural attributes of mixed-conifer forests in Yosemite National Park and found that unburned *A. magnifica* sites evenly represented four structural classes: sparse cover, shorter canopy cover, multistory canopy cover, and top story cover; similar sites burned at low to moderate severity primarily occupied the sparse cover and top story categories, indicating that fire had potentially reduced the density of understory trees.

Although both density and basal area of stems <30.0 cm dbh were affected by fire, the impact on structural composition was only apparent when structural communities were characterized by relative density. In the relative density ordination DC1 and DC2 were associated with a high concentration of unburned sites (Figure 2.5 A). In contrast, unburned sites were not clustered around DC1 and DC2 in the ordination of relative basal area. This suggests that lower-severity fire is effective at altering structure in the density dimension by reducing the

abundance of small diameter trees, while structural communities as defined by basal area are conserved.

Fire severity and multiple fires

Relationships between structural composition, RdNBR, and number of fires were tenuous, if not entirely nonexistent (Figure 2.5 B, C, D, and E). The disconnect between structural communities and RdNBR could reflect (1) limitations of the RdNBR metric, or (2) error stemming from how plot RdNBR was calculated. RdNBR is considered a useful metric of fire severity because it correlates with the Composite Burn Index, which measures both tree-related and non-tree-related fire effects and combines them into a single index (Miller and Thode 2007; Key 2006); while I was primarily interested in fire effects on trees, RdNBR assesses fire severity at a coarser resolution (Miller et al. 2009). Alternatively, RdNBR values could have under- or overestimated fire severity because they represented the mean RdNBR of the hectare surrounding each plot. It is possible that some plots experienced undifferentiated severity but were assigned higher values due to higher-severity fire in adjacent areas or vice versa. However, even if the RdNBR values were representative, undifferentiated severity, which characterized eight sites, could correspond to any of several circumstances: (1) a subcanopy burn, (2) a very light homogeneous burn, or (3) vegetation at the site actually remained unburned (Kolden et al. 2012). The effects of a subcanopy burn of undifferentiated severity could be equivalent to a low-severity burn; similarly, a low-severity burn in an area of dense canopy could be equivalent to a moderate-severity burn in a more open forest.

Number of fires also did not appear to influence structural communities. Given that previous fire occurrence can lead to a 90% reduction in subsequent fire size, allegedly reburned sites could have remained undisturbed despite their residence within fire perimeters (Scholl and

Taylor 2010). Alternatively, multiple fires may not have affected structure because trees that survived one fire would be likely to survive subsequent fires due to fuel reduction, consistent or increasing bark thickness, and unchanging microtopography.

Conclusions

This study examined forest structure from three perspectives: (1) the sum of structural elements expressed in basal area and stem density, (2) the relative proportion of diameter classes, and (3) the individual diameter class. High variability characterized each of these attributes of forest structure. Similar structural communities extended throughout lower and upper montane forests and were not a product of biophysical parameters. Lower-severity fire exclusively impacted the smaller diameter classes, altering the structural community as represented by density but not basal area. Therefore, conservation of forest structure as described by basal area could be maintained with fire into the future, irrespective of species compositional shifts. If conservation of forest structure is a management goal, the range of disturbances that affect the structural communities – not just fire – should be included in assessment and monitoring.

ACKNOWLEDGEMENTS

This work was made possible by funding from the Byron and Alice Lockwood Endowed Fellowship and the National Park Service.

I am grateful to my advisor, Jim Lutz, and my committee chair, Greg Ettl, for guidance, mentorship, and support throughout this project. I appreciate the involvement of Don McKenzie, who served on my committee and contributed to additional learning during this process. I thank Gus Smith, the Yosemite Fire Ecologist, for his direction during data collection; I am appreciative of the expertise and leadership of the field crew he assembled: Justin Romanowitz, who organized the logistics of data collection, Tim Martel, and Kevin Song. Additionally, I am indebted to the members of the Sustainable Forestry Lab and the Fire and Mountain Ecology Lab for their friendship and advice. Lastly, I would like to recognize Sean Jeronimo, who provided counsel at key moments and kept morale high.

REFERENCES

Agee, J.K. 1993. Fire Ecology of Pacific Northwest Forests. Island Press, Washington D.C..

Allen, C.D., A. Macalady, H. Chenchouni, D. Bachelet, N. McDowell, M. Vennetier, P. Gonzales, T. Hogg, A. Rigling, D. Breshears, et al. 2010. A global overview of drought and heat-induced tree mortality reveals emerging climate change risks for forests. Forest Ecology and Management **259**: 660–684.

Beaty, R.M., and A.H. Taylor. 2007. Fire disturbance and forest structure in old-growth mixed conifer forests in the northern Sierra Nevada, California. Journal of Vegetation Science **18**: 879-890.

Bekker, M.F., and A.H. Taylor. 2010. Fire disturbance, forest structure, and stand dynamics in montane forests of the southern Cascades, Thousand Lakes Wilderness, California USA. Ecoscience **17**: 59-72.

Caprio, A.C., and T.W. Swetnam. 1995. Historic fire regimes along an elevational gradient on the west slope of the Sierra Nevada, California. Proceedings of the Symposium on Fire in Wilderness and Park Management. USDA Forest Service General Technical Report INT-GTR-320, Missoula, Montana.

Collins, B.M., R.G. Everett, and S.L. Stephens. 2011. Impacts of fire exclusion and recent managed fire on forest structure in old growth Sierra Nevada mixed-conifer forests. Ecosphere **2**: art51.

Curtis, J.T., and R.P. McIntosh. 1951. An upland forest continuum in the prairie-forest border region of Wisconsin. Ecology **32**: 476-496.

Das, A.J., N.L. Stephenson, A. Flint, T. Das, and P.J. van Mantgem. 2013. Climatic correlates of tree mortality in water- and energy-limited forests. PLoS ONE 8(7): e69917.

Eidenshink, J., B. Schwind, K. Brewer, Z. Zhu, B. Quayle, and S. Howard. 2007. A project for monitoring trends in burn severity. Fire Ecology **3**: 3-21.

Faith, D.P., P.R. Minchin, and L. Belbin. 1987. Compositional dissimilarity as a robust measure of ecological distance. Vegetatio **69**: 57-68.

Fellows, A.W., and M.L. Goulden. 2008. Has fire suppression increased the amount of carbon stored in western U.S. forests? Geophysical Research Letters **35**: L12404, doi:10.1029/2008GL033965.

Fites-Kaufman, J., P. Rundel, N. Stephenson, and D.A. Weixelman. 2007. Montane and subalpine vegetation of the Sierra Nevada and Cascade Ranges. Pages 456-501 *in* M. Barbour, T. Keeler-Wolf, and A. A. Schoenherr, editors. Terrestrial Vegetation of California. University of California Press, Berkeley, California.

Flora of North America Editorial Committee. 1993-2007. Flora of North America. Oxford University Press, New York, New York.

Franklin, J.F., T.A. Spies, R. Van Pelt, A.B. Carey, D.A. Thornburgh, D.R. Berg, D.B. Lindenmayer, M.E. Harmon, W.S. Keeton, D.C. Shaw, K. Bible, and J.Q. Chen. 2002. Disturbances and structural development of natural forest ecosys- tems with silvicultural implications, using Douglas-fir forests as an example. For. Ecol. Manage. **155**: 399–423.

Hubbert, K.R., J.L. Beyers, and R.C. Graham. 2001. Roles of weathered bedrock and soil in seasonal water relations of *Pinus jeffreyi* and *Arctostaphylos patula*. Canadian Journal of Forest Research **31**: 1947-1957.

Intergovernmental Panel on Climate Change (IPCC). 2007. Climate Change 2007: The Scientific Basis. Contribution of Working Group I to the Fourth Assessment Report of the

Intergovernmental Panel on Climate Change [Solomon, S., D. Qin, M. Manning, Z. Chen, M. Marquis, K.B. Averyt, M. Tignor, and H.L. Miller (eds.)]. Cambridge University Press, Cambridge, United Kingdom and New York, NY, USA.

Iverson, L.R., and D. McKenzie. 2013. Tree-species range shifts in a changing climate: detecting, modeling, assisting. Landscape Ecology **28**:879–889.

Johnstone, J.F., T.S. Rupp, M. Olson, and D. Verbyla. 2011. Modeling impacts of fire severity on successional trajectories and future fire behavior in Alaskan boreal forests. Landscape Ecology **26**: 487-500.

Kane, V.R., J.A. Lutz, S.L. Roberts, D.F. Smith, R.J. McGaughey, N.A. Povak, and M.L. Brooks. 2013. Landscape-scale effects of fire severity on mixed-conifer and red fir forest structure in Yosemite National Park. Forest Ecology and Management **287**: 17-31.

Kane, V.R., R. McGaughey, J.D. Bakker, R. Gersonde, J.A. Lutz, and J.F. Franklin. 2010. Comparisons between field– and LiDAR-based measures of stand structural complexity. Canadian Journal of Forest Research **40**: 761-773.

Kane, V.R., M. North, J.A. Lutz, D. Churchill, S.L. Roberts, D.F. Smith, R.J. McGaughey, J.T. Kane, and M.L. Brooks. In press. Assessing fire-mediated change to forest spatial structure using a fusion of Landsat and airborne LiDAR data in Yosemite National Park. Remote Sensing of Environment.

Keeler-Wolf, T., P.E. Moore, E.T. Reyes, J.M. Menke, D.N. Johnson, and D.L. Karavides. 2012. Yosemite National Park Vegetation Classification and Mapping Project Report. Natural Resource Report NPS/YOSE/NRTR-2012/598. National Park Service Fort Collins, Colorado.

Key, C.H. 2006. Ecological and sampling constraints on defining landscape fire severity. Fire Ecology **2**: 34-59.

Key, C.H., and N.C. Benson. 2006. Landscape Assessment: Ground measure of severity, the Composite Burn Index, and remote sensing of severity, the Normalized Burn Ratio. In: D.C. Lutes, R.E. Keane, J.F. Caratti, C.H. Key, N.C. Benson, S. Sutherland, and L.J. Gangi. 2005. FIREMON: Fire Effects Monitoring and Inventory System. USDA Forest Service, Rocky Mountain Research Station, Ogden, UT. Gen. Tech. Rep. RMRS-GTR-164-CD: LA1-51.

Kilgore, B.M., and G.S. Briggs. 1972. Restoring fire to high elevation forests in California. J. Forestry **70**: 266-271.

Klyver, F.D. 1931. Major Plant Communities in a Transect of the Sierra Nevada Mountains of California. Ecology **12**: 1-17.

Kobe, R.K., S.W. Pacala, J.A. Silander, Jr., and C.D. Canham. 1995. Juvenile tree survivorship as a component of shade tolerance. Ecological Applications **5**: 517-532.

Kolden, C.A., J.A. Lutz, C.H. Key, J.T. Kane, and J.W. van Wagtendonk. 2012. Mapped versus actual burned area within wildfire perimeters: Characterizing the unburned. Forest Ecology and Management **286**: 38-47.

Lindenmayer, D.B., W.F. Laurence, and J.F. Franklin. 2012. Global decline in large old trees. Science **338**: 1305-1306.

Littell, J.S., D. McKenzie, D.L. Peterson, and A.L. Westerling. 2009. Climate and wildfire area burned in western U.S. ecoprovinces, 1916-2003. Ecological Applications **19**: 1003-1021.

Logan, J.A., W.W. Macfarlane, and L. Willcox. 2010. Whitebark pine vulnerability to climate change induced mountain pine beetle disturbance in the Greater Yellowstone Ecosystem. Ecological Applications **20**: 895-902.

Lutz, J.A., A.J. Larson, J.A. Freund, M.E. Swanson, and K.J. Bible. 2013. The ecological importance of large-diameter trees to forest structural heterogeneity. PLoS ONE **8**: e82784. doi: http://dx.plos.org/10.1371/journal.pone.0082784.

Lutz, J.A., A.J. Larson, M.E. Swanson, and J.A. Freund. 2012. Ecological importance of large-diameter trees in a temperate mixed-conifer forest. PLoS ONE **7**: e36131. doi: 10.1371/journal.pone.0036131.

Lutz, J.A., C.H. Key, C.A. Kolden, J.T. Kane, and J.W. van Wagtendonk. 2011. Fire frequency, area burned, and severity: A quantitative approach to defining normal fire year. Fire Ecology **7**: 51-65.

Lutz, J.A., J.W. van Wagtendonk, and J.F. Franklin. 2009a. Twentieth-century decline of large-diameter trees in Yosemite National Park, California, USA. Forest Ecology and Management **257**: 2296-2307.

Lutz, J.A., J.W. van Wagtendonk, and J.F. Franklin. 2010. Climatic water deficit, tree species ranges, and climate change in Yosemite National Park. Journal of Biogeography **37**: 936-950.

Lutz, J.A., J.W. van Wagtendonk, A.E. Thode, J.D. Miller, and J.F. Franklin. 2009b. Climate, lightning ignitions, and fire severity in Yosemite National Park, California, USA. International Journal of Wildland Fire **18**: 765-774.

Marks, P.L., and F.H. Bormann. 1972. Revegetation following forest cutting: mechanisms for return to steadystate nutrient cycling. Science **176**: 914–915.

McCune, B., and J.B. Grace. 2002. Analysis of Ecological Communities. MjM Software Design, Gleneden Beach, OR.

McKenzie, D., D.W. Peterson, D.L. Peterson, and P.E. Thornton. 2003. Climatic and biophysical controls on conifer species distributions in mountain forests of Washington State, USA. Journal of Biogeography **30**: 1093-1108.

McKenzie, D., Z. Gedalof, D.L. Peterson, and P. Mote. 2004. Climatic change, wildfire, and conservation. Conservation Biology **18**: 890-902.

Miller, J.D., and A.E. Thode. 2007. Quantifying burn severity in a heterogeneous landscape with a relative version of the delta Normalized Burn Ratio (dNBR). Remote Sensing of Environment **109**: 66-80.

Miller, J.D., B.M. Collins, J.A. Lutz, S.L. Stephens, J.W. van Wagtendonk, and D.A. Yasuda. 2012a. Differences in wildfires among ecoregions and land management agencies in the Sierra Nevada region, California, USA. Ecosphere **3**: art80.

Miller, J.D., C.N. Skinner, H.D. Safford, E.E. Knapp, and C.M. Ramirez. 2012b. Trends and causes of severity, size, and number of fires in northwestern California, USA. Ecological Applications **22**: 184–203.

Miller, J.D., E.E. Knapp, C.H. Key, C.N. Skinner, C.J. Isbell, R.M. Creasy, and J.W. Sherlock. 2009. Calibration and validation of the relative differenced Normalized Burn Ratio (RdNBR) to three measures of fire severity in the Sierra Nevada and Klamath Mountains, California, USA. Remote Sensing of Environment 113: 645-656.

National Wildfire Coordination Group. 2007. Glossary of wildland fire terminology. US National Wildfire Coordination Group Report PMS-205 (Ogden, UT).

North, M., J. Innes, and H. Zald. 2007. Comparison of thinning and prescribed fire restoration treatments to Sierran mixed-conifer historic conditions. Canadian Journal of Forest Research **37**: 331-342.

Oksanen, J., F.G. Blanchet, R. Kindt, P. Legendre, P.R. Minchin, R.B. O'Hara, G.L. Simpson, P. Solymos, M.H. Stevens, and H. Wagner. 2013. vegan: Community Ecology Package. R package version 2.0-10. http://CRAN.R-project.org/package=vegan.

Oosting, H.J., and W.D. Billings. 1943. The Red Fir Forest of the Sierra Nevada: Abietum Magnificae. Ecological Monographs **13**: 259–274.

Pacala, S.W., and D.H. Deutschman. 1995. Details that matter: the spatial distribution of individual trees maintains forest ecosystem function. Oikos **74**: 357-365.

Parker, A.J. 1982. Environmental and compositional ordinations of conifer forests in Yosemite National Park, California. Madroño **29**: 109-118.

Parker, A.J. 1984. Mixed forests of red fir and white fir in Yosemite National Park, California. American Midland Naturalist **112**: 15-23.

Parker, A.J. 1986a. Environmental and historical factors affecting red and white fir regeneration in ecotonal forests. Forest Science **32**: 339-347.

Parker, A.J. 1986b. Persistence of lodgepole pine forests in the central Sierra Nevada. Ecology **67**: 1560-1567.

Parker, A.J. 1989. Forest/environment relationships in Yosemite National Park, California, United States. Vegetation **82**: 41-54.

Parsons, D.J., and S.H. Debenedetti. 1979. Impact of fire suppression on a mixed-conifer forest. Forest Ecology and Management **2**: 21-33.

Peet, R.K. 1981. Changes in biomass and production during secondary forest succession. Pages 324–338 in D.C. West, H.H. Shugart, and D.B. Botkin, editors. Forest succession. Springer-Verlag, New York, New York, USA.

PRISM. 2012. Climatological Normals, 1971-2000. The PRISM Group, Oregon State University.

R Development Core Team. 2013. R: A language and environment for statistical computing. R Foundation for Statistical Computing, Vienna, Austria. ISBN 3-900051-07-0, URL http://www.R-project.org/.

Scholl, A.E., and A.H. Taylor. 2010. Fire regimes, forest change, and self-organization in an old-growth mixed-conifer forest, Yosemite National Park, USA. Ecological Applications **20**: 362-380.

Schwilk, D.W., E.E. Knapp, S.M. Ferrenberg, J.E. Keeley, and A.C. Caprio. 2006. Tree mortality from fire and bark beetles following early and late season prescribed fires in a Sierra Nevada mixed-conifer forest. Forest Ecology and Management **232**: 36-45.

Sequoia and Kings Canyon National Parks Photo Interpretation Report. 2007. USGS-NPS Vegetation Mapping Program. Environmental Systems Research Institute, Inc. Redlands, CA.

Shugart, H.H., D.C. West, and W.R. Emanuel. 1981. Patterns and dynamics of forests: an application of simulation models. Pages 74–94 in D. C. West, H. H. Shugart, and D. B. Botkin, editors. Forest succession. Springer-Verlag, New York, New York, USA.

Stephenson, N.L. 1990. Climatic control of vegetation distribution - the role of the water balance. American Naturalist **135**: 649-670.

Stephenson, N.L. 1998. Actual evapotranspiration and deficit: biologically meaningful correlates of vegetation distribution across spatial scales. Journal of Biogeography **25**: 855-870.

Stephenson, N.L., A.J. Das, R. Condit, S.E. Russo, P.J. Baker, et al. 2014. Rate of tree carbon accumulation increases continuously with tree size. Nature 10.1038/nature12914.

Sugihara, N.G., J.W. van Wagtendonk, and J. Fites-Kaufman. 2006. Fire as an ecological process. Pages 58-74 *in* N.G. Sugihara, J.W. van Wagtendonk, K.E. Shaffer, J. Fites-Kaufman, and A.E. Thode, editors. Fire in California's Ecosystems. University of California Press, Berkeley, California.

Taylor, A., and C.B. Halpern. 1991. The structure and dynamics of *Abies magnifica* forests in the southern Cascade Range, USA. Journal of Vegetation Science **2**:180-200.

Thode, A.E., J.W. van Wagtendonk, J.D. Miller, and J.F. Quinn. 2011. Quantifying the fire regime distributions of severity in Yosemite National Park, California, USA. International Journal of Wildland Fire **20**: 223-239.

Van Cleve, K., and L.A. Viereck. 1981. Forest succession in relation to nutrient cycling in the boreal forest of Alaska. Pages 185-211 in D. C. West, H. H. Shugart, and D. B. Botkin, editors. Forest succession. Springer-Verlag, New York, New York, USA.

van Mantgem, P.J., N.L. Stephenson, E. Knapp, J. Battles, and J.E. Keeley. 2011. Long-term effects of prescribed fire on mixed conifer forest structure in the Sierra Nevada, California. Forest Ecology and Management **261**: 989-994.

van Mantgem, P.J., J.C.B. Nesmith, M. Keifer, and M. Brooks. 2013. Tree mortality patterns following prescribed fire for *Pinus* and *Abies* across the southwestern United States. Forest Ecology and Management **289**: 463-469.

van Wagtendonk, J.W. 1994. Spatial patterns of lightning strikes and fires in Yosemite National Park. Proceedings of the 12th Conference on Fire and Forest Meteorology **12**: 223-231.

van Wagtendonk, J.W. Fire as a physical process. 2006. Pages 38-57 in: N.G. Sugihara, J.W. van Wagtendonk, J. Fites-Kaufman, K.E. Shaffer, and A.E. Thode (eds.). Fire in California's ecosystems. University of California Press, Berkeley.

van Wagtendonk, J.W. 2007. The history and evolution of wildland fire use. Fire Ecology **3**: 3-17.

van Wagtendonk, J.W., and J. Fites-Kaufman. 2006. Sierra Nevada bioregion. Pages 264-294 *in* N.G. Sugihara, J.W. van Wagtendonk, K.E. Shaffer, J. Fites-Kaufman, and A.E. Thode, editors. Fire in California's Ecosystems. University of California Press, Berkeley, California.

van Wagtendonk, J.W., and J.A. Lutz. 2007. Fire regime attributes of wildland fires in Yosemite National Park, USA. Fire Ecology **3**: 34-52.

van Wagtendonk, J.W., K.A. van Wagtendonk, and A.E. Thode. 2012. Factors associated with the severity of intersecting fires in Yosemite National Park, California, USA. Fire Ecology **8**: 11-31.

Vankat, J.L. 1982. A gradient perspective on the vegetation of Sequoia National Park, California. Madroño **29**: 200-214.

Vankat, J.L., and J. Major. 1978. Vegetation changes in Sequoia National Park, California. Journal of Biogeography **5**: 377-402.

Webster, K.M., and C.B. Halpern. 2010. Long-term vegetation responses to reintroduction and repeated use of fire in mixed-conifer forests of the Sierra Nevada. Ecosphere **1**: art9.

Westerling, A.L., H.G. Hidalgo, D.R. Cayan, and T.W. Swetnam. 2006. Warming and earlier spring increase western US forest wildfire activity. Science **313**: 940-943.

APPENDIX I: TREE AND SHRUB SPECIES

Table A.1. Tree species present in 97 plots located in lower and upper montane forests of Yosemite and Sequoia & Kings Canyon National Parks. Nomenclature follows *Flora of North America Editorial Committee, eds.*.

Tree species	Species code	Family	Common name
Conifers			
Abies concolor	ABCO	Pinaceae	white fir
Abies magnifica	ABMA	Pinaceae	red fir
Calocedrus decurrens	CADE	Cupressaceae	incense-cedar
Juniperus occidentalis var. *australis*	JUOC	Cupressaceae	Western juniper
Pinus contorta var. *murrayana*	PICO	Pinaceae	Sierra lodgepole pine
Pinus jeffreyi	PIJE	Pinaceae	Jeffrey pine
Pinus lambertiana	PILA	Pinaceae	sugar pine
Pinus monticola	PIMO	Pinaceae	Western white pine
Pinus ponderosa	PIPO	Pinaceae	ponderosa pine
Pseudotsuga menziesii	PSME	Pinaceae	Douglas-fir
Tsuga mertensiana	TSME	Pinaceae	mountain hemlock
Hardwoods			
Cornus nuttallii	CONU	Cornaceae	Pacific dogwood
Quercus chrysolepis	QUCH	Fagaceae	canyon live oak
Quercus kelloggii	QUKE	Fagaceae	California black oak

Table A.2. Shrub species present in 97 plots located in lower and upper montane forests of Yosemite and Sequoia & Kings Canyon National Parks. Nomenclature follows *Flora of North America Editorial Committee, eds.*.

Shrub species	Species code	Family	Common name
Alnus spp.	ALSP	Betulaceae	alder
Arctostaphylos patula	ARPA	Ericaceae	greenleaf manzanita
Ceanothus cordulatus	CECO	Rhamnaceae	mountain whitethorn
Ceanothus integerrimus	CEIN	Rhamnaceae	deer brush
Ceanothus parvifolius	CEPA	Rhamnaceae	littleleaf ceanothus
Chamaebatia foliolosa	CHFO	Rosaceae	mountain misery
Chrysolepis sempervirens	CHSE	Fagaceae	bush chinquapin
Cornus nuttallii	CONU	Cornaceae	Pacific dogwood
Prunus emarginata	PREM	Rosaceae	bitter cherry
Prunus virginiana	PRVI	Rosaceae	chokecherry
Quercus chrysolepis	QUCH	Fagaceae	canyon live oak
Quercus spp.	QUSP	Fagaceae	oak
Ribes nevadense	RINE	Grossulariaceae	Sierra currant
Ribes roezlii	RIRO	Grossulariaceae	Sierra gooseberry

Table A.3. Prevalence of shrub species among 97 plots located in lower and upper montane forests of Yosemite and Sequoia & Kings Canyon National Parks. Species are ordered firstly by overall frequency of occurrence and secondly by overall total cover.

Shrub species	Frequency of occurrence		Total cover (m^2)	
	Burned	Unburned	Burned	Unburned
ARPA	16	8	820	1979
CECO	16	2	1469	201
CHSE	9	5	303	726
CHFO	10	3	4948	1133
RIRO	5	1	85	25
QUSP	1	1	294	268
QUCH	0	2	0	286
PREM	1	78	10	78
PRVI	2	0	12	0
CEIN	1	0	337	0
RINE	1	0	87	0
CONU	1	0	53	0
ALSP	0	1	0	27
CEPA	1	0	12	0

APPENDIX II: PLOT LOCATIONS AND ATTRIBUTES

Table A.4. Locations and characteristics of 105 plots located in lower and upper montane forests of Yosemite and Sequoia & Kings Canyon National Parks. Forest alliance and association codes are provided in Table 1.4.

Plot	Easting (UTM)	Northing (UTM)	Elevation (m)	Slope (°)	Aspect	Soil water capacity (mm)	Forest alliance	Forest association
Yosemite National Park								
P000	247652	4206725	1,595	15	SW	49	**5**	17
P002	250952	4185809	1,468	25	SW	85	**6**	18
P003	251010	4185799	1,487	21	W	85	**6**	18
P004	247531	4209343	1,665	11	SE	118	**6**	18
P005	252422	4184475	1,633	15	N	161	**1**	2
P006	252107	4186833	1,560	5	NW	205	**6**	18
P007	252514	4190105	1,595	19	N	72	**1**	2
P008	247833	4209607	1,695	13	SE	118	**6**	18
P009	251973	4190028	1,555	12	N	72	**1**	2
P010	252007	4186341	1,600	13	W	205	**6**	18
P011	249857	4205613	1,620	2	W	76	**5**	17
P012	253000	4204848	1,580	7	NW	53	**5**	17
P013	252071	4185221	1,510	14	NW	134	**1**	2
P014	257277	4188267	1,695	14	SE	108	**1**	2
P015	250898	4186863	1,460	21	NE	205	**1**	2
P016	248074	4209201	1,620	12	SE	118	**6**	18
P017	249378	4205629	1,665	4	E	68	**6**	18
P018	252983	4184793	1,610	7	W	134	**1**	2
P019	252802	4184672	1,665	15	NW	161	**1**	2
P020	252120	4185462	1,545	17	S	134	**6**	18
P021	270906	4176726	2,290	16	W	81	**3**	9
P023	256607	4179995	1,610	15	S	67	**1**	2
P024	255768	4179772	1,630	14	S	67	**6**	18
P028	289296	4205492	2,625	9	E	48	**4**	11
P029	290044	4205532	2,705	9	NW	59	**2**	7
P036	249988	4213234	2,115	12	SE	108	**1**	3
P043	269604	4162265	2,200	9	S	118	**3**	9
P060	249280	4213391	2,000	20	W	88	**5**	14
P061	256626	4184171	2,030	20	NW	54	**3**	9
P062	256424	4184163	2,030	19	NE	54	**3**	9
P063	256816	4192320	2,000	10	N	72	**1**	2
P065	254771	4182231	1,890	13	SE	107	**1**	2
P066	264392	4160868	1,793	14	NW	94	**1**	2

Plot	Easting (UTM)	Northing (UTM)	Elevation (m)	Slope (°)	Aspect	Soil water capacity (mm)	Forest alliance	Forest association
P067	265118	4162362	1,760	22	N	94	**1**	2
P068	248831	4210524	1,750	6	SW	118	**6**	18
P069	256745	4191588	1,890	4	SW	108	**1**	1
P071	263324	4169272	1,760	16	W	120	**1**	2
P072	261872	4171251	1,895	4	W	72	**1**	2
P073[§]	253115	4183246	1,915	10	W	72	**1**	2
P074	257175	4191304	1,880	15	W	72	**3**	8
P076	261180	4172061	1,810	12	S	94	**1**	1
P079	257156	4188544	1,770	10	W	64	**5**	17
P082	248479	4211366	1,775	8	NW	53	**6**	18
P084	248919	4213351	1,905	13	W	53	**5**	13
P085	252709	4181771	1,940	4	W	127	**1**	2
P087	258524	4186417	2,012	12	NE	127	**1**	3
P088	258564	4186233	2,021	4.5	NE	100	**1**	3
P109	268266	4157544	1,377	13	N	78	**6**	18
P110	264676	4162004	1,750	34	W	94	**1**	2
P111	267531	4156640	1,338	12	SW	205	**6**	18
P112[§]	267562	4157064	1,401	10	S	205	**6**	18
P113[§]	263526	4160989	1,666	13	NE	94	**1**	2
P114	263354	4162884	1,545	23	SW	67	**6**	18
P115	262916	4166844	1,710	13	SW	94	**1**	2
P116	264818	4163275	1,660	14	N	94	**1**	2
P117	270763	4154249	1,895	17	SW	111	**1**	2
P118	268841	4153873	1,770	13	E	129	**1**	2
P119[§]	269749	4153747	1,773	6	W	111	**1**	2
P133	282817	4159220	2,372	12	SE	69	**5**	13
P153	285692	4161153	2,607	9	NW	81	**2**	7
P154	284977	4160297	2,635	6	NE	47	**2**	7
P179	265455	4170505	2,344	10	S	69	**5**	17
P260	282477	4158986	2,382	17	NE	48	**2**	5
P261	266057	4170394	2,389	6	SW	69	**5**	17
P262	265736	4170605	2,374	4	S	69	**5**	17
P263	289917	4205579	2,680	11	S	59	**4**	11
P264	289238	4205276	2,630	13	E	48	**4**	11
Sequoia & Kings Canyon National Park								
P136	351115	4033432	2,495	17	W	89	**3**	9
P137	348583	4079822	2,375	8	NW	89	**3**	9
P138	350276	4038660	2,540	20	NE	82	**2**	6
P139	348407	4065375	2,535	18	NE	90	**3**	9
P140	348980	4080400	2,490	14	SW	104	**5**	14

Plot	Easting (UTM)	Northing (UTM)	Elevation (m)	Slope (°)	Aspect	Soil water capacity (mm)	Forest alliance	Forest association
P141[§]	349902	4040379	2,310	10	W	86	**3**	9
P142	349568	4065863	2,490	24	W	99	**5**	14
P145	350489	4039294	2,045	29	NW	83	**2**	4
P148	348239	4035597	2,010	11	S	129	**6**	19
P149	350458	4072351	1,600	18	N	123	**6**	19
P156	359211	4073580	1,620	5	SE	131	**6**	19
P158	353226	4066286	2,180	1	NE	80	**4**	12
P159	347674	4062887	2,550	11	N	79	**4**	11
P160	352779	4066456	2,195	0	N	98	**5**	17
P162	347473	4062271	2,550	11	NE	77	**4**	11
P168	349628	4077764	1,960	12	SW	98	**5**	17
P170	349622	4077904	1,985	6	S	98	**5**	17
P172	349406	4031220	2,245	23	W	101	**5**	14
P174	349720	4031042	2,285	24	S	108	**5**	14
P186	350703	4038144	2,545	27	S	93	**3**	9
P187[§]	352978	4034266	2,600	20	NW	83	**2**	6
P188	354852	4035089	2,335	23	N	103	**3**	10
P190	350031	4075549	1,790	17	W	138	**6**	18
P192	351796	4065235	2,235	10	NW	98	**5**	14
P193	351921	4065378	2,220	11	NW	82	**4**	12
P195	350590	4065082	2,355	7	S	101	**5**	14
P196	355503	4035605	2,435	29	SW	96	**5**	14
P197	353514	4066071	2,180	8	NW	95	**5**	14
P198	350149	4064610	2,360	10	E	93	**5**	15
P251	349763	4064549	2,390	6	S	98	**5**	17
P252	348417	4065760	2,495	10	SE	90	**3**	9
P253[§]	360282	4064793	2,680	20	S	85	**2**	5
P254	354361	4034428	2,600	14	N	81	**2**	6
P255	350797	4032895	2,525	10	NW	80	**2**	6
P256[§]	351343	4027792	2,615	8	S	81	**2**	5
P257	350991	4028245	2,645	7	SW	83	**2**	4
P258	350160	4039119	2,415	5	NW	83	**2**	4
P259	349909	4038809	2,490	14	NE	83	**2**	4

[§]Eight plots were removed from analysis either due to lack of fire severity data or because the plot had experienced high-severity fire.

APPENDIX III: FIRE HISTORY OF BURNED PLOTS

Table A.5. Fire attributes of 59 plots burned since 1930 located in lower and upper montane forests of Yosemite and Sequoia & Kings Canyon National Parks. Each fire at a site is listed as an individual entry. LTG = lightning; MI = management ignited; Human = unintentional ignition caused by human activity. RdNBR = Relative differenced Normalized Burn Ratio (Miller and Thode 2007).

Plot	Year	RdNBR	Size (ha)	Cause	Name
P000	1996	480	23,938.7	LTG	Ackerson
P002	1992	55	209.6	MI	South Fork
P003	1992	81	209.6	MI	South Fork
P011	1978	-	2,074.3	MI	-
P011	1996	548	23,938.7	LTG	Ackerson
P012	1996	521	23,938.7	LTG	Ackerson
P017	1978	-	2,074.3	MI	-
P017	1996	355	23,938.7	LTG	Ackerson
P018	2005	163	699.0	MI	PW3-23
P019	2005	145	699.0	MI	PW3-23
P020	1992	124	209.6	MI	South Fork
P023	2009	412	0.0	MI	Big Meadow
P024	2009	400	0.0	MI	Big Meadow
P028	1988	174	182.3	LTG	Elbow
P029	1988	-10	182.3	LTG	Elbow
P036	1997	481	993.4	MI	Kibbie Relight
P060	1997	304	993.4	MI	Kibbie Relight
P061	1989	179	688.4	MI	Pw3
P061	2002	1	1,360.3	MI	PW-3 Gin Flat
P062	1989	-1	688.4	MI	Pw3
P062	2002	251	1,360.3	MI	PW-3 Gin Flat
P063	1996	-10	23,938.7	LTG	Ackerson
P065	1979	-	1,932.5	MI	-
P065	1980	-	830.4	MI	-
P065	2009	412	0.0	MI	Big Meadow
P066	2008	173	249.5	MI	Wawona NW
P068	1986	60	583.6	LTG	Eleanor
P068	1999	326	1,042.3	LTG	Eleanor
P073[§]	1993	-	37.4	MI	-
P073[§]	2002	-	31.4	MI	YI Burn
P085	2005	162	104.3	MI	PW5-AD
P087	1989	19	688.4	MI	Pw3
P087	2002	188	1,360.3	MI	PW-3 Gin Flat
P088	1989	59	688.4	MI	Pw3
P088	2002	176	1,360.3	MI	PW-3 Gin Flat
P110	2007	35	447.9	LTG	Jack WF
P111	1970	-	178.9	MI	-
P111	1973	-	36.1	MI	-
P111	1975	-	18.7	MI	-

Plot	Year	RdNBR	Size (ha)	Cause	Name
P111	2005	45	57.4	MI	Soupbowl
P112[§]	1970	-	178.9	MI	-
P112[§]	1971	-	62.1	MI	-
P112[§]	1985	-	36.9	MI	So. Wawona 3/4
P112[§]	1994	-	56.5	MI	Studhorse
P112[§]	2002	-	21.3	MI	Studhorse 4
P113[§]	2008	715	249.5	MI	Wawona NW
P119[§]	1990	-	11.7	MI	M Grove
P119[§]	1997	-	17.3	MI	Mg #9
P119[§]	2008	434	53.5	MI	Mariposa Grove
P136	2002	279	489.4	MI	Tar Gap RX
P137	2005	126	3,947.3	LTG	Comb
P138	2003	142	1,098.4	MI	Atwood
P139	2003	187	1,404.8	LTG	Williams
P140	2005	345	3,947.3	LTG	Comb
P141[§]	1947	-	149.6	Human	Castle Gro
P148	1994	-	55.7	MI	Paradise
P148	1995	158	843.1	MI	Mineral 1
P148	2003	228	1,098.4	MI	Atwood
P149	1997	-	149.8	MI	Sheep Creek
P149	2010	178	3,650.1	LTG	Sheep Complex
P158	1974	-	1,218.4	LTG	Comanche
P158	1985	444	1,152.2	LTG	Sugarloaf
P159	2003	19	1,404.8	LTG	Williams
P160	1974	-	1,218.4	LTG	Comanche
P160	1985	32	1,152.2	LTG	Sugarloaf
P168	1980	-	3,368.8	Human	Lewis Crk
P168	1998	358	645.2	MI	Lewis Creek
P168	2005	257	3,947.3	LTG	Comb
P170	1980	-	3,368.8	Human	Lewis Crk
P170	1998	229	645.2	MI	Lewis Creek
P170	2005	308	3,947.3	LTG	Comb
P186	1946	-	90.0	Human	Atwell Mil
P186	2003	160	1,098.4	MI	Atwood
P187[§]	1999	-	248.3	MI	Tar Gap
P190	1980	-	3,368.8	Human	Lewis Crk
P190	1998	274	645.2	MI	Lewis Creek
P192	1974	-	1,218.4	LTG	Comanche
P192	1985	95	1,152.2	LTG	Sugarloaf
P193	1974	-	1,218.4	LTG	Comanche
P193	1985	160	1,152.2	LTG	Sugarloaf
P195	1974	-	1,218.4	LTG	Comanche
P195	1985	9	1,152.2	LTG	Sugarloaf
P195	2003	454	1,404.8	LTG	Williams
P196	2005	535	344.6	MI	Highbrid E
P197	1974	-	1,218.4	LTG	Comanche
P197	1985	159	1,152.2	LTG	Sugarloaf

Plot	Year	RdNBR	Size (ha)	Cause	Name
P198	1974	-	1,218.4	LTG	Comanche
P198	1985	164	1,152.2	LTG	Sugarloaf
P251	1974	-	1,218.4	LTG	Comanche
P251	1985	489	1,152.2	LTG	Sugarloaf
P251	2003	-174	1,404.8	LTG	Williams
P252	2003	159	1,404.8	LTG	Williams
P253[§]	1977	-	4,216.3	LTG	Ferguson
P255	2002	105	489.4	MI	Tar Gap RX
P256[§]	2009	-	268.7	LTG	Horse
P263	1988	115	182.3	LTG	Elbow
P264	1988	160	182.3	LTG	Elbow

[§]Eight plots were removed from analysis either due to lack of fire severity data or because the plot had experienced high-severity fire.

APPENDIX IV: DIAMETER DISTRIBUTIONS BY SPECIES

Diameter distributions for 105 plots that correspond by plot number to the location, site attribute, and fire history data in Appendices II and III.

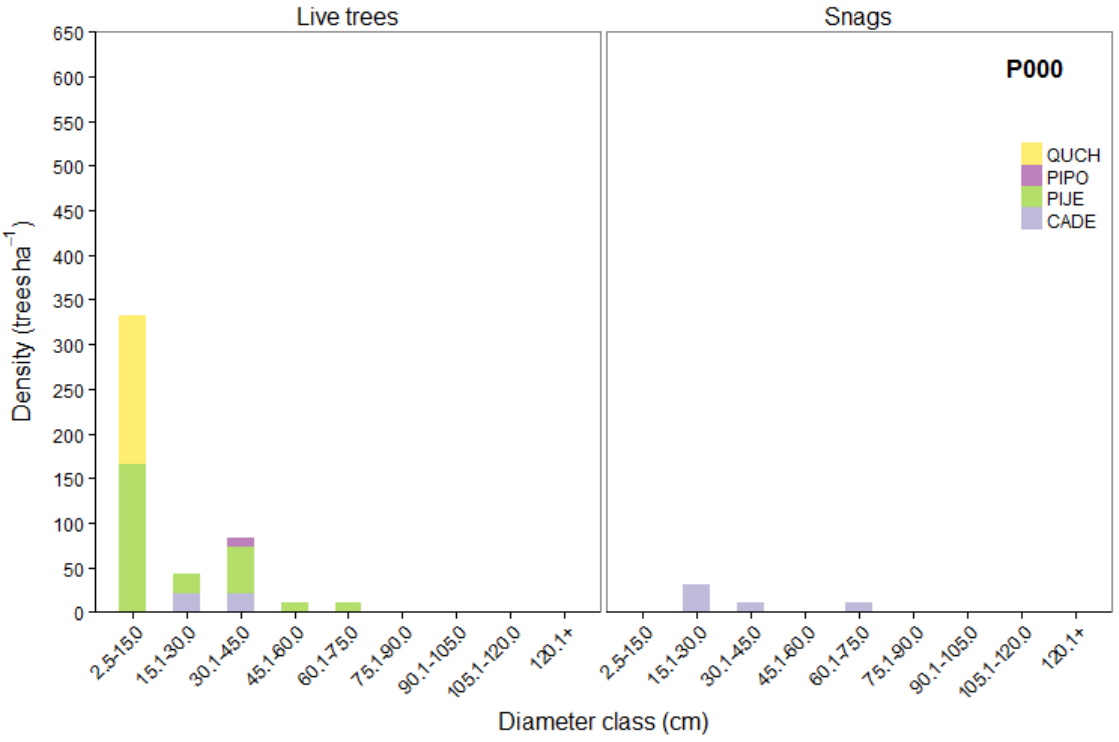

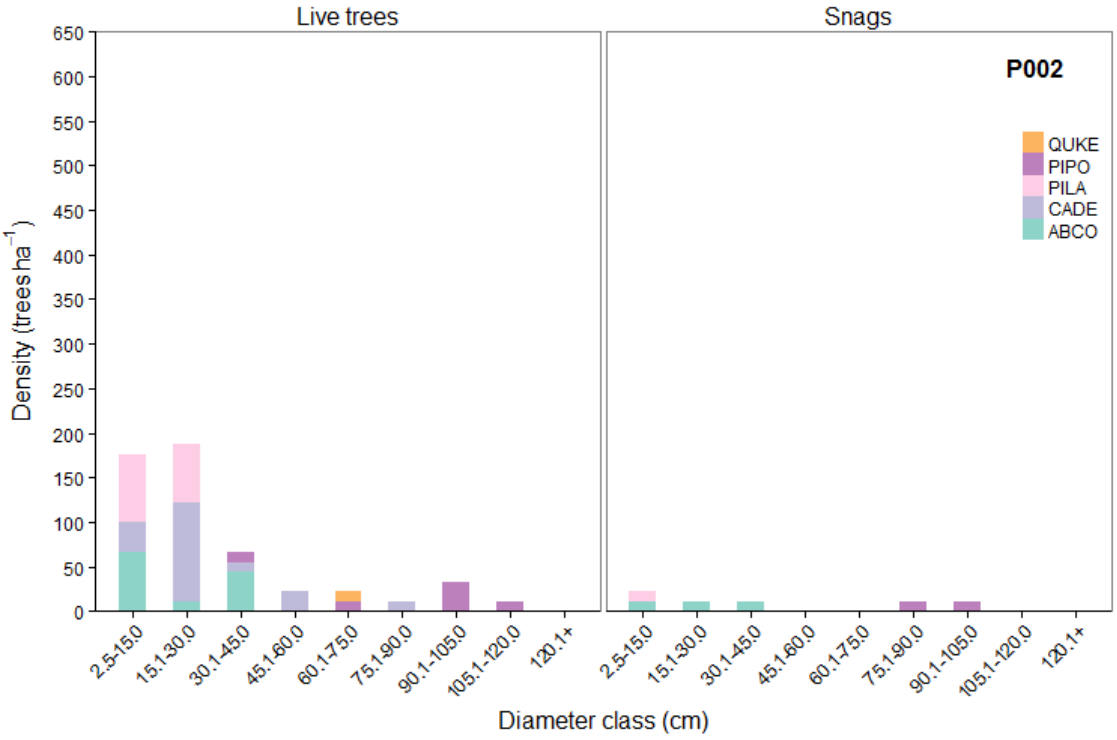
Live trees
Snags
P002
QUKE
PIPO
PILA
CADE
ABCO
Density (trees ha^{-1})
650
600
550
500
450
400
350
300
250
200
150
100
50
0
2.5-15.0
15.1-30.0
30.1-45.0
45.1-60.0
60.1-75.0
75.1-90.0
90.1-105.0
105.1-120.0
120.1+
Diameter class (cm)

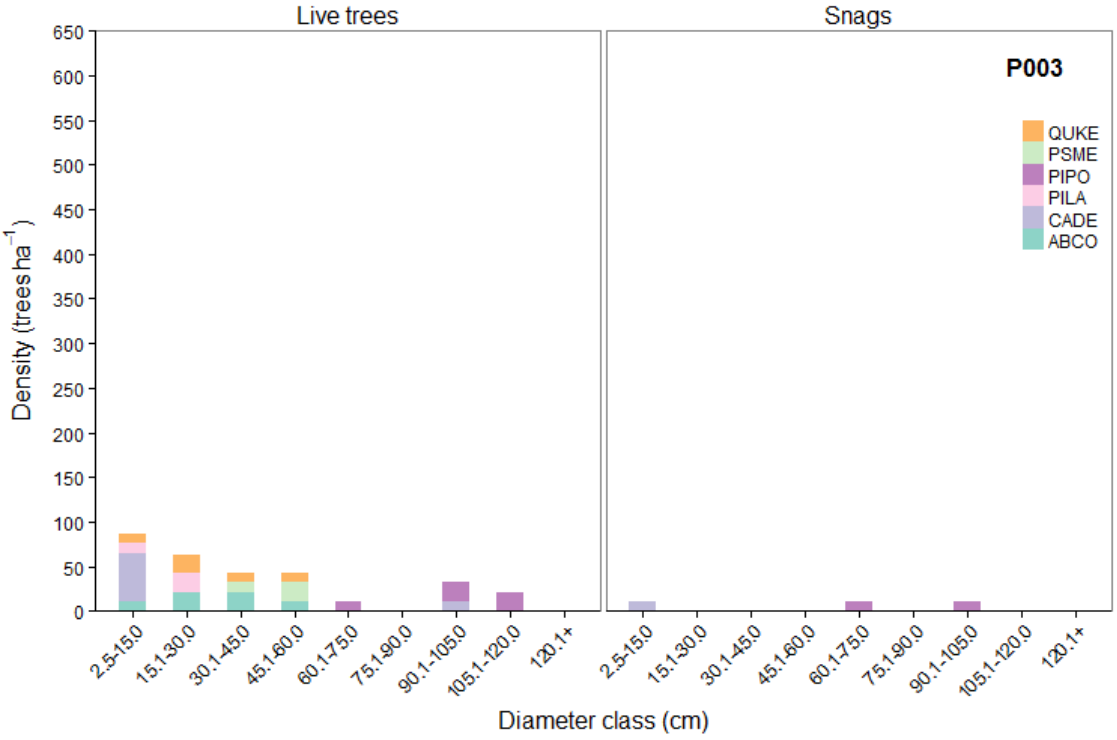
Live trees
Snags
P003
QUKE
PSME
PIPO
PILA
CADE
ABCO
Density (trees ha^{-1})
650
600
550
500
450
400
350
300
250
200
150
100
50
0
2.5-15.0
15.1-30.0
30.1-45.0
45.1-60.0
60.1-75.0
75.1-90.0
90.1-105.0
105.1-120.0
120.1+
Diameter class (cm)

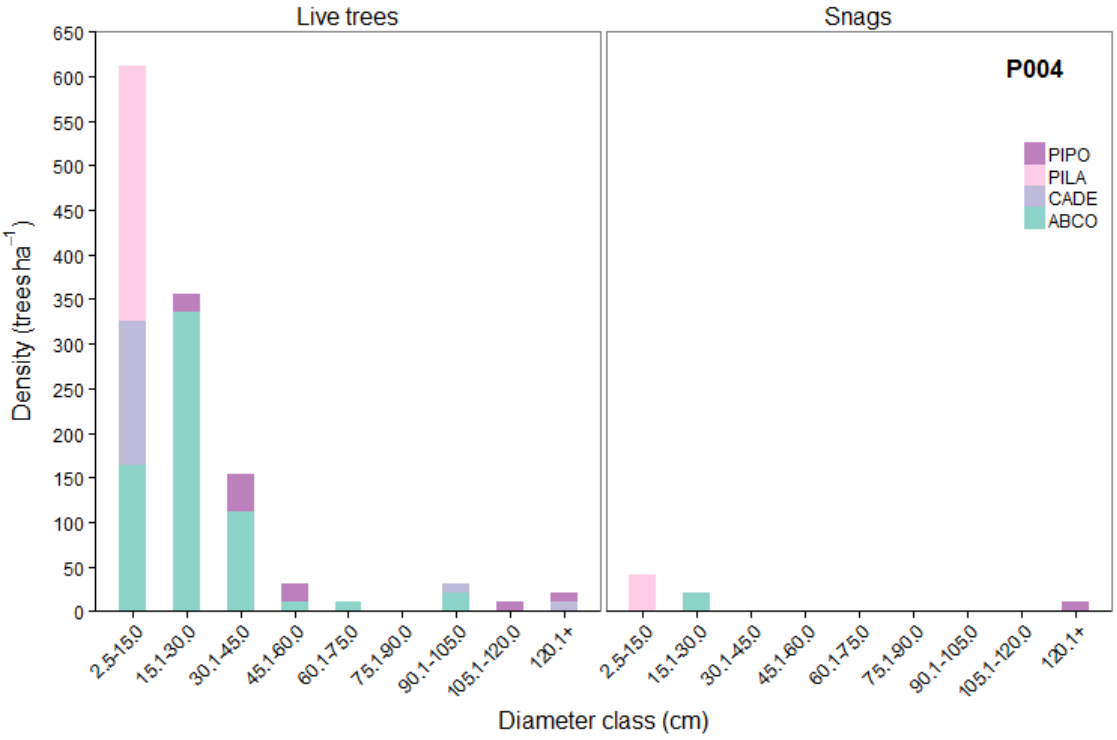
Live trees
Snags
P004
PIPO
PILA
CADE
ABCO
Density (trees ha^{-1})
650
600
550
500
450
400
350
300
250
200
150
100
50
0
2.5-15.0
15.1-30.0
30.1-45.0
45.1-60.0
60.1-75.0
75.1-90.0
90.1-105.0
105.1-120.0
120.1+
Diameter class (cm)

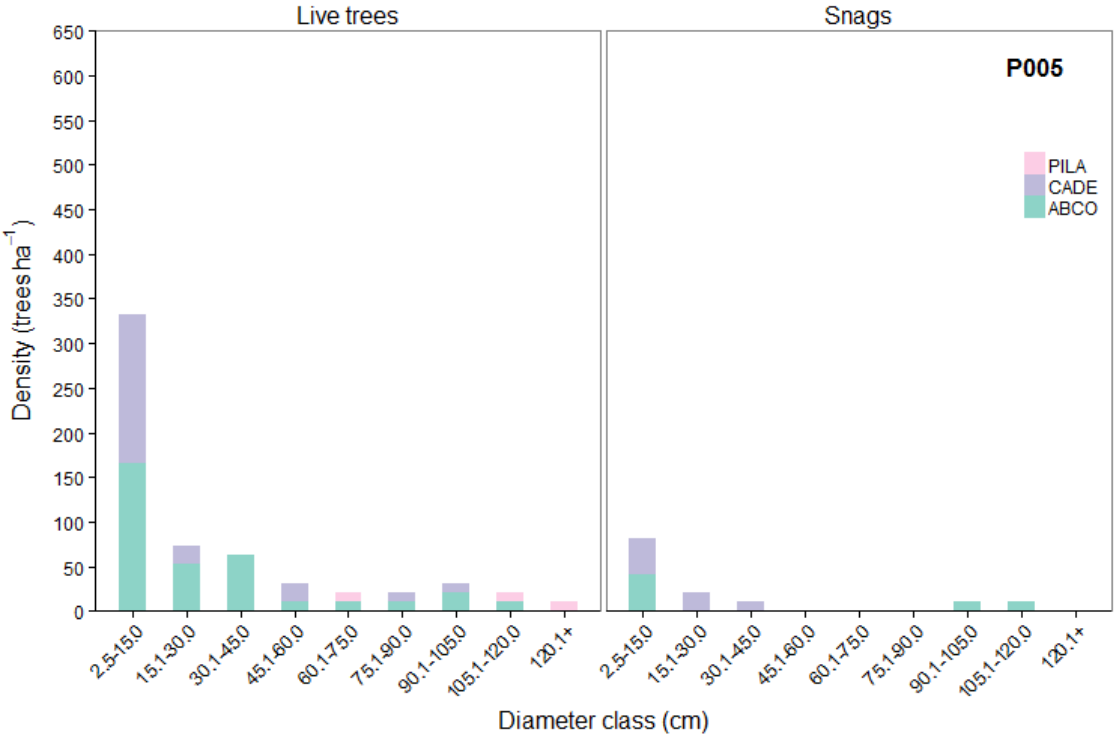
Live trees
Snags
P005
PILA
CADE
ABCO
Density (trees ha^{-1})
650
600
550
500
450
400
350
300
250
200
150
100
50
0
2.5-15.0
15.1-30.0
30.1-45.0
45.1-60.0
60.1-75.0
75.1-90.0
90.1-105.0
105.1-120.0
120.1+
Diameter class (cm)

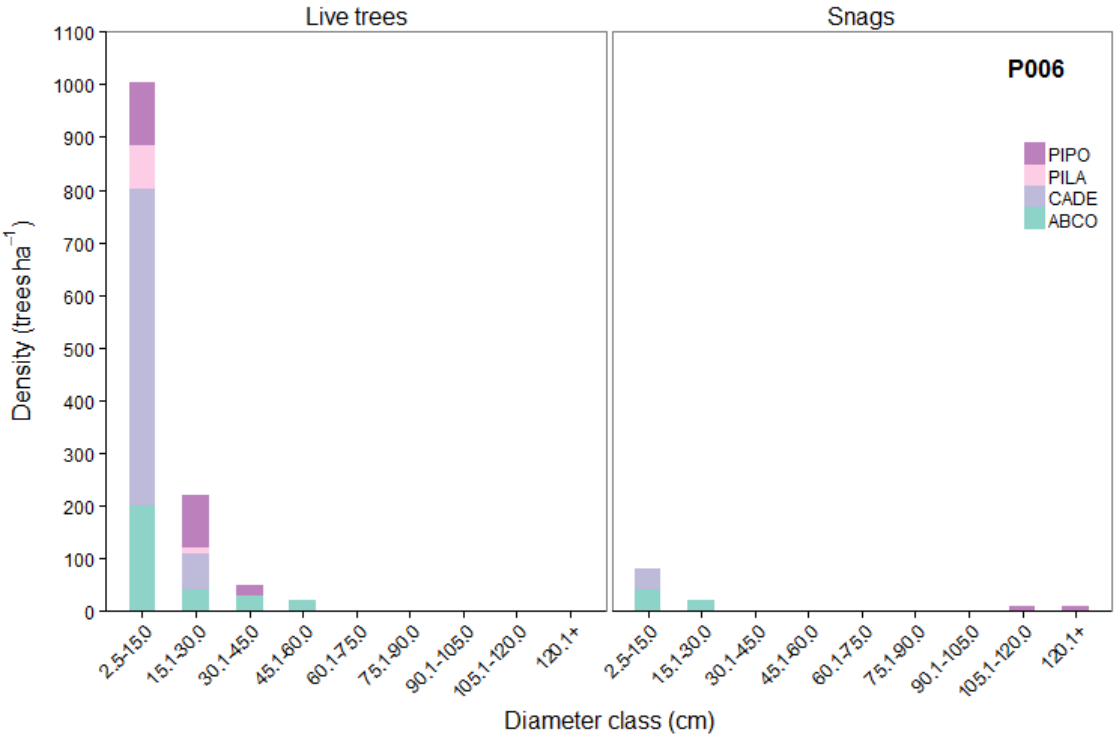
Live trees
Snags
P006
PIPO
PILA
CADE
ABCO
Density (trees ha^{-1})
0
100
200
300
400
500
600
700
800
900
1000
1100
2.5-15.0
15.1-30.0
30.1-45.0
45.1-60.0
60.1-75.0
75.1-90.0
90.1-105.0
105.1-120.0
120.1+
Diameter class (cm)

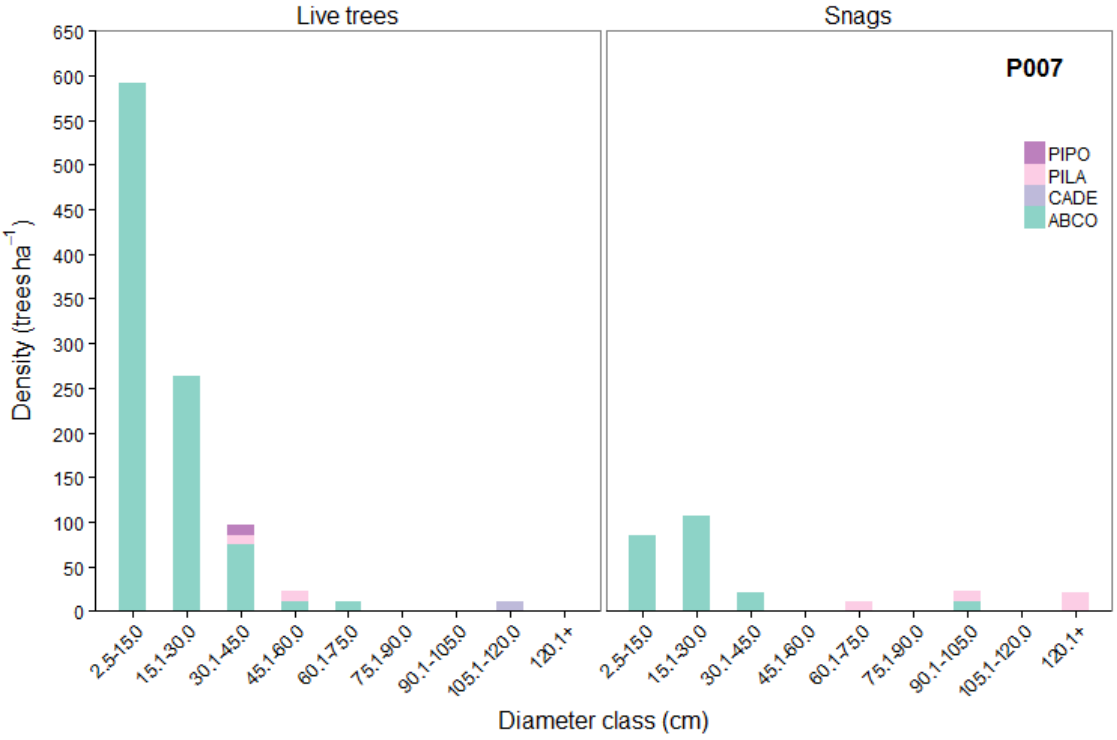
Live trees
Snags
P007
PIPO
PILA
CADE
ABCO
Density (trees ha^{-1})
0
50
100
150
200
250
300
350
400
450
500
550
600
650
2.5-15.0
15.1-30.0
30.1-45.0
45.1-60.0
60.1-75.0
75.1-90.0
90.1-105.0
105.1-120.0
120.1+
Diameter class (cm)

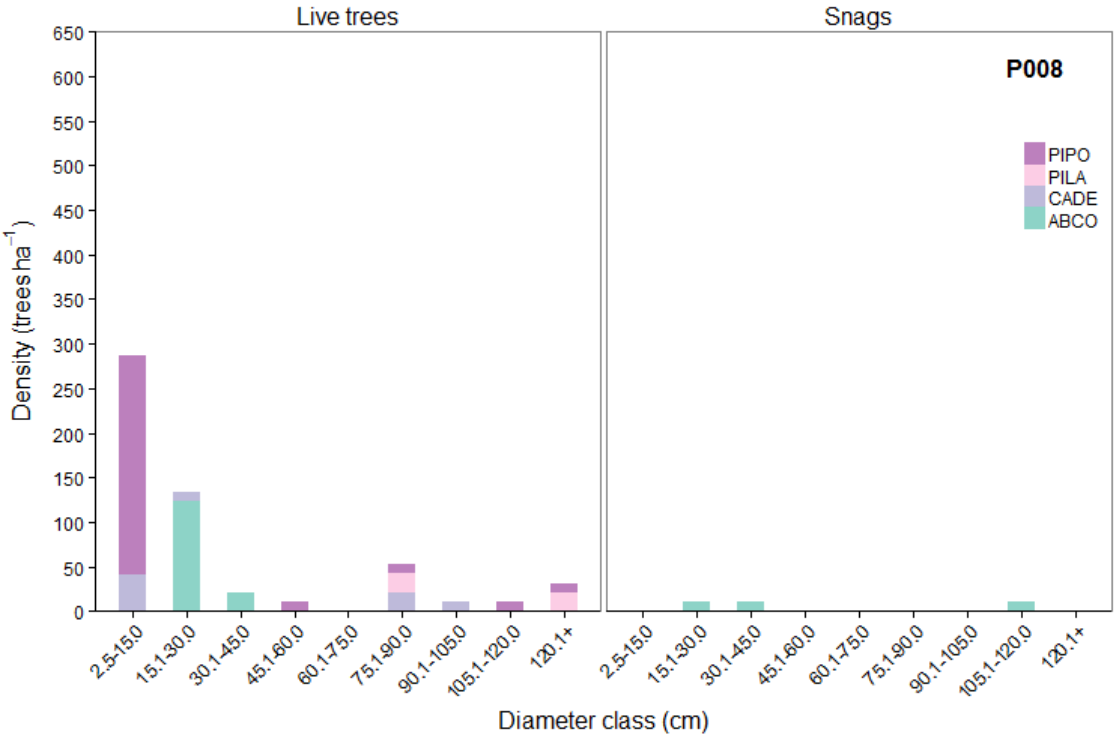
Live trees
Snags
P008
PIPO
PILA
CADE
ABCO
Density (trees ha^{-1})
650
600
550
500
450
400
350
300
250
200
150
100
50
0
2.5-15.0
15.1-30.0
30.1-45.0
45.1-60.0
60.1-75.0
75.1-90.0
90.1-105.0
105.1-120.0
120.1+
Diameter class (cm)

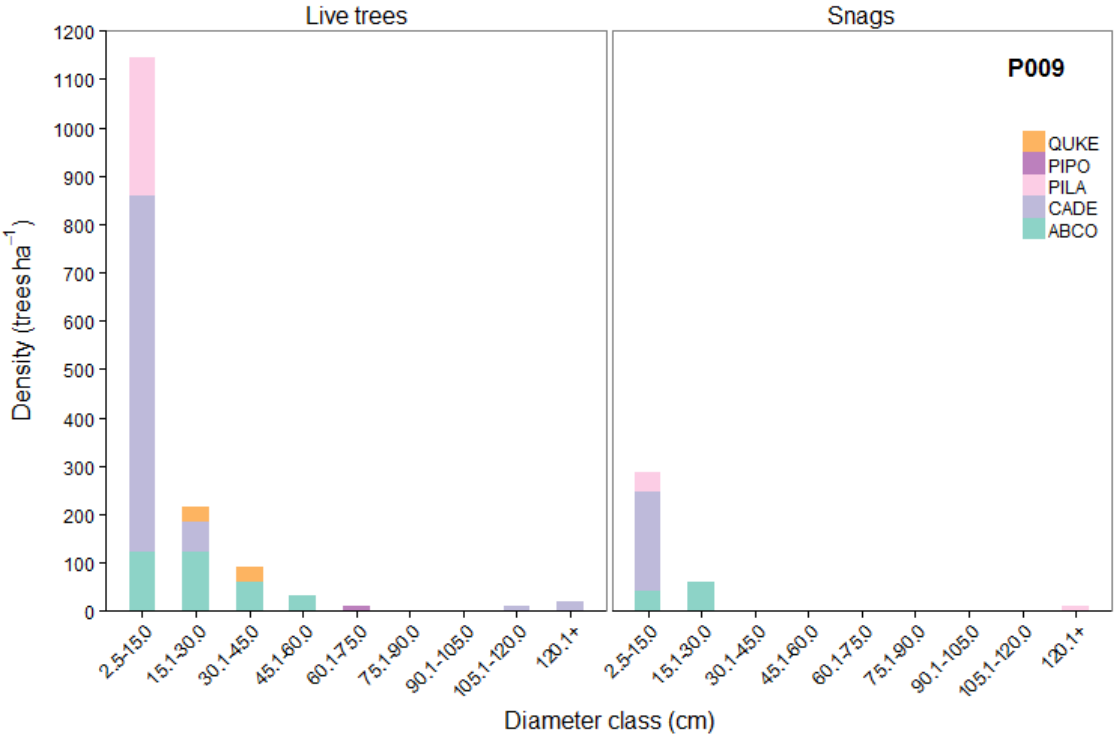
Live trees
Snags
P009
QUKE
PIPO
PILA
CADE
ABCO
Density (trees ha^{-1})
1200
1100
1000
900
800
700
600
500
400
300
200
100
0
2.5-15.0
15.1-30.0
30.1-45.0
45.1-60.0
60.1-75.0
75.1-90.0
90.1-105.0
105.1-120.0
120.1+
Diameter class (cm)

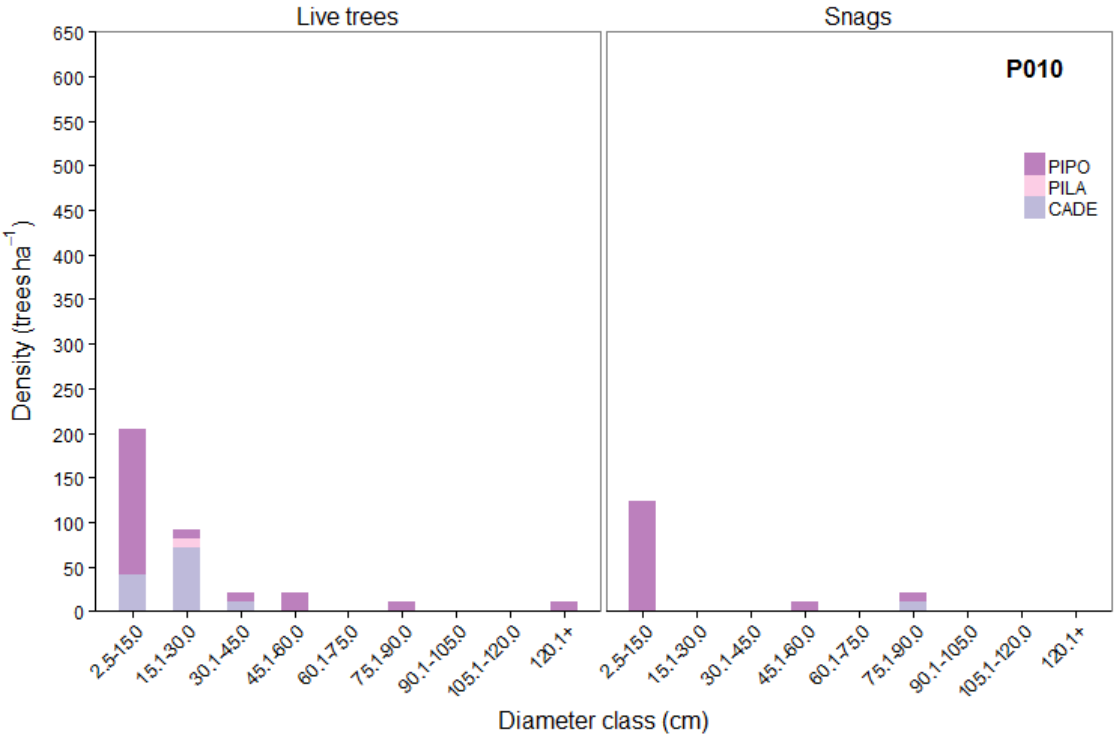
Live trees
Snags
P010
PIPO
PILA
CADE
Density (trees ha^{-1})
650
600
550
500
450
400
350
300
250
200
150
100
50
0
2.5-15.0
15.1-30.0
30.1-45.0
45.1-60.0
60.1-75.0
75.1-90.0
90.1-105.0
105.1-120.0
120.1+
Diameter class (cm)

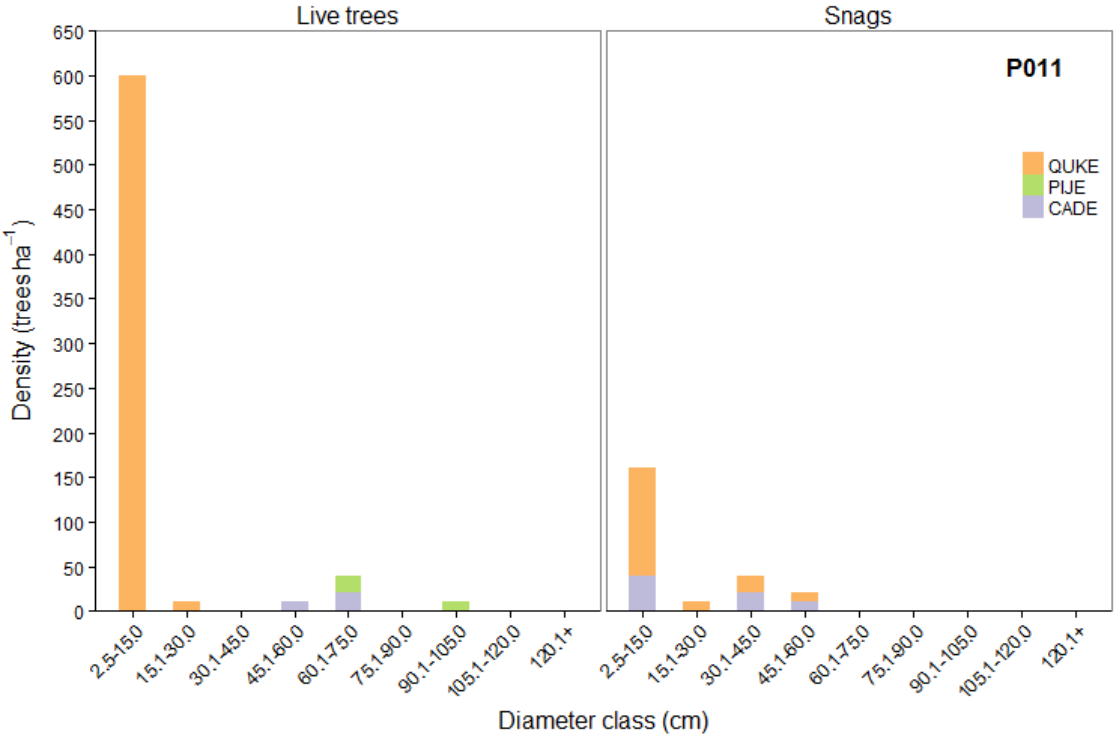
Live trees
Snags
P011
QUKE
PIJE
CADE
Density (trees ha^{-1})
650
600
550
500
450
400
350
300
250
200
150
100
50
0
2.5-15.0
15.1-30.0
30.1-45.0
45.1-60.0
60.1-75.0
75.1-90.0
90.1-105.0
105.1-120.0
120.1+
Diameter class (cm)

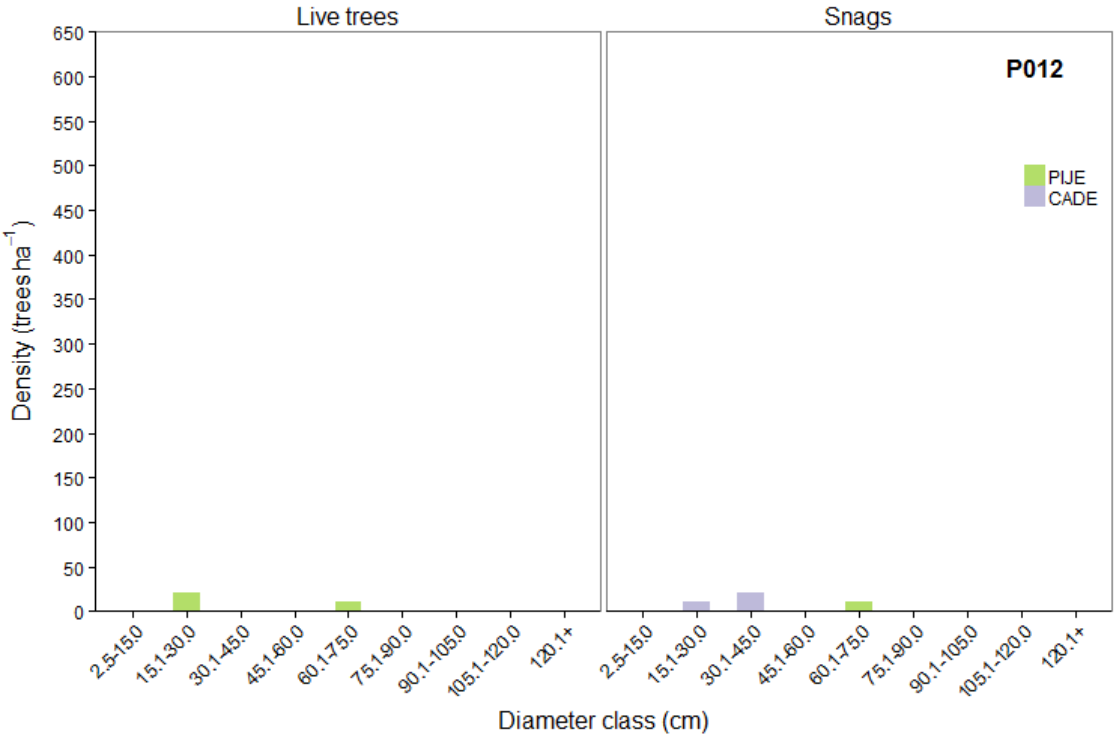
Live trees
Snags
P012
PIJE
CADE
Density (trees ha^{-1})
650
600
550
500
450
400
350
300
250
200
150
100
50
0
2.5-15.0
15.1-30.0
30.1-45.0
45.1-60.0
60.1-75.0
75.1-90.0
90.1-105.0
105.1-120.0
120.1+
Diameter class (cm)

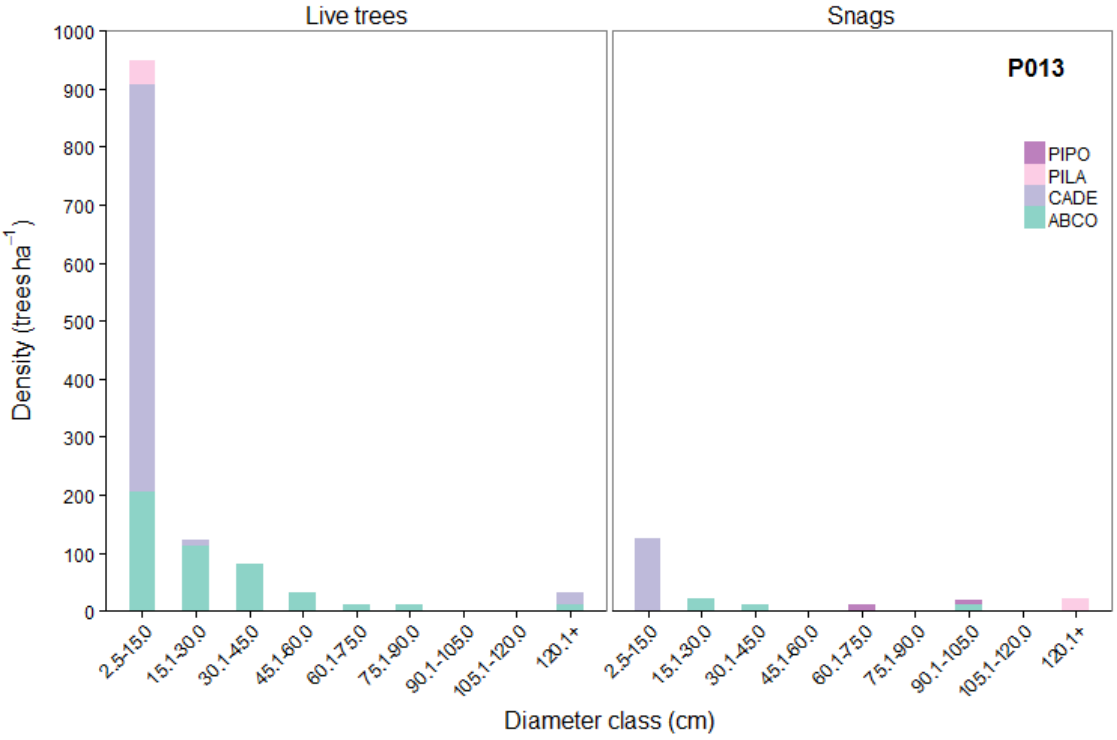
Live trees
Snags
P013
PIPO
PILA
CADE
ABCO
Density (trees ha^{-1})
1000
900
800
700
600
500
400
300
200
100
0
2.5-15.0
15.1-30.0
30.1-45.0
45.1-60.0
60.1-75.0
75.1-90.0
90.1-105.0
105.1-120.0
120.1+
Diameter class (cm)

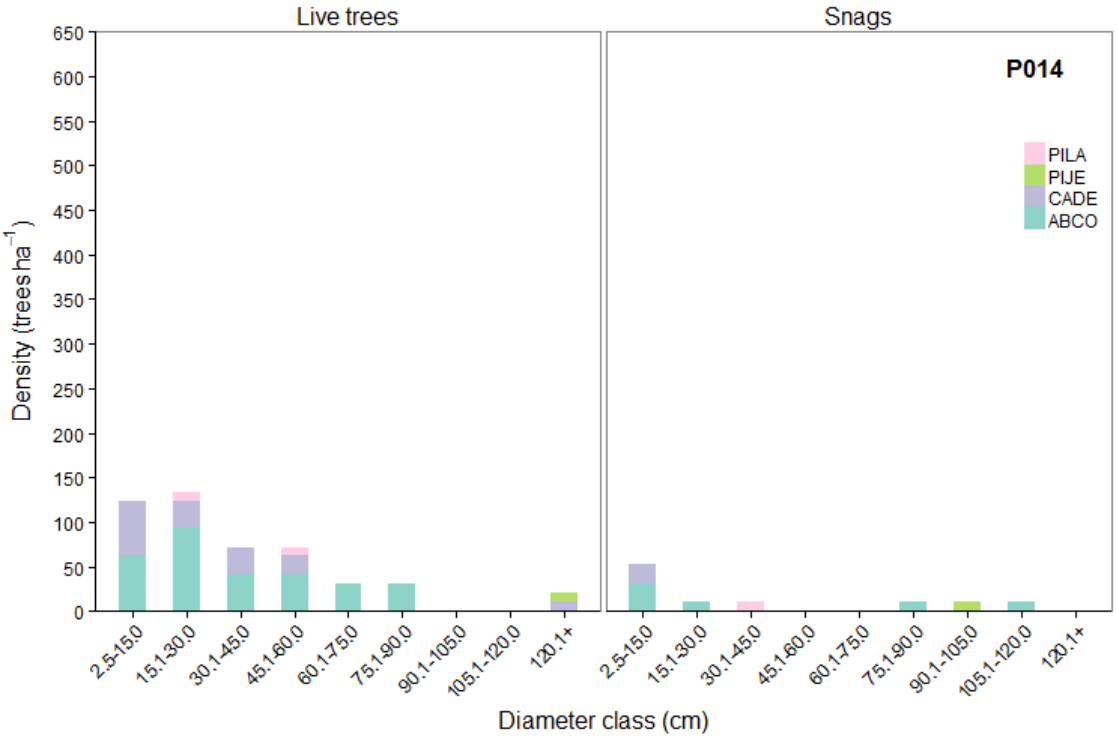
Live trees
Snags
P014
PILA
PIJE
CADE
ABCO
Density (trees ha^{-1})
650
600
550
500
450
400
350
300
250
200
150
100
50
0
2.5-15.0
15.1-30.0
30.1-45.0
45.1-60.0
60.1-75.0
75.1-90.0
90.1-105.0
105.1-120.0
120.1+
Diameter class (cm)

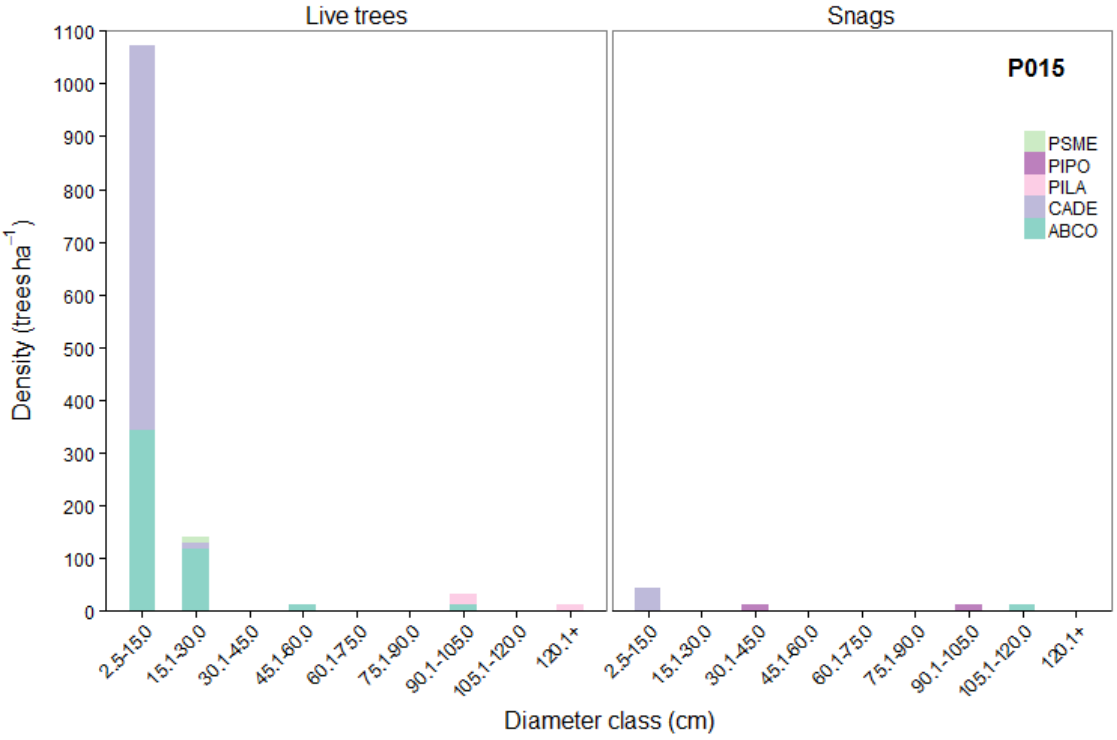
Live trees
Snags
P015
PSME
PIPO
PILA
CADE
ABCO
Density (trees ha^{-1})
1100
1000
900
800
700
600
500
400
300
200
100
0
2.5-15.0
15.1-30.0
30.1-45.0
45.1-60.0
60.1-75.0
75.1-90.0
90.1-105.0
105.1-120.0
120.1+
Diameter class (cm)

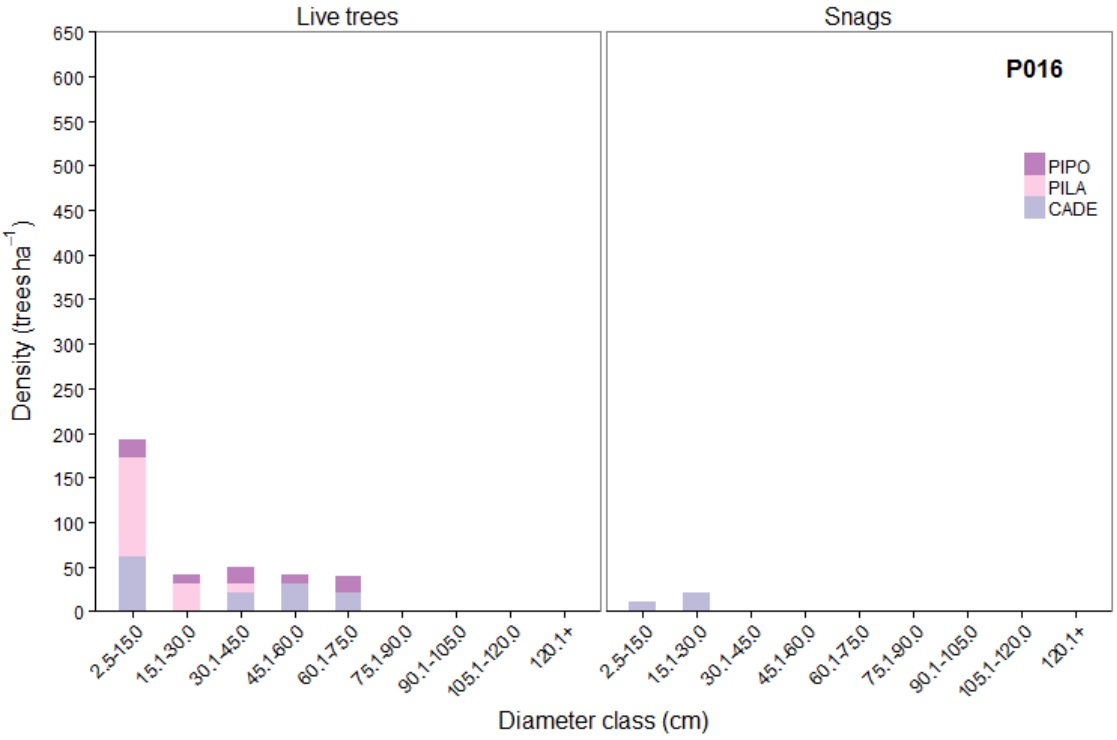
Live trees
Snags
P016
PIPO
PILA
CADE
Density (trees ha^{-1})
650
600
550
500
450
400
350
300
250
200
150
100
50
0
2.5-15.0
15.1-30.0
30.1-45.0
45.1-60.0
60.1-75.0
75.1-90.0
90.1-105.0
105.1-120.0
120.1+
Diameter class (cm)

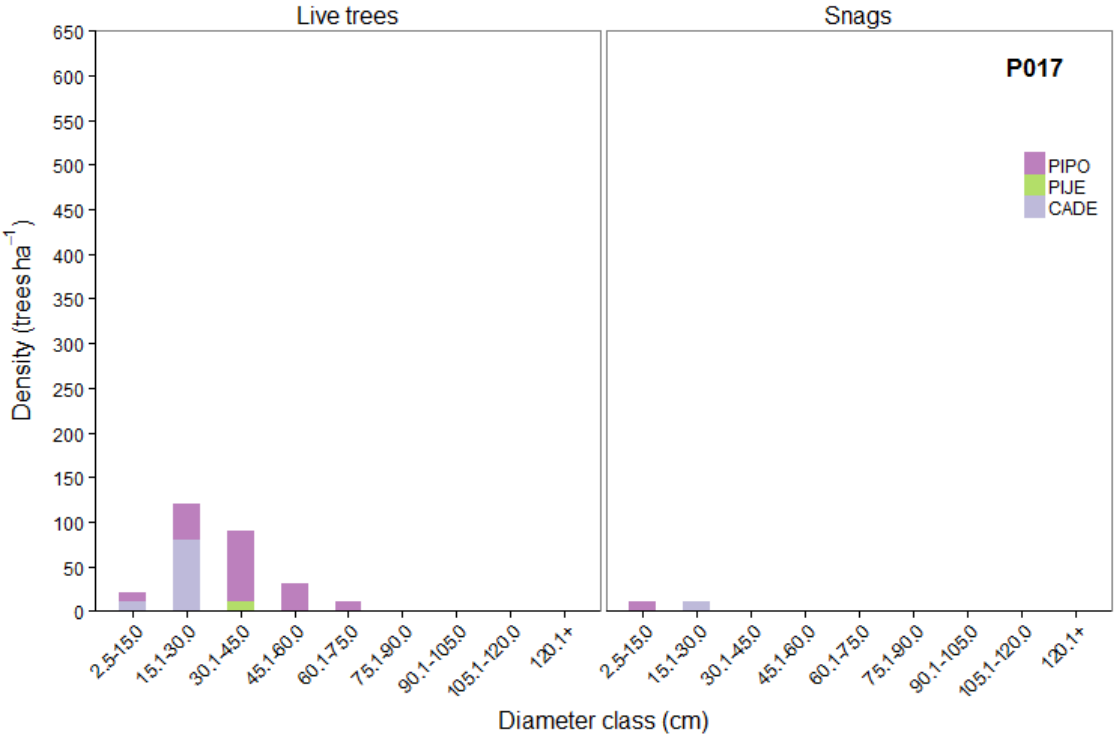
Live trees
Snags
P017
PIPO
PIJE
CADE
Density (trees ha^{-1})
650
600
550
500
450
400
350
300
250
200
150
100
50
0
2.5-15.0
15.1-30.0
30.1-45.0
45.1-60.0
60.1-75.0
75.1-90.0
90.1-105.0
105.1-120.0
120.1+
Diameter class (cm)

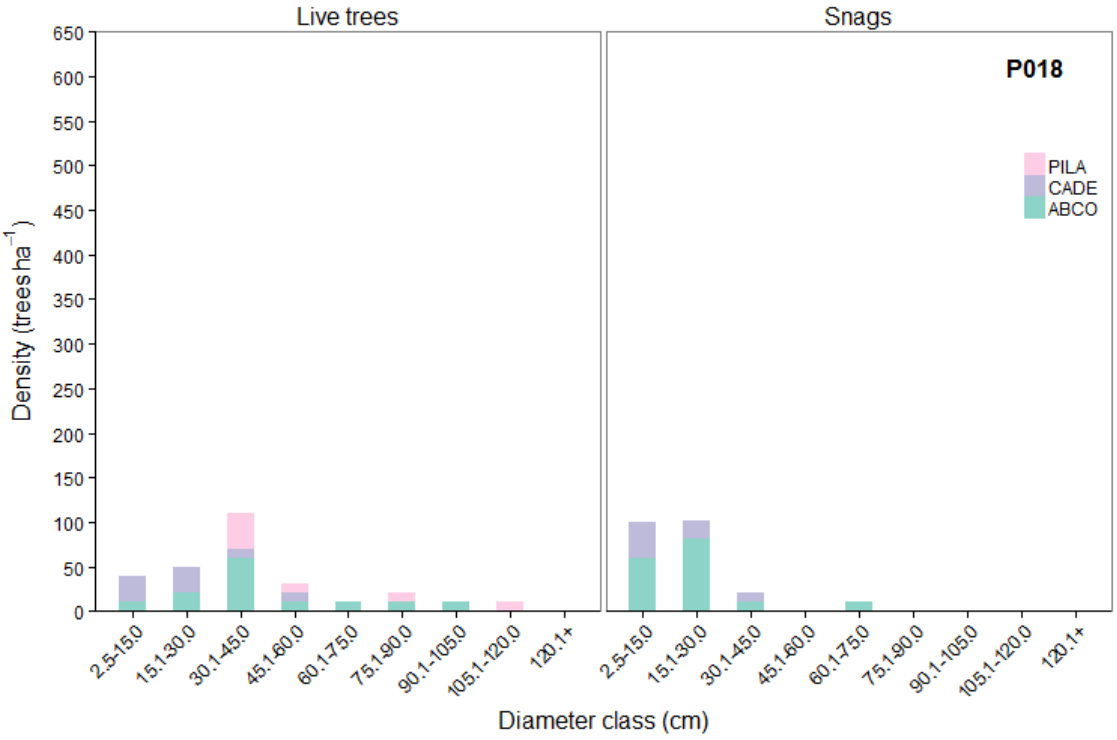
Live trees
Snags
P018
PILA
CADE
ABCO
Density (trees ha^{-1})
650
600
550
500
450
400
350
300
250
200
150
100
50
0
2.5-15.0
15.1-30.0
30.1-45.0
45.1-60.0
60.1-75.0
75.1-90.0
90.1-105.0
105.1-120.0
120.1+
Diameter class (cm)

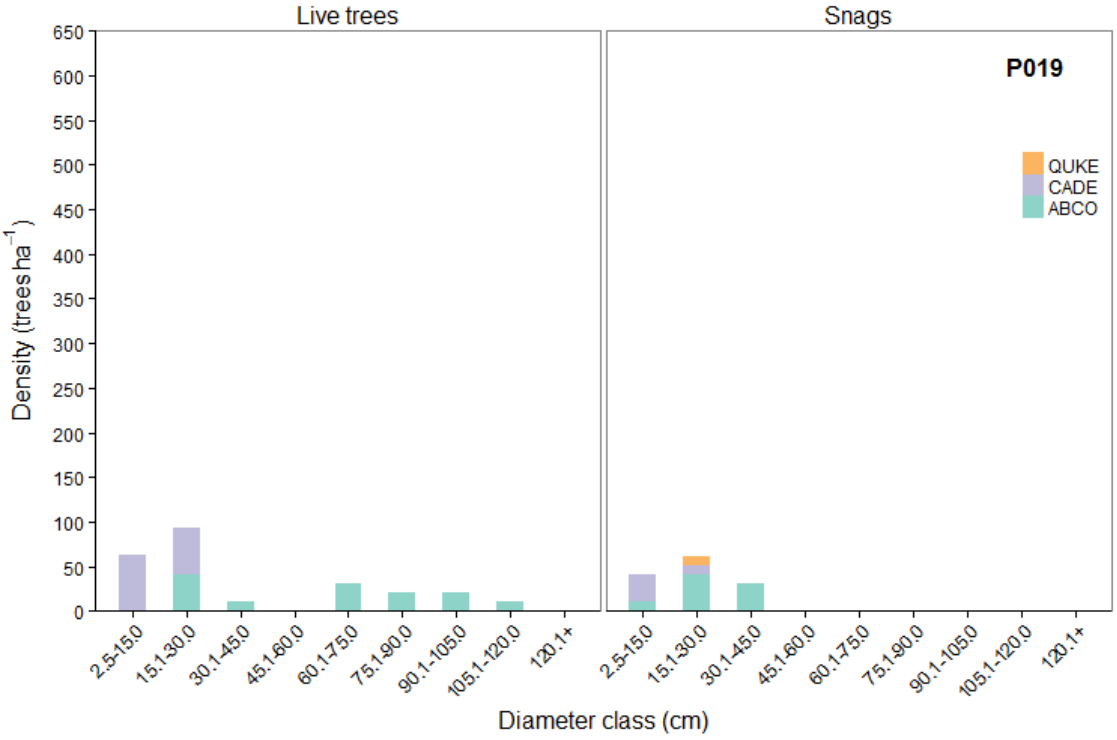
Live trees
Snags
P019
QUKE
CADE
ABCO
Density (trees ha^{-1})
650
600
550
500
450
400
350
300
250
200
150
100
50
0
2.5-15.0
15.1-30.0
30.1-45.0
45.1-60.0
60.1-75.0
75.1-90.0
90.1-105.0
105.1-120.0
120.1+
Diameter class (cm)

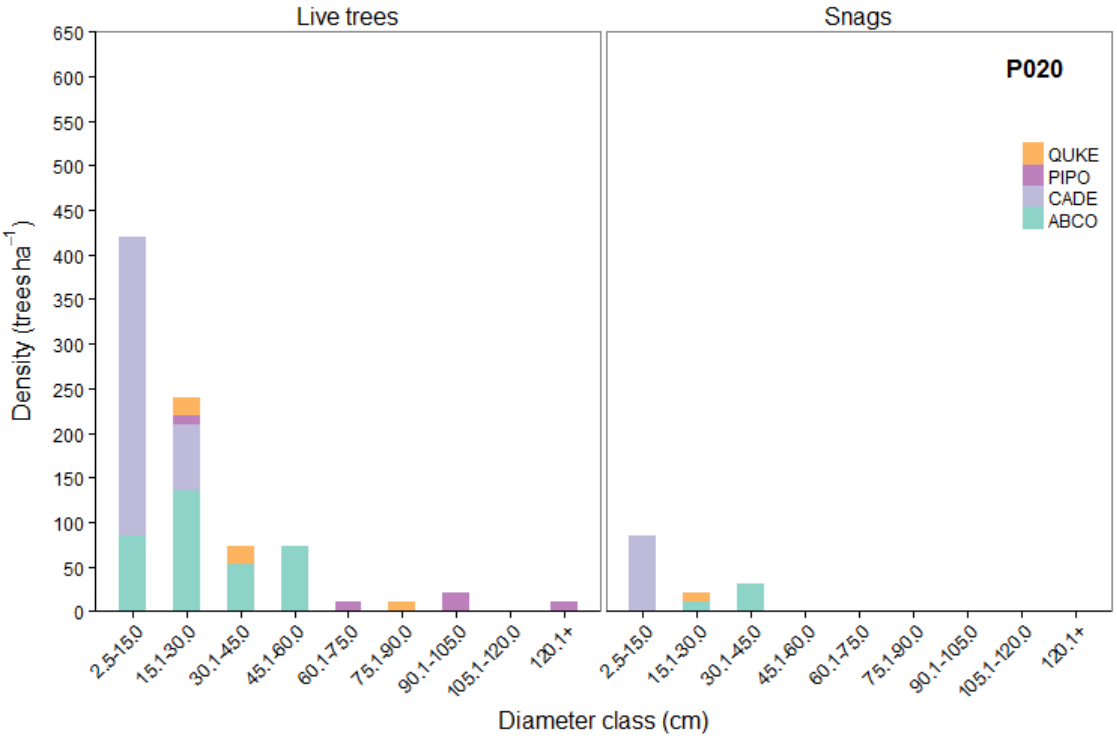
Live trees
Snags
P020
QUKE
PIPO
CADE
ABCO
Density (trees ha^{-1})
650
600
550
500
450
400
350
300
250
200
150
100
50
0
2.5-15.0
15.1-30.0
30.1-45.0
45.1-60.0
60.1-75.0
75.1-90.0
90.1-105.0
105.1-120.0
120.1+
Diameter class (cm)

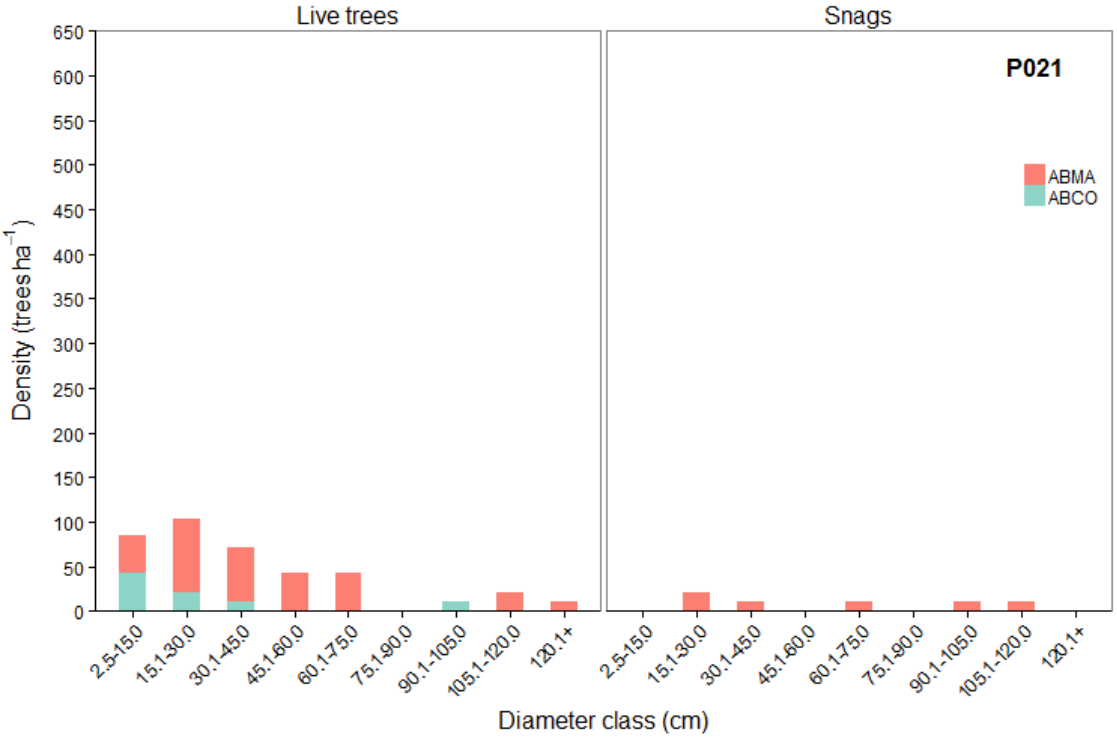
Live trees
Snags
P021
ABMA
ABCO
Density (trees ha^{-1})
650
600
550
500
450
400
350
300
250
200
150
100
50
0
2.5-15.0
15.1-30.0
30.1-45.0
45.1-60.0
60.1-75.0
75.1-90.0
90.1-105.0
105.1-120.0
120.1+
Diameter class (cm)

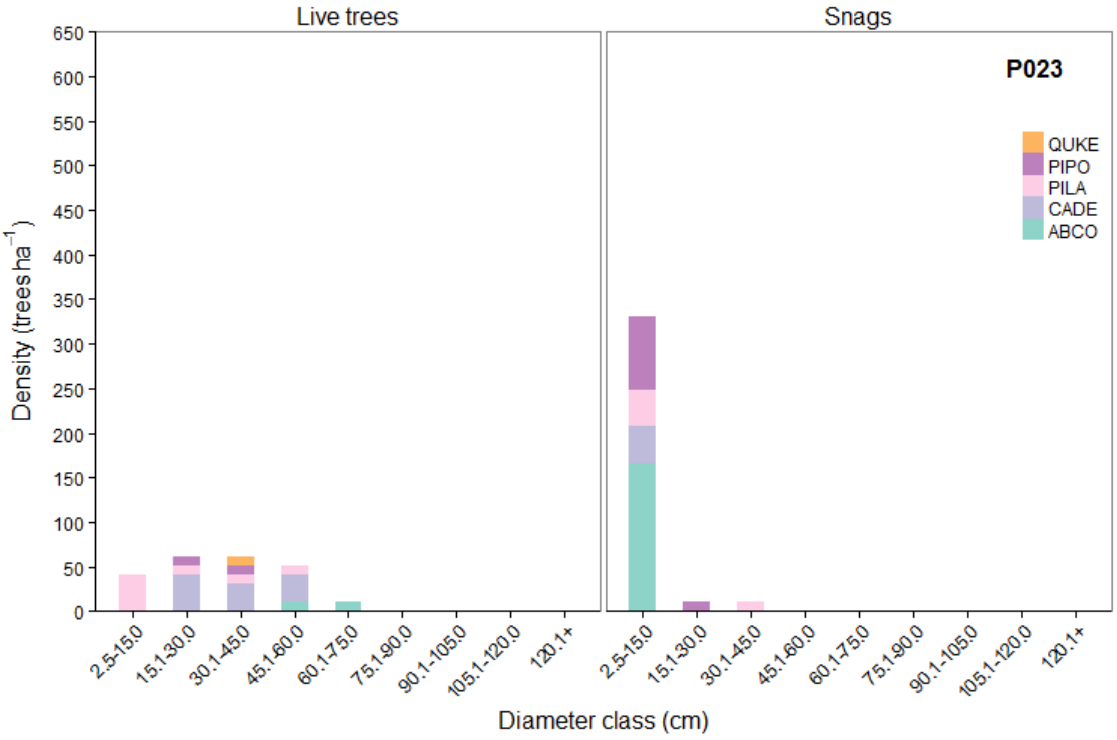
Live trees
Snags
P023
QUKE
PIPO
PILA
CADE
ABCO
Density (trees ha^{-1})
650
600
550
500
450
400
350
300
250
200
150
100
50
0
2.5-15.0
15.1-30.0
30.1-45.0
45.1-60.0
60.1-75.0
75.1-90.0
90.1-105.0
105.1-120.0
120.1+
Diameter class (cm)

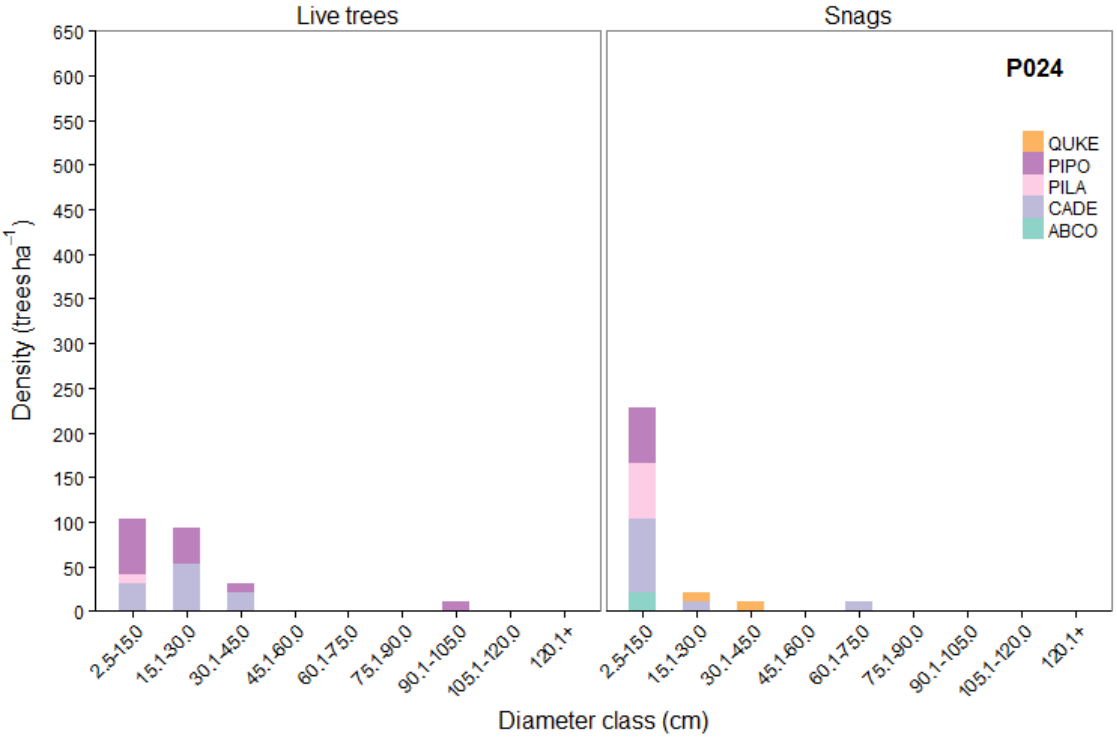
Live trees
Snags
P024
QUKE
PIPO
PILA
CADE
ABCO
Density (trees ha^{-1})
650
600
550
500
450
400
350
300
250
200
150
100
50
0
2.5-15.0
15.1-30.0
30.1-45.0
45.1-60.0
60.1-75.0
75.1-90.0
90.1-105.0
105.1-120.0
120.1+
Diameter class (cm)

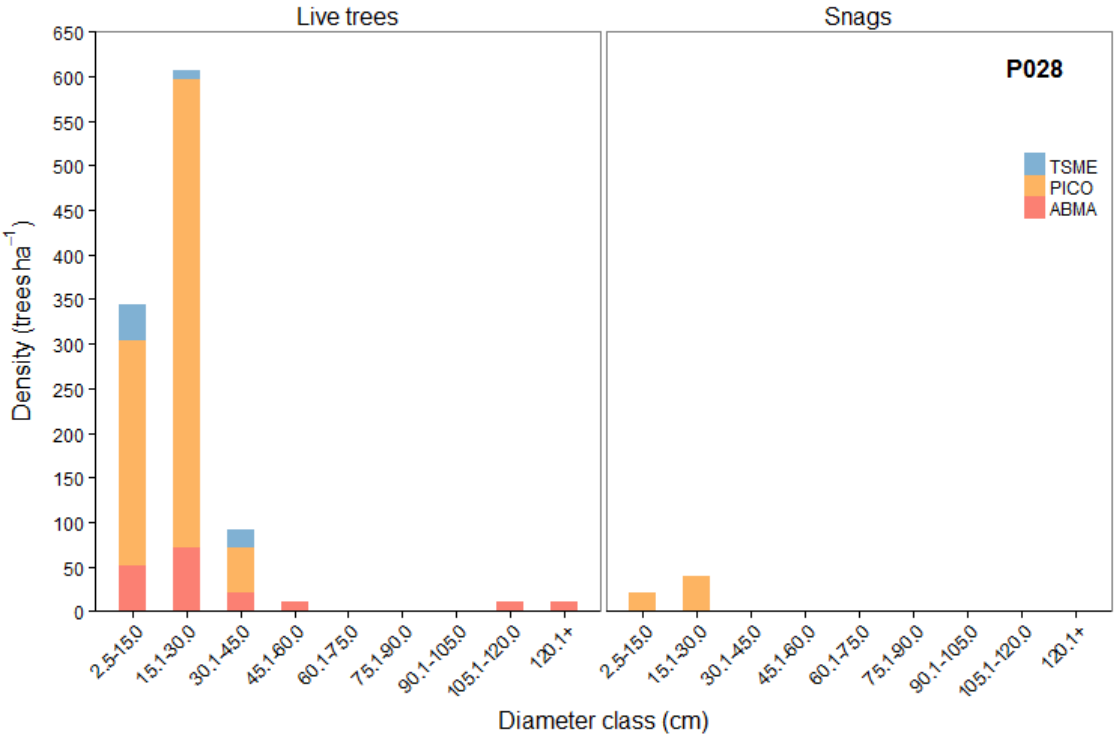
Live trees
Snags
P028
TSME
PICO
ABMA
Density (trees ha^{-1})
650
600
550
500
450
400
350
300
250
200
150
100
50
0
2.5-15.0
15.1-30.0
30.1-45.0
45.1-60.0
60.1-75.0
75.1-90.0
90.1-105.0
105.1-120.0
120.1+
Diameter class (cm)

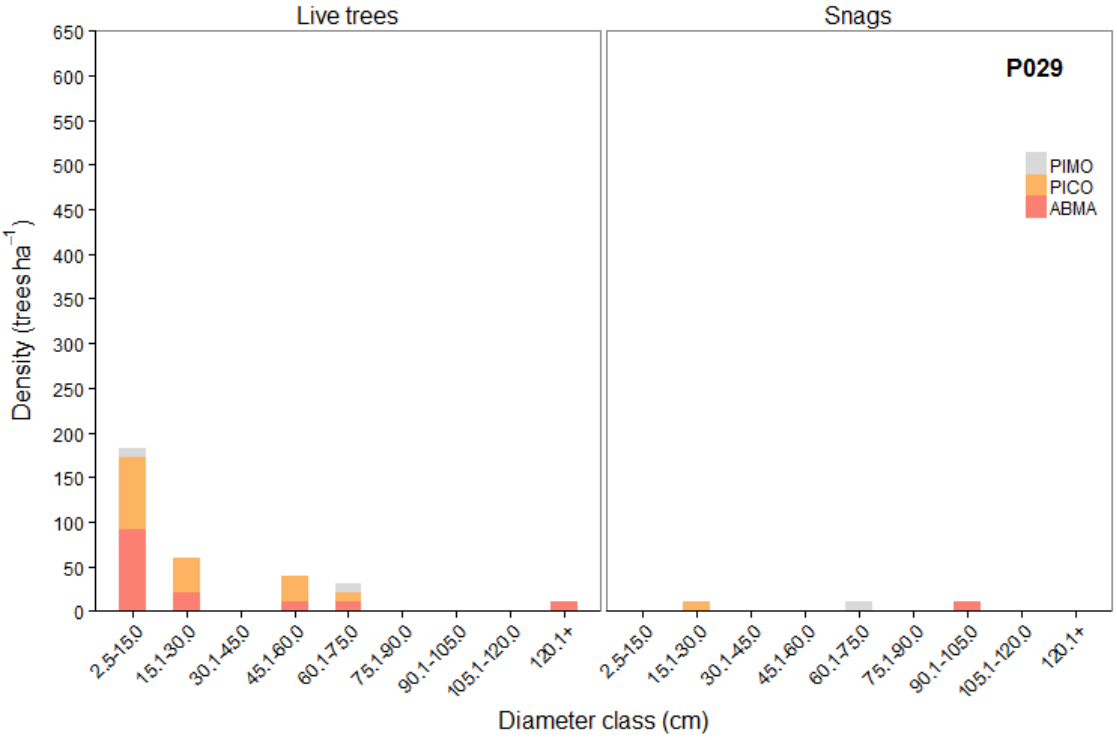
Live trees
Snags
P029
PIMO
PICO
ABMA
Density (trees ha^{-1})
650
600
550
500
450
400
350
300
250
200
150
100
50
0
2.5-15.0
15.1-30.0
30.1-45.0
45.1-60.0
60.1-75.0
75.1-90.0
90.1-105.0
105.1-120.0
120.1+
Diameter class (cm)

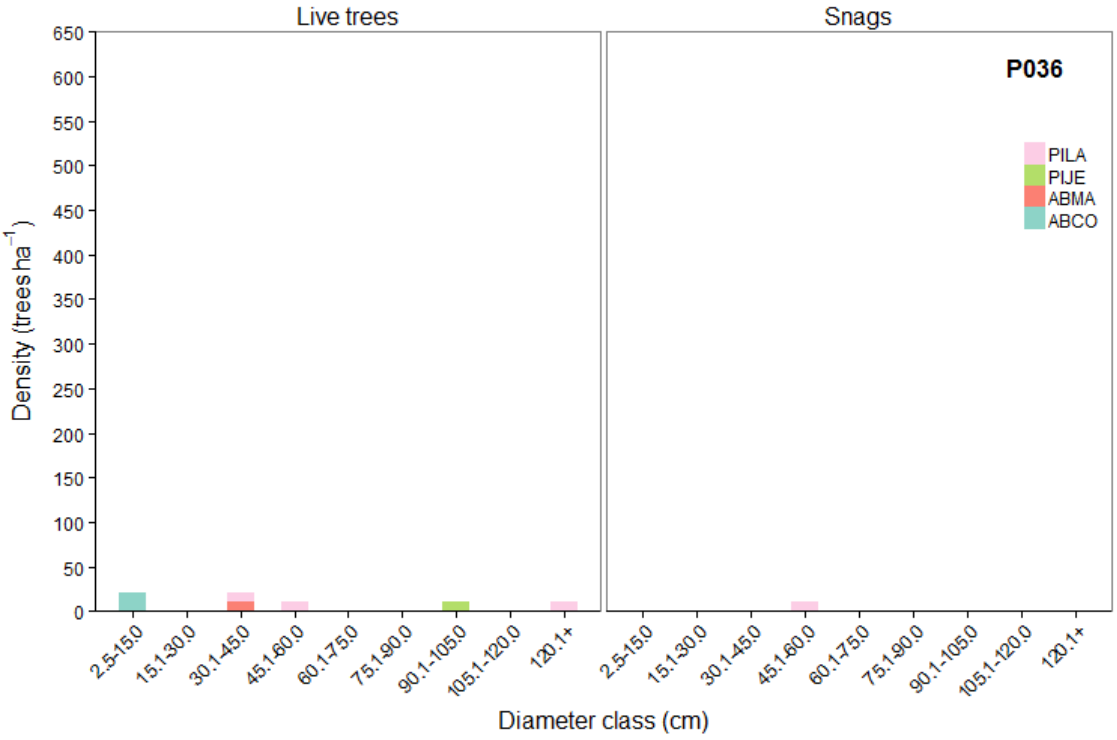
Live trees
Snags
P036
PILA
PIJE
ABMA
ABCO
Density (trees ha^{-1})
650
600
550
500
450
400
350
300
250
200
150
100
50
0
2.5-15.0
15.1-30.0
30.1-45.0
45.1-60.0
60.1-75.0
75.1-90.0
90.1-105.0
105.1-120.0
120.1+
Diameter class (cm)

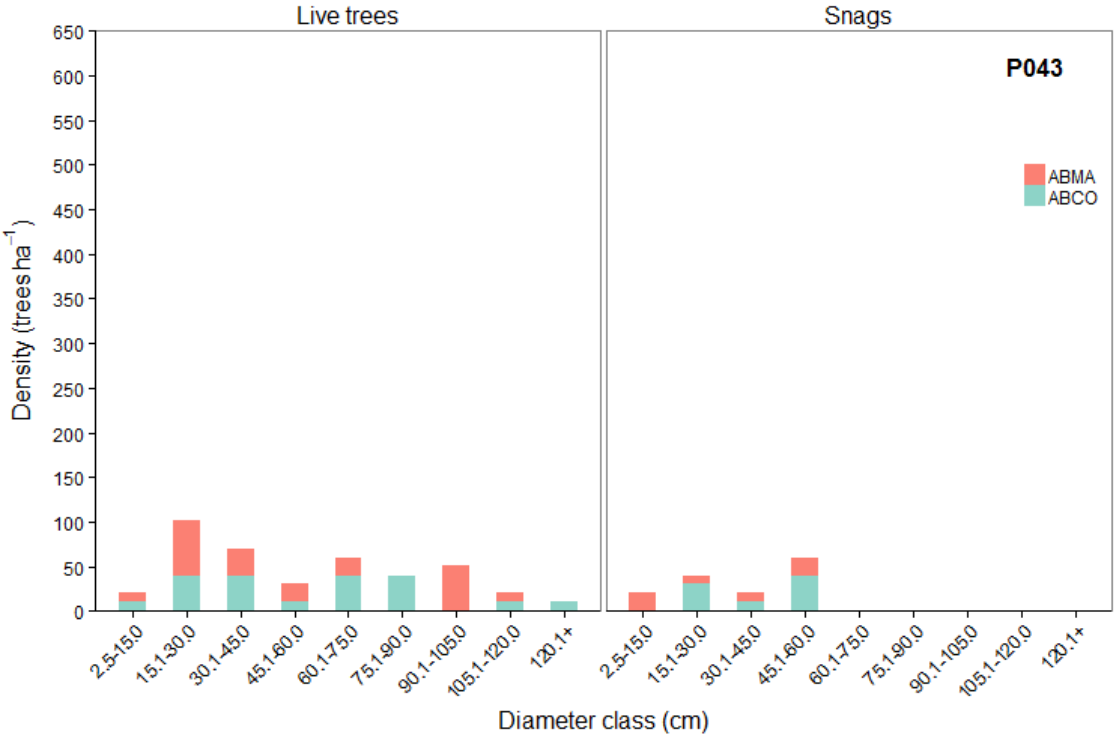
Live trees
Snags
P043
ABMA
ABCO
Density (trees ha^{-1})
650
600
550
500
450
400
350
300
250
200
150
100
50
0
2.5-15.0
15.1-30.0
30.1-45.0
45.1-60.0
60.1-75.0
75.1-90.0
90.1-105.0
105.1-120.0
120.1+
Diameter class (cm)

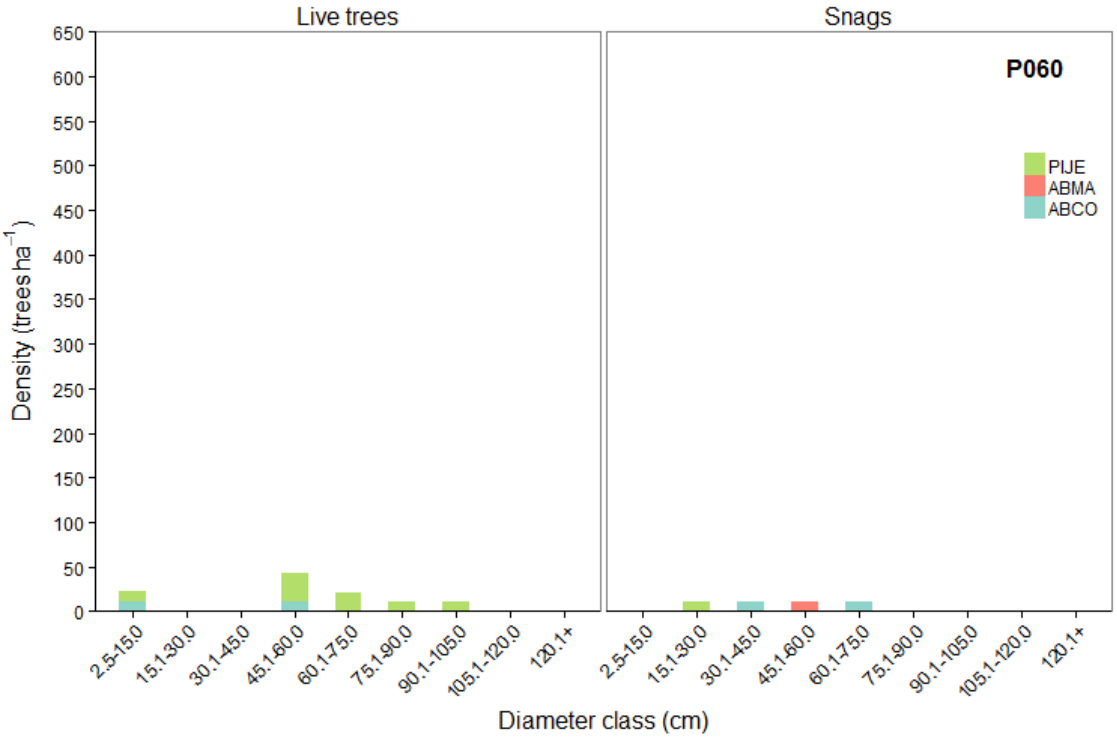
Live trees
Snags
P060
PIJE
ABMA
ABCO
Density (trees ha^{-1})
650
600
550
500
450
400
350
300
250
200
150
100
50
0
2.5-15.0
15.1-30.0
30.1-45.0
45.1-60.0
60.1-75.0
75.1-90.0
90.1-105.0
105.1-120.0
120.1+
Diameter class (cm)

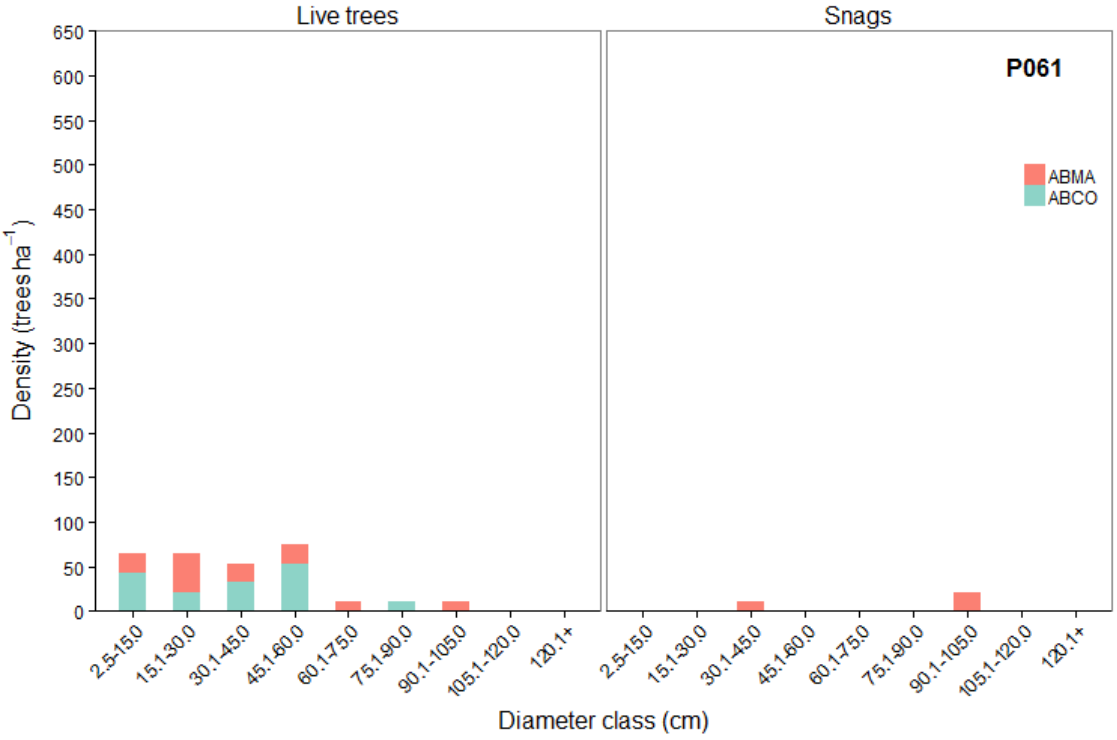
Live trees
Snags
P061
ABMA
ABCO
Density (trees ha^{-1})
650
600
550
500
450
400
350
300
250
200
150
100
50
0
2.5-15.0
15.1-30.0
30.1-45.0
45.1-60.0
60.1-75.0
75.1-90.0
90.1-105.0
105.1-120.0
120.1+
Diameter class (cm)

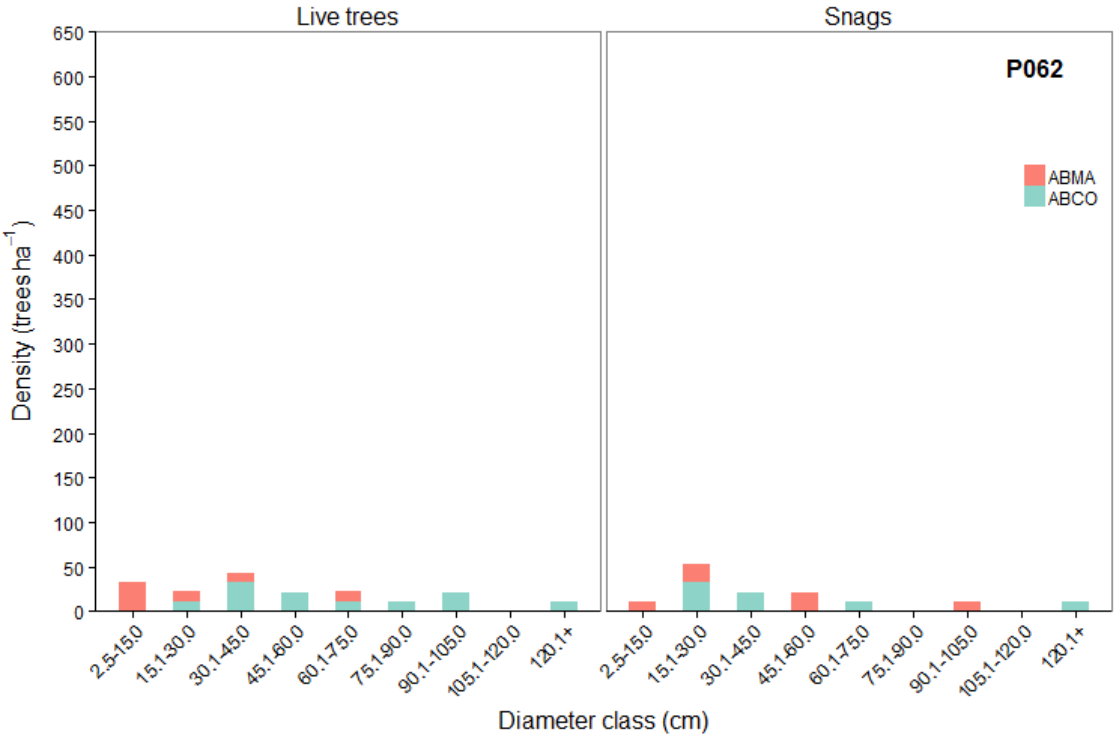
Live trees
Snags
P062
ABMA
ABCO
Density (trees ha^{-1})
650
600
550
500
450
400
350
300
250
200
150
100
50
0
2.5-15.0
15.1-30.0
30.1-45.0
45.1-60.0
60.1-75.0
75.1-90.0
90.1-105.0
105.1-120.0
120.1+
Diameter class (cm)

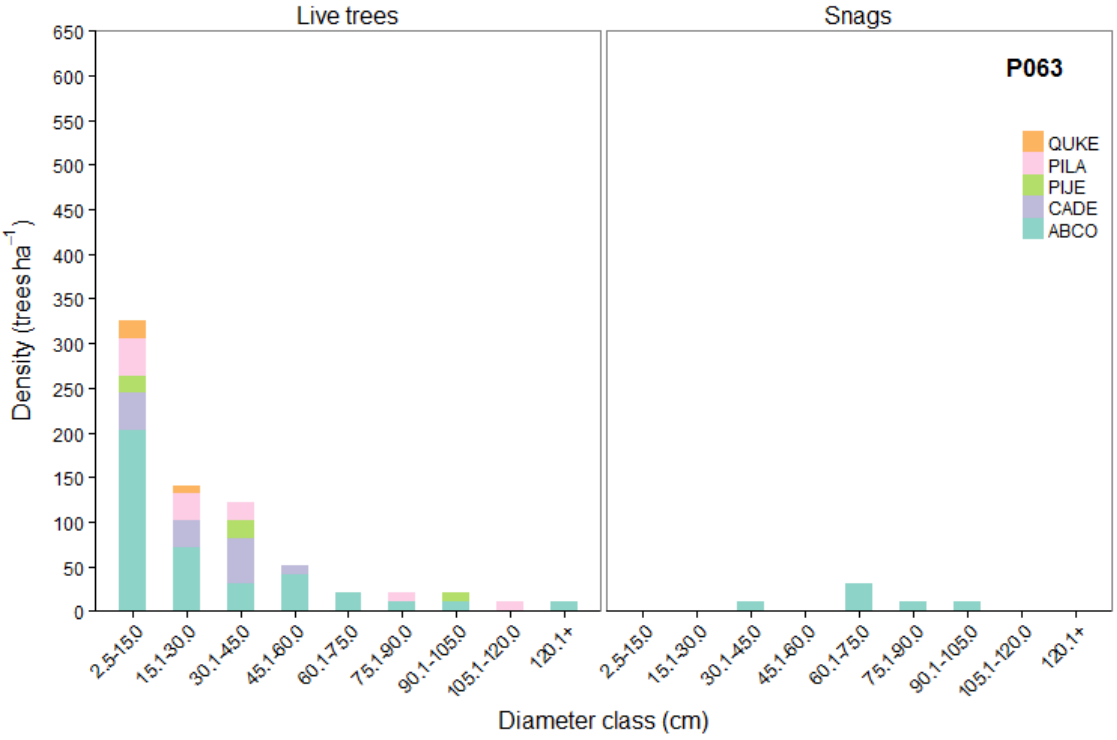
Live trees
Snags
P063
QUKE
PILA
PIJE
CADE
ABCO
Density (trees ha^{-1})
650
600
550
500
450
400
350
300
250
200
150
100
50
0
2.5-15.0
15.1-30.0
30.1-45.0
45.1-60.0
60.1-75.0
75.1-90.0
90.1-105.0
105.1-120.0
120.1+
Diameter class (cm)

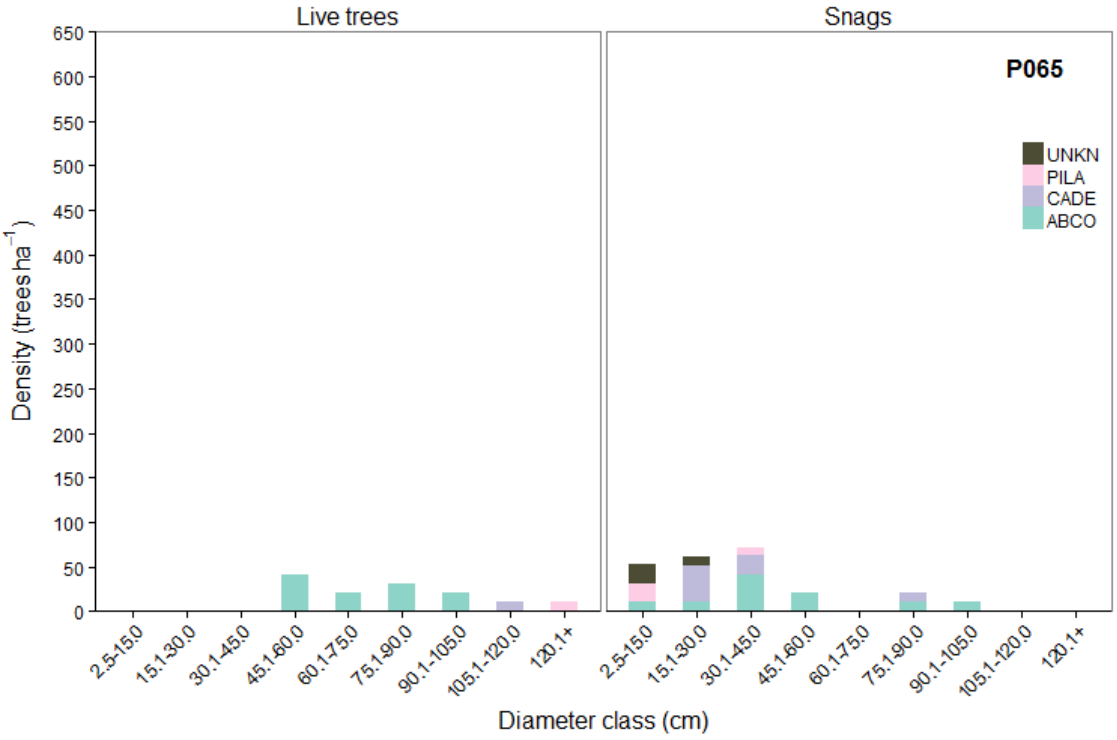
Live trees
Snags
P065
UNKN
PILA
CADE
ABCO
Density (trees ha^{-1})
650
600
550
500
450
400
350
300
250
200
150
100
50
0
2.5-15.0
15.1-30.0
30.1-45.0
45.1-60.0
60.1-75.0
75.1-90.0
90.1-105.0
105.1-120.0
120.1+
Diameter class (cm)

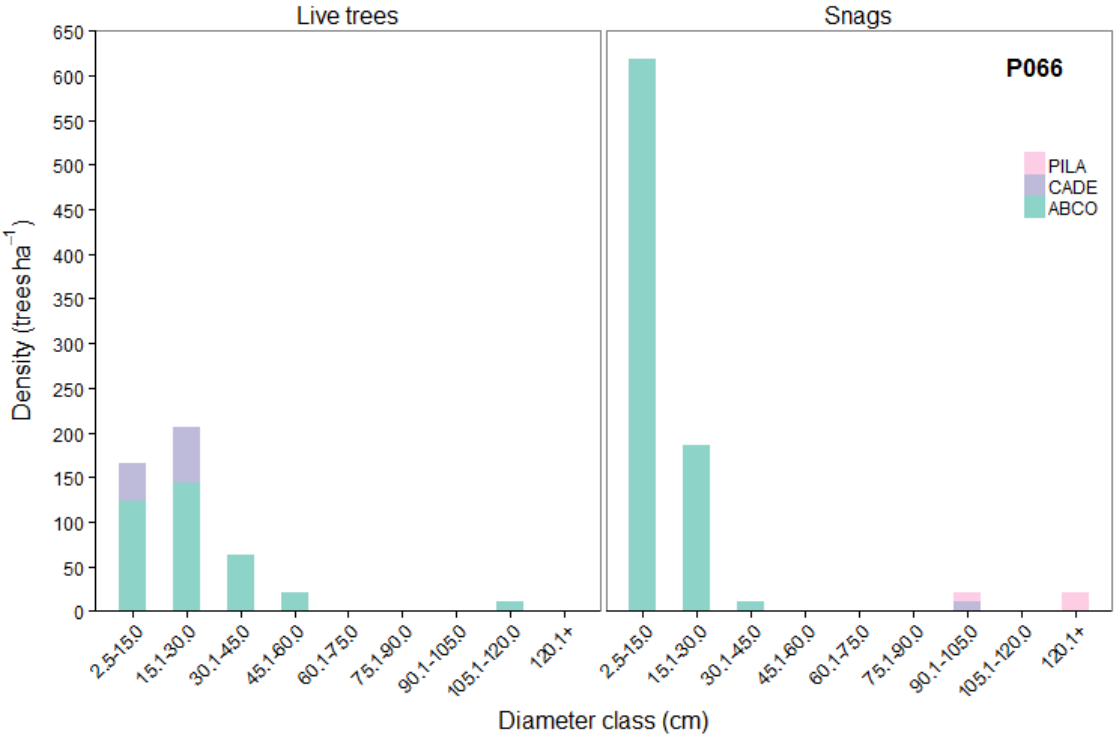
Live trees
Snags
P066
PILA
CADE
ABCO
Density (trees ha^{-1})
650
600
550
500
450
400
350
300
250
200
150
100
50
0
2.5-15.0
15.1-30.0
30.1-45.0
45.1-60.0
60.1-75.0
75.1-90.0
90.1-105.0
105.1-120.0
120.1+
Diameter class (cm)

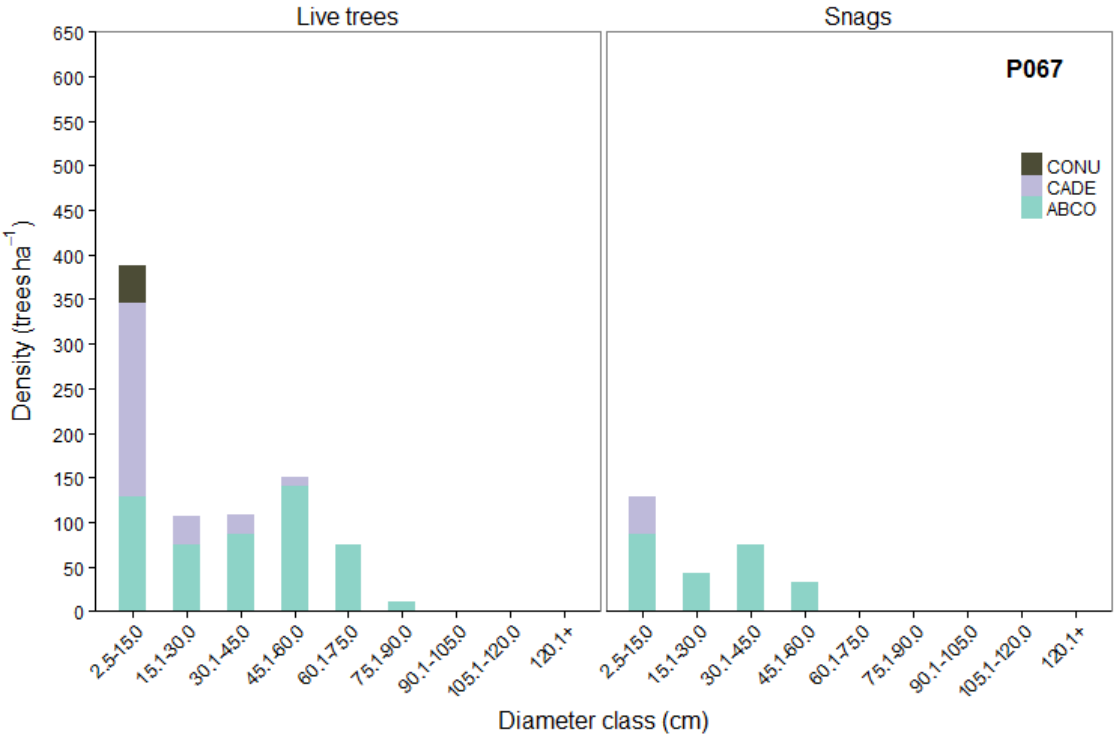
Live trees
Snags
P067
CONU
CADE
ABCO
Density (trees ha^{-1})
650
600
550
500
450
400
350
300
250
200
150
100
50
0
2.5-15.0
15.1-30.0
30.1-45.0
45.1-60.0
60.1-75.0
75.1-90.0
90.1-105.0
105.1-120.0
120.1+
Diameter class (cm)

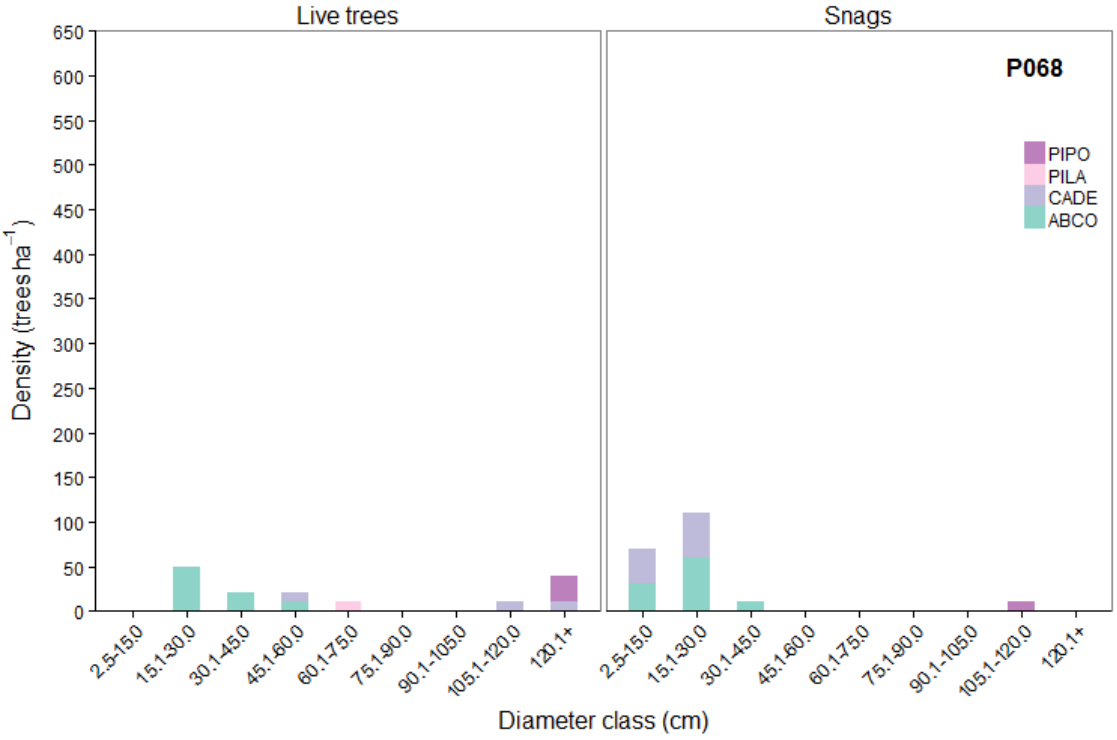
Live trees
Snags
P068
PIPO
PILA
CADE
ABCO
Density (trees ha^{-1})
650
600
550
500
450
400
350
300
250
200
150
100
50
0
2.5-15.0
15.1-30.0
30.1-45.0
45.1-60.0
60.1-75.0
75.1-90.0
90.1-105.0
105.1-120.0
120.1+
Diameter class (cm)

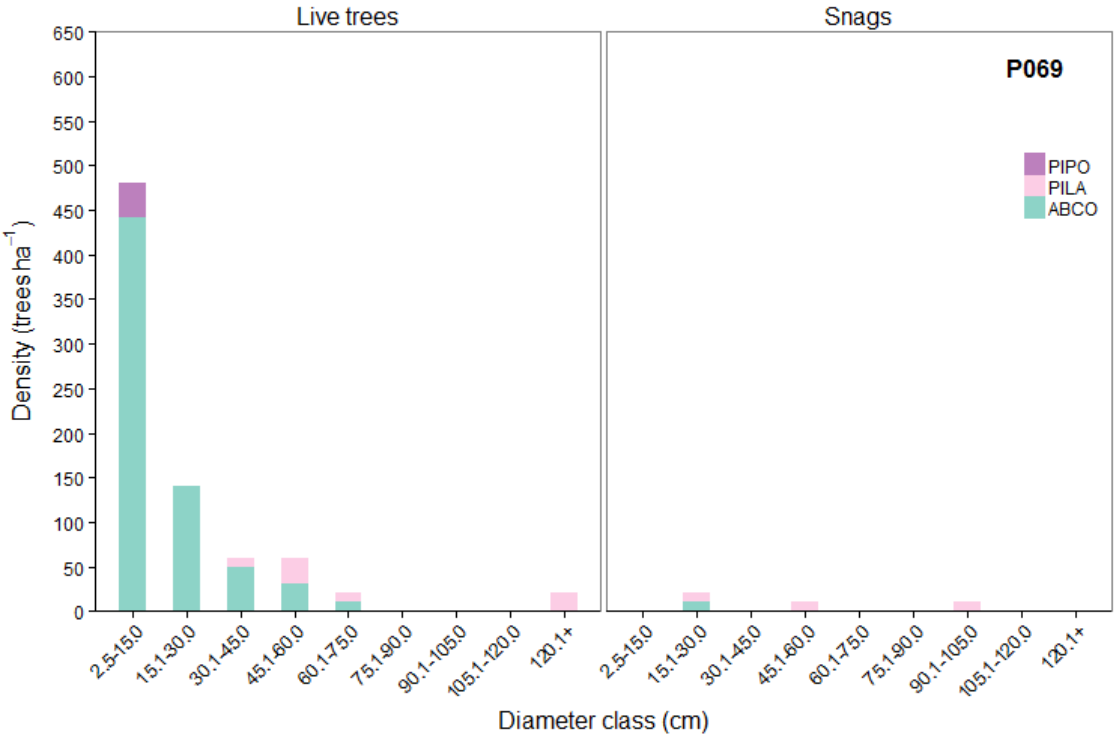
Live trees
Snags
P069
PIPO
PILA
ABCO
Density (trees ha^{-1})
650
600
550
500
450
400
350
300
250
200
150
100
50
0
2.5-15.0
15.1-30.0
30.1-45.0
45.1-60.0
60.1-75.0
75.1-90.0
90.1-105.0
105.1-120.0
120.1+
Diameter class (cm)

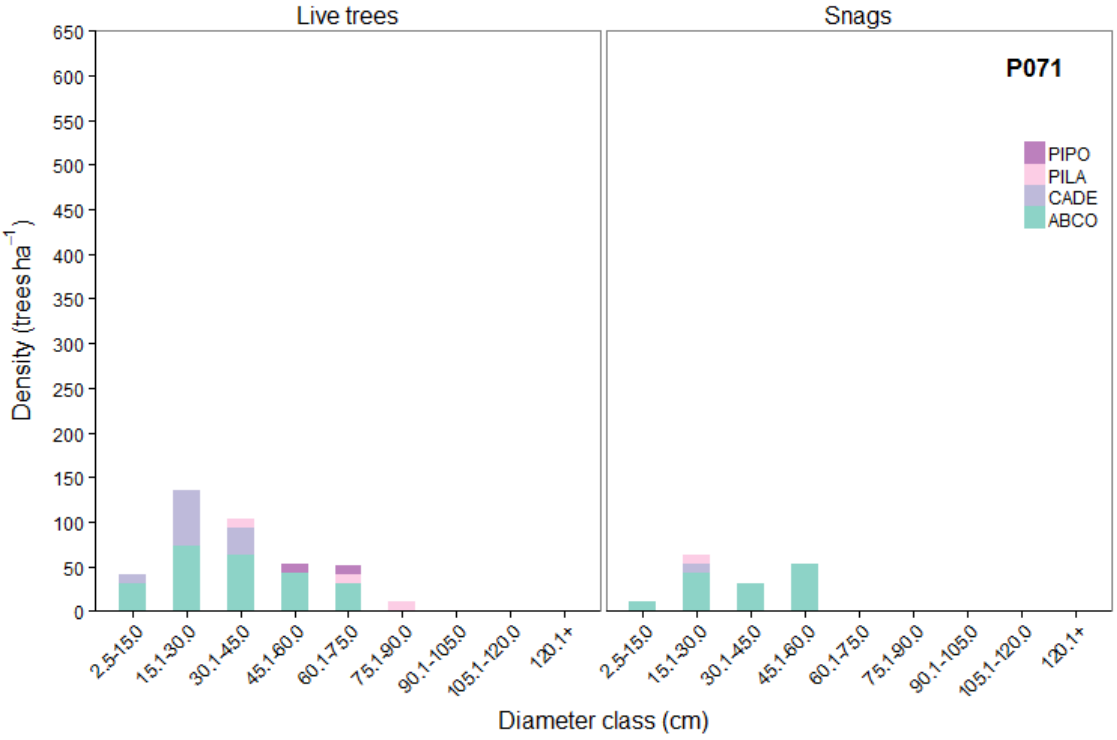
Live trees
Snags
P071
PIPO
PILA
CADE
ABCO
Density (trees ha^{-1})
650
600
550
500
450
400
350
300
250
200
150
100
50
0
2.5-15.0
15.1-30.0
30.1-45.0
45.1-60.0
60.1-75.0
75.1-90.0
90.1-105.0
105.1-120.0
120.1+
Diameter class (cm)

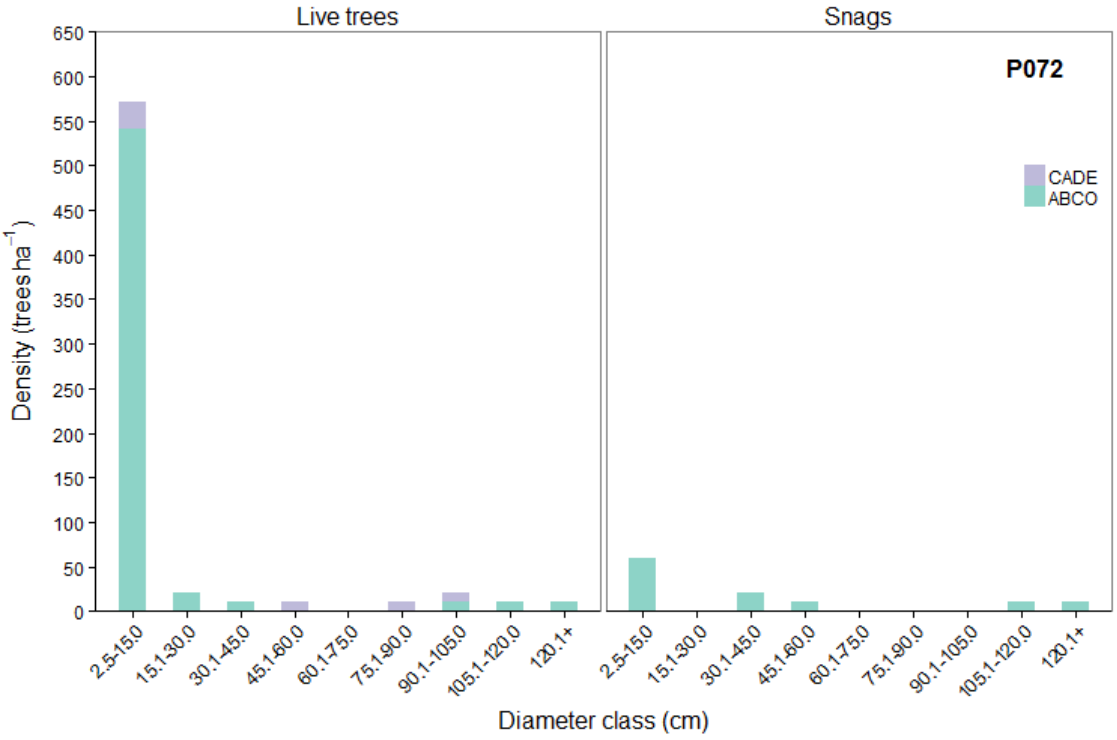
Live trees
Snags
P072
CADE
ABCO
Density (trees ha^{-1})
650
600
550
500
450
400
350
300
250
200
150
100
50
0
2.5-15.0
15.1-30.0
30.1-45.0
45.1-60.0
60.1-75.0
75.1-90.0
90.1-105.0
105.1-120.0
120.1+
Diameter class (cm)

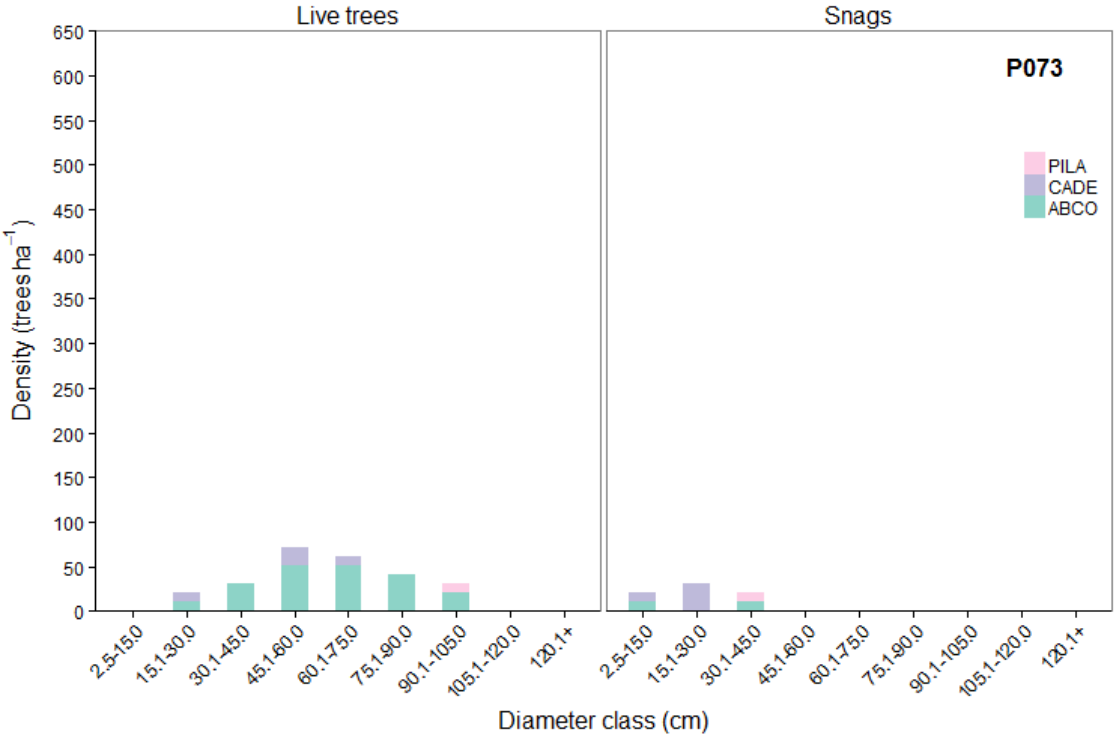
Live trees
Snags
P073
PILA
CADE
ABCO
Density (trees ha^{-1})
650
600
550
500
450
400
350
300
250
200
150
100
50
0
2.5-15.0
15.1-30.0
30.1-45.0
45.1-60.0
60.1-75.0
75.1-90.0
90.1-105.0
105.1-120.0
120.1+
Diameter class (cm)

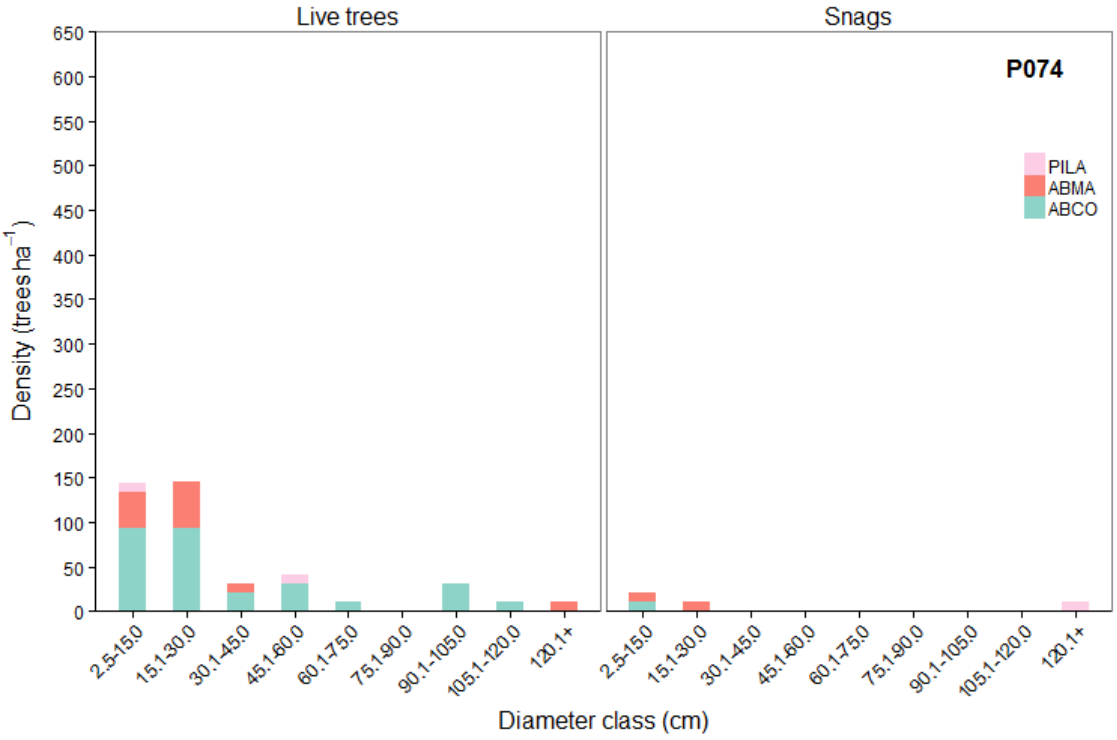
Live trees
Snags
P074
PILA
ABMA
ABCO
Density (trees ha^{-1})
650
600
550
500
450
400
350
300
250
200
150
100
50
0
2.5-15.0
15.1-30.0
30.1-45.0
45.1-60.0
60.1-75.0
75.1-90.0
90.1-105.0
105.1-120.0
120.1+
Diameter class (cm)

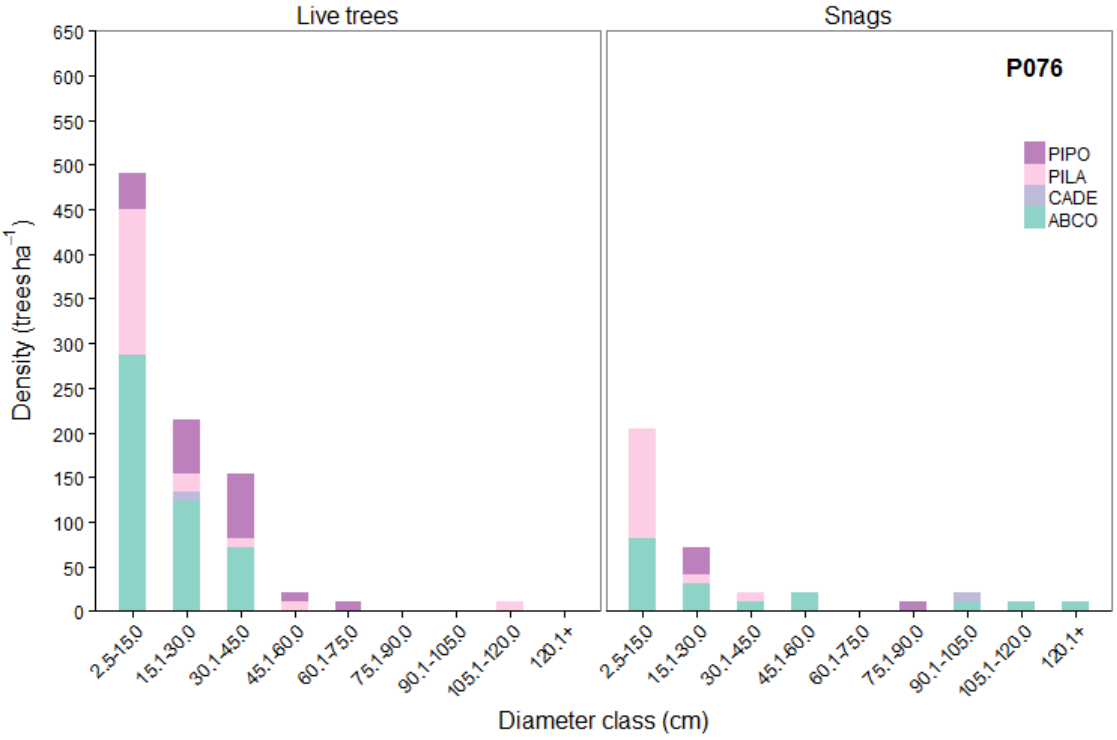
Live trees
Snags
P076
PIPO
PILA
CADE
ABCO
Density (trees ha^{-1})
650
600
550
500
450
400
350
300
250
200
150
100
50
0
2.5-15.0
15.1-30.0
30.1-45.0
45.1-60.0
60.1-75.0
75.1-90.0
90.1-105.0
105.1-120.0
120.1+
Diameter class (cm)

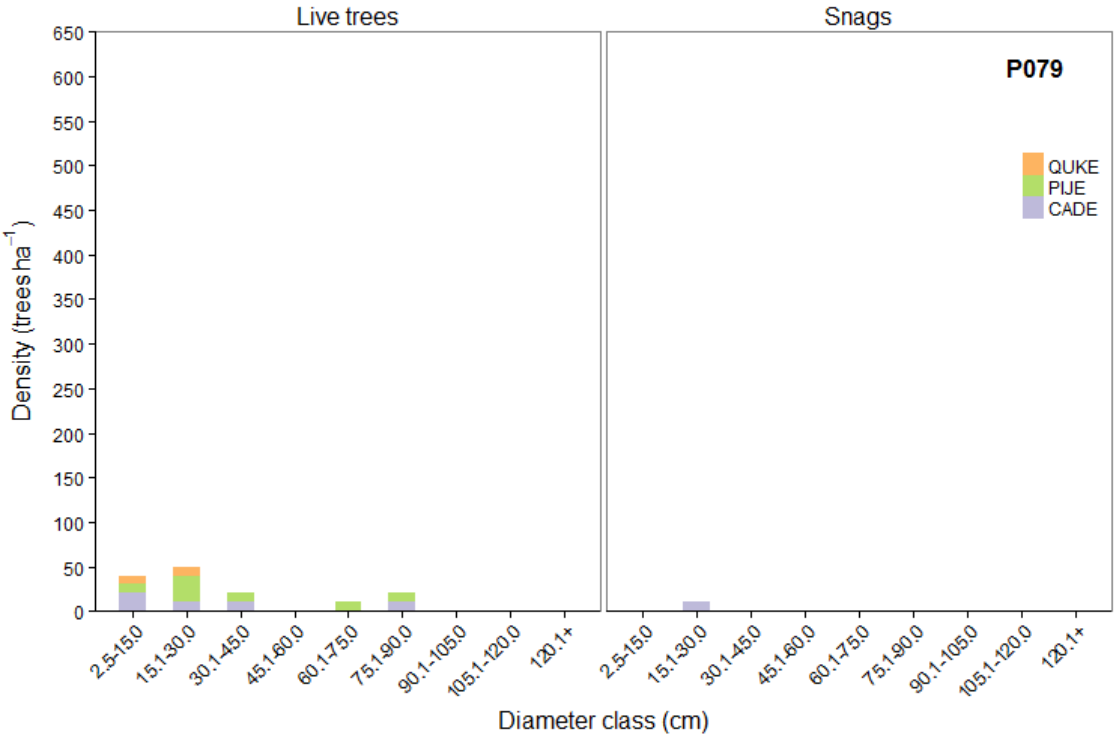
Live trees
Snags
P079
QUKE
PIJE
CADE
Density (trees ha^{-1})
650
600
550
500
450
400
350
300
250
200
150
100
50
0
2.5-15.0
15.1-30.0
30.1-45.0
45.1-60.0
60.1-75.0
75.1-90.0
90.1-105.0
105.1-120.0
120.1+
Diameter class (cm)

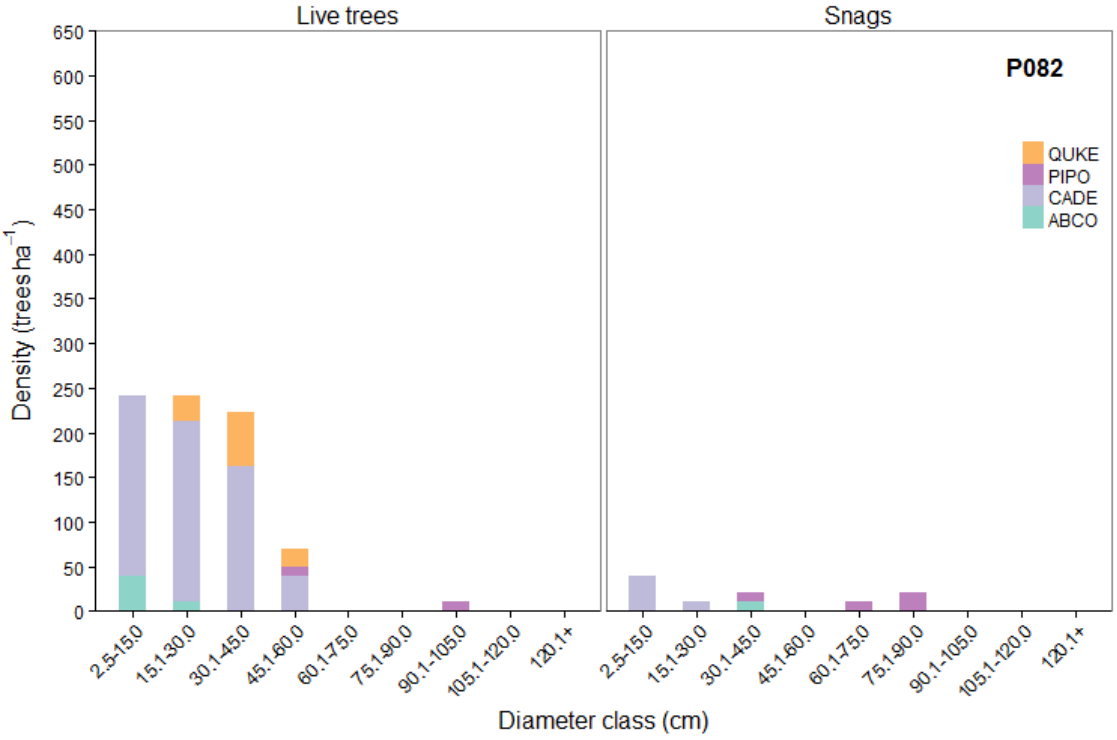
Live trees
Snags
P082
QUKE
PIPO
CADE
ABCO
Density (trees ha^{-1})
650
600
550
500
450
400
350
300
250
200
150
100
50
0
2.5-15.0
15.1-30.0
30.1-45.0
45.1-60.0
60.1-75.0
75.1-90.0
90.1-105.0
105.1-120.0
120.1+
Diameter class (cm)

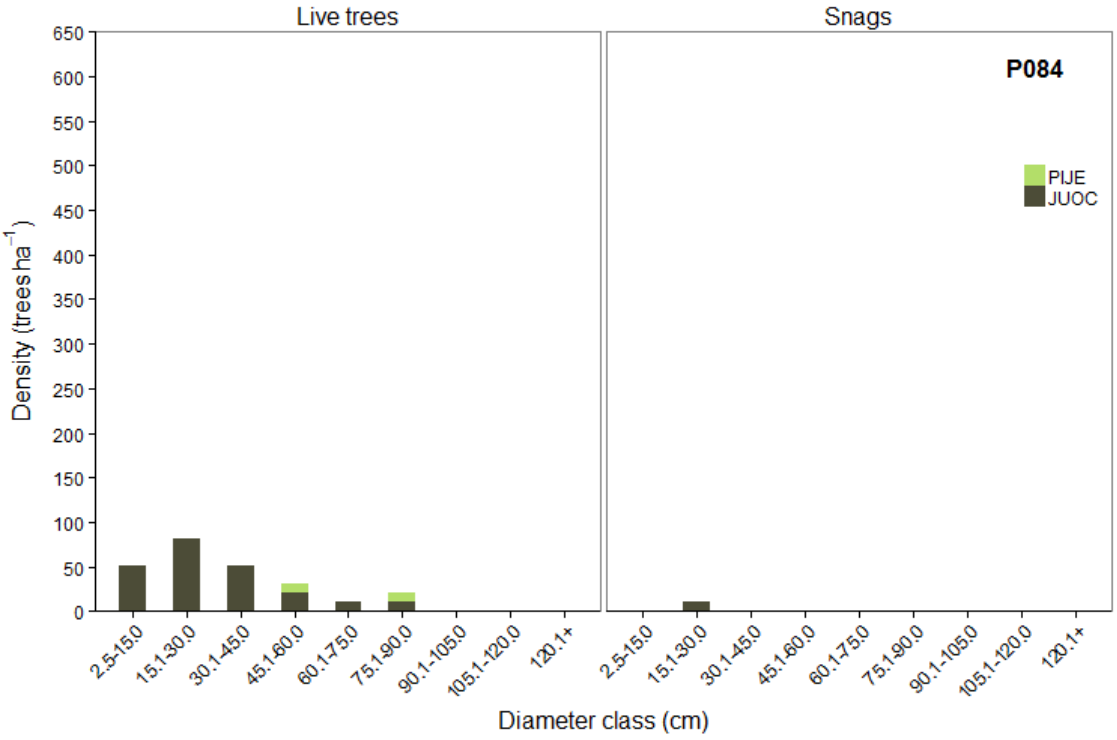
Live trees
Snags
P084
PIJE
JUOC
Density (trees ha^{-1})
650
600
550
500
450
400
350
300
250
200
150
100
50
0
2.5-15.0
15.1-30.0
30.1-45.0
45.1-60.0
60.1-75.0
75.1-90.0
90.1-105.0
105.1-120.0
120.1+
Diameter class (cm)

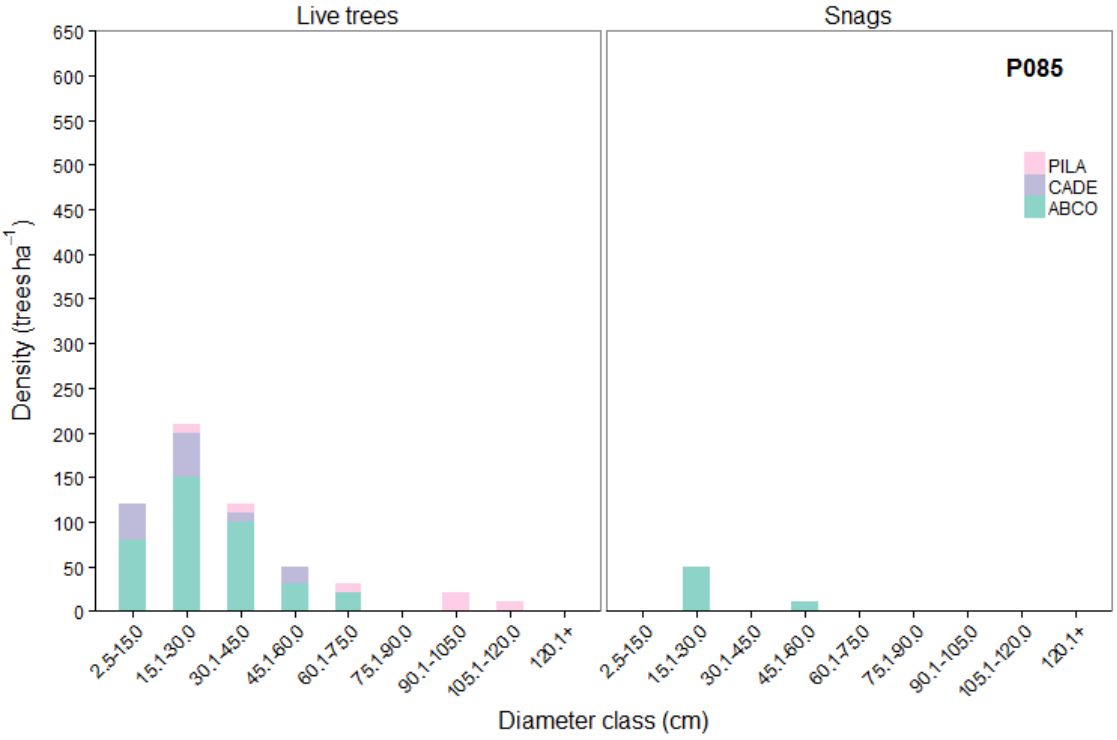
Live trees
Snags
P085
PILA
CADE
ABCO
Density (trees ha^{-1})
650
600
550
500
450
400
350
300
250
200
150
100
50
0
2.5-15.0
15.1-30.0
30.1-45.0
45.1-60.0
60.1-75.0
75.1-90.0
90.1-105.0
105.1-120.0
120.1+
Diameter class (cm)

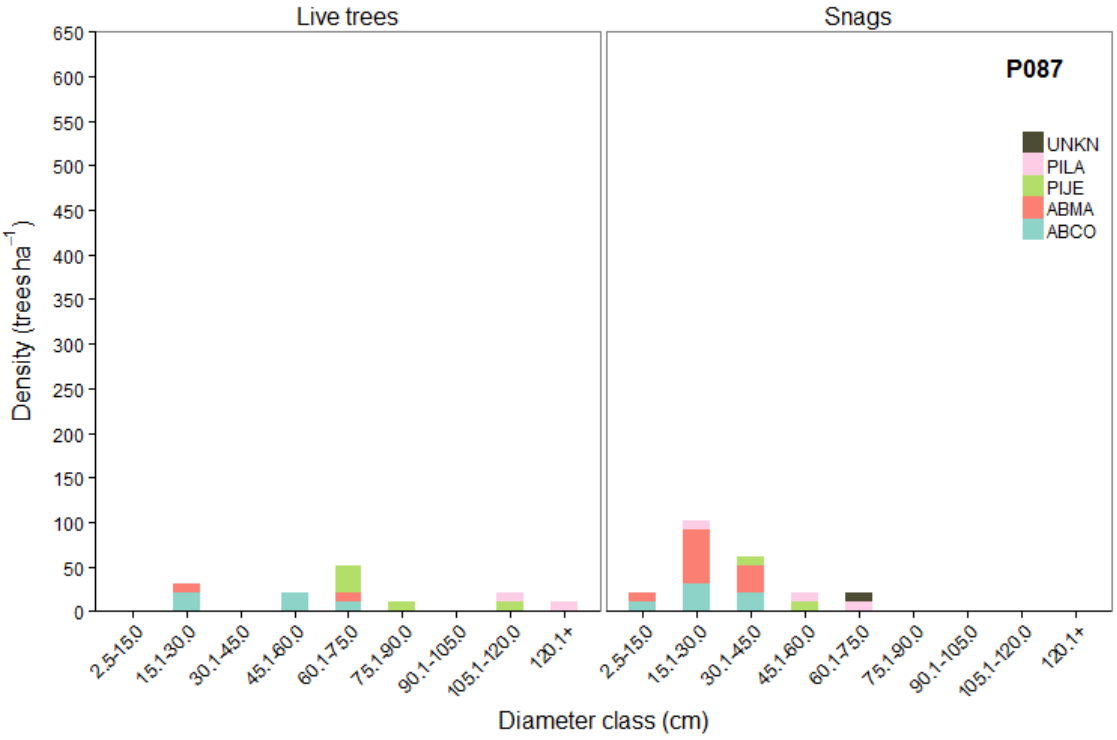
Live trees
Snags
P087
UNKN
PILA
PIJE
ABMA
ABCO
Density (trees ha^{-1})
650
600
550
500
450
400
350
300
250
200
150
100
50
0
2.5-15.0
15.1-30.0
30.1-45.0
45.1-60.0
60.1-75.0
75.1-90.0
90.1-105.0
105.1-120.0
120.1+
Diameter class (cm)

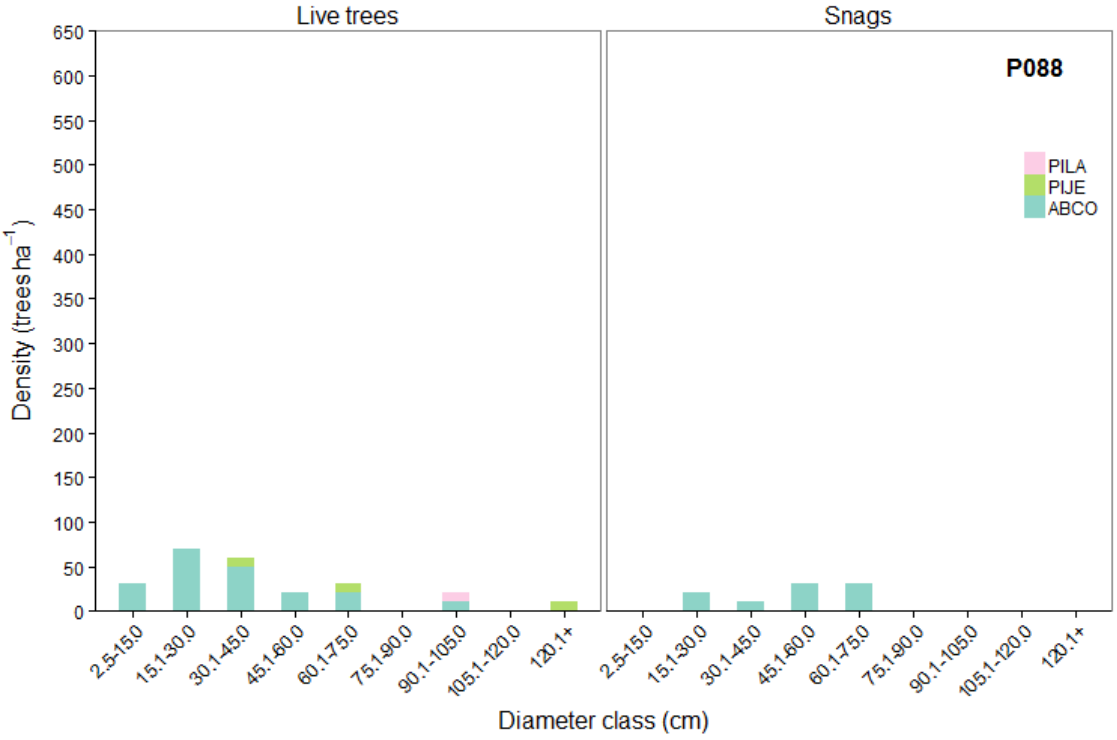
Live trees
Snags
P088
PILA
PIJE
ABCO
Density (trees ha^{-1})
650
600
550
500
450
400
350
300
250
200
150
100
50
0
2.5-15.0
15.1-30.0
30.1-45.0
45.1-60.0
60.1-75.0
75.1-90.0
90.1-105.0
105.1-120.0
120.1+
Diameter class (cm)

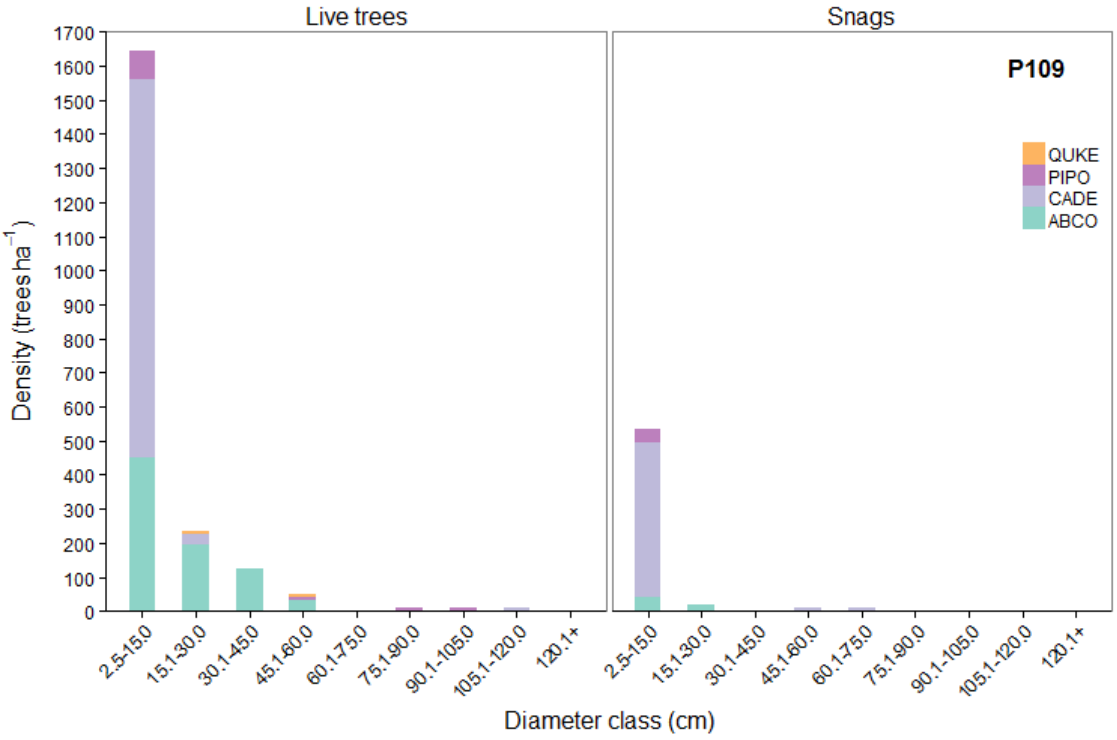
Live trees
Snags
P109
QUKE
PIPO
CADE
ABCO
Density (trees ha^{-1})
1700
1600
1500
1400
1300
1200
1100
1000
900
800
700
600
500
400
300
200
100
0
2.5-15.0
15.1-30.0
30.1-45.0
45.1-60.0
60.1-75.0
75.1-90.0
90.1-105.0
105.1-120.0
120.1+
Diameter class (cm)

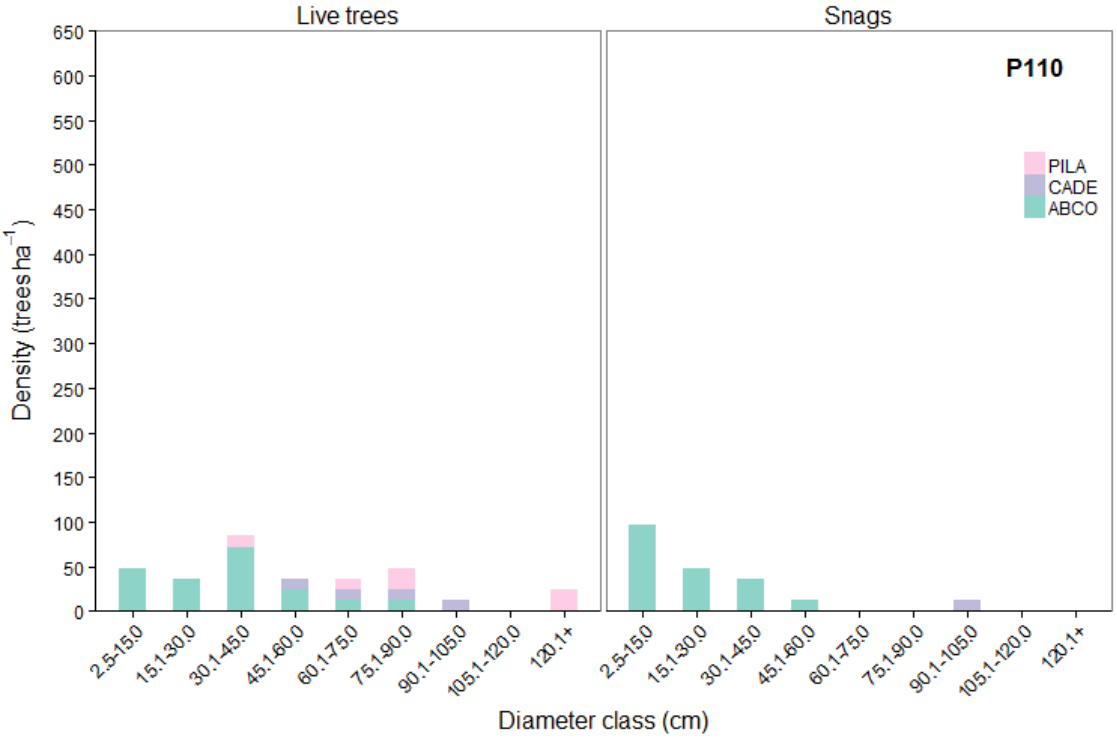
Live trees
Snags
P110
PILA
CADE
ABCO
Density (trees ha^{-1})
650
600
550
500
450
400
350
300
250
200
150
100
50
0
2.5-15.0
15.1-30.0
30.1-45.0
45.1-60.0
60.1-75.0
75.1-90.0
90.1-105.0
105.1-120.0
120.1+
Diameter class (cm)

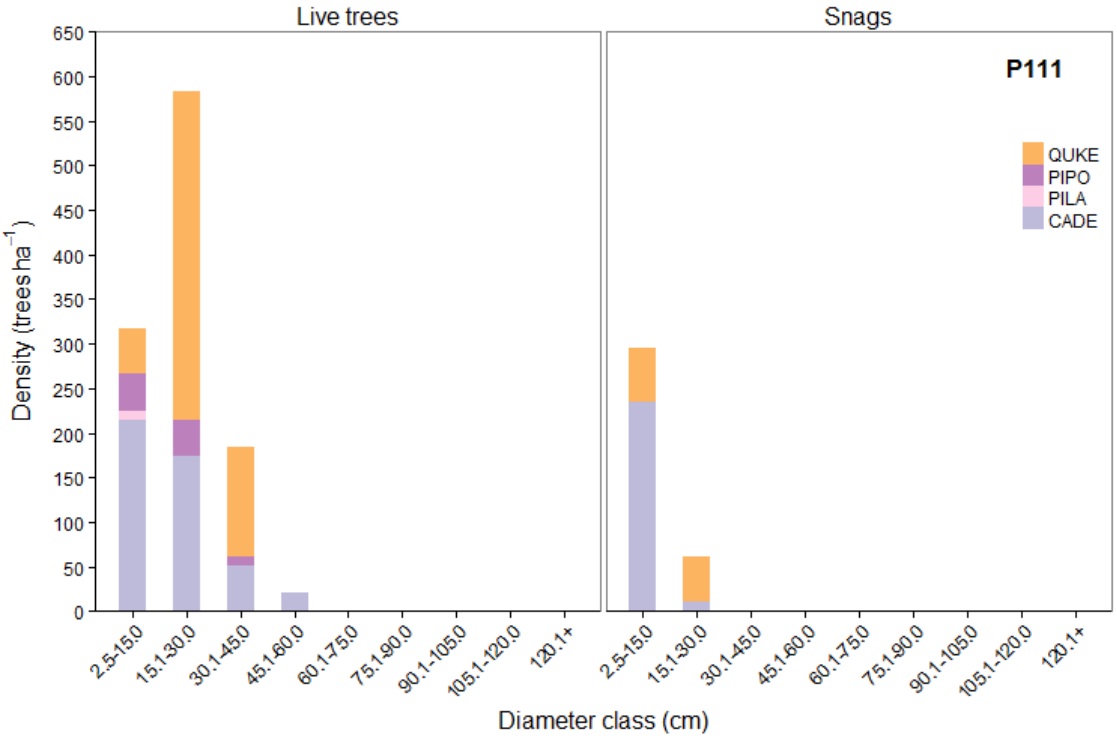
Live trees
Snags
P111
QUKE
PIPO
PILA
CADE
Density (trees ha^{-1})
650
600
550
500
450
400
350
300
250
200
150
100
50
0
2.5-15.0
15.1-30.0
30.1-45.0
45.1-60.0
60.1-75.0
75.1-90.0
90.1-105.0
105.1-120.0
120.1+
Diameter class (cm)

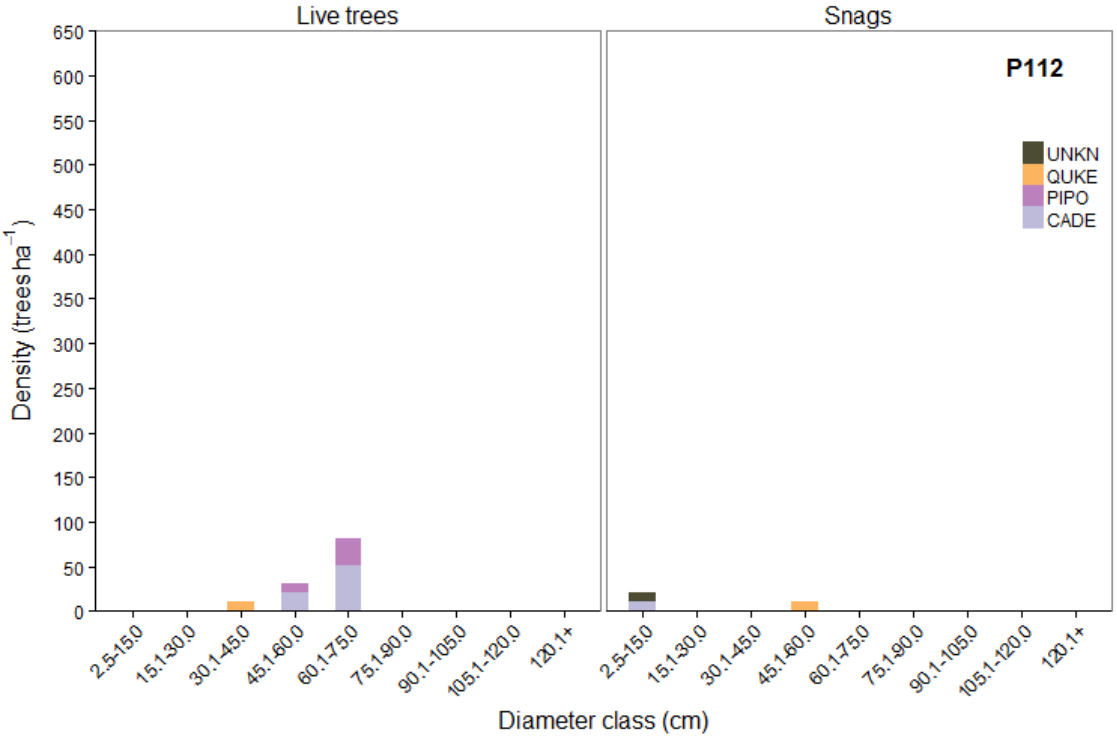
Live trees
Snags
P112
UNKN
QUKE
PIPO
CADE
Density (trees ha^{-1})
650
600
550
500
450
400
350
300
250
200
150
100
50
0
2.5-15.0
15.1-30.0
30.1-45.0
45.1-60.0
60.1-75.0
75.1-90.0
90.1-105.0
105.1-120.0
120.1+
Diameter class (cm)

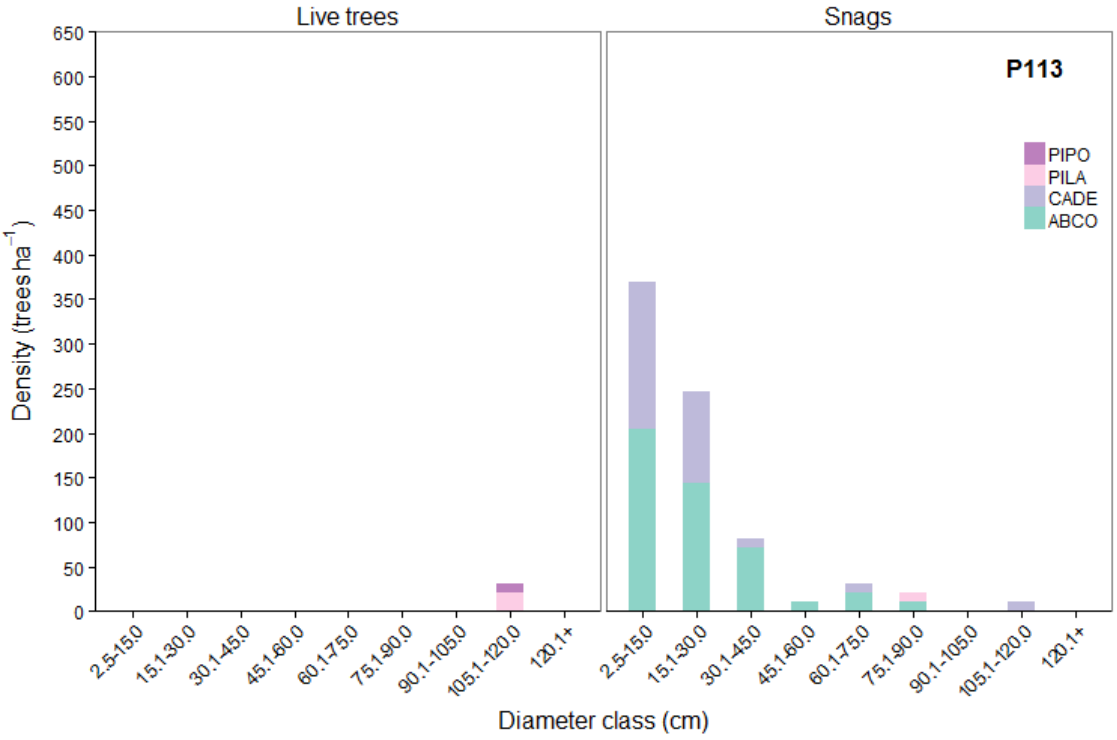
Live trees
Snags
P113
PIPO
PILA
CADE
ABCO
Density (trees ha^{-1})
650
600
550
500
450
400
350
300
250
200
150
100
50
0
2.5-15.0
15.1-30.0
30.1-45.0
45.1-60.0
60.1-75.0
75.1-90.0
90.1-105.0
105.1-120.0
120.1+
Diameter class (cm)

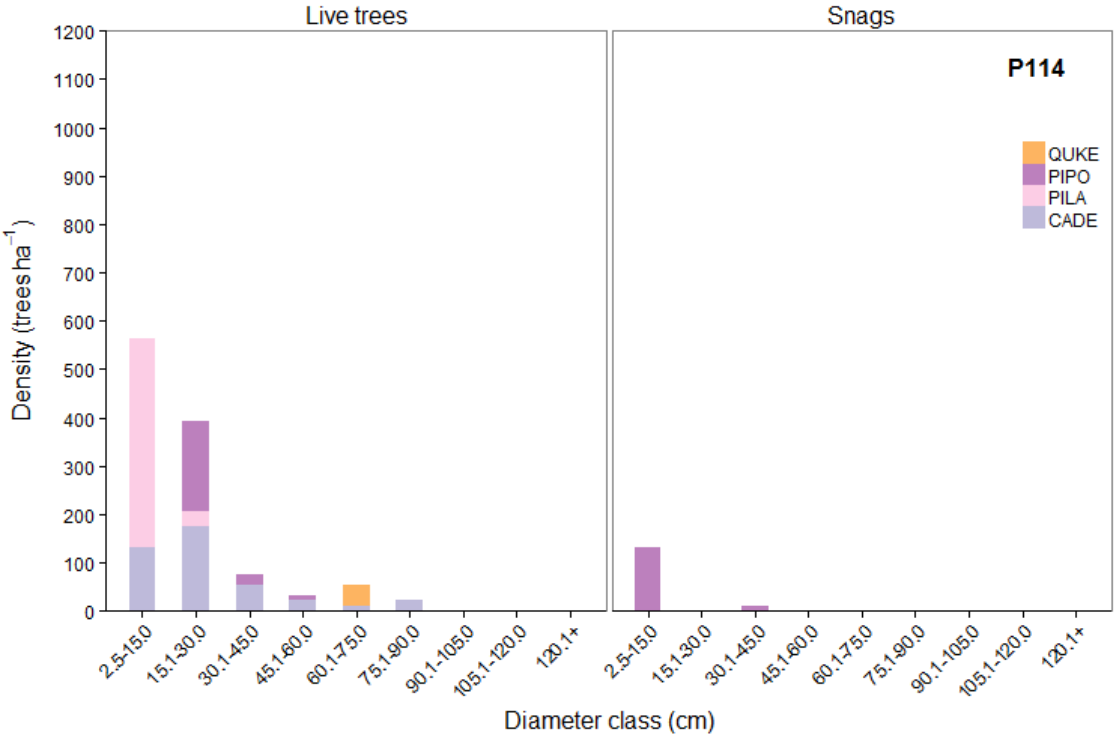
Live trees
Snags
P114
QUKE
PIPO
PILA
CADE
Density (trees ha^{-1})
1200
1100
1000
900
800
700
600
500
400
300
200
100
0
2.5-15.0
15.1-30.0
30.1-45.0
45.1-60.0
60.1-75.0
75.1-90.0
90.1-105.0
105.1-120.0
120.1+
Diameter class (cm)

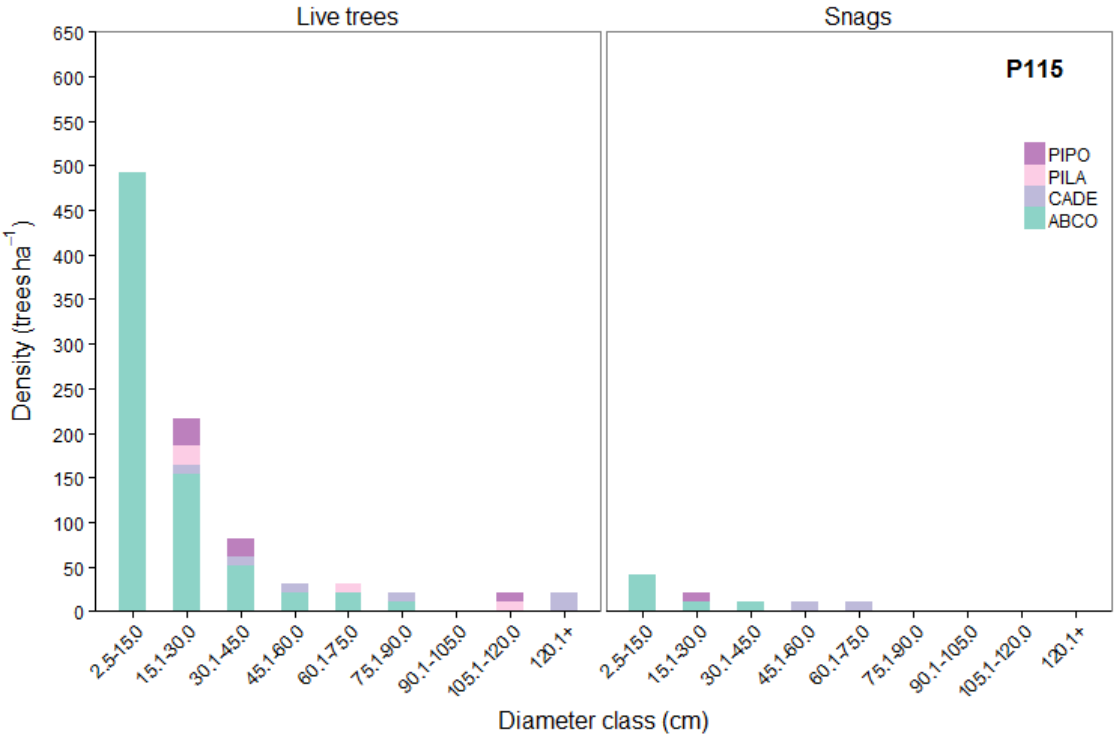
Live trees
Snags
P115
PIPO
PILA
CADE
ABCO
Density (trees ha^{-1})
650
600
550
500
450
400
350
300
250
200
150
100
50
0
2.5-15.0
15.1-30.0
30.1-45.0
45.1-60.0
60.1-75.0
75.1-90.0
90.1-105.0
105.1-120.0
120.1+
Diameter class (cm)

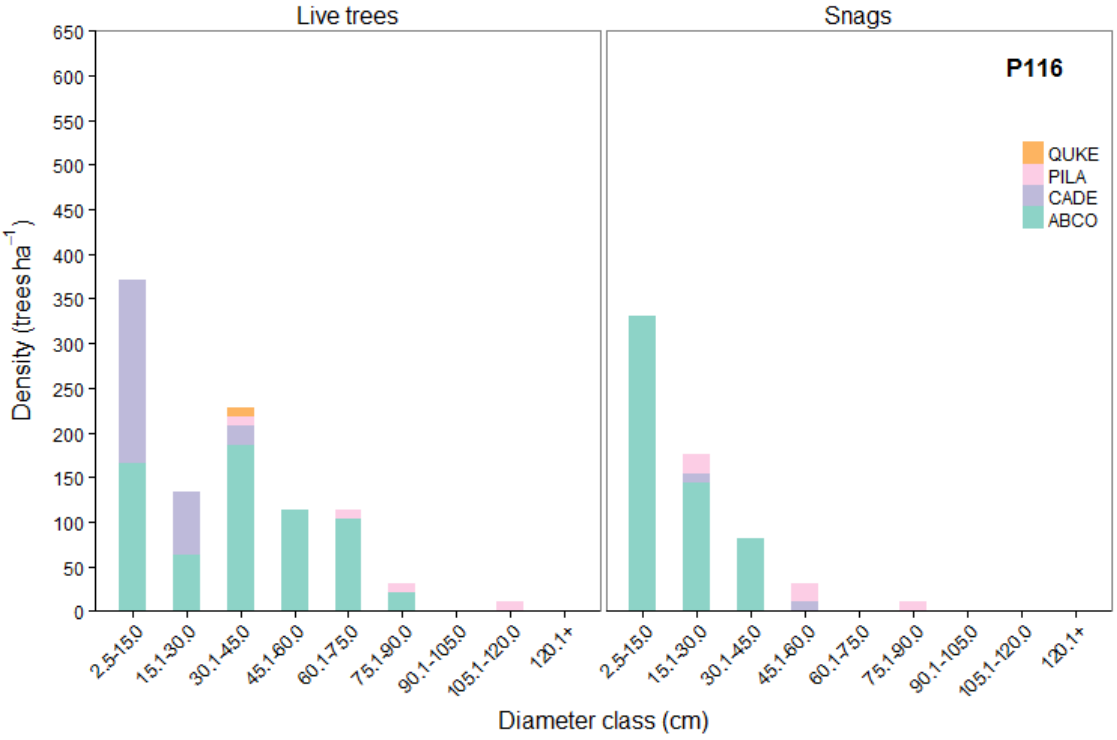
Live trees
Snags
P116
QUKE
PILA
CADE
ABCO
Density (trees ha^{-1})
650
600
550
500
450
400
350
300
250
200
150
100
50
0
2.5-15.0
15.1-30.0
30.1-45.0
45.1-60.0
60.1-75.0
75.1-90.0
90.1-105.0
105.1-120.0
120.1+
Diameter class (cm)

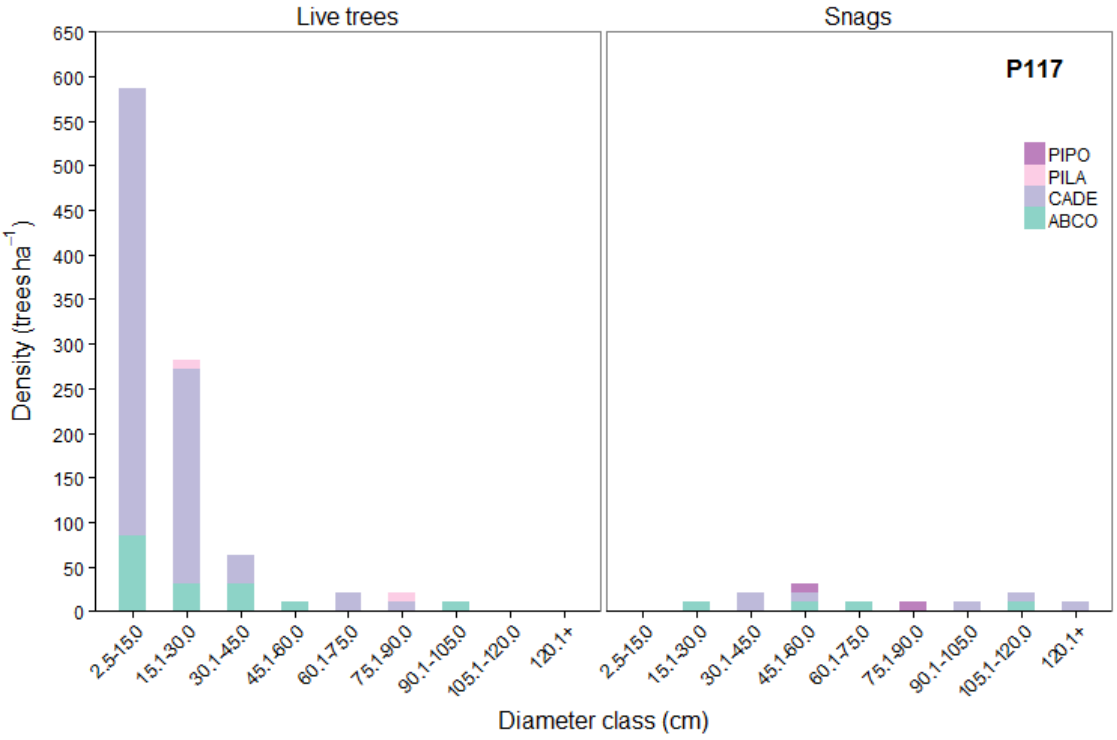
Live trees
Snags
P117
PIPO
PILA
CADE
ABCO
Density (trees ha^{-1})
650
600
550
500
450
400
350
300
250
200
150
100
50
0
2.5-15.0
15.1-30.0
30.1-45.0
45.1-60.0
60.1-75.0
75.1-90.0
90.1-105.0
105.1-120.0
120.1+
Diameter class (cm)

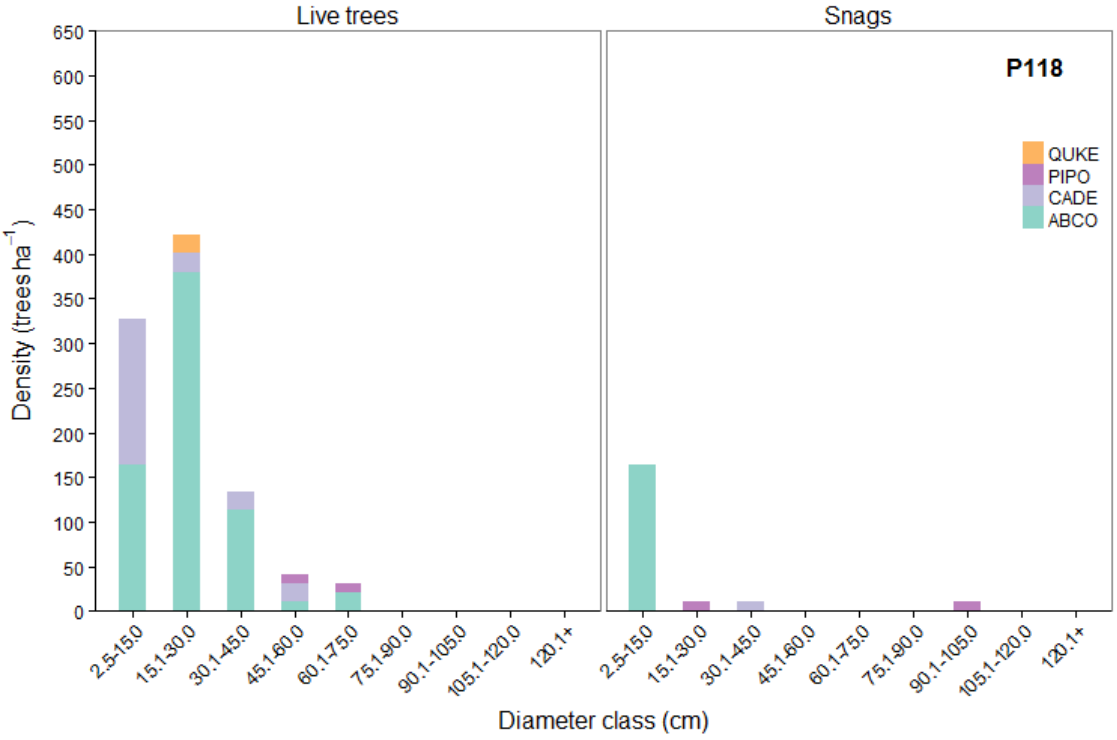
Live trees
Snags
P118
QUKE
PIPO
CADE
ABCO
Density (trees ha^{-1})
650
600
550
500
450
400
350
300
250
200
150
100
50
0
2.5-15.0
15.1-30.0
30.1-45.0
45.1-60.0
60.1-75.0
75.1-90.0
90.1-105.0
105.1-120.0
120.1+
Diameter class (cm)

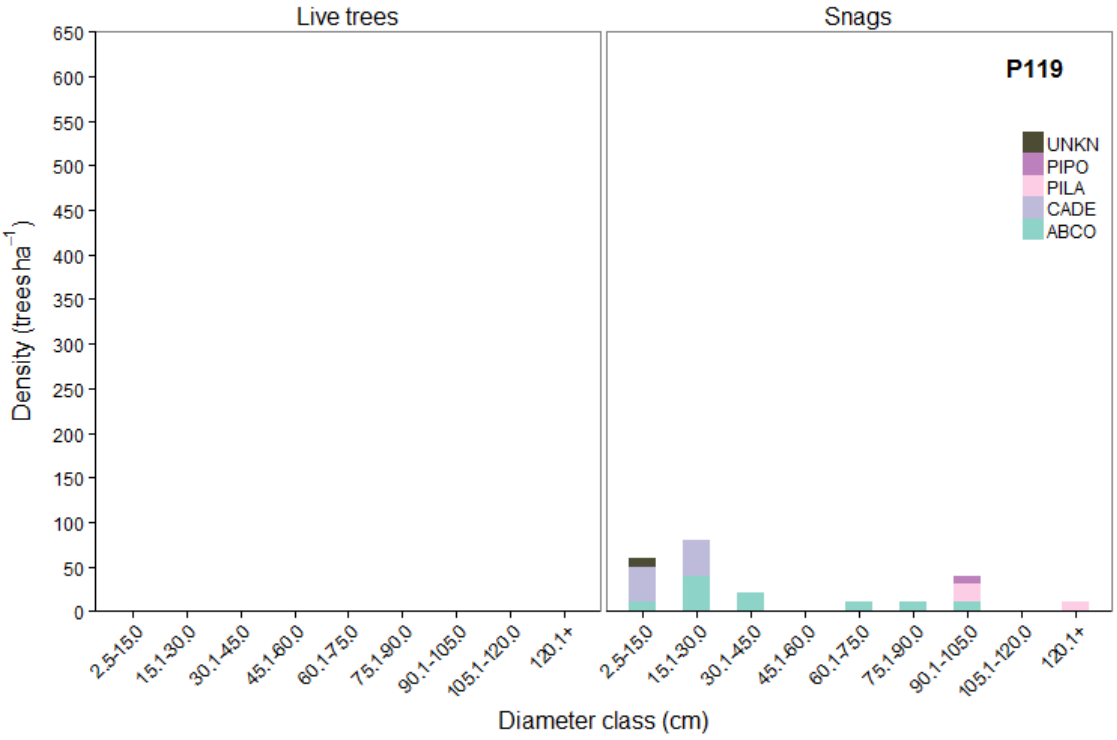
Live trees
Snags
P119
UNKN
PIPO
PILA
CADE
ABCO
Density (trees ha^{-1})
650
600
550
500
450
400
350
300
250
200
150
100
50
0
2.5-15.0
15.1-30.0
30.1-45.0
45.1-60.0
60.1-75.0
75.1-90.0
90.1-105.0
105.1-120.0
120.1+
Diameter class (cm)

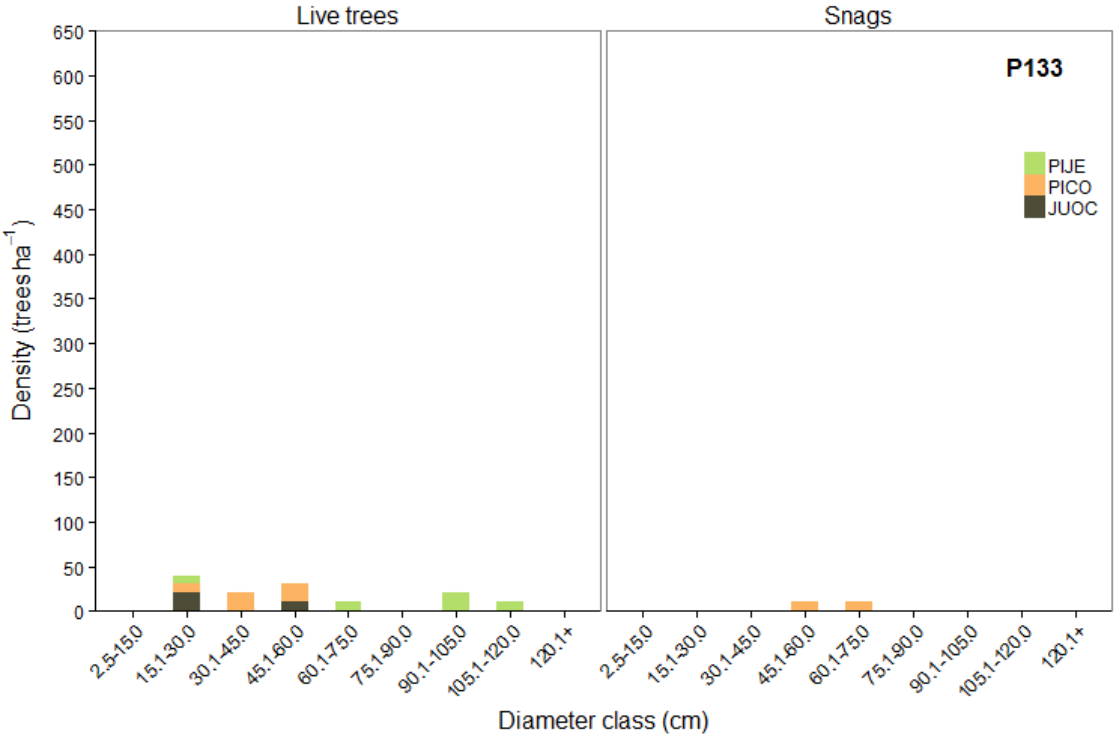
Live trees
Snags
P133
PIJE
PICO
JUOC
Density (trees ha^{-1})
650
600
550
500
450
400
350
300
250
200
150
100
50
0
2.5-15.0
15.1-30.0
30.1-45.0
45.1-60.0
60.1-75.0
75.1-90.0
90.1-105.0
105.1-120.0
120.1+
Diameter class (cm)

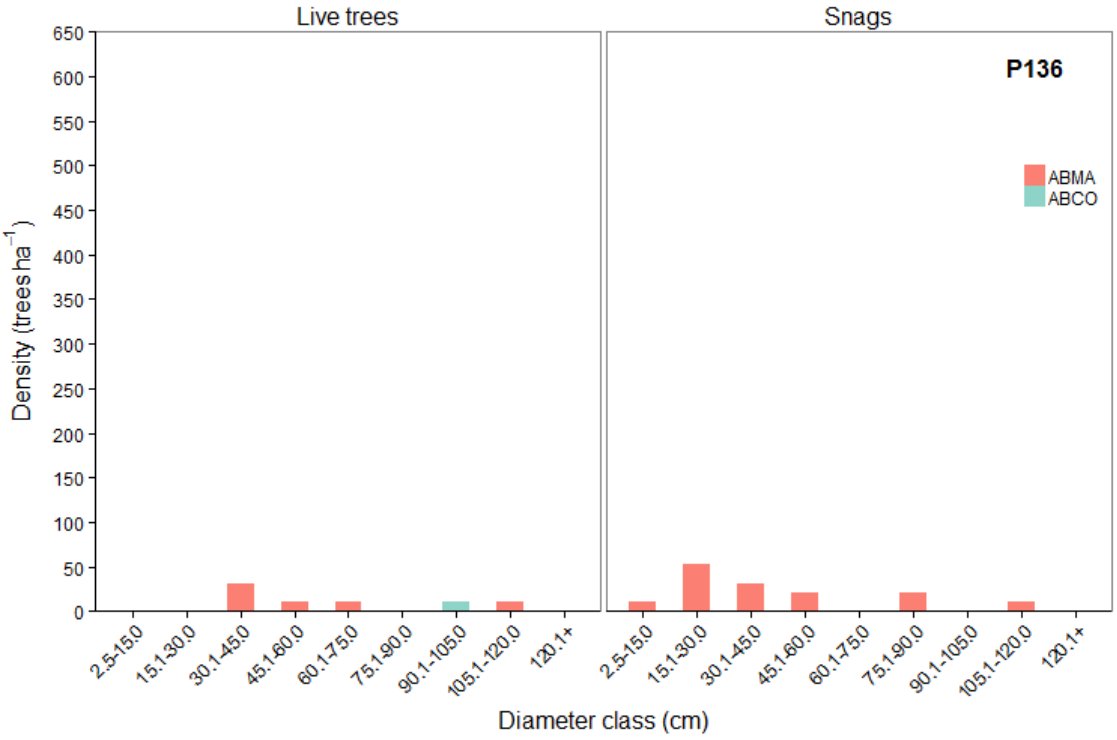
Live trees
Snags
P136
ABMA
ABCO
Density (trees ha^{-1})
650
600
550
500
450
400
350
300
250
200
150
100
50
0
2.5-15.0
15.1-30.0
30.1-45.0
45.1-60.0
60.1-75.0
75.1-90.0
90.1-105.0
105.1-120.0
120.1+
Diameter class (cm)

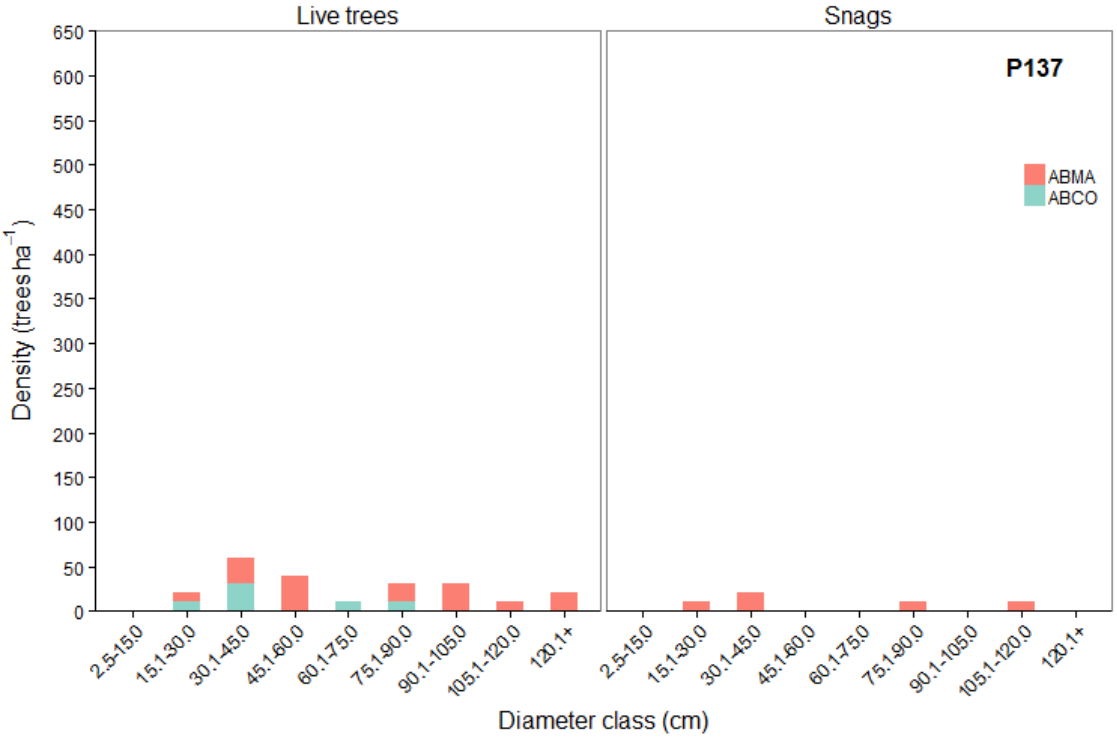
Live trees
Snags
P137
ABMA
ABCO
Density (trees ha^{-1})
650
600
550
500
450
400
350
300
250
200
150
100
50
0
2.5-15.0
15.1-30.0
30.1-45.0
45.1-60.0
60.1-75.0
75.1-90.0
90.1-105.0
105.1-120.0
120.1+
Diameter class (cm)

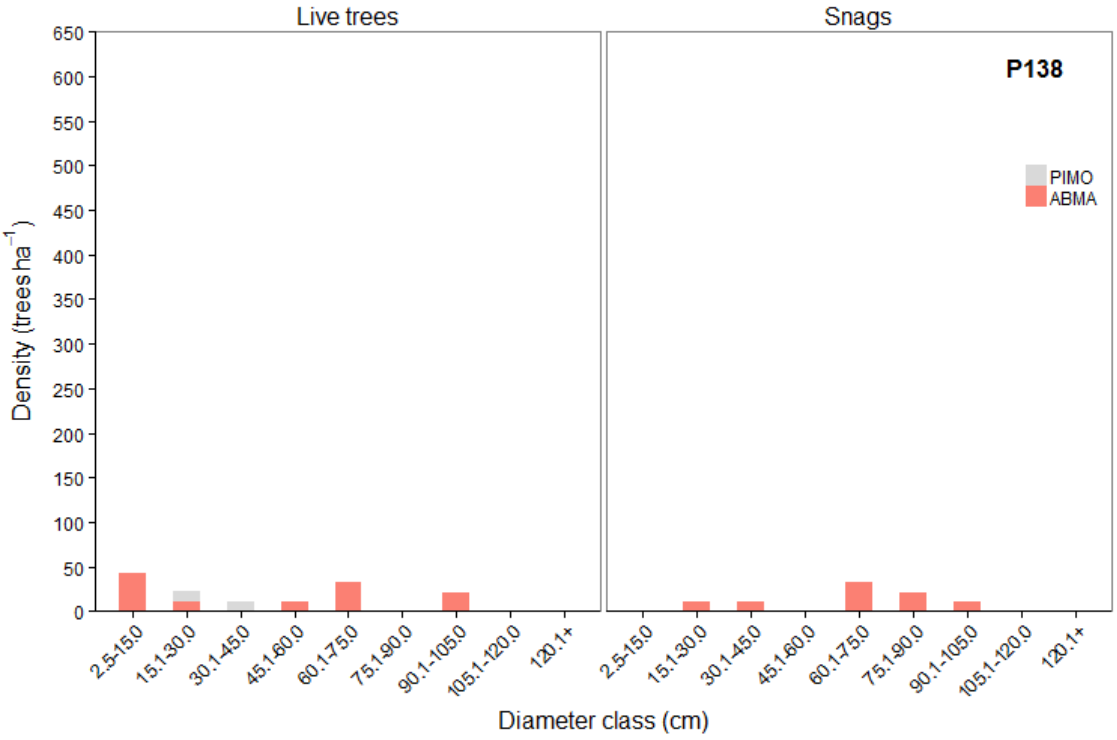
Live trees
Snags
P138
PIMO
ABMA
Density (trees ha^{-1})
650
600
550
500
450
400
350
300
250
200
150
100
50
0
2.5-15.0
15.1-30.0
30.1-45.0
45.1-60.0
60.1-75.0
75.1-90.0
90.1-105.0
105.1-120.0
120.1+
Diameter class (cm)

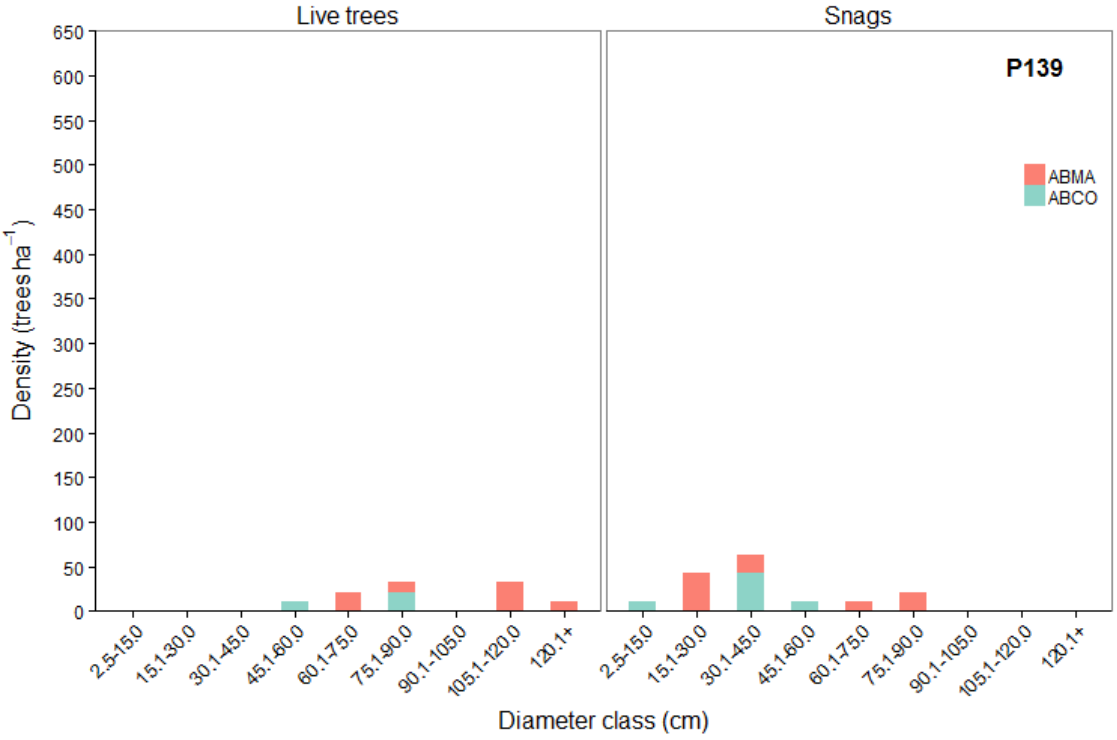
Live trees
Snags
P139
ABMA
ABCO
Density (trees ha^{-1})
650
600
550
500
450
400
350
300
250
200
150
100
50
0
2.5-15.0
15.1-30.0
30.1-45.0
45.1-60.0
60.1-75.0
75.1-90.0
90.1-105.0
105.1-120.0
120.1+
Diameter class (cm)

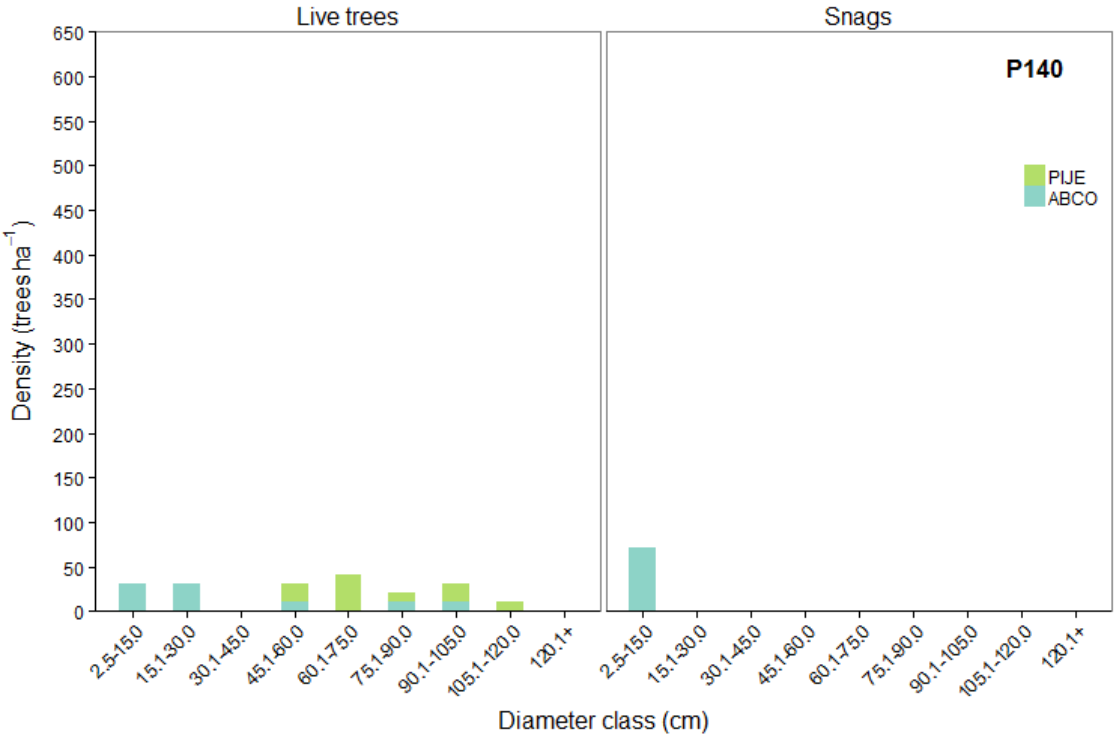
Live trees
Snags
P140
PIJE
ABCO
Density (trees ha^{-1})
650
600
550
500
450
400
350
300
250
200
150
100
50
0
2.5-15.0
15.1-30.0
30.1-45.0
45.1-60.0
60.1-75.0
75.1-90.0
90.1-105.0
105.1-120.0
120.1+
Diameter class (cm)

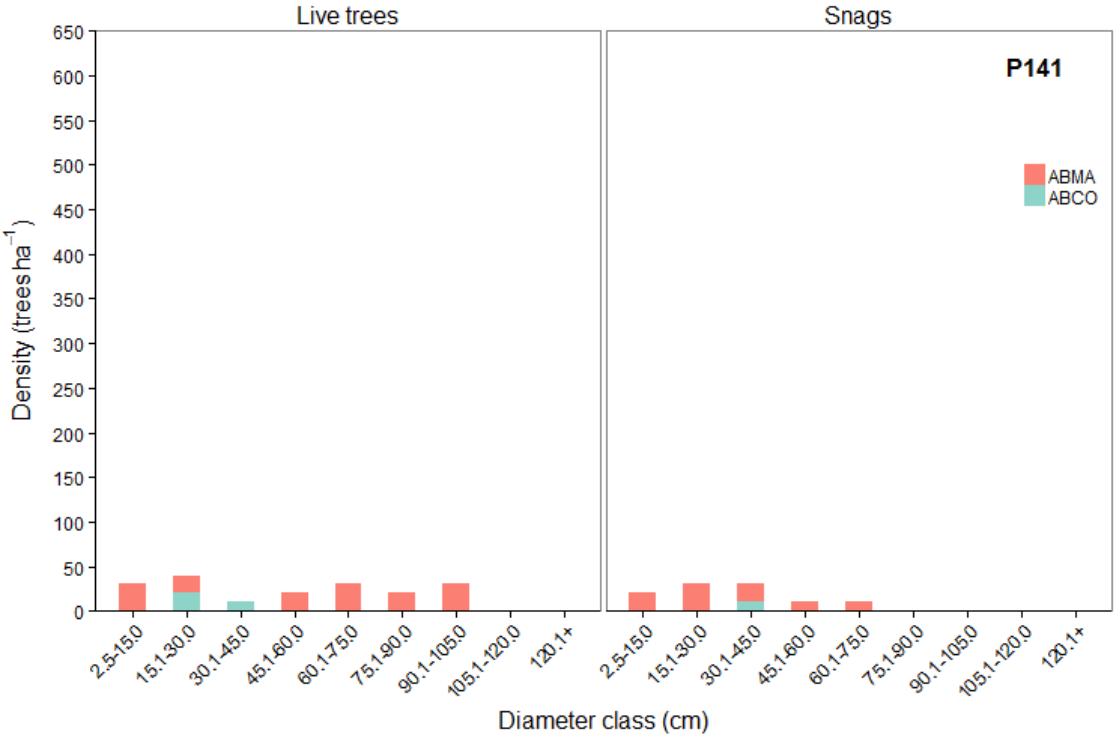
Live trees
Snags
P141
ABMA
ABCO
Density (trees ha^{-1})
650
600
550
500
450
400
350
300
250
200
150
100
50
0
2.5-15.0
15.1-30.0
30.1-45.0
45.1-60.0
60.1-75.0
75.1-90.0
90.1-105.0
105.1-120.0
120.1+
Diameter class (cm)

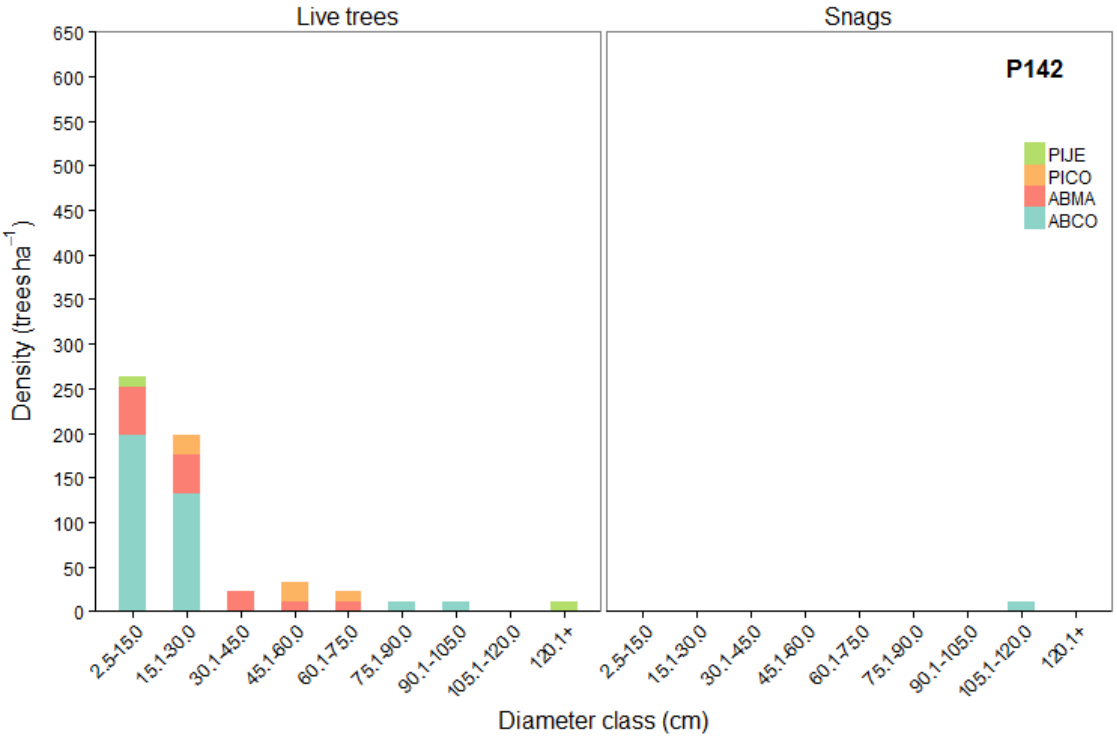
Live trees
Snags
P142
PIJE
PICO
ABMA
ABCO
Density (trees ha^{-1})
650
600
550
500
450
400
350
300
250
200
150
100
50
0
2.5-15.0
15.1-30.0
30.1-45.0
45.1-60.0
60.1-75.0
75.1-90.0
90.1-105.0
105.1-120.0
120.1+
Diameter class (cm)

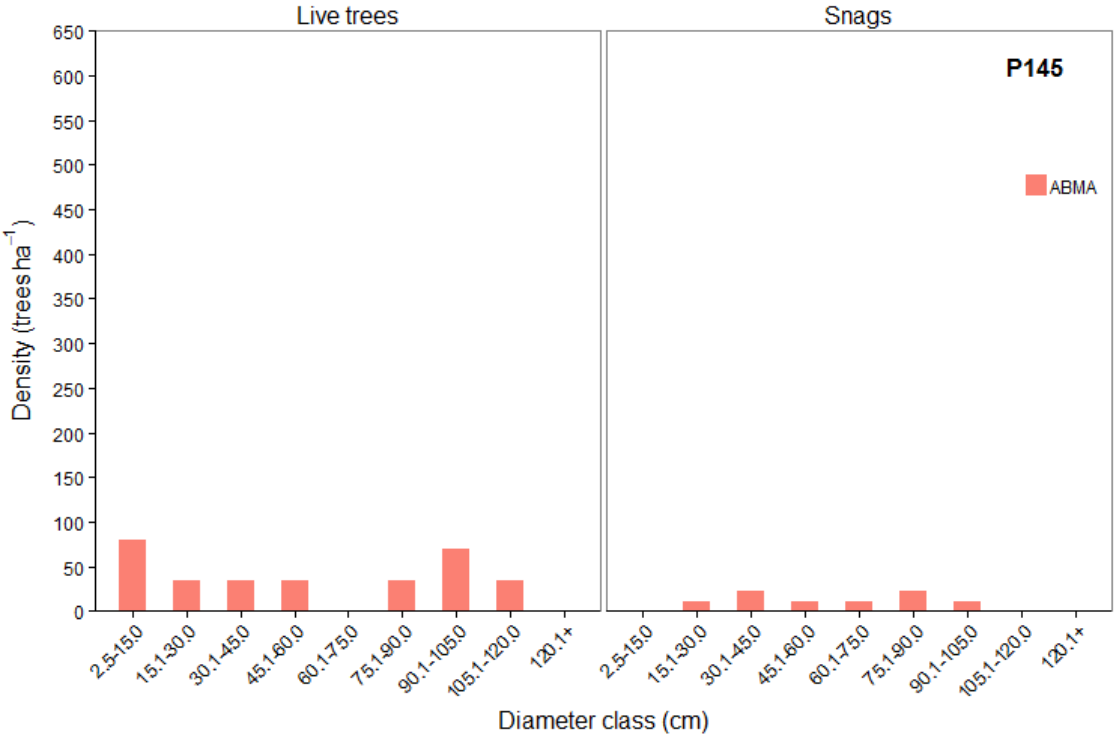
Live trees
Snags
P145
ABMA
Density (trees ha^{-1})
650
600
550
500
450
400
350
300
250
200
150
100
50
0
2.5-15.0
15.1-30.0
30.1-45.0
45.1-60.0
60.1-75.0
75.1-90.0
90.1-105.0
105.1-120.0
120.1+
Diameter class (cm)

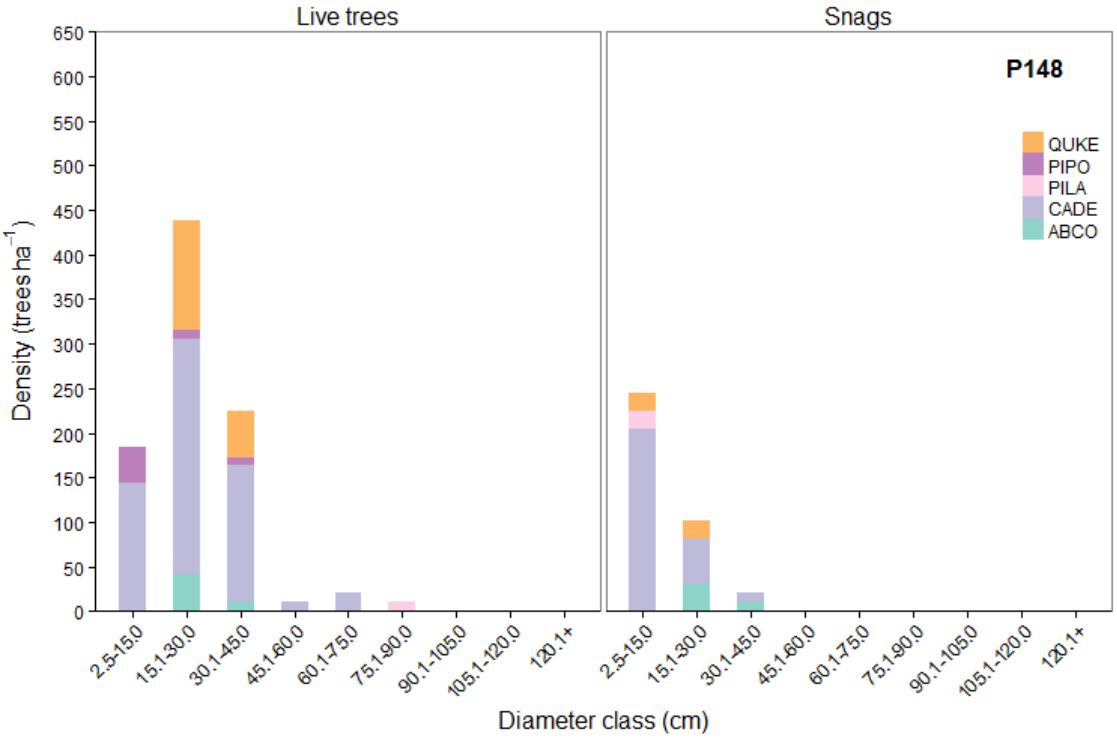
Live trees
Snags
P148
QUKE
PIPO
PILA
CADE
ABCO
Density (trees ha^{-1})
0
50
100
150
200
250
300
350
400
450
500
550
600
650
2.5-15.0
15.1-30.0
30.1-45.0
45.1-60.0
60.1-75.0
75.1-90.0
90.1-105.0
105.1-120.0
120.1+
Diameter class (cm)

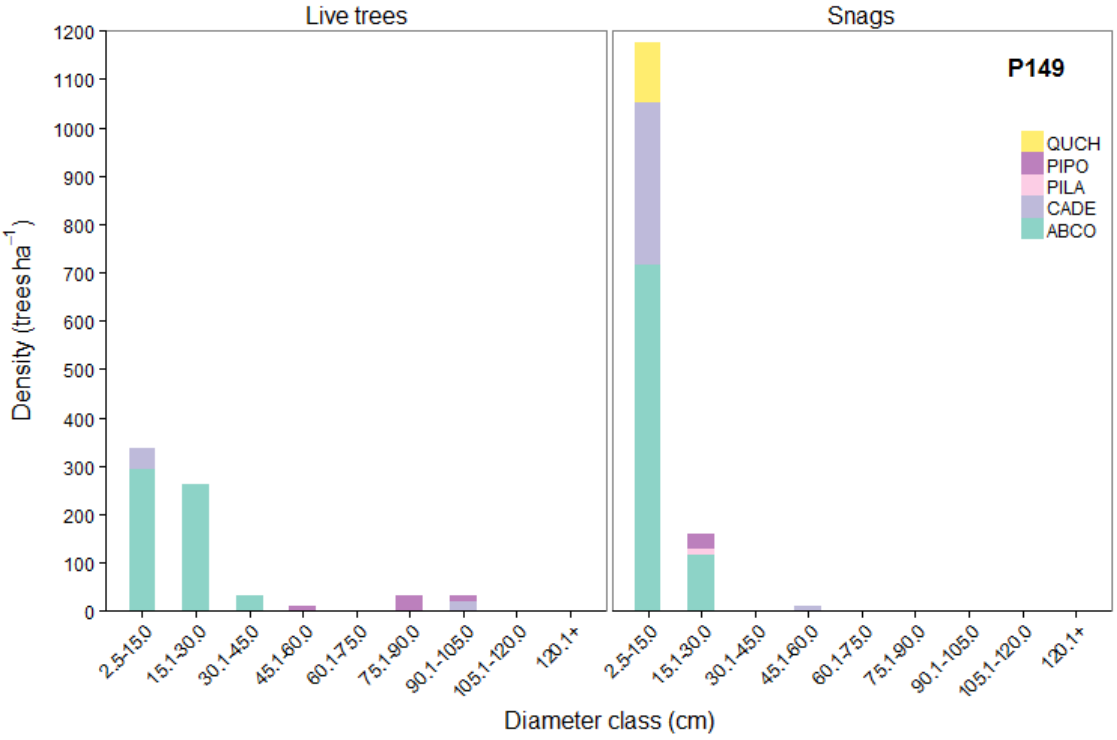
Live trees
Snags
P149
QUCH
PIPO
PILA
CADE
ABCO
Density (trees ha^{-1})
0
100
200
300
400
500
600
700
800
900
1000
1100
1200
2.5-15.0
15.1-30.0
30.1-45.0
45.1-60.0
60.1-75.0
75.1-90.0
90.1-105.0
105.1-120.0
120.1+
Diameter class (cm)

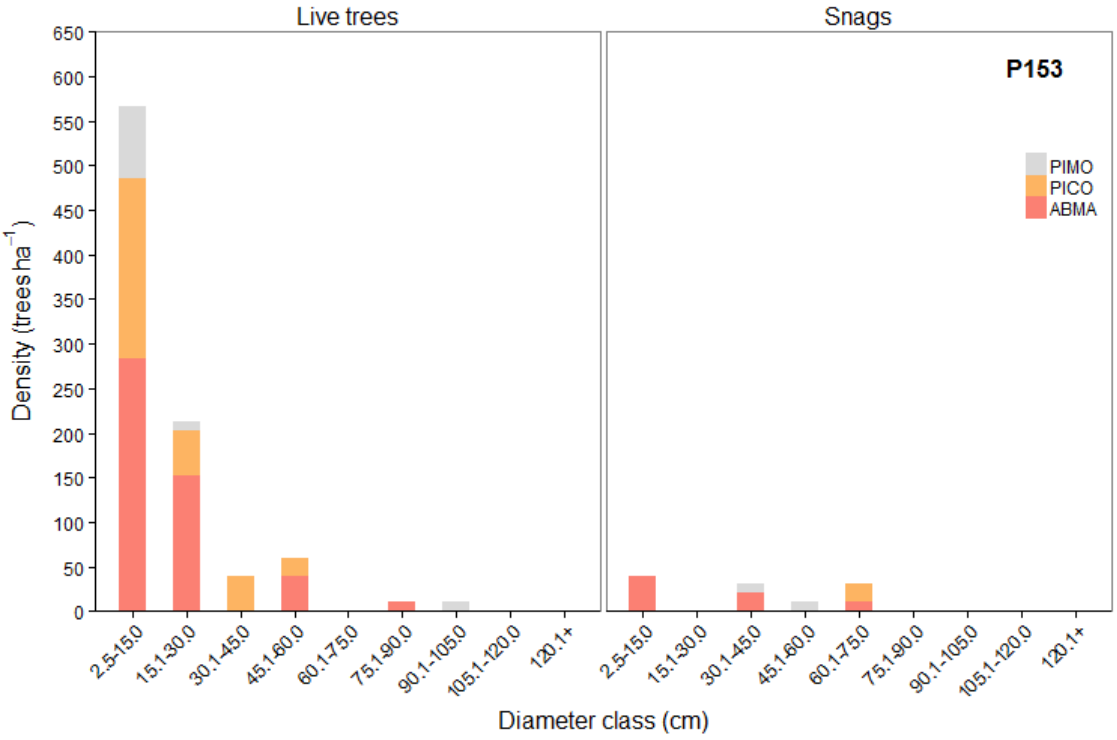
Live trees
Snags
P153
PIMO
PICO
ABMA
Density (trees ha^{-1})
650
600
550
500
450
400
350
300
250
200
150
100
50
0
2.5-15.0
15.1-30.0
30.1-45.0
45.1-60.0
60.1-75.0
75.1-90.0
90.1-105.0
105.1-120.0
120.1+
Diameter class (cm)

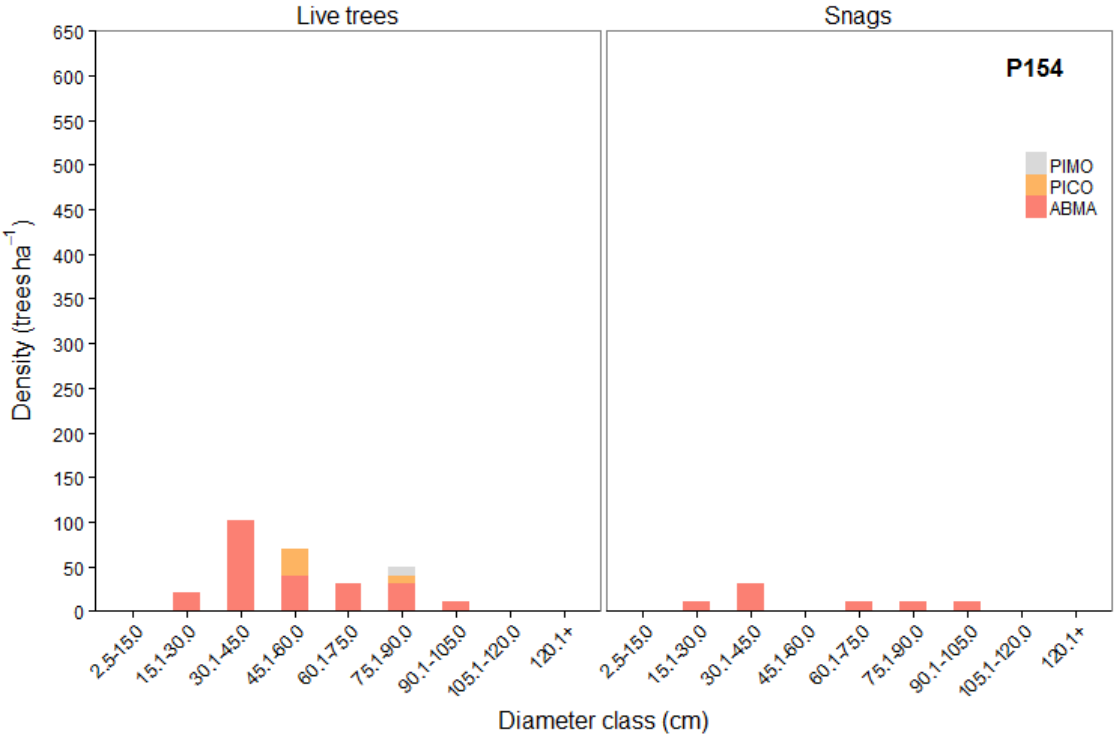
Live trees
Snags
P154
PIMO
PICO
ABMA
Density (trees ha^{-1})
650
600
550
500
450
400
350
300
250
200
150
100
50
0
2.5-15.0
15.1-30.0
30.1-45.0
45.1-60.0
60.1-75.0
75.1-90.0
90.1-105.0
105.1-120.0
120.1+
Diameter class (cm)

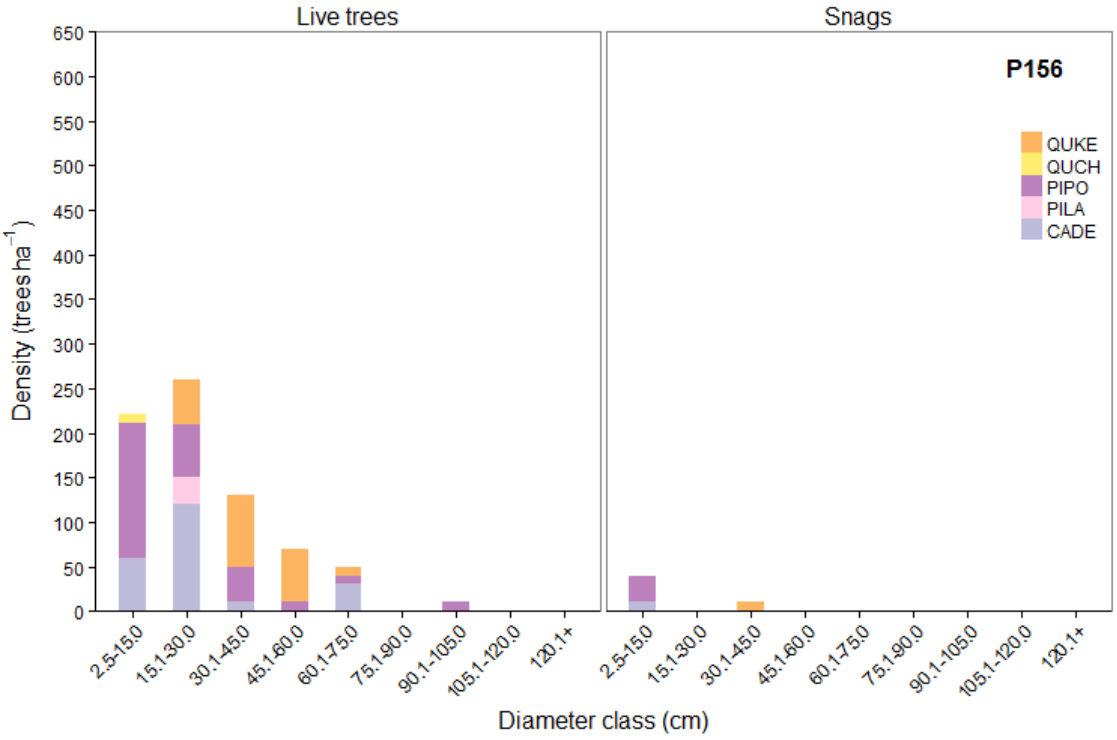
Live trees
Snags
P156
QUKE
QUCH
PIPO
PILA
CADE
Density (trees ha^{-1})
650
600
550
500
450
400
350
300
250
200
150
100
50
0
2.5-15.0
15.1-30.0
30.1-45.0
45.1-60.0
60.1-75.0
75.1-90.0
90.1-105.0
105.1-120.0
120.1+
Diameter class (cm)

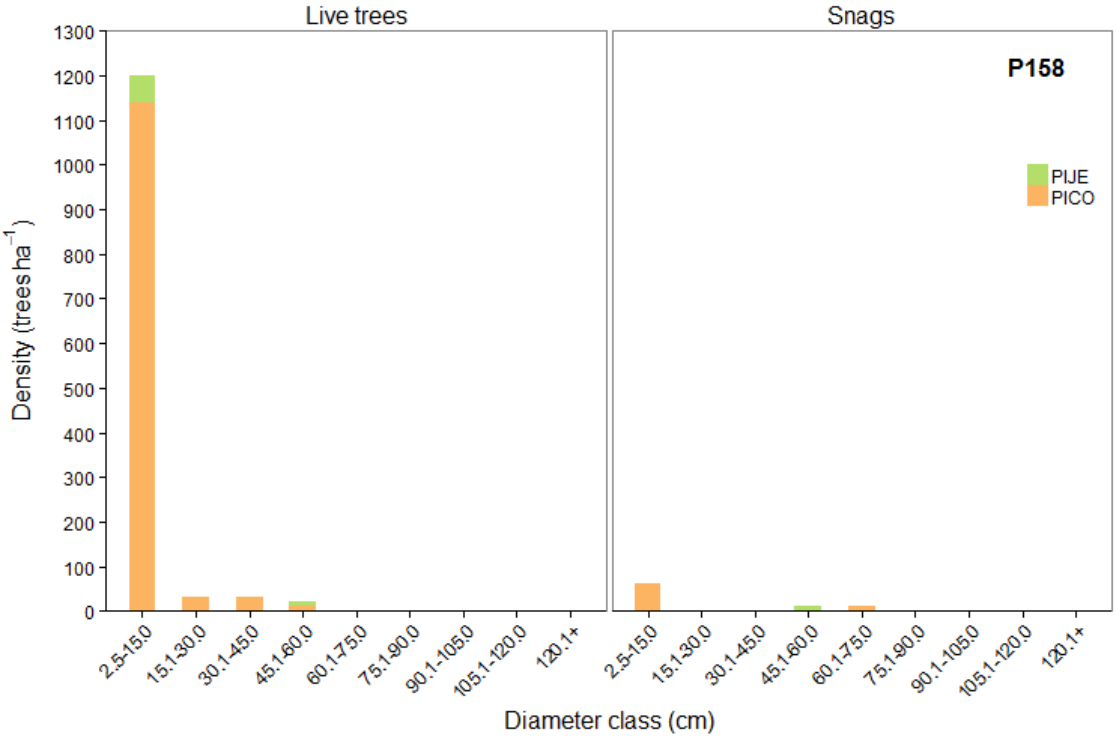
Live trees
Snags
P158
PIJE
PICO
Density (trees ha^{-1})
1300
1200
1100
1000
900
800
700
600
500
400
300
200
100
0
2.5-15.0
15.1-30.0
30.1-45.0
45.1-60.0
60.1-75.0
75.1-90.0
90.1-105.0
105.1-120.0
120.1+
Diameter class (cm)

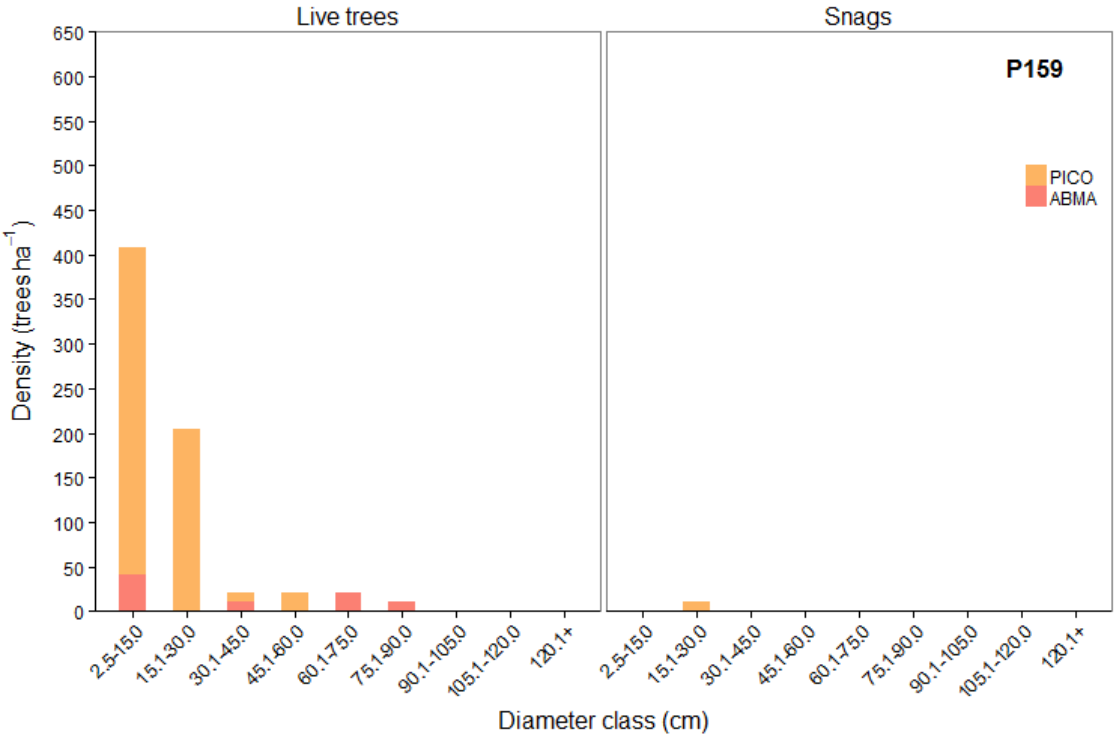
Live trees
Snags
P159
PICO
ABMA
Density (trees ha^{-1})
650
600
550
500
450
400
350
300
250
200
150
100
50
0
2.5-15.0
15.1-30.0
30.1-45.0
45.1-60.0
60.1-75.0
75.1-90.0
90.1-105.0
105.1-120.0
120.1+
Diameter class (cm)

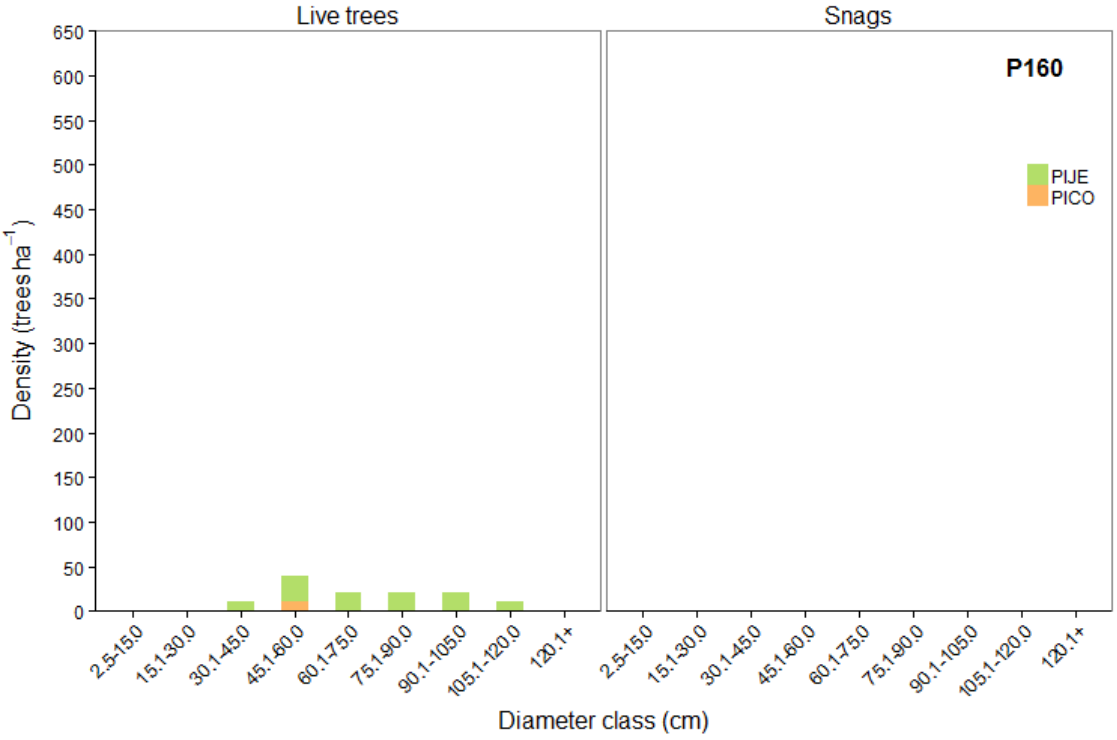
Live trees
Snags
P160
PIJE
PICO
Density (trees ha^{-1})
650
600
550
500
450
400
350
300
250
200
150
100
50
0
2.5-15.0
15.1-30.0
30.1-45.0
45.1-60.0
60.1-75.0
75.1-90.0
90.1-105.0
105.1-120.0
120.1+
Diameter class (cm)

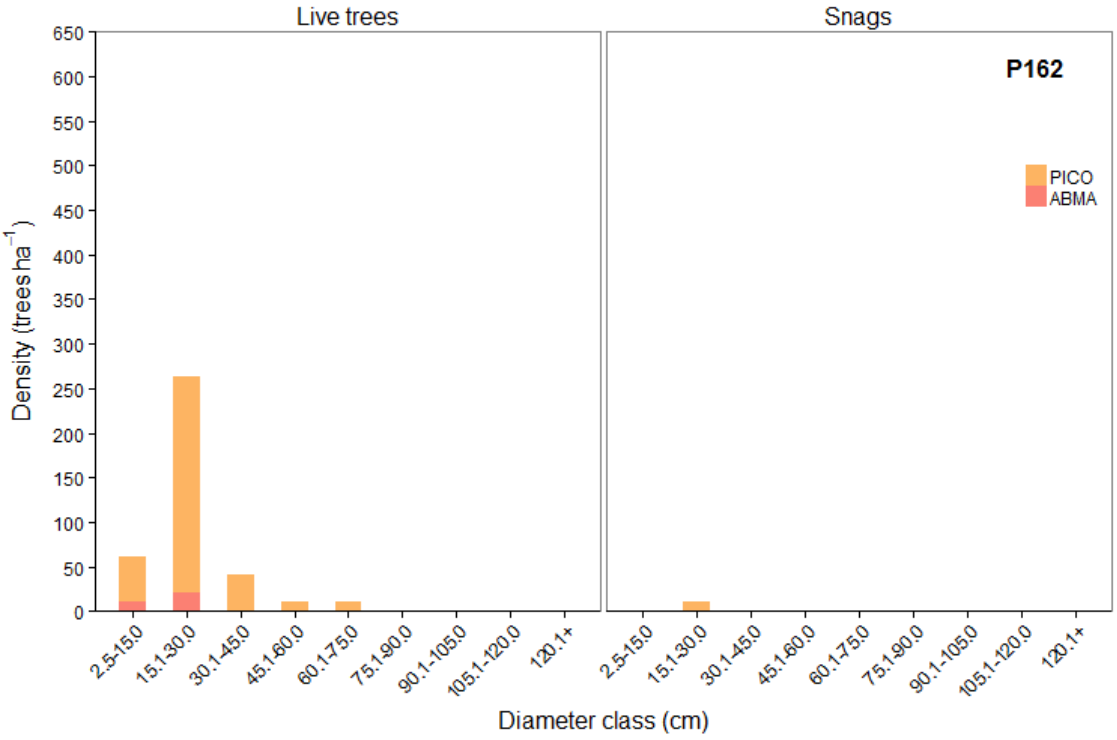
Live trees
Snags
P162
PICO
ABMA
Density (trees ha^{-1})
650
600
550
500
450
400
350
300
250
200
150
100
50
0
2.5-15.0
15.1-30.0
30.1-45.0
45.1-60.0
60.1-75.0
75.1-90.0
90.1-105.0
105.1-120.0
120.1+
Diameter class (cm)

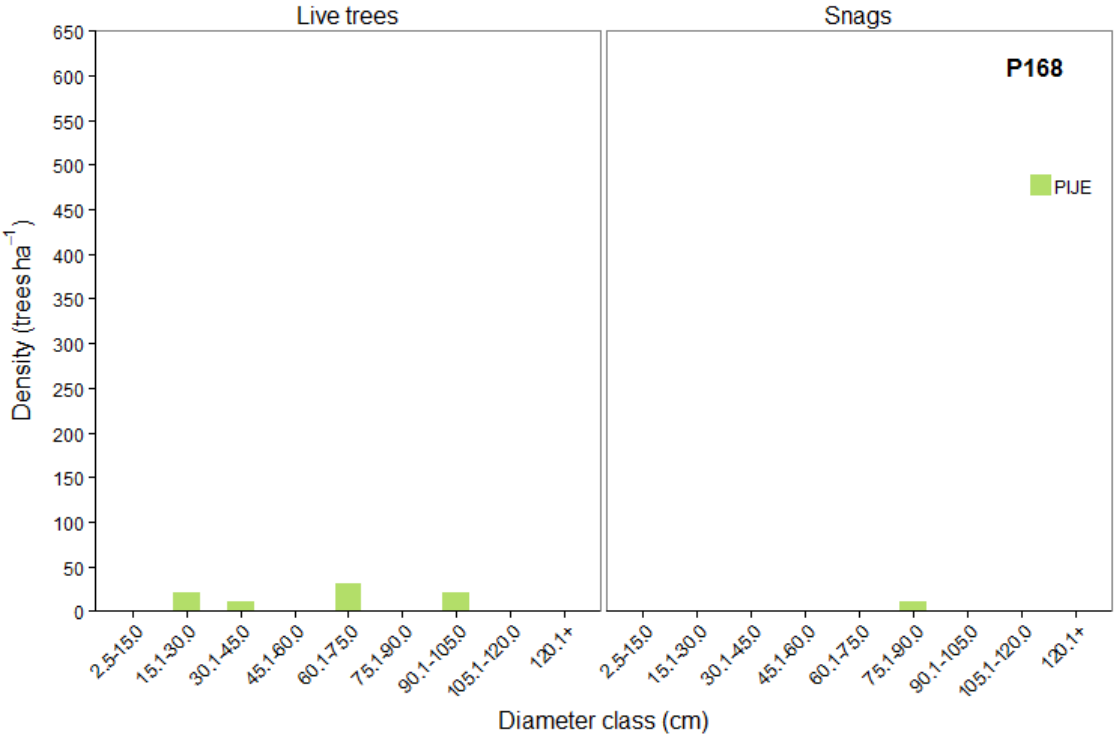
Live trees
Snags
P168
PIJE
Density (trees ha^{-1})
650
600
550
500
450
400
350
300
250
200
150
100
50
0
2.5-15.0
15.1-30.0
30.1-45.0
45.1-60.0
60.1-75.0
75.1-90.0
90.1-105.0
105.1-120.0
120.1+
Diameter class (cm)

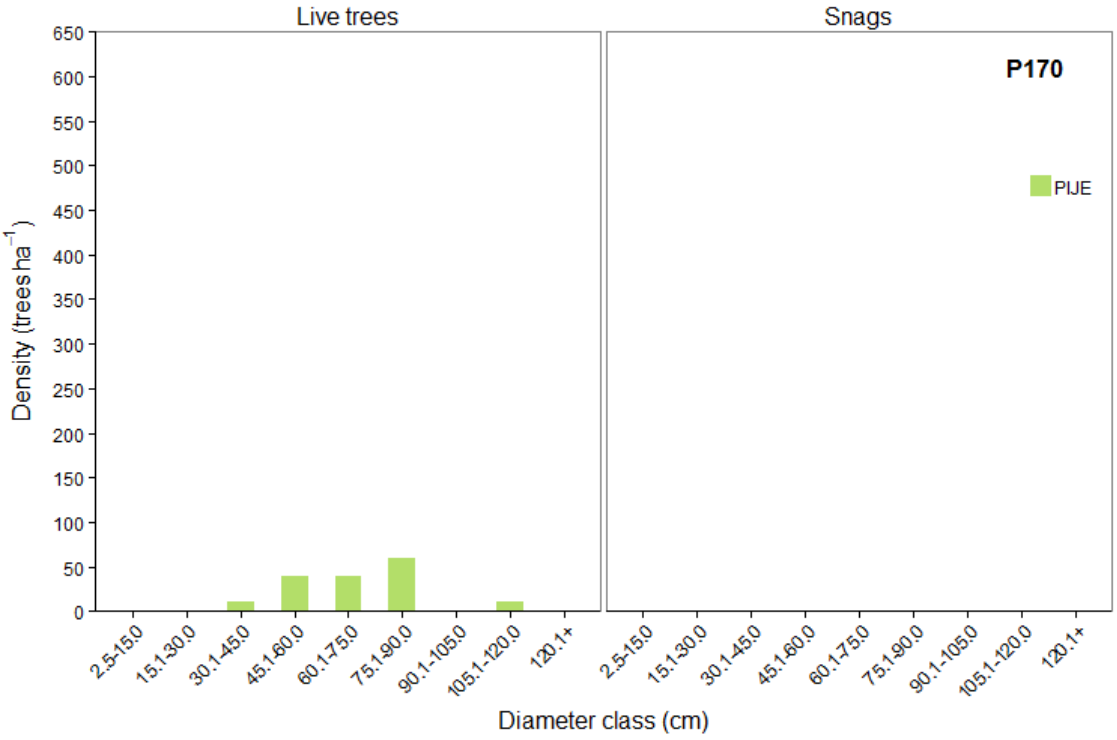
Live trees
Snags
P170
PIJE
Density (trees ha^{-1})
650
600
550
500
450
400
350
300
250
200
150
100
50
0
2.5-15.0
15.1-30.0
30.1-45.0
45.1-60.0
60.1-75.0
75.1-90.0
90.1-105.0
105.1-120.0
120.1+
Diameter class (cm)

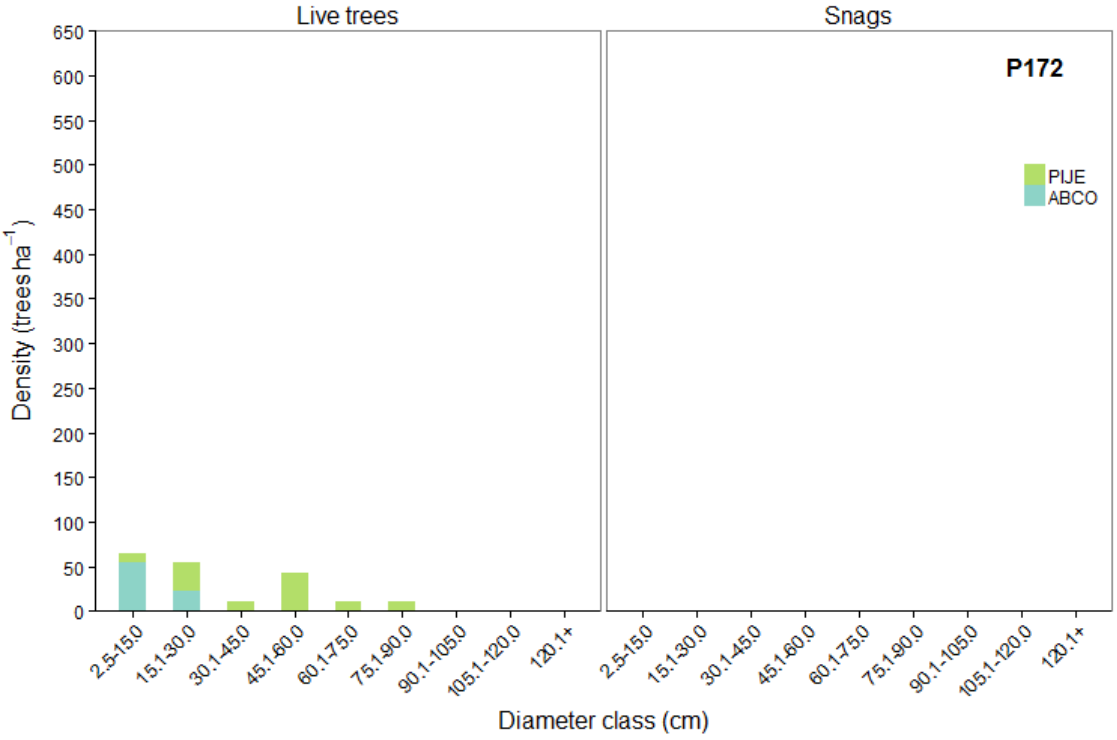
Live trees
Snags
P172
PIJE
ABCO
Density (trees ha^{-1})
650
600
550
500
450
400
350
300
250
200
150
100
50
0
2.5-15.0
15.1-30.0
30.1-45.0
45.1-60.0
60.1-75.0
75.1-90.0
90.1-105.0
105.1-120.0
120.1+
Diameter class (cm)

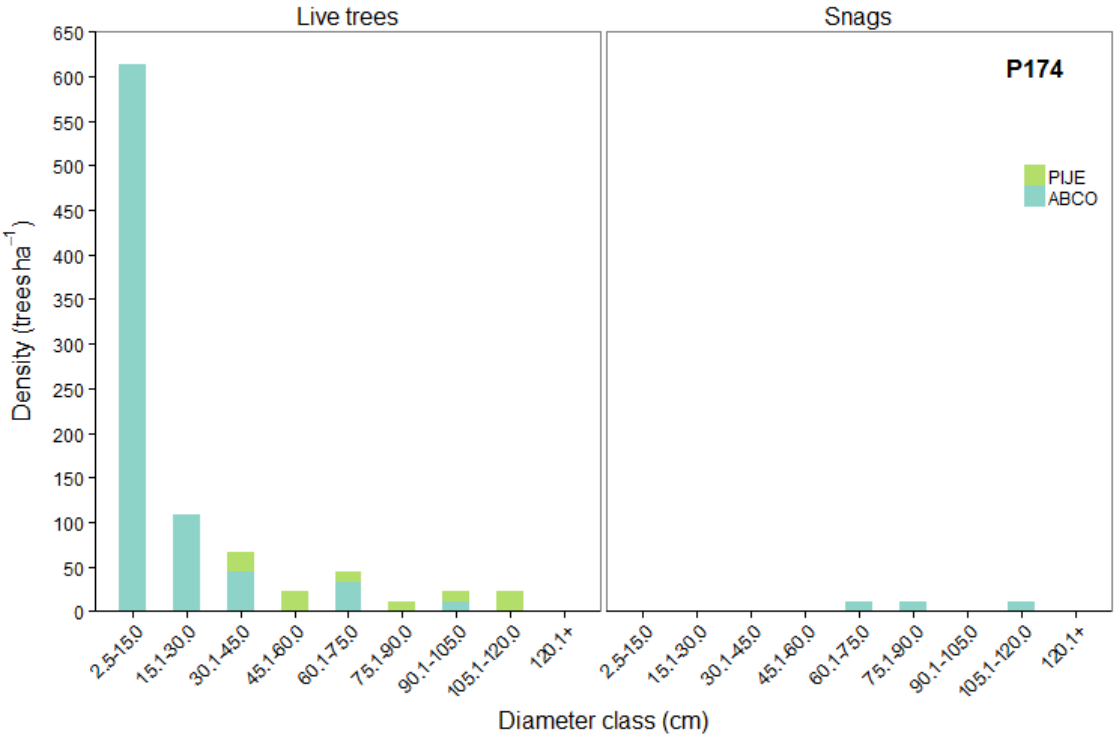
Live trees
Snags
P174
PIJE
ABCO
Density (trees ha^{-1})
650
600
550
500
450
400
350
300
250
200
150
100
50
0
2.5-15.0
15.1-30.0
30.1-45.0
45.1-60.0
60.1-75.0
75.1-90.0
90.1-105.0
105.1-120.0
120.1+
Diameter class (cm)

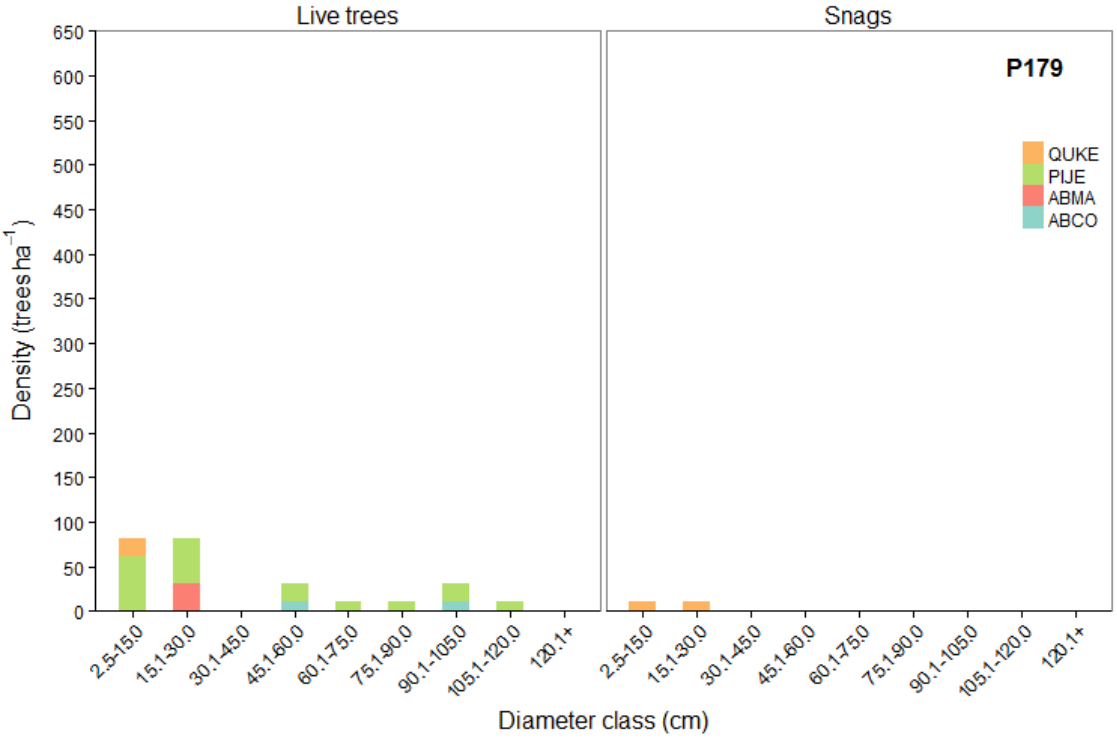
Live trees
Snags
P179
QUKE
PIJE
ABMA
ABCO
Density (trees ha^{-1})
650
600
550
500
450
400
350
300
250
200
150
100
50
0
2.5-15.0
15.1-30.0
30.1-45.0
45.1-60.0
60.1-75.0
75.1-90.0
90.1-105.0
105.1-120.0
120.1+
Diameter class (cm)

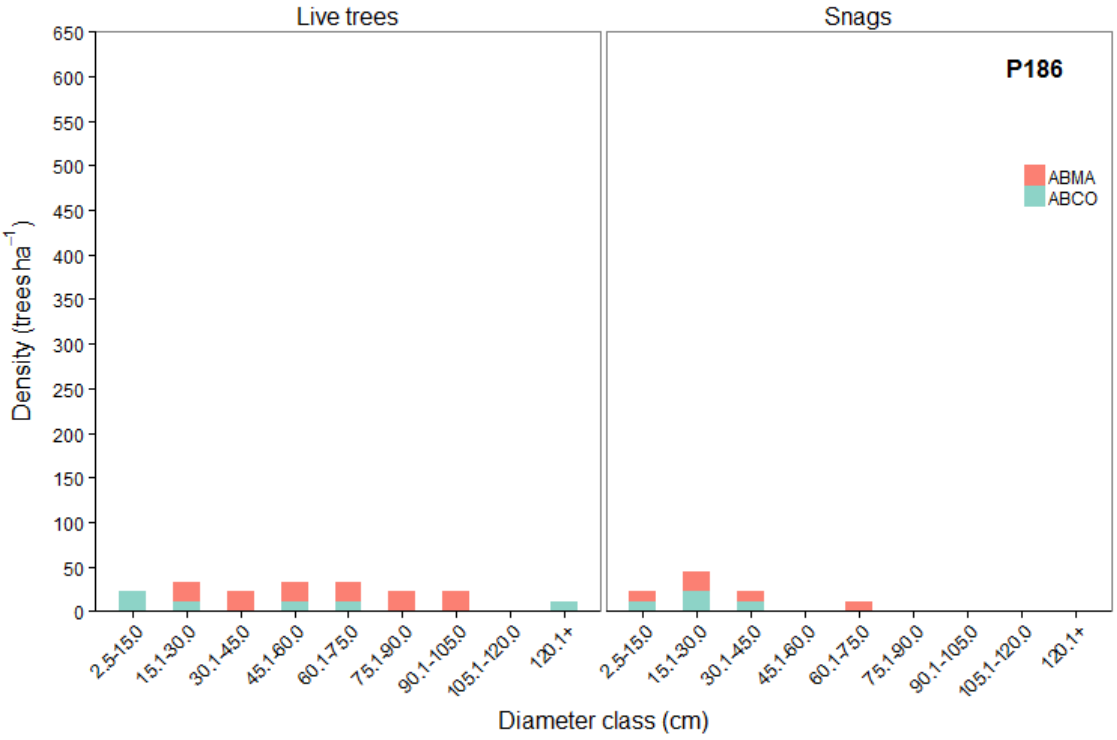
Live trees
Snags
P186
ABMA
ABCO
Density (trees ha^{-1})
650
600
550
500
450
400
350
300
250
200
150
100
50
0
2.5-15.0
15.1-30.0
30.1-45.0
45.1-60.0
60.1-75.0
75.1-90.0
90.1-105.0
105.1-120.0
120.1+
Diameter class (cm)

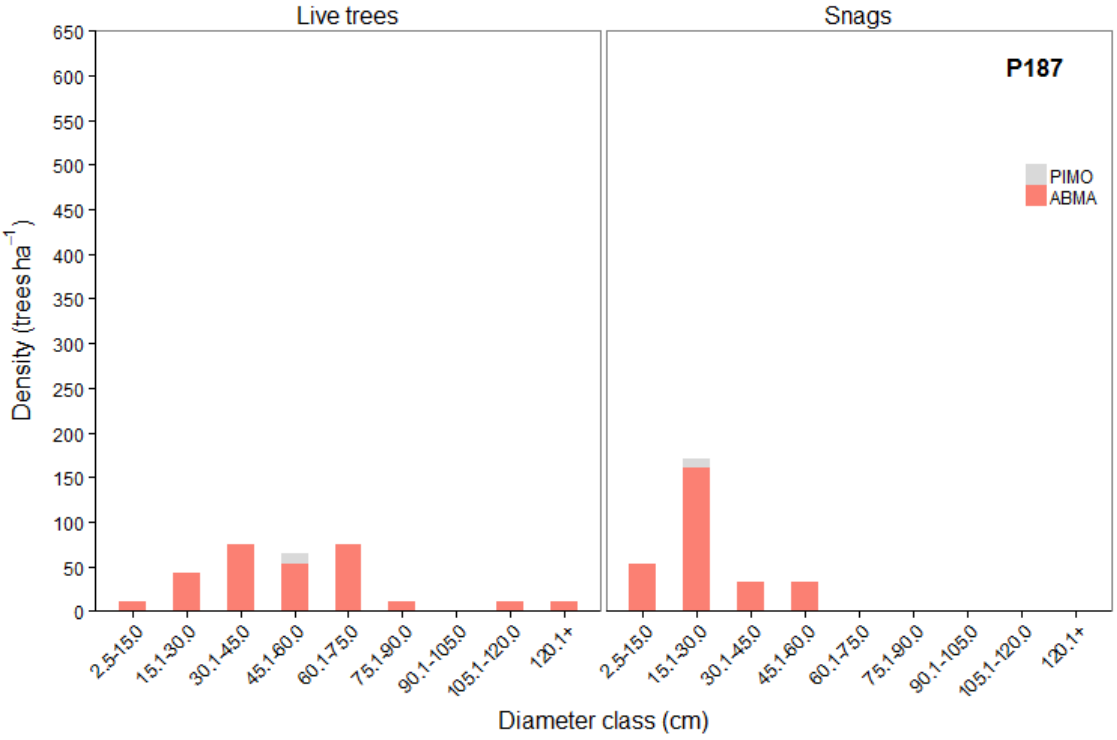
Live trees
Snags
P187
PIMO
ABMA
Density (trees ha^{-1})
650
600
550
500
450
400
350
300
250
200
150
100
50
0
2.5-15.0
15.1-30.0
30.1-45.0
45.1-60.0
60.1-75.0
75.1-90.0
90.1-105.0
105.1-120.0
120.1+
Diameter class (cm)

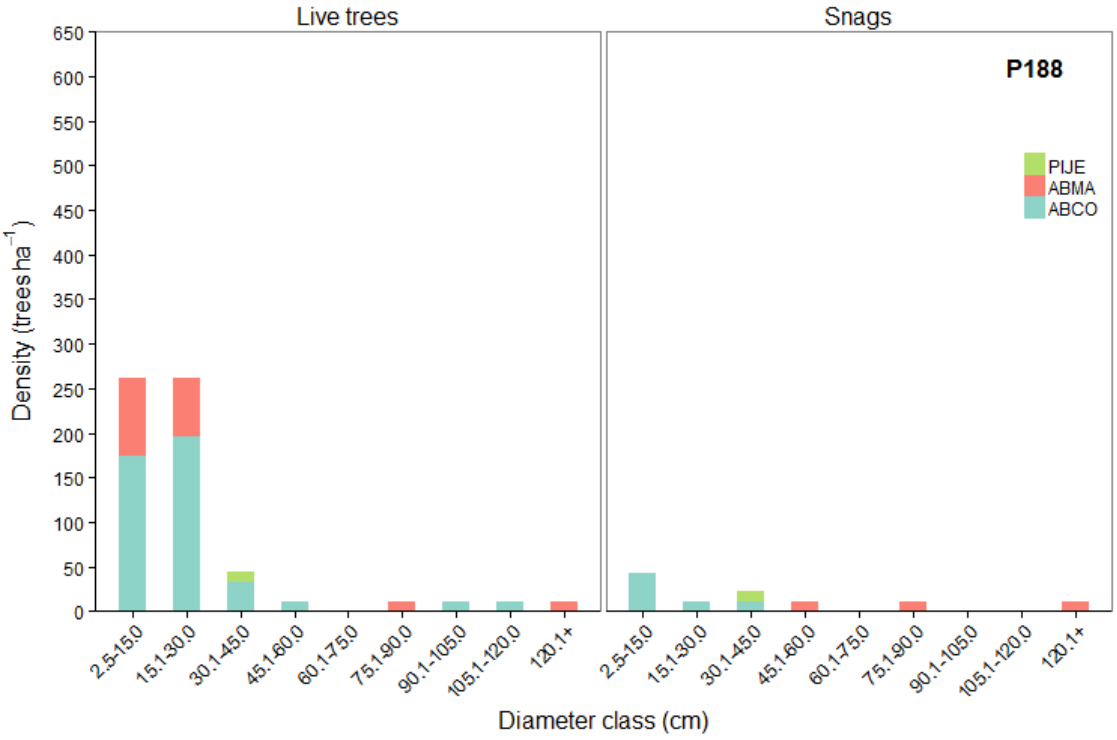
Live trees
Snags
P188
PIJE
ABMA
ABCO
Density (trees ha^{-1})
650
600
550
500
450
400
350
300
250
200
150
100
50
0
2.5-15.0
15.1-30.0
30.1-45.0
45.1-60.0
60.1-75.0
75.1-90.0
90.1-105.0
105.1-120.0
120.1+
Diameter class (cm)

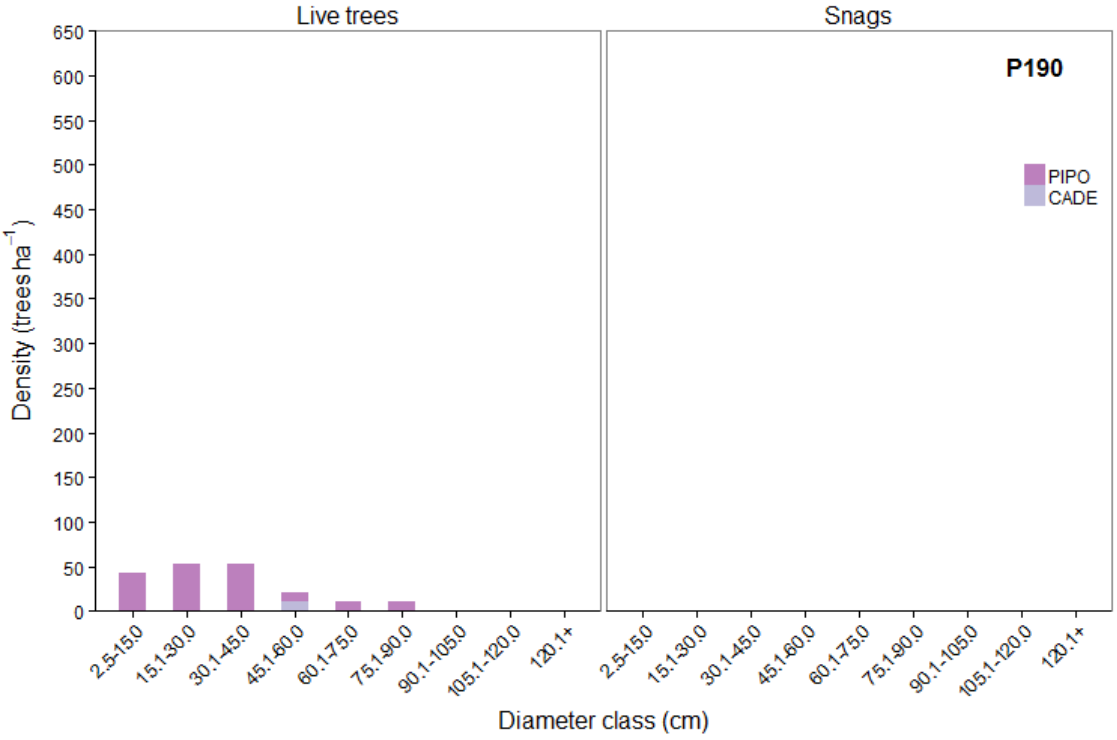
Live trees
Snags
P190
PIPO
CADE
Density (trees ha^{-1})
650
600
550
500
450
400
350
300
250
200
150
100
50
0
2.5-15.0
15.1-30.0
30.1-45.0
45.1-60.0
60.1-75.0
75.1-90.0
90.1-105.0
105.1-120.0
120.1+
Diameter class (cm)

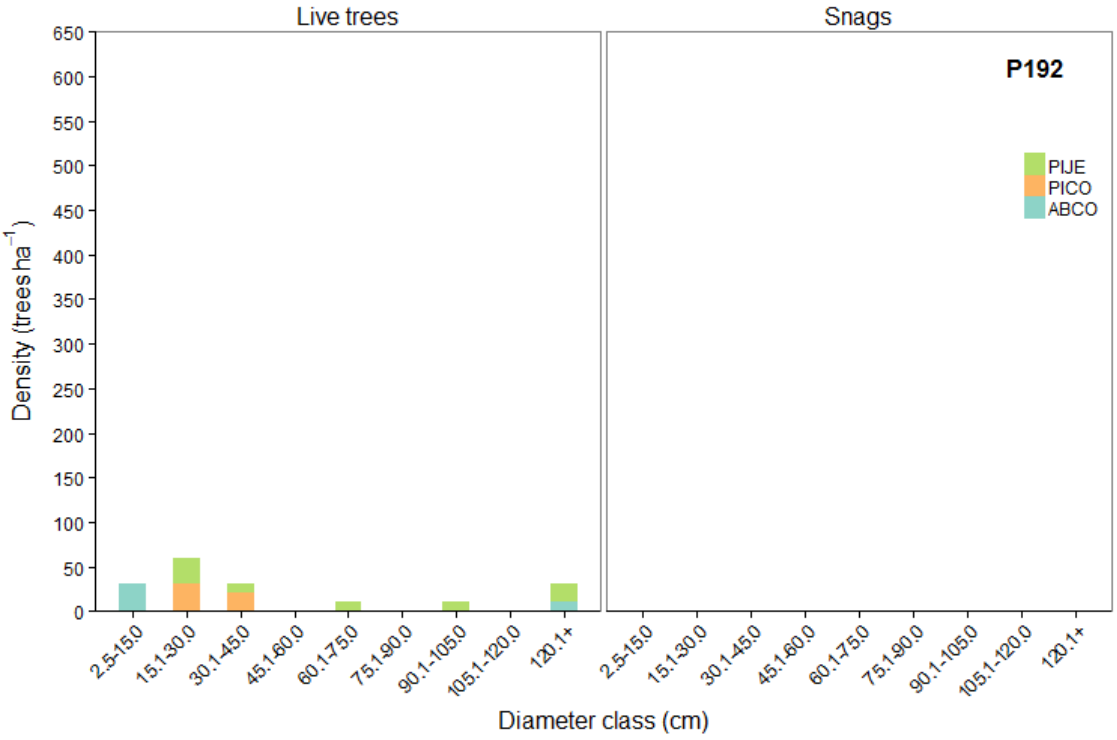
Live trees
Snags
P192
PIJE
PICO
ABCO
Density (trees ha^{-1})
650
600
550
500
450
400
350
300
250
200
150
100
50
0
2.5-15.0
15.1-30.0
30.1-45.0
45.1-60.0
60.1-75.0
75.1-90.0
90.1-105.0
105.1-120.0
120.1+
Diameter class (cm)

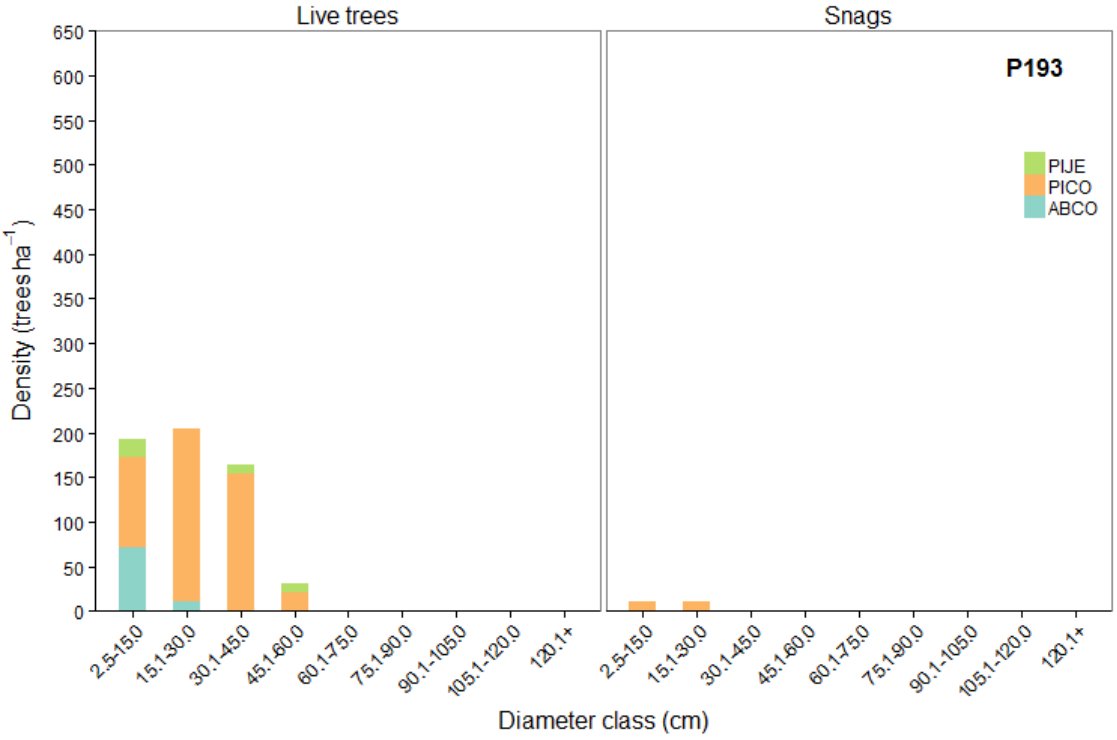
Live trees
Snags
P193
PIJE
PICO
ABCO
Density (trees ha^{-1})
650
600
550
500
450
400
350
300
250
200
150
100
50
0
2.5-15.0
15.1-30.0
30.1-45.0
45.1-60.0
60.1-75.0
75.1-90.0
90.1-105.0
105.1-120.0
120.1+
Diameter class (cm)

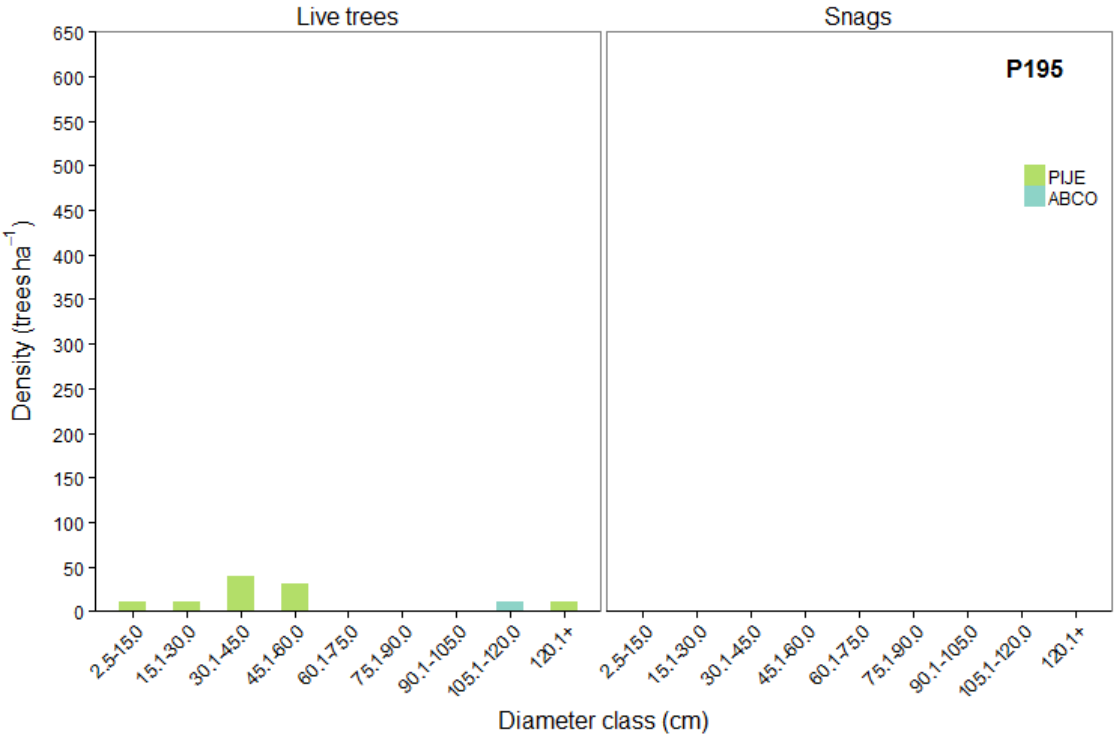
Live trees
Snags
P195
PIJE
ABCO
Density (trees ha^{-1})
650
600
550
500
450
400
350
300
250
200
150
100
50
0
2.5-15.0
15.1-30.0
30.1-45.0
45.1-60.0
60.1-75.0
75.1-90.0
90.1-105.0
105.1-120.0
120.1+
Diameter class (cm)

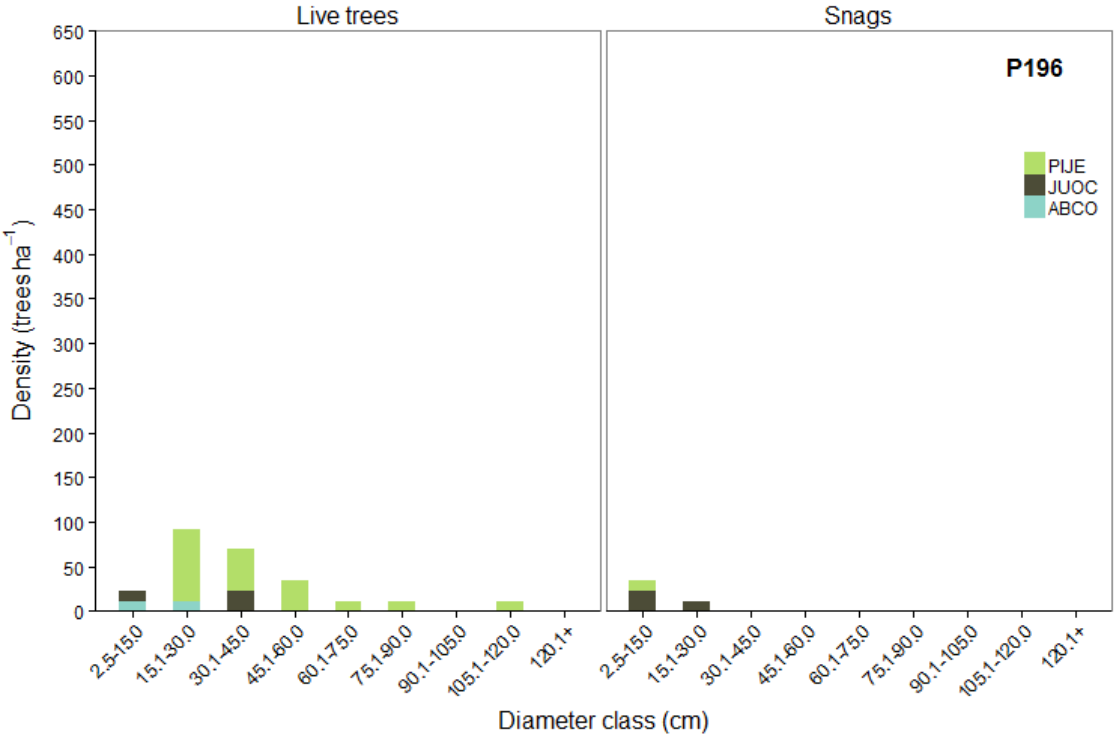
Live trees
Snags
P196
PIJE
JUOC
ABCO
Density (trees ha^{-1})
650
600
550
500
450
400
350
300
250
200
150
100
50
0
2.5-15.0
15.1-30.0
30.1-45.0
45.1-60.0
60.1-75.0
75.1-90.0
90.1-105.0
105.1-120.0
120.1+
Diameter class (cm)

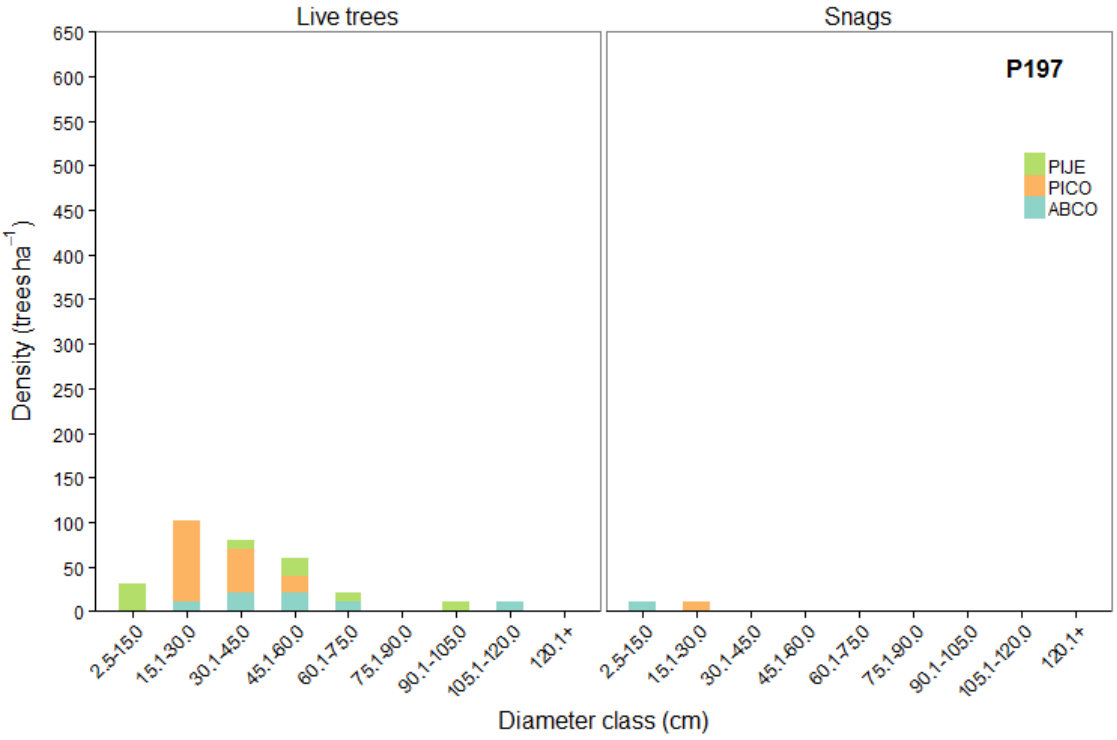
Live trees
Snags
P197
PIJE
PICO
ABCO
Density (trees ha^{-1})
650
600
550
500
450
400
350
300
250
200
150
100
50
0
2.5-15.0
15.1-30.0
30.1-45.0
45.1-60.0
60.1-75.0
75.1-90.0
90.1-105.0
105.1-120.0
120.1+
Diameter class (cm)

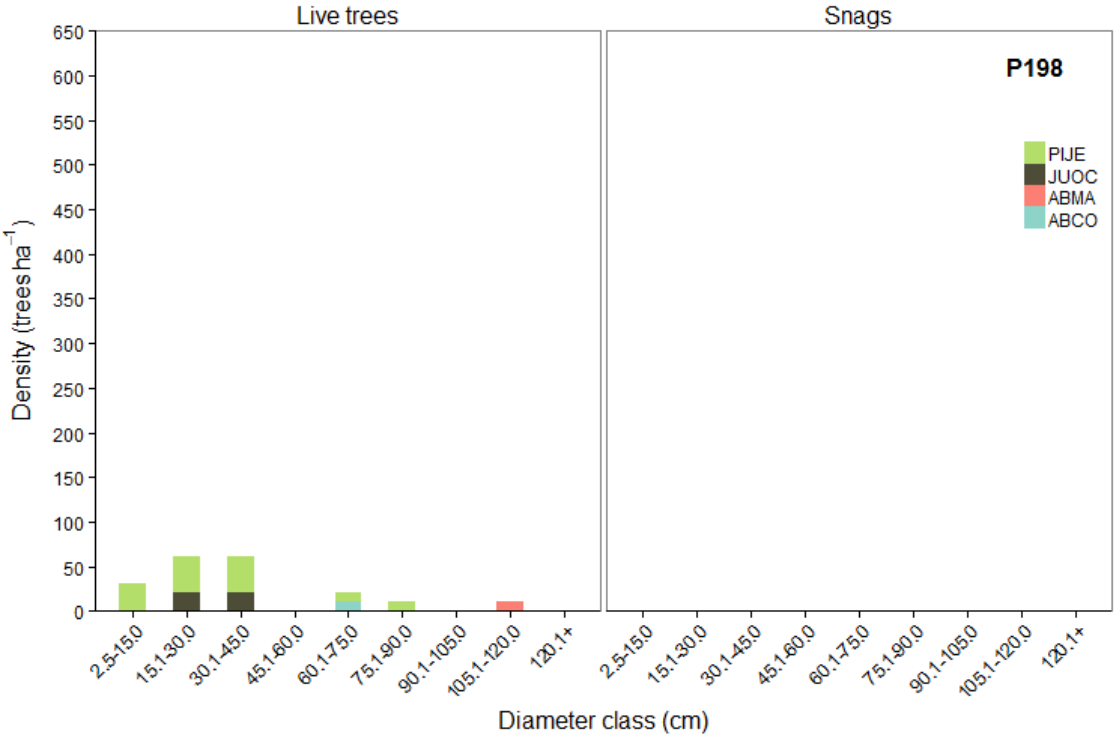
Live trees
Snags
P198
PIJE
JUOC
ABMA
ABCO
Density (trees ha^{-1})
650
600
550
500
450
400
350
300
250
200
150
100
50
0
2.5-15.0
15.1-30.0
30.1-45.0
45.1-60.0
60.1-75.0
75.1-90.0
90.1-105.0
105.1-120.0
120.1+
Diameter class (cm)

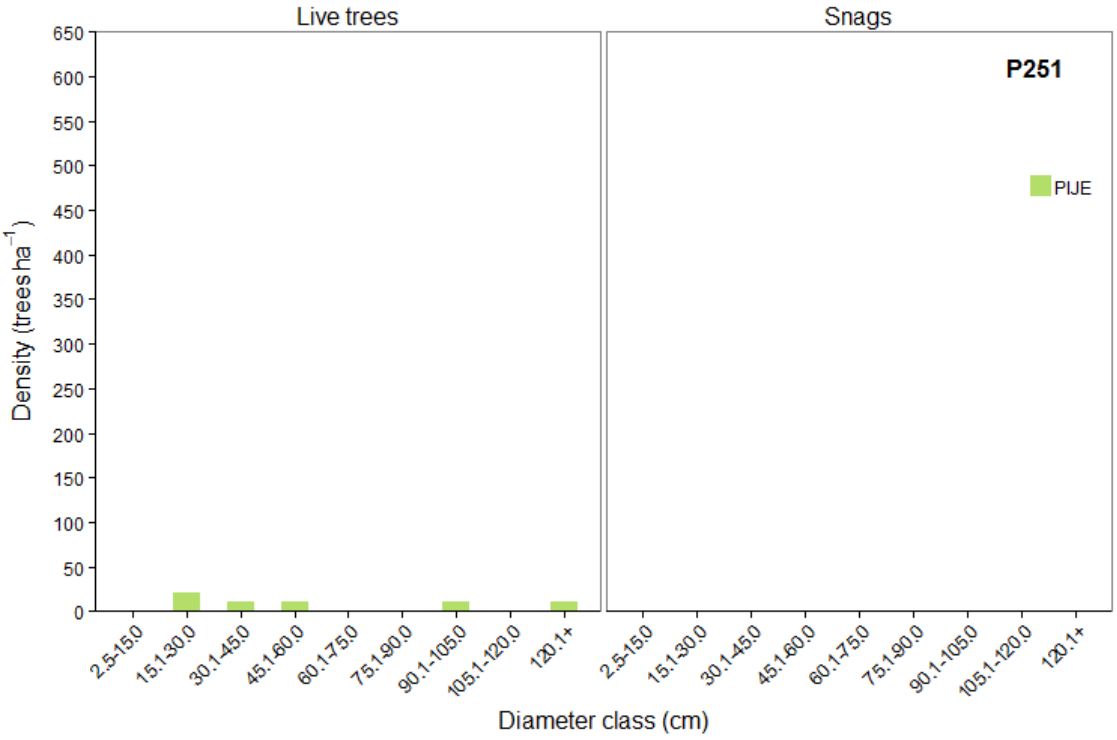
Live trees
Snags
P251
PIJE
Density (trees ha^{-1})
650
600
550
500
450
400
350
300
250
200
150
100
50
0
2.5-15.0
15.1-30.0
30.1-45.0
45.1-60.0
60.1-75.0
75.1-90.0
90.1-105.0
105.1-120.0
120.1+
Diameter class (cm)

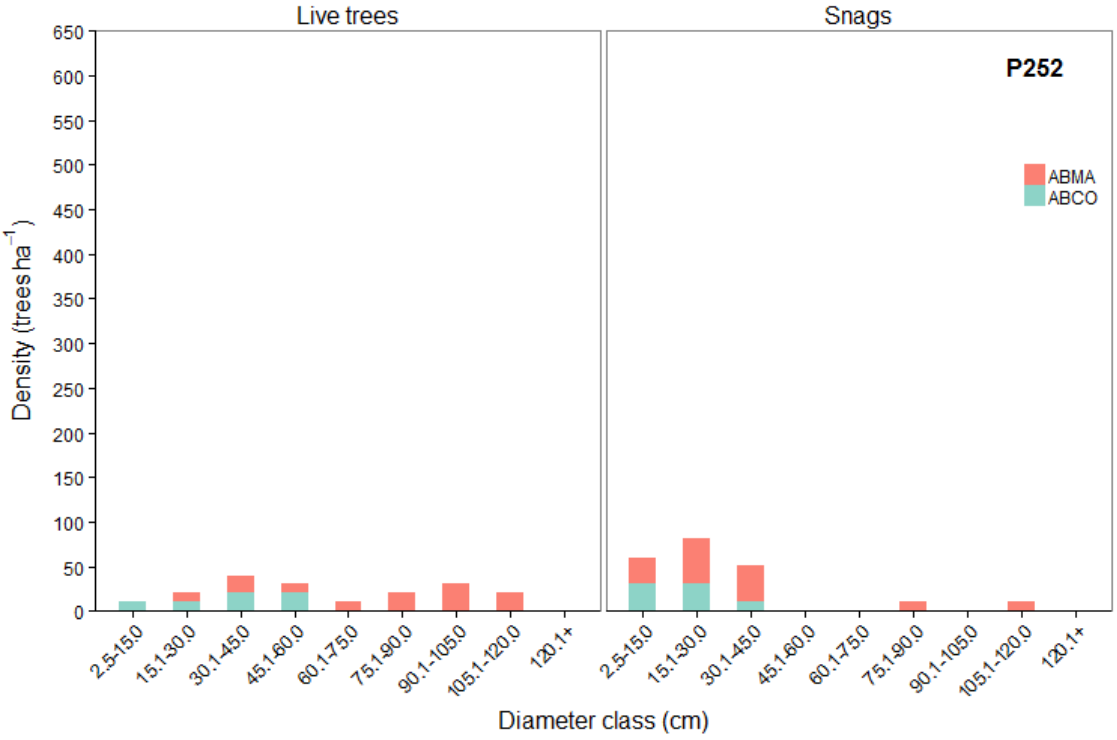
Live trees
Snags
P252
ABMA
ABCO
Density (trees ha^{-1})
650
600
550
500
450
400
350
300
250
200
150
100
50
0
2.5-15.0
15.1-30.0
30.1-45.0
45.1-60.0
60.1-75.0
75.1-90.0
90.1-105.0
105.1-120.0
120.1+
Diameter class (cm)

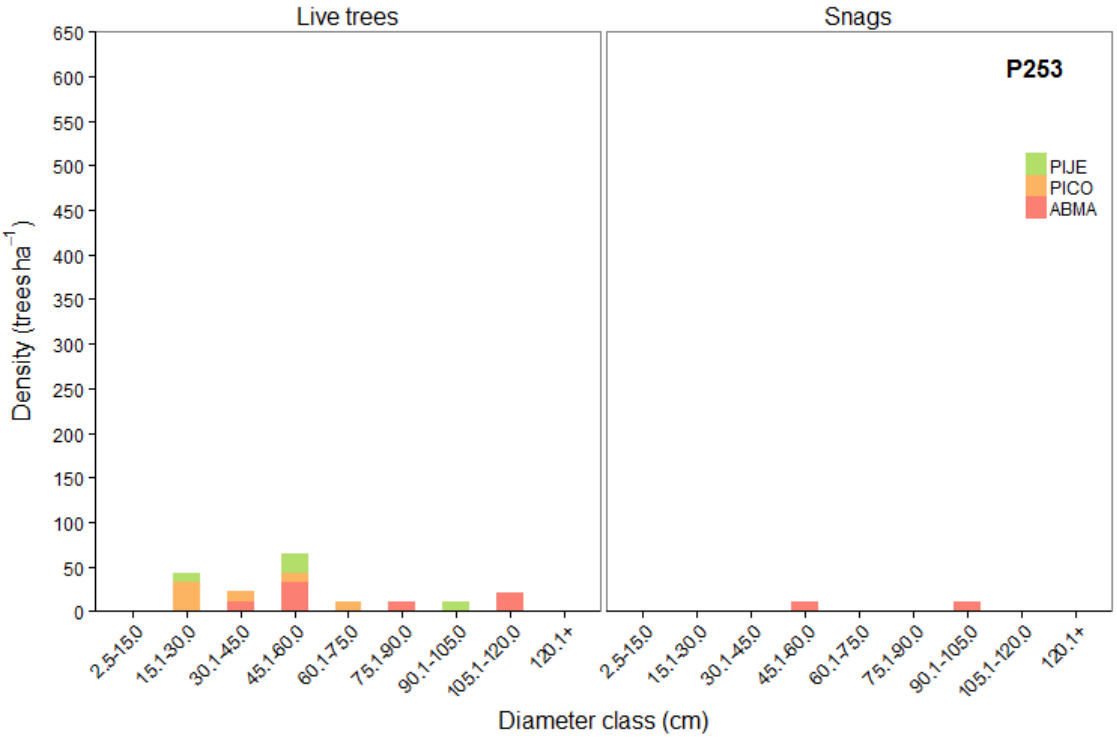
Live trees
Snags
P253
PIJE
PICO
ABMA
Density (trees ha^{-1})
650
600
550
500
450
400
350
300
250
200
150
100
50
0
2.5-15.0
15.1-30.0
30.1-45.0
45.1-60.0
60.1-75.0
75.1-90.0
90.1-105.0
105.1-120.0
120.1+
Diameter class (cm)

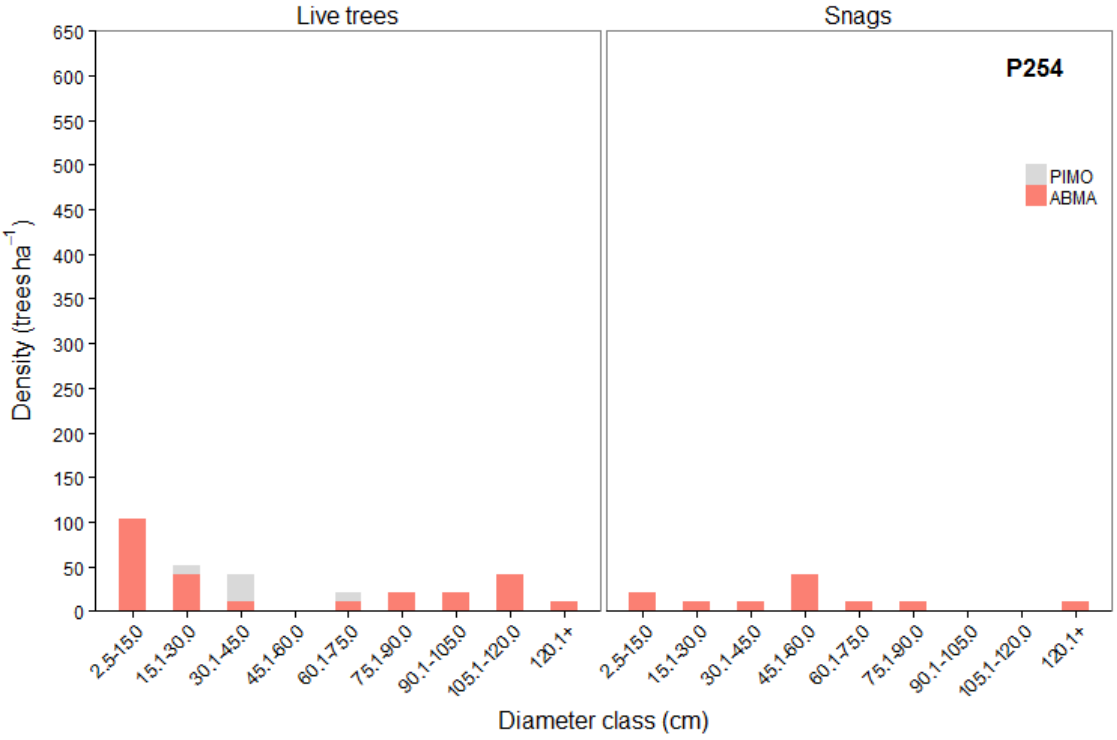
Live trees
Snags
P254
PIMO
ABMA
Density (trees ha^{-1})
650
600
550
500
450
400
350
300
250
200
150
100
50
0
2.5-15.0
15.1-30.0
30.1-45.0
45.1-60.0
60.1-75.0
75.1-90.0
90.1-105.0
105.1-120.0
120.1+
Diameter class (cm)

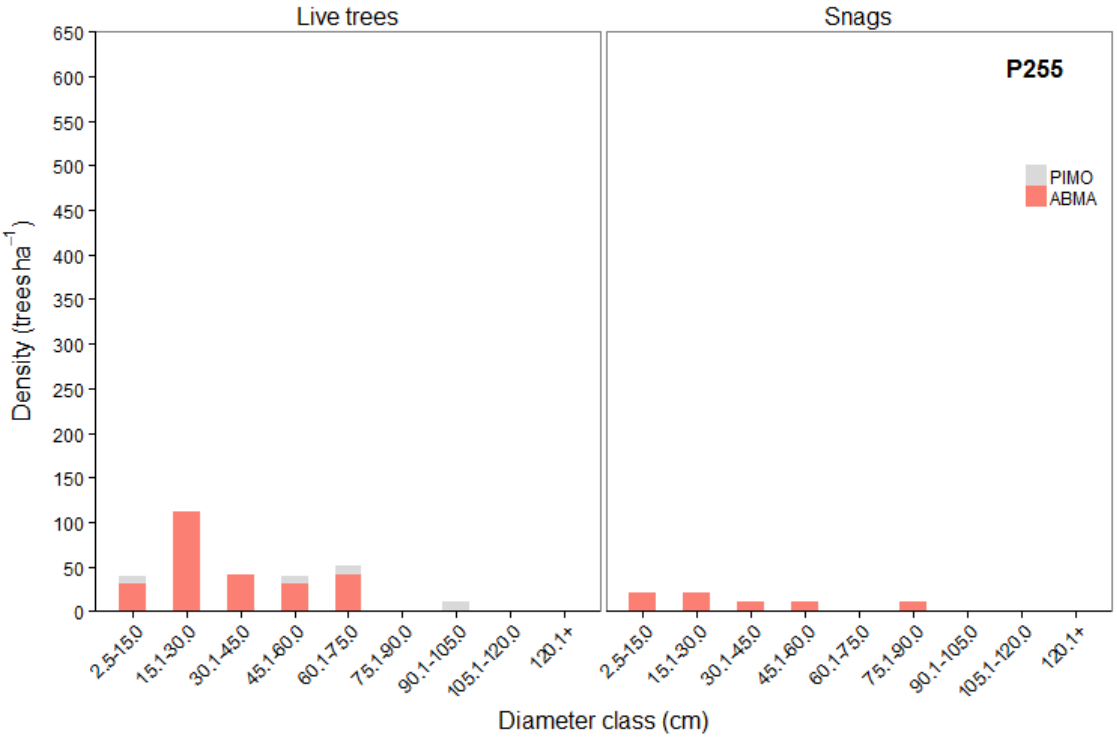
Live trees
Snags
P255
PIMO
ABMA
Density (trees ha^{-1})
650
600
550
500
450
400
350
300
250
200
150
100
50
0
2.5-15.0
15.1-30.0
30.1-45.0
45.1-60.0
60.1-75.0
75.1-90.0
90.1-105.0
105.1-120.0
120.1+
Diameter class (cm)

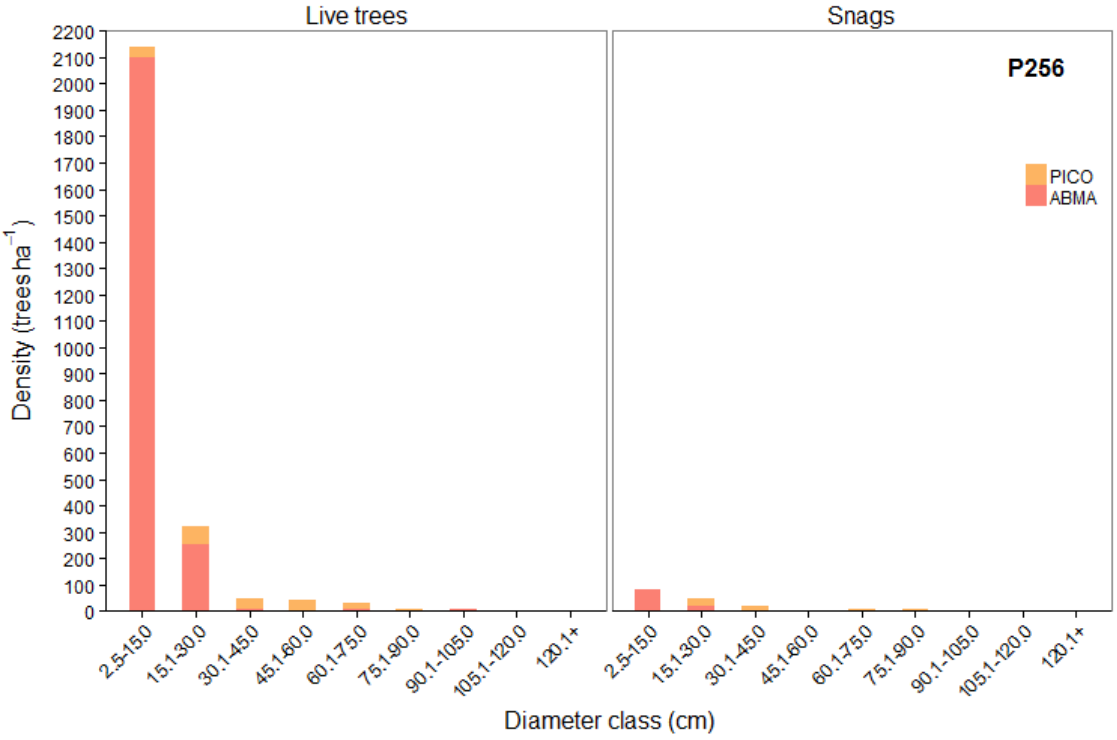
Live trees
Snags
P256
PICO
ABMA
Density (trees ha^{-1})
2200
2100
2000
1900
1800
1700
1600
1500
1400
1300
1200
1100
1000
900
800
700
600
500
400
300
200
100
0
2.5-15.0
15.1-30.0
30.1-45.0
45.1-60.0
60.1-75.0
75.1-90.0
90.1-105.0
105.1-120.0
120.1+
Diameter class (cm)

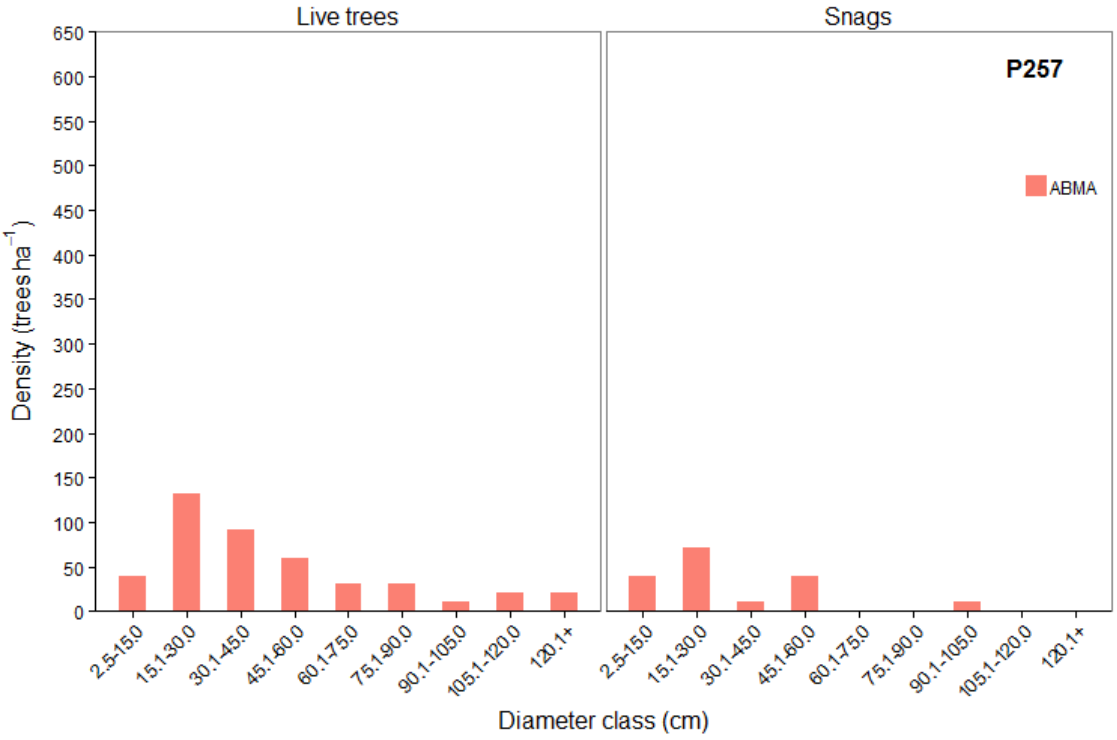
Live trees
Snags
P257
ABMA
Density (trees ha^{-1})
650
600
550
500
450
400
350
300
250
200
150
100
50
0
2.5-15.0
15.1-30.0
30.1-45.0
45.1-60.0
60.1-75.0
75.1-90.0
90.1-105.0
105.1-120.0
120.1+
Diameter class (cm)

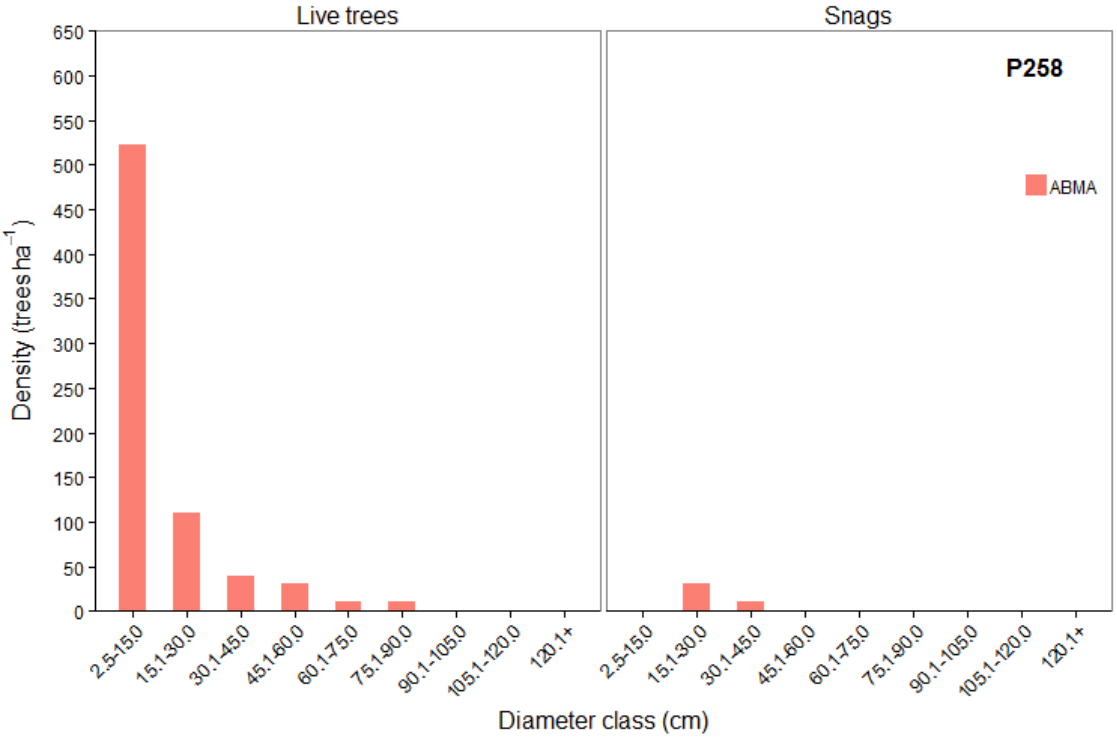
Live trees
Snags
P258
ABMA
Density (trees ha^{-1})
650
600
550
500
450
400
350
300
250
200
150
100
50
0
2.5-15.0
15.1-30.0
30.1-45.0
45.1-60.0
60.1-75.0
75.1-90.0
90.1-105.0
105.1-120.0
120.1+
Diameter class (cm)

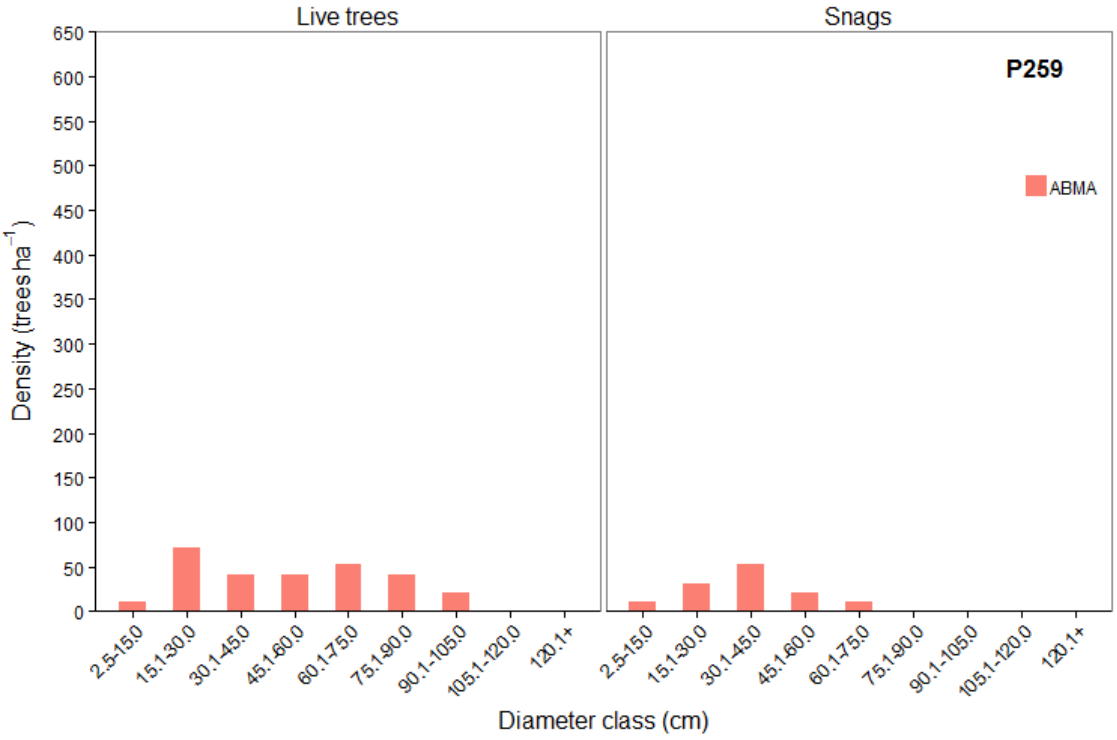
Live trees
Snags
P259
ABMA
Density (trees ha^{-1})
650
600
550
500
450
400
350
300
250
200
150
100
50
0
2.5-15.0
15.1-30.0
30.1-45.0
45.1-60.0
60.1-75.0
75.1-90.0
90.1-105.0
105.1-120.0
120.1+
Diameter class (cm)

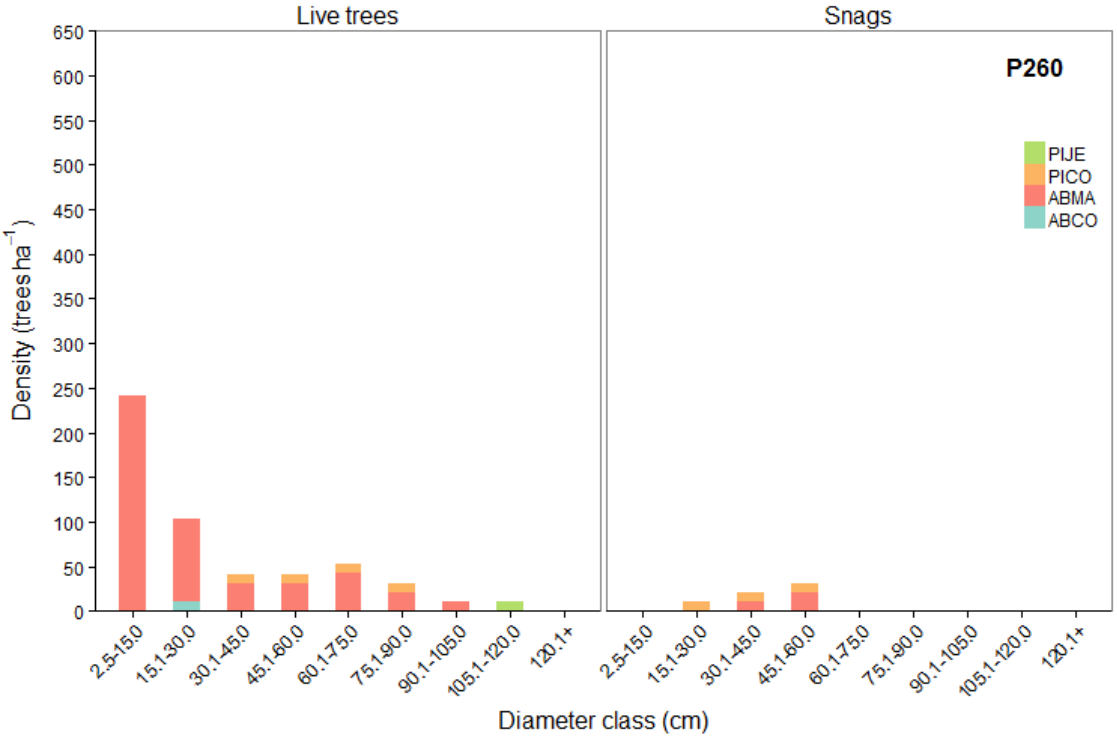
Live trees
Snags
P260
PIJE
PICO
ABMA
ABCO
Density (trees ha^{-1})
650
600
550
500
450
400
350
300
250
200
150
100
50
0
2.5-15.0
15.1-30.0
30.1-45.0
45.1-60.0
60.1-75.0
75.1-90.0
90.1-105.0
105.1-120.0
120.1+
Diameter class (cm)

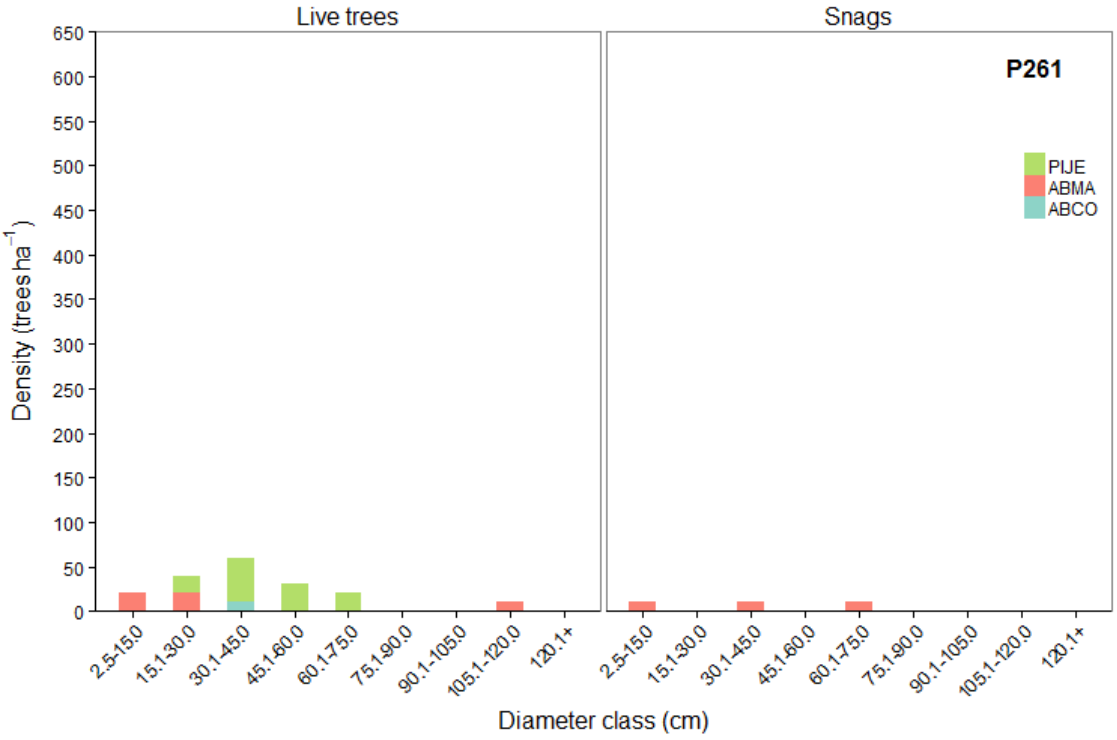
Live trees
Snags
P261
PIJE
ABMA
ABCO
Density (trees ha^{-1})
650
600
550
500
450
400
350
300
250
200
150
100
50
0
2.5-15.0
15.1-30.0
30.1-45.0
45.1-60.0
60.1-75.0
75.1-90.0
90.1-105.0
105.1-120.0
120.1+
Diameter class (cm)

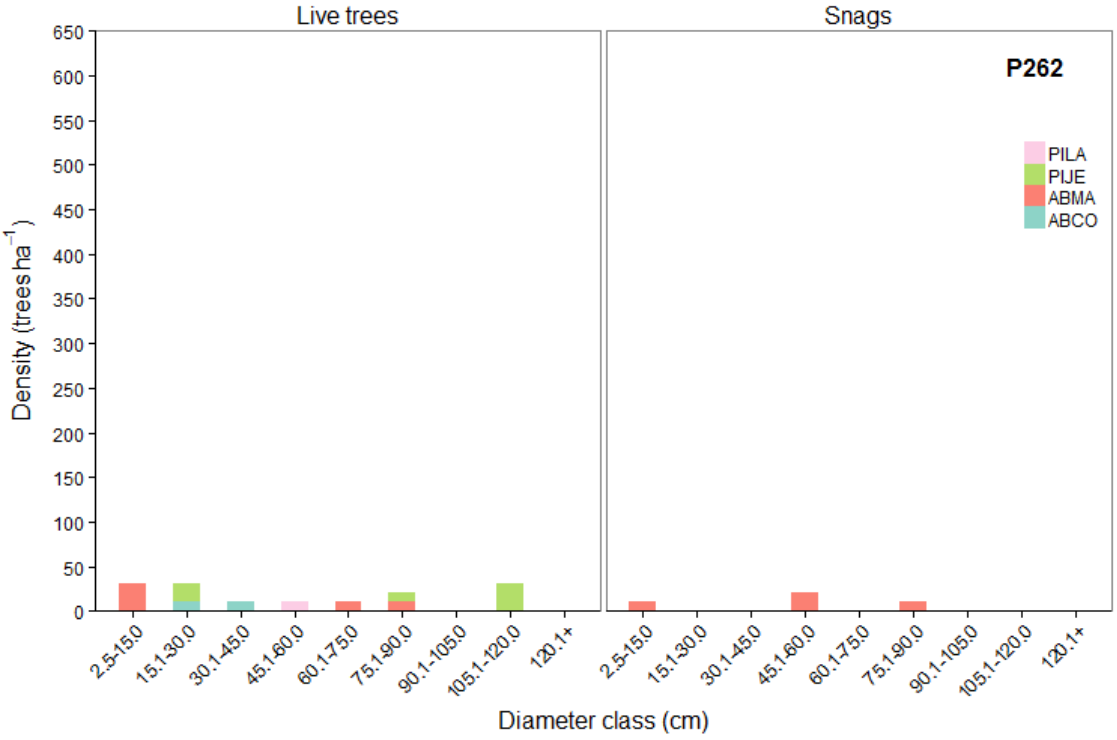
Live trees
Snags
P262
PILA
PIJE
ABMA
ABCO
Density (trees ha^{-1})
650
600
550
500
450
400
350
300
250
200
150
100
50
0
2.5-15.0
15.1-30.0
30.1-45.0
45.1-60.0
60.1-75.0
75.1-90.0
90.1-105.0
105.1-120.0
120.1+
Diameter class (cm)

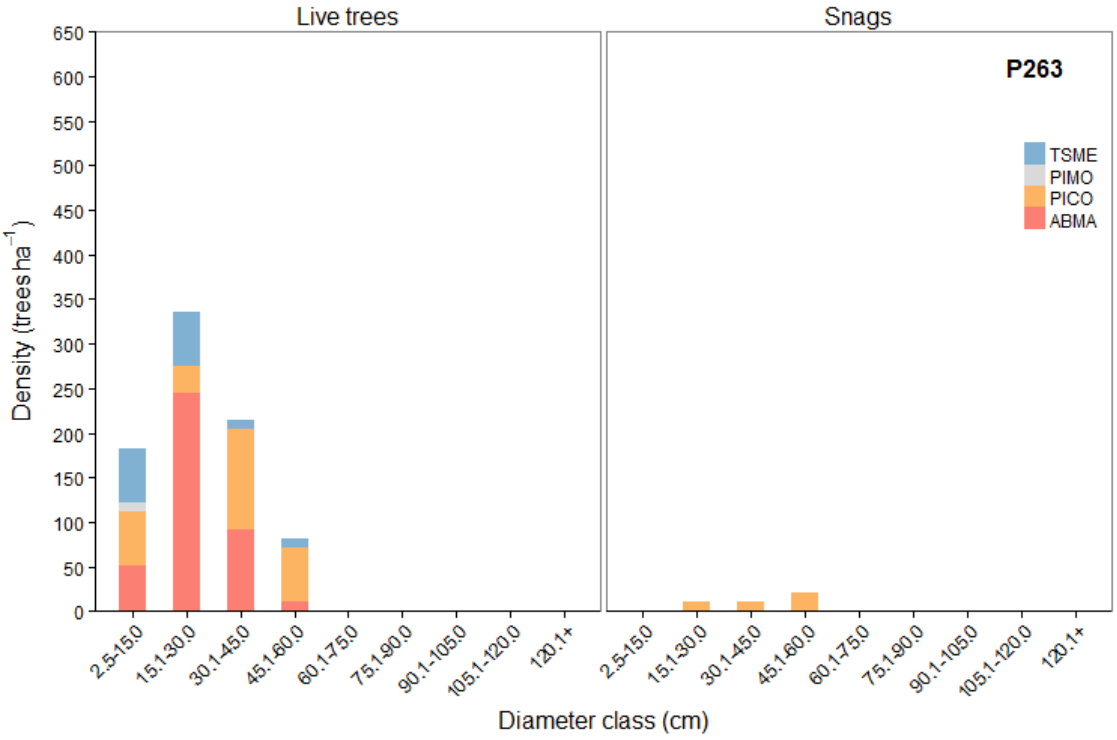
Live trees
Snags
P263
TSME
PIMO
PICO
ABMA
Density (trees ha^{-1})
650
600
550
500
450
400
350
300
250
200
150
100
50
0
2.5-15.0
15.1-30.0
30.1-45.0
45.1-60.0
60.1-75.0
75.1-90.0
90.1-105.0
105.1-120.0
120.1+
Diameter class (cm)

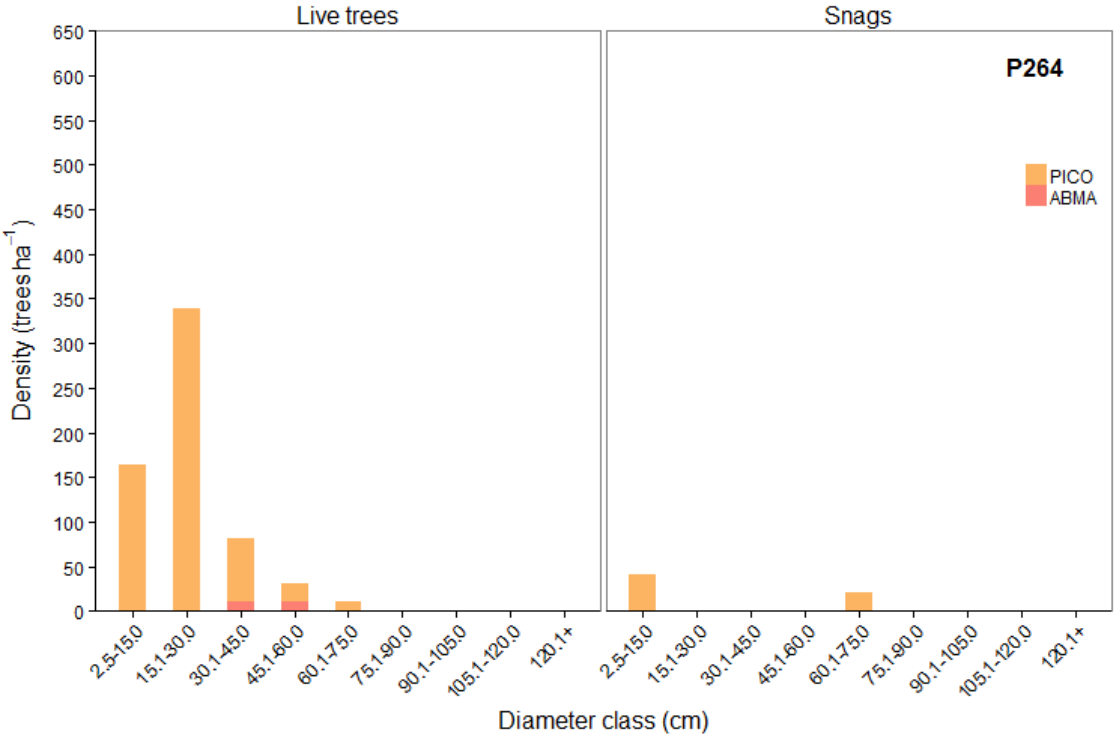
Live trees
Snags
P264
PICO
ABMA
Density (trees ha^{-1})
650
600
550
500
450
400
350
300
250
200
150
100
50
0
2.5-15.0
15.1-30.0
30.1-45.0
45.1-60.0
60.1-75.0
75.1-90.0
90.1-105.0
105.1-120.0
120.1+
Diameter class (cm)

APPENDIX V: COMPARISON OF DISTANCE MEASURES

Selecting an appropriate distance measure is an important step in NMDS ordination. I used the Bray-Curtis distance measure in Chapter I because it is appropriate when data matrices are sparse and particularly when a large proportion of plots do not share any species in common. For Chapter II, however, the decision was less obvious. The data matrices of Chapter II (plots by diameter classes) were not sparse; only two pairs of plots had no diameter classes in common. Therefore, both the Euclidean and Bray-Curtis distance measures could have been appropriate.

The Bray-Curtis dissimilarity is defined as: BC = 1 - (2C/(A+B)), where BC is the dissimilarity between two plots, C is the sum of the lesser abundances for all species that occur in both plots, A is the total abundance of everything in one site, and B is the total abundance of everything in the other site. Therefore, BC represents the proportion of abundance that differs between the two sites. Euclidean distance, in contrast, is an extension of the Pythagorean theorem, $\sqrt{A^2 + B^2} = C$, in species (or diameter class) space, where each orthogonal axis represents a species (or a diameter class). Variable A represents the difference in abundance for one species between two plots, B represents the difference in abundance for another species between the plots, and C is the distance in species space between the two plots. Because the Bray-Curtis distance measure is based on proportional differences and the Euclidean distance measure is based on absolute differences, these measures can yield different results.

I ordinated the relative basal area and density data using both the Bray-Curtis and Euclidean distance measures and compared the results (Figures A.1 and A.2). The diameter classes (not shown) retained the same relative spatial pattern in both ordinations regardless of which distance measure was used. Stress associated with the Euclidean distance ordinations was marginally lower (Table A.6). In the relative density ordination the position of one plot (P087)

was more sensitive to the distance measure relative to other plots (Figure A.1). In the relative basal area ordination the positions of two plots (P024 and P158) were more sensitive to the distance measure relative to other plots (Figure A.2). P024 exhibited the greatest response to distance measure. Over half (0.529) of the basal area of this plot was in DC7; the remainder was distributed among DC1 through DC3. Therefore, the Euclidean distance was marginally better for these data given that P024 was located near the DC7 centroid when the Euclidean distance measure was used. The Bray-Curtis measure, in contrast, gave greater weight to the three diameter classes that contained nearly half the basal area.

Despite these subtle differences, the correlations between the relative density ordinations and between the relative basal area ordinations as determined by Procrustes analyses were high (Table A.6). Procrustes analysis is a technique that determines the correlation between two ordinations (Kane et al. 2010; McCune and Grace 2002). In Procrustes analysis the axes of one ordination (i.e., the ordination based on Euclidean distance) are rotated and rescaled until all points are as close as possible to their locations in another ordination (i.e., the ordination based on Bray-Curtis distance). The rotation and rescaling of the ordination axes is based on minimization of the sum of squares error (m^2), which is computed from the distances between matching points in the two ordinations (i.e., Procrustes residuals). A correlation-like metric, Procrustes R = sqrt(1- m^2), is then computed, and its significance (p) is determined by permutations of the data. Procrustes analysis was conducted in the R statistical language (version 3.0.2; R Development Core Team, 2013) with the function "protest" in the vegan package (version 2.0-10; Oksanen et al. 2013).

Based on these analyses I decided to use the Bray-Curtis distance measure in Chapter II to maintain consistency with Chapter I and because there was no compelling reason not to use it.

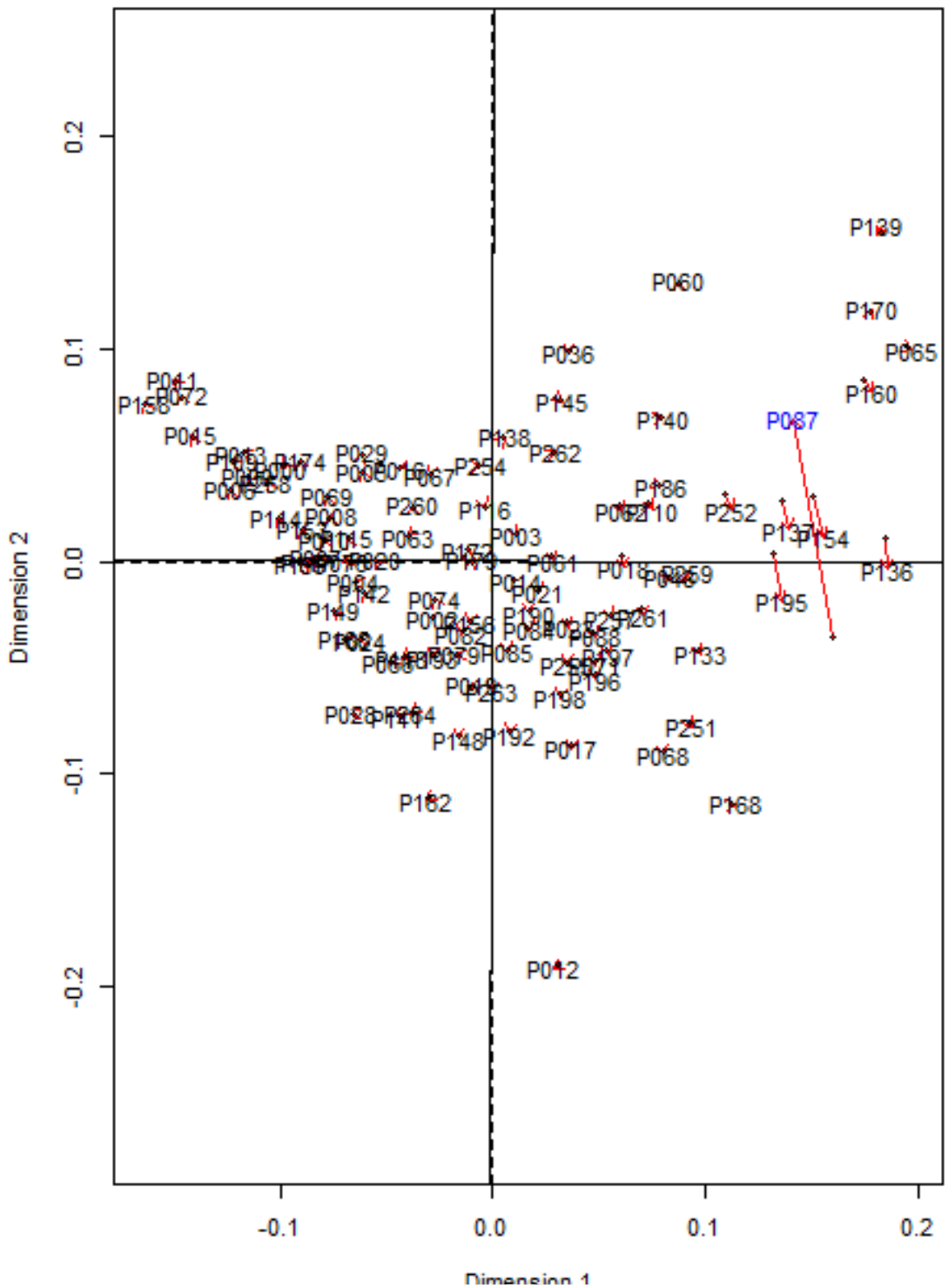

Figure A.1. Procrustes analysis of relative density attributed to nine diameter classes, comparing an ordination based on Bray-Curtis distance to an ordination based on Euclidean distance. Plot labels represent the ordination based on Bray-Curtis distance; red arrows point to the same plot as ordinated with the Euclidean distance measure. Blue text identifies the plot that was most sensitive to distance measure. The ordination based on Euclidean distance was rotated (solid axes) and rescaled to match the ordination based on Bray-Curtis distance (dotted axes).

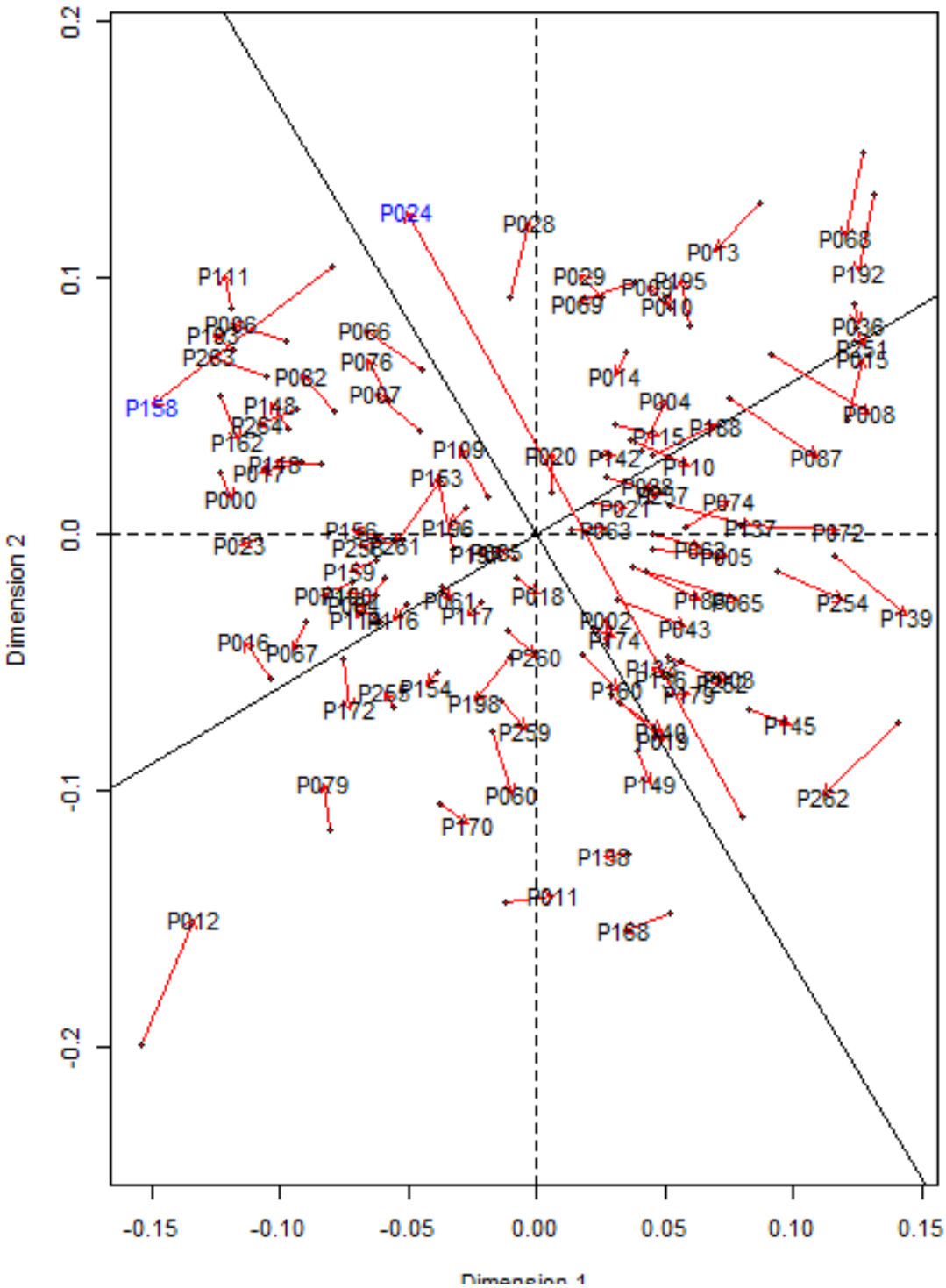

Figure A.2. Procrustes analysis of relative basal area attributed to nine diameter classes, comparing an ordination based on Bray-Curtis distance to an ordination based on Euclidean distance. Plot labels represent the ordination based on Bray-Curtis distance; red arrows point to the same plot as ordinated with the Euclidean distance measure. Blue text identifies the plots that were most sensitive to distance measure. The ordination based on Euclidean distance was rotated (solid axes) and rescaled to match the ordination based on Bray-Curtis distance (dotted axes).

Table A.6. Comparison of NMDS ordinations based on the Bray-Curtis and Euclidean distance measures.

	Bray-Curtis stress	Euclidean stress	Procrustes *R*	*p*-value
Relative density	0.130	0.098	0.98	0.001
Relative basal area	0.218	0.199	0.94	0.001